Evaluation of Cover Materials for a Large Scale Test Facility at Key Lake

A Thesis
Submitted to the College of Graduate Studies and Research
in Partial Fulfilment of the Requirements
for the Degree of Master of Science
in the
Department of Civil Engineering
University of Saskatchewan, Saskatoon, SK, Canada

by
Nan H. Lee
September 1999

In presenting this thesis in partial fulfilment of the requirements for a Postgraduate degree from the University of Saskatchewan, I agree that the Libraries of this University may make it freely available for inspection. I further agree that permission for copying of this thesis in any manner, in whole or in part, for scholarly purposes may be granted by the professors who supervised my thesis work, or in their absence, by the Head of the Department or Dean of the College in which my thesis work was done. It is understood that any copying or publication or use of my thesis or parts thereof for financial gain shall not be allowed without my written permission. It is also understood that due recognition shall be given to me and the University of Saskatchewan in any scholarly use which may be made of any material in my thesis.

Request for permission to copy or to make any other use of material in this thesis in whole or in part should be addressed to:

Head of Department of Civil Engineering
University of Saskatchewan
57 Campus Drive
Saskatoon, SK
Canada
S7N 5A9

ABSTRACT

Engineered soil cover systems have gained popularity in recent years as a preferred method of decommissioning and reclaiming waste management facilities. The main functions of a soil cover system are to minimize water infiltration, limit gas migration, resist weathering and erosion, and provide support for vegetation.

In 1992, Cameco Corporation constructed a large scale non-vegetated prototype soil cover at Key Lake in north-central Saskatchewan. Their main objective was to evaluate the suitability of using local tills and sands for cover materials during future decommissioning of various waste management facilities at the site. An instrumentation and monitoring program was initiated in 1993 to verify the field performance of the soil cover system.

The prototype soil cover was constructed over leached cobble ore that was enclosed within a double lined containment system. The soil cover consisted of a 60 cm layer of outwash glacial sand overlain by a 60 cm layer of compacted till. The test facility is essentially a large scale lysimeter whereby net infiltration is determined by monitoring the change in water table depth, the quantity of water removed from the facility, and the soil moisture profile.

The instrumentation and monitoring program included a weather station, thermal conductivity sensors and neutron probe access holes, a Bowen Ratio Instrumentation, and a runoff collection and monitoring system. A laboratory program was undertaken to define pertinent soil parameters such as the soil-water characteristic curve and hydraulic conductivity. Laboratory calibration of the neutron probe was also carried out. A field soil testing program was completed to determine *in situ* density and hydraulic conductivity.

The weather monitoring program yielded reliable precipitation, air temperature, and wind speed data. Instrumentation error was noted for relative humidity, net radiation, and pan evaporation parameters. The surface runoff monitoring system provided reliable runoff data

on a real time basis. The thermal conductivity sensors were found to underestimate the soil moisture content, while the neutron probe was found to overestimate. The laboratory testing indicated that the outwash sand and the compacted till possessed similar soil water characteristic curves. The similarities in their water storage and release characteristics preclude the ability of these soils to form an effective capillary barrier when the till is overlain by the outwash sand. The field investigation has revealed that the soil cover system was underlain by a layer of extraneous sand and till material, most likely used to grade the facility prior to constructing the soil cover.

The field performance of an engineered soil cover system is determined by the net infiltration through the system. The net infiltration for the 1996-1997 monitoring year was estimated to be 52% (287 mm) of the total annual precipitation (555 mm of precipitation from October 1996 to April 1997, inclusively). There was an insignificant change in the subsurface soil moisture storage. The surface runoff was recorded to be 6% (35 mm) of the total annual precipitation. The actual evaporation was estimated to be 30% (167 mm).

The evaluation of the soil cover design has suggested that the Key Lake outwash sand overlain by the Key Lake till will not form a capillary barrier. Furthermore, the thickness of the till layer far exceeded the evaporative zone depth of the material, and therefore, infiltrated water could not have been extracted through evaporation even if the two soils had formed a capillary barrier. The net water storage capacity of the cover system was found to be inadequate (12 mm) to store larger rainfall events, thus further contributing to net infiltration. Incorporating surface vegetation has the potential to increase the total storage capacity to 42 mm; vegetation will also increase total evapotranspiration.

A detailed analysis of the surface runoff and infiltration characteristics has indicated that runoff was governed by rainfall intensity and antecedent soil moisture conditions. Surface runoff was generated regardless of soil moisture conditions when the 15-minute rainfall intensity exceeded 1.4 mm. This intensity corresponds to a surface hydraulic conductivity (till) of 1.5×10^{-6} m/s; the laboratory determined hydraulic conductivity was 2.0×10^{-7} m/s.

ACKNOWLEDGMENTS

I would like to acknowledge Nick Holl of Cameco Corporation. His confidence in my abilities has spurred on this thesis. I am grateful to Mr. Holl for entrusting me with this project, and for providing financial support for this thesis research. I would like to thank Trevor Hamm of Cameco Corporation for his assistance and encouragement. The success of the field instrumentation program, the runoff monitoring in particular, is accredited to his diligent involvement. I am also grateful to the crew at Key Lake for their assistance.

I would like to thank Dr. G. Putz for encouraging me to apply for a scholarship, and Dr. D.E. Pufahl and the University of Saskatchewan for granting me the university scholarship.

I am grateful to my supervisors Dr. S.L. Barbour and Dr. G.W. Wilson for their friendship and their insightful suggestions. Their enthusiasm and optimism are infectious. Their insatiable curiosity and desire for knowledge, coupled with a passion for teaching others make them superb researchers, and challenging supervisors. I would like to acknowledge the members of my examination committee, Drs. D.E. Pufahl, D.G. Fredlund, and M.D. Haug for their encouragement, expertise, and advise throughout my research. A special thanks is extended to Dr. D.G. Fredlund and his research team, F. Shuai, J. Yazdani, M. Feng, and J. Gan, for generously contributing Beta-97 sensors toward this project.

I have made many new friends and acquaintances, and each of them have contributed to this research through their assistance, encouragement, and friendship. Thank you to Lori and Greg Newman, Alex Kozlow, Mike O'Kane, Dale Pavier, Brenda Bews, Brian Ayres, Debbie Pfeifer, Karen Wog, Andrew Durham, James Wilson, and Jack Woo.

It would not have been possible for me to pursue this personal endeavor without the love and constant encouragement from my husband, Dave Neuburger, and my daughters Sarah and Laura. I am grateful to my daughters' caregiver Xiuli Yang, whose loving and competent care accorded me the peace of mind to complete this thesis.

TABLE OF CONTENTS

Chapter Two: LITERATURE REVIEW AND THEORY (continued)

Chapter Three: CAMECO INSTRUMENTATION PROGRAM

Chapter Four: LABORATORY AND FIELD PROGRAM

Chapter Five: DATA PRESENTATION AND DISCUSSION

Chapter Five: DATA PRESENTATION AND DISCUSSION (continued)

Chapter Six: ANALYSIS AND INTERPRETATION

LIST OF TABLES

LIST OF FIGURES

Chapter One
INTRODUCTION

1.1 GENERAL BACKGROUND

Engineered soil cover systems have gained popularity in recent years as a preferred method of decommissioning and reclaiming waste management facilities. Research and development in the area of soil cover designs have been abundant and fruitful in the last decade (Vanapalli *et al.*, 1997). The main functions of a soil cover are to minimize water infiltration, limit gas migration into or out of the waste being contained, resist weathering and erosion, and provide support for vegetation.

In 1992, Cameco Corporation (Cameco) constructed a large scale non-vegetated prototype soil cover at the Key Lake Heap Leach Test Facility (HLTF) in north-central Saskatchewan. Cameco's main objective was to evaluate the suitability of using local tills and sands for cover materials during future decommissioning of various waste management facilities at the site. An extensive instrumentation and monitoring program was initiated in 1993 to verify the field performance of the constructed soil cover system.

1.2 SITE DESCRIPTION

The Key Lake Operation (Key Lake) is located in north-central Saskatchewan approximately 350 air miles (560 km) north of Saskatoon at latitude 57°11' north and longitude 105°34' west (*Figure 1.1*). Cameco is currently the operator and majority owner of Key Lake .

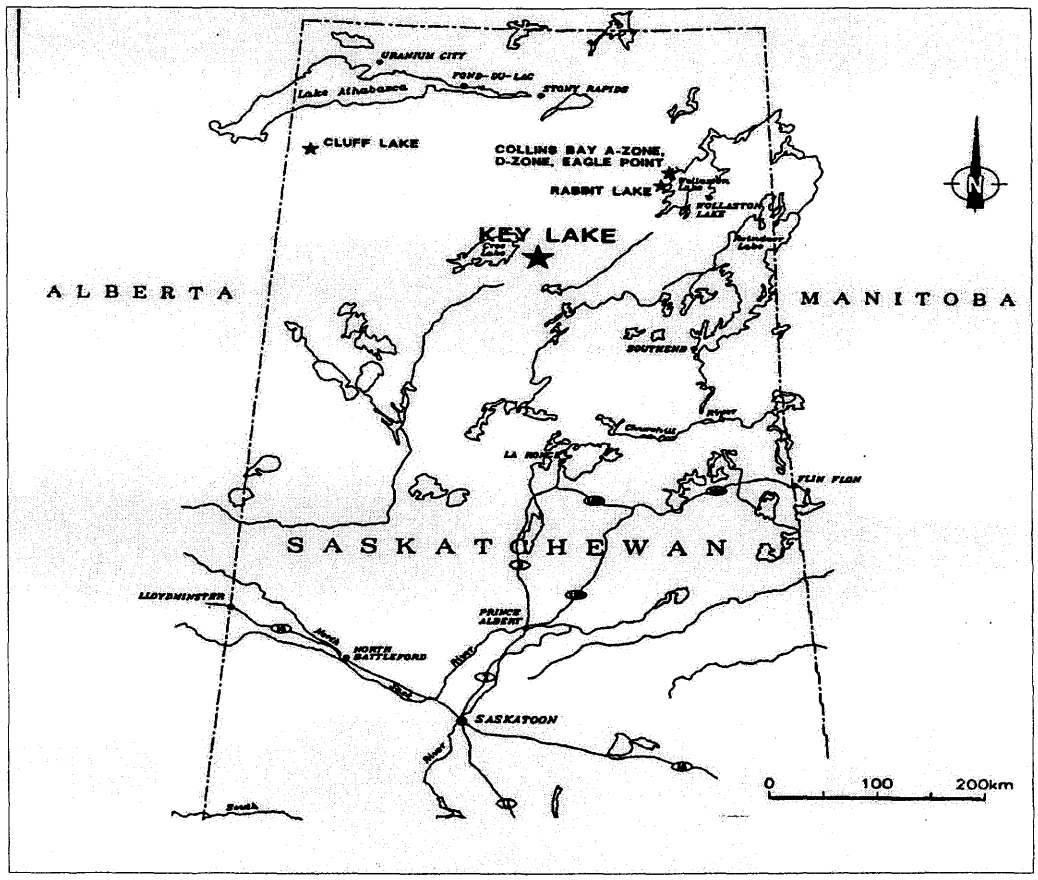

Figure 1.1 Location of Key Lake Operation (after Amok Ltd., 1992)

Mining activities at Key Lake commenced with the Gaertner ore body in 1982. The Gaertner pit was mined out by 1987. The Development of the Deilmann ore body commenced in 1986, and the mining and stockpiling activities continued until 1997. During its production, Key Lake maintained its status as the world's largest uranium mining operation with an average annual total output of approximately 14 million pounds of U_3O_8. The milling of the stockpiled ore is expected to continue till mid 1999.

Key Lake is located in the continental subarctic region of north-central Saskatchewan. This region is characterized by short cool summers and long cold winters . The warmest month of the year is July, and the coldest is January, with a mean daily temperature of 16.1°C and -22.4°C, respectively. The mean number of frost days is 222 days per year. The precipitation

typically occurs as snow from October to April, and as rain from May to September. The mean annual total precipitation is 458 mm with 35% falling as snow, and 65% as rain (Cameco 1994).

Key Lake lies within the southerly boundary of the Athabaska basin. The region has undergone substantial glacial erosion and deposition over recent geological history. It is overlain by unconsolidated Quaternary glacial deposits that consist of streamline forms (drumlins), moraines (ground moraines), ice-contact forms (eskers and kames), and proglacial (outwash) deposits (Cameco 1994).

The till deposits are present in ground moraines and drumlins consisting of unsorted and unstratified sandy materials with angular to sub-rounded grey sandstone fragments. Ground moraines are relatively flat, and 5 to 20 meters in thickness. Drumlins are smooth streamlined hills, 500 to 2000 meters long, 300 to 1000 meters wide, and over 50 meters high. These deposits consist primarily of sand (68%), gravel (20%), silt (8.5%), and clay (3.5%). The sand deposits are found in outwash plains with some deposits exceeding 80 meters in thickness. The outwash plains are flat to gently sloping stratified sand and gravel deposits, commonly pitted with kettle holes (Cameco 1994).

The vegetation in the area is typically subarctic with a prevalence of jack pine and spruce, and occasional birch; the trees are generally stunted due to poor soil conditions (Cameco 1994).

1.3 KEY LAKE WASTE MANAGEMENT FACILITIES

Cameco's decommissioning plan identifies two waste management facilities; the surface Tailings Management Facility (TMF) and the waste rock and overburden stockpiles, which may require some form of a soil cover system. The surface TMF is a subaerial tailings containment facility brought into operation in 1983. It comprises an area of approximately

30 ha at the bottom, and 45 ha at the top. It was designed to have a final storage capacity of approximately 5.6 x 10^6 m^3. It has a base seal of 200 mm of compacted mixed glacial till and bentonite that is overlain by a 1 metre thick sand filter layer. Three sides are built with compacted glacial till, while the fourth side is composed of compacted glacial till on the outside and sand and gravel on the inside. The conceptual decommissioning plan proposes to cap the surface TMF with an engineered cover that will minimized infiltration into the facility.

A waste rock characterization study carried out in 1993 described the waste rock piles to be at least 85% sandstone with lesser amounts of overburden or basement rock (SRK Canada Inc., 1993). The sulphide contents of the rock piles were reported to be relatively low, and acidic drainage was not anticipated. The basement rock, however, have reactive sulphide minerals with a potential for oxidation and metal leaching. Therefore, the placement of recently excavated basement material over the existing rock piles may have resulted in an increase in potential contaminant loads. The studies on final waste rock decommissioning are ongoing, and the final decommissioning plan remains to be completed. Nevertheless, it is anticipated that some form of a till cover may be required to minimize infiltration into these stockpiles.

1.4 HEAP LEACH TEST FACILITY TEST COVER

The test soil cover facility, referred to as the Heap Leach Test Facility (HLTF), is a double plastic lined containment area that was originally constructed in 1987 to study leachate recovery rates from low-grade cobble ore. The leaching program was concluded at the end of 1989. The remaining leachate was pumped to the mill; the facility was subsequently flushed, and neutralization was completed in the spring of 1992 (Cameco 1995).

In 1993, a test soil cover was installed as part of the decommissioning process for this facility. It consisted of 60 cm of compacted glacial outwash sand overlain by 60 cm of

compacted glacial till. The instrumentation and monitoring equipment were installed in stages between 1992 and 1994 to study the process of surface runoff, infiltration, and evaporation on a scale representative of actual field conditions. The collection of field data began in 1994. The details of the HLTF test cover are contained in Chapter 3.

1.5 RESEARCH OBJECTIVES, SCOPE, and METHODOLOGY

The contamination potential of waste management facilities is governed by the quantity of net infiltration and gas migration into and out of the waste containment system. The net infiltration is determined by the evaporation, transpiration, and surface runoff processes. These processes are dictated by parameters such as climatic conditions, vegetation, and soil properties. Defining decommissioning scenarios and requirements using various types of cover materials and design alternatives thus requires a clear understanding of these processes.

The objectives of this research program are:

- to evaluate the performance of the test cover as designed and as constructed;
- to assess the suitability of using local tills and sands for future decommissioning of waste management facilities at Key Lake; and
- to formulate a criteria for future cover designs at Cameco's Key Lake Operation.

The project scope and methodology are:

- a literature review of the theory and the fundamental processes pertaining to the design of soil cover systems;
- assessment of the existing field data and implementation of an additional field instrumentation program;
- a laboratory program to determine pertinent soil properties; and
- verification of the overall water balance.

Chapter Two
LITERATURE REVIEW AND THEORY

2.1 INTRODUCTION

An effective soil cover design requires identification of soil parameters and design factors that impact the cover performance, as well as climatic conditions that dictate its longterm integrity. The assessment of a soil cover system requires a good understanding of surface water partitioning and energy balance at the soil-atmosphere interface. Furthermore, an extensive instrumentation and monitoring is typically needed to verify the actual field performance.

This chapter presents a literature review and related theoretical background pertaining to:

- the design of soil cover systems (section 2.2);
- the surface and subsurface hydrology characterization, such as precipitation, infiltration, runoff, and evaporation, that are required to represent water partitioning and the energy balance at the soil-atmosphere interface (sections 2.3 to 2.6); and
- the instrumentation used to assess temporal variations in subsurface soil-water content and soil suction (sections 2.6, and 2.7).

A review of instrumentation available for the measurement of precipitation, infiltration, surface runoff, and evaporation are presented in their respective sections (i.e., sections 2.3 to 2.6).

The relevant literary and theoretical framework is presented in Chapter 2. The literature review provides an outline of the fundamentals of soil cover design, and the processes that govern the overall water balance such as precipitation, infiltration, runoff, and evaporation. The details of the Heap Leach Test Facility test cover and the existing instrumentation and monitoring program are presented in Chapter 3. The existing program included a weather station, a runoff monitoring system, thermal conductivity soil suction sensors, neutron probe access holes, and thermistors.

The additional field and laboratory program carried out to complement the existing data is described in Chapter 4. The field program involved installation of new matric suction sensors and a Bowen Ratio Station. The laboratory program determined pertinent soil parameters such as the grain size distribution, the specific gravity, the hydraulic conductivity, and the soil-water characteristic curve. A laboratory calibration of the neutron probe was also undertaken.

The results of the field instrumentation and monitoring efforts and the laboratory programs are presented in Chapter 5. Chapter 6 provides the analysis and the interpretation of the overall water balance, and the discussion on the performance and the effectiveness of the HLTF test cover. A detailed analysis of the runoff and infiltration characteristics are presented in Chapter 6. The conclusions and recommendations arising from this research program are provided in Chapter 7.

2.2 DESIGNING A SOIL COVER SYSTEM

An optimal soil cover design is inherently site specific, given that: its performance is weather dependant; the material utilized is typically limited to what is readily available in the vicinity of the waste management facility; the performance specification of the proposed cover is dictated in part by the nature of the disposed material; and the contamination potential is dependent on the regional hydrology and regulatory requirements.

Engineered soil covers are generally designed to provide one or more of the following functions:

- capillary barrier for limiting oxygen diffusion (Nicholson *et al.*, 1989; Bennet and Ritchie 1991; Yanful 1991; O'Kane 1996; Wilson *et al.*, 1997);
- capillary barrier for limiting water influx (Weeks *et al.*, 1992; Benson *et al.*, 1994; Bell *et al.*, 1995; Swanson 1995; Woyshner and Yanful, 1995; O'Kane *et al.*,1995);
- subsurface moisture storage for delayed evaporation (Fayer *et al.*, 1992; Weeks *et al.*, 1992; Anderson *et al.*, 1993; Bews *et al.*, 1997; Stormont and Morris, 1998);
- erosion protection (Bell *et al.*, 1995; Swanson 1995);
- protection against freeze/thaw or dessication (Mohamed *et al.*, 1993; O'Kane 1996);
- support for vegetation (Fayer *et al.*, 1992; O'Kane 1996; Bews *et al.*, 1997);
- capillary barrier against migration of salt into upper layers (Haug *et al.*, 1991); and
- capillary barrier against radon gas emission.

2.2.1 Fundamentals of Soil Layering

The capillary barrier concept and the fundamentals of soil layering has succinctly been presented by O'Kane (1996). A brief overview is provided in this thesis.

A capillary barrier soil cover design typically consists of two or more layers of soils that differ significantly in their ability to store and transmit water, thus creating a barrier to

subsurface moisture flow and gas migration. A capillary barrier is formed when a fine textured material overlies a coarse textured material (Nicholson, 1989; Barbour 1990; Akindunni *et al.*, 1991). Under drainage conditions, the lowest suction that the underlying coarse layer will attain, is the suction at its residual water content (Nicholson 1989; Akindunni *et al.*, 1991). The underlying coarse textured material, therefore, prevents the fine textured material from draining.

When the overlying fine material has an air entry value much greater than the matric suction attained in the underlying coarse layer at residual water content, then the fine layer will remain near saturation at considerable heights above the water table (Nicholson 1989). Under evaporative conditions, however, soil suction in the coarse layer will continue to increase due to evaporative demand (Barbour and Yanful, 1994).

To reduce drying and dessication in the near saturated fine layer, coarse/loose layers are often placed on top. This uppermost loose layer provides protection against erosion, protection against freeze/thaw or dessication, and supports vegetation. This surficial layer also functions as a moisture storage layer where infiltration is stored to supply moisture for vegetative growth and evaporative demand during subsequent dry periods.

2.2.2 Soil Cover and Site Climatic Conditions

Designing an optimum and effective soil cover system requires understanding the soil-atmosphere interaction. The site climatic conditions dictate the overall design and impact the longterm cover performance. For example, a design that incorporates freeze/thaw or dessication protection (Mohamed *et al*, 1993) differs from a design that resists high intensity rainfall erosion (Bews *et al.*, 1997). Maintaining a near saturated subsurface layer as an oxygen and moisture limiting barrier is attainable for humid and tropical climatic conditions; but it is difficult to maintain at arid sites. Consequently, the success of any soil cover design is dependent on how well it reflects and adapts to site specific climatic conditions. Examples of soil cover designs below, illustrate their adaptability and variability.

Arid Climatic Zone: Golden Sunlight Mine

The Golden Sunlight Mine is located in an arid alpine environment in Montana (Swanson 1995). The cover system consists of 60 cm of oxidized waste rock overlain by 60 cm of local topsoil material. It was designed to reduce infiltration, provide erosion control, and support vegetative growth. Moisture is stored and released in the upper vegetated topsoil layer, and the subsurface oxidized waste rock layer is maintained in a dry condition.

Semi-Arid Climatic Zone: Kidston Gold Mine

The Kidston Gold Mine in North Queensland, Australia, is located in a semi-arid climatic zone with extreme wet and dry seasons (Bews *et al.*, 1997). Maintaining a subsurface layer near saturation to limit oxygen diffusion into the underlying acid generating mine waste rock is not practical, nor possible, during the dry season. Consequently, the cover system is designed with a 250 cm thick non-compacted weathered material with a large moisture storage capacity. The soil cover is designed to accept and store infiltration during high intensity rainfalls. The stored infiltration is then released by evapotranspiration during subsequent dry periods. The vegetation plays a primary role by significantly extending the depth from which water is removed through evapotranspiration.

Humid Alpine Climatic Zone: Equity Silver Mine

The Equity Silver Mine is located in a humid alpine environment in the central interior of British Columbia (O'Kane 1996). The soil cover system consists of 50 cm of compacted till overlain by 30 cm of non-compacted till. Water and oxygen influx into the underlying acid generating waste rock is controlled by the low hydraulic conductivity compacted layer maintained at a high degree of saturation. The non-compacted till layer provides for moisture storage to satisfy evaporative demand. It also provides protection from freeze/thaw dessication and supports vegetation.

Maritime Continental Climatic Zone: Heath Steel Mine

The Heath Steel Mine is located in a maritime continental climatic zone in New Brunswick (Bell *et al.*, 1995). The soil cover system consists of, from bottom to top, 30 cm of sand base, 60 cm of compacted till, 30 cm of sand and gravel, and 10 cm of gravel. The sand and gravel layer serves to reduce evaporation and dessication of the underlying compacted till layer. The gravel layer on surface provides for erosion protection. The cover system is designed to minimize water and oxygen influx to the acid generating mine waste rock below.

Tropical Climatic Zone: Rum Jungle Mine

The Rum Jungle Mine is located in the Northern Territory, Australia, in a tropical climatic environment (Bennet and Ritchie, 1991). The three layer composite cover system consists of, from bottom to top, 22.5 cm of compacted clay, 25 cm of sandy clay loam, and 15 cm of gravelly sand. The compacted clay layer was designed to remain saturated to serve as a moisture and oxygen barrier. The sandy clay loam layer was designed to retain moisture for vegetation, and to prevent dessication of the underlying clay layer. The top gravelly sand layer was designed to provide protection against erosion and to reduce evaporation.

2.2.3 Soil Cover Material Utilized

The material most likely used for the construction of a soil cover is typically limited to locally available soil (subsection 2.2.2). The soil properties define the ability of a soil cover to create and to maintain a capillary barrier. The candidate soil must have appropriate moisture storage/release characteristics (soil-water characteristic curve), provide a low rate of water infiltration (hydraulic conductivity), provide resistence to surficial erosion, and be able to support vegetation. A successful design requires identification of relevant soil parameters and rationalization of soil layer sequencing. As well, the soil cover material's role in the soil-atmosphere interaction and the hydrological process must be clearly understood.

2.2.4 Soil Cover Performance Specification

Soil cover performance specification must be based on the design objectives, which may include control of water infiltration and gas migration, evaporation and transpiration, and surface erosion control. Soil cover materials, layer sequences, layer thickness, and placement techniques, must all be specified to achieve the design objectives. Considerations must be made to account for longterm modification to the initial structural integrity: e.g., freeze/thaw or dessication, mineralogical transformation, and root growth.

The performance specification is also dictated in part by the type of waste material being covered. An acid producing pyritic mine waste requires a barrier that minimizes water infiltration and/or oxygen diffusion into the underlying waste layer. At Heath Steel Mine, the placement of the sand base layer was prescribed by elevated temperatures within the waste rock piles. A compacted till soil cover over salt tailings (Haug *et al.*, 1991) was designed with a coarse boulder barrier layer to prevent the movement of dissolved salt into the overlying compacted till layer. For uranium tailings, a saturated barrier layer is needed to minimize radon gas emission from the uranium waste material (Ayres 1998).

2.2.5 Assessing a Soil Cover System

To verify the performance of a soil cover system, the surface water and energy balance estimates at the soil-atmosphere interface are required in accordance with the *Conservation of Mass* and the *Conservation of Energy*. The surface water balance involves precipitation which partitions into runoff and infiltration. The infiltrated water subsequently separates into subsurface storage, deep percolation, evaporation, and transpiration. The processes of infiltration and evapotranspiration govern the exchange of water between the soil surface and the atmosphere. The process of evaporation is driven by a combination of energy input from radiation, sensible heat energy from the atmosphere or ground, and a loss of heat energy in the evaporating body. Therefore, an energy balance is also required at the soil-atmosphere interface.

2.3 PRECIPITATION

The physics and meteorology of precipitation is not within the scope of this review. This section is limited to the measurement of precipitation which is required as an input to the surface water balance calculation.

2.3.1 Measurement of Rainfall

Rainfall may be measured by one or more of the methods described below.

A non-recording *storage gauge* simply consists of a straight sided cylinder. In its simplest form, the total accumulated depth is recorded manually using a calibrated measuring stick on a daily basis. A more elaborate system may consist of an electric transducer linked to a datalogger that measures the fluid level in the gauge at regular time intervals. The gauge may be partially filled with antifreeze in colder regions to prevent rainwater from freezing, and also to melt snowfall. A thin film of oil is typically added to prevent evaporation.

A *weighing recording gauge* consists of a cylindrical collection vessel mounted on a mechanical scale. A datalogger is used to record accumulated weight at regular intervals. This device is relatively expensive and requires regular servicing (Goodison *et al.*, 1981).

A *tipping bucket rain gauge* is the most popular of all recording rain gauges. The gauge consists of a collecting funnel that directs rain water to one of a pair of vessels of known volume. The pair of vessels are balanced on a fulcrum so that when one vessel is filled, it tips and empties, and the other vessel is brought into position for filling. The gauge is linked to a datalogger that records the time each vessel tips and empties, and thus the rainfall intensity is recorded. This method is applicable for remote and continuous monitoring.

An *Optical precipitation gauge* is a new generation of rain gauge that uses infrared technology. Precipitation (rainfall or snowfall) causes a disturbance to an infrared beam

between an infrared light emitting diode and a sensor. A datalogger is used to record the disturbance at a prescribed time interval, which is then used to calculate rainfall and snowfall intensities. It is the most expensive of all methods.

2.3.2 Measurement of Snowfall and Snowcover

The measurement of snowfall using a *standard precipitation gauge* (i.e., a cylindrical container mounted above ground surface) is made possible by placing a charge of antifreeze which melts the snow prior to measurement. This method, however, is typically fraught with difficulties. Snow often piles up at the gauge orifice and subsequently blows off. Furthermore, gauge induced wind eddies prevent significant amounts of snow from entering the gauge. Snowfall measurements using this method typically underestimate snowfall by 30% (Dingman 1994), and thus, snowfall is generally measured by other means.

Universal surface precipitation gauge measures snowfall water equivalent by recording an increase in weight on the collector (Waring and Jones, 1980). Installation of these gauges is elaborate and expensive, and therefore they are not widely used. The snowcover depth can be determined by observing the height of the snow surface against a fixed ruler called a *snow stake*. Snow drifting can yield erroneous readings, and actual water equivalent of the snowcover cannot be determined using this method.

Snowcover water equivalent can be estimated via a *snow survey*. Snow surveys are typically done periodically at fixed locations. At each survey point, a coring tube equipped with a saw toothed cutting rim (snow tube) is inserted vertically to the surface. The snow depth is read against markings on the outside of the tube and the tube is then pushed a few centimeters into the soil to secure a small plug of soil to hold the snow in place. The tube is subsequently extracted and weighed on a specially calibrated scale (a spring balance) that is tared and reads directly in centimeters or inches of water equivalent. Snow tubes can be made of aluminum or fibreglass, and can range in diameter from 3.8 cm to 7.6 cm. It has been found that snow tubes tend to overestimate water equivalent by up to 10% (Goodison *et al.*, 1981).

2.3.3 Factors Affecting Precipitation Measurement Accuracy

The factors that affect measurement accuracy are the gauge orifice size and orientation, the orifice height and wind shielding, distance to obstructions, splash and evaporation effects, instrument errors, and errors due to fog and low intensity rainfalls.

When the gauge opening is greater than 30 mm, the orifice size has negligible effect on the fraction of the true precipitation that enters the gauge. Gauges that project above ground result in wind eddies that tend to reduce the amount of smaller raindrops and snowflakes that enter the gauge. Wind shields minimize this eddie effect for snowflakes; they have very little effect on raindrops. Deficiencies of 10% for rain and 30% for snow are common (Dingman 1994).

The optimum location for a rain gauge is within an open space in a fairly uniform enclosure of trees, shrubs, fences, or other objects so that wind effects are reduced. Rain falling onto a water surface too near the orifice can cause water to splash out. Errors due to evaporation can be overcome by adding a thin film of oil. Instrument errors can result from the mechanics of operation. Tipping bucket rain gauges often under-record during heavy rains, and weighing gauges tend to become less sensitive as the weight of collected water increases. Overall instrument errors are typically 1% to 5% of the total (Winter 1981).

Occult precipitation is precipitation that occurs when clouds encounter trees or other vegetation. This precipitation is not captured by standard gauges, but it may be significant for many areas. For example, fog drip accounts for about 450 mm/year at elevations above 1200 m in northern New England; it totals 800 mm/year in a Douglas fir forest in Oregon. When a significant source of precipitation occurs as low intensity rain, the *trace amounts* that are not recorded can represent a significant portion of the overall precipitation.

Winter (1981) concluded that overall errors in point measurement can be from 5% to 15% for longterm data, and as high as 75% for individual storms.

2.4 INFILTRATION

Horton (1933) defined *infiltration* as "*the physical process by which rain enters the soil*". Water infiltrates due to the combined effects of gravity and soil matric suction. Horton also coined the term *infiltration capacity* as "*the rate at which a given soil can absorb rainfall when the soil is in a specified condition*"

Horton stated that at a given point, the rate of infiltration generally changes systematically with time for each rainfall event. Infiltration is typified by a high infiltration rate at the start of the event when water enters the soil layer and goes into storage; this is followed by a rapid decline as the surface layer becomes saturated, and an asymptotic approach to a near-constant value (i.e. *infiltration capacity*) approximately equal to the saturated hydraulic conductivity (k_{sat}) of the near surface soil (Mein and Larsen, 1973). Subsequent excess rainfall accumulates on a surface as ponding or surface runoff.

2.4.1 Factors Affecting Infiltration Rate

In general, the infiltration rate has been found to be highly variable, and the factors that control the process of infiltration are still not adequately defined. Nonetheless, it is acknowledged that infiltration is influenced by climatic fluxes and the depth of ponding on surface, the saturated hydraulic conductivity of the near surface soil, antecedent soil moisture and suction conditions, surface topography; and the infiltrating water temperature.

The surface hydraulic conductivity can be modified by external factors such as the presence of organic matter, a low permeable frozen layer, freeze/thaw or dessication, drying and crack formation, inwashing of fine sediments, raindrop compaction, formation of soil crust, and swelling during the wet season. Upward flow of air during infiltration has also been found to decrease the hydraulic conductivity (Freyberg *et al.*, 1980). Thus, the effective surface hydraulic conductivity can either be greater or less than the nominal hydraulic conductivity. The hydraulic conductivity is also directly related to the viscosity of water, while the

viscosity is particularly sensitive to changes in temperature. Klock (1972) measured the infiltration rate to be twice as large at 25^{0}C than what was measured at 0^{0}C.

2.4.2 Modeling Infiltration

Infiltration can be simulated using saturated/unsaturated flow equations. Quantitative models that are currently used by researchers assume vertical movement of liquid water through a soil medium. The effects of temperature or osmotic gradients are generally ignored, and airflow in the soil medium is assumed to have an insignificant effect. While the latter assumption has some justification (Youngs 1988), water movement in response to thermal and osmotic gradients can be important for water infiltration under freezing or thawing conditions (Sophocleous 1979; Newman and Wilson, 1997). There are three popular methods of quantitatively modeling infiltration: the Richards equation (Smith and Woolhiser, 1971), the Green-Ampt model (Smith 1976; Rawls *et al.* 1990; Stone *et al.*, 1993, 1994), and the Phillip's infiltration model (Morel-Seytoux and Khanji, 1974; Smith 1976).

Richards Equation

Richards (1931) equation is derived by combining Darcy's law for vertical unsaturated flow with the *Conservation of Mass*. It is the basic theoretical equation for transient one-dimensional vertical unsaturated flow in a homogeneous porous medium. By dividing the soil into thin layers (spatial discretization) and small increments of time, numerical solutions using the Richards equation are possible (Whisler and Bouwer, 1970). Richards equation is used as a basis for many numerical infiltration models. However, numerical solutions using Richards equation are considered to be computationally intensive, and require soil data that is typically unavailable for most locations.

Green-Ampt Infiltration Model

Green and Ampt (1911) proposed a model that treated the soil as a bundle of capillary tubes

whereby soil water is considered to move as a unit with a sharp wetting front. The Green-Ampt infiltration model incorporates Darcy's law and assumes infiltration from a ponded surface into a deep homogeneous soil of uniform antecedent water content. The Green-Ampt model incorporates three empirical parameters: conductivity, water content, and potential. These parameters have been correlated with some success to soil textural classification (Rawls and Brankensiek, 1983). It is a finite-difference formulation that captures the essential aspects of the infiltration process. That is, the complete infiltration up to the time of ponding, and the quasi-exponential decline of infiltration rate thereafter. The model parameters are measurable physical properties that can be calibrated based on measurable field data (Essen 1989; Risse *et al.*, 1994).

Mein and Larson (1973) noted a good correlation between computed infiltration using the Green-Ampt model and the numerical solution of the Richards equation. It has been shown that the Green-Ampt model predicts infiltration and surface runoff better than the Soil Conservation Services (SCS) curve number method, both for small plots and watershed size areas (Rawls and Brankensiek, 1988; Van Mullen 1991a and 1991b). Changes and adaptations to the Green-Ampt model have evolved over the years to overcome some of the model's shortcomings. These include, conditions of unsteady rainfall (Chu 1978) and multi-storm infiltration and redistribution (Ogden, 1997); a layered soil profile (Brankensiek and Rawls, 1983; Chu 1985; Kim and Chung, 1994); initial soil water content adjustment (Chu 1995); and the effects of crusted soils (Ahuja 1983; Rawls *et al.*, 1990).

Phillips Infiltration Model

J. R. Philip (1957) derived an analytic expression for cumulative infiltration with time after water has ponded on surface. The Philip's model is often used for characterizing the spatial variability of infiltrometer measurements. The Philip's approach only applies after the time of ponding, thus, the initial infiltration rate and the time of ponding must first be calculated and specified. Whisler and Bouwer (1970) compared the results of the Green- Ampt and the Philip's model with field data and concluded that the Green-Ampt model was more practical.

2.4.3 Flow Through Macropores

Flow through macropores caused by frost action, drying , animal burrowing, or decayed roots can substantially increase the rate of infiltration through the development of a secondary flow system. Beven and Germann (1982) observed that as the water input rate exceeds the infiltration capacity of the soil, water begins to flow down the walls of the macropores, and lateral infiltration into the soil matrix is initiated. The flow of water in the macropores effectively increases the surface area available for infiltration.

Macropores typically constitute a small portion of the total voids, but they may dominate vertical flow rates during infiltration (Thomas and Phillips, 1979; Smettem and Kirkby, 1990). The effect of macropores is dependent on the spacing between the pores, the pattern of rainfall intensities, and the hydraulic characteristics of the soil matrix. The nature of flow in the macropore system is not well defined. The spatial and temporal variability of macropore distribution and connectivity renders modeling of flow through macropores a very difficult task (Beven and Germann, 1981; Bronswijk 1988).

2.4.4 Spatial and Temporal Variability of Infiltration

Field infiltration rate studies for small experimental sites all indicate a high degree of spatial variability (Sharma *et al.*, 1980; Springer and Gifford, 1980; Tricker 1981; Wilcock and Essery 1984; Berndtsson 1987). Temporal variability in the rate of infiltration was also noted by Wilcock and Essery (1984) with average infiltration capacity considerably higher during summer than in winter.

The typically large spatial and temporal variability encountered for these relatively small test sites highlights the difficulty associated with using point estimates of infiltration for computing overall watershed infiltration rates. The spatial variability of precipitation, topography, vegetative cover, and soil properties further exacerbate this task.

2.4.5 Infiltration Measurement

The *infiltration capacity* can be estimated using single ring or double ring infiltrometers. The temporal and spatial variations in subsurface soil moisture content can be used to calculate the infiltration rate during a rainfall event. Field test plots are often used to monitor water input rates and runoff in order to indirectly estimate infiltration.

A *ring infiltrometer* is a device used for direct field measurement of infiltration capacity over a small area (0.01 to 0.10 m^2). A ring infiltrometer consists of an impermeable ring extending several centimeters above and below the soil surface. Ponding is created by direct flooding of the surface, or by applying a sufficiently high rate of simulated rainfall. The measured infiltration rate overestimates the actual infiltration capacity due to lateral movement of water in response to matric suction gradient (Hills 1971). Correction factors to account for the capillary effect when using single ring infiltrometer has been proposed by Tricker (1978). A *double ring infiltrometer* reduces the effects of lateral moisture movement by using two concentric rings. Infiltration capacity has been shown to have high spatial variability, thus multiple readings are typically required.

Infiltration rates can be indirectly determined by monitoring runoff from small *field test plots* on which the corresponding rainfall intensity or the rate of artificial rainfall application is known (Nassif and Wilson, 1975; Weeks *et al.*, 1992). Infiltration rates can be directly measured by use of lysimeters (Benson *et al.*, 1994). Weighing lysimeters are widely used for field assessment of infiltration rates (Kirkham *et al.*, 1984; Young *et al.*, 1996).

Infiltration can also be estimated by monitoring changes in soil moisture or soil suction with depth (Benson *et al.*, 1994; Bell *et al.*, 1995; O'Kane 1996; Young *et al.*, 1997). Changes in soil moisture can be monitored using probes such as a neutron moisture probe or time domain reflectometry probes (section 2.6). Changes in soil suction can be monitored using tensiometers or thermal conductivity sensors (section 2.7). Infiltration rate is then determined from the increase in soil-water content with depth during a water input event.

2.5 SURFACE RUNOFF

Understanding and conceptualizing watershed runoff mechanisms have been the main focus of hydrologists in recent years. The impetus behind their preoccupation is the economic and sociological benefits associated with successful flood prediction and forecasting.

The process of evaporation, transpiration, and infiltration are relatively well understood, and the physics behind these processes have been well defined. Consequently, there are many theoretical and theory based empirical models that predict these parameters within acceptable level of accuracy. The surface runoff mechanism is highly stochastic in nature, and accurate runoff prediction remains elusive. Many existing runoff models are expedient formulations based on heuristic and empirical relations that appear to give "reasonable" results.

Surface runoff, or *overland flow*, was originally estimated indirectly as the quantity that exceeded infiltration during a water input event. Horton's (1933) concept of *infiltration capacity* was considered to be the principle process responsible for runoff.

Small scale field studies and laboratory investigations into the runoff mechanism are limited, and their results are in general inadequate or inconclusive (Smith and Woolhiser, 1971; Smith and Chery, 1973; Simanton and Renard, 1982; O'Kane 1996). Model verification is carried out mainly on small watershed monitoring results, and the models tend to be semi-analytical for use in flood forecasting (Sivapalan 1987; Moore and Grayson, 1991; Stone *et al.*, 1992; Larsen *et al.*, 1994; Coles *et al.*, 1997; Zollweg *et al.*, 1996; Melone *et al.*, 1998).

2.5.1 Surface Runoff Mechanism

Surface runoff occurs along a sloping surface that is either impermeable, saturated from above, or saturated from below. It is generally agreed that surface runoff results from an *infiltration excess*, or from a *saturation excess* process. In recent years, the *throughflow* process has also been recognized as an important runoff mechanism.

Infiltration Excess Runoff

The *Infiltration excess* runoff (Hortonian flow) is named after R.E. Horton who described the process in the 1930s. The Hortonian overland flow concept became widely accepted as the principle process, and it remains entrenched in many modern day runoff models.

The infiltration excess runoff occurs when the rainfall intensity exceeds the *infiltration capacity* of the soil at any location. That is, when the water input rate exceeds the saturated hydraulic conductivity of the surface layer after surface ponding has occurred. However, the water input rate is greater than the saturated hydraulic conductivity for only relatively intense rainfall events on fine grained soils (*Figure 2.1*). The actual occurrence of this is generally uncommon, and it is rendered more infrequent since the effective surface hydraulic conductivity is generally increased by the presence of macropores and biological activities.

Hortonian flow is found to be prevalent in impermeable areas, and in areas where frost or human activity has reduced the surface hydraulic conductivity (Moore and Grayson, 1991). Hortonian flow is considered to be an important runoff mechanism for semi-arid to arid regions where rainfall tends to be intense, and the natural surface hydraulic conductivity is low (Freeze 1974; Sivapalan 1987; Goodrich *et al.,* 1994; Mack 1995). Coles *et al.* (1997) and Martinez-Mena *et al.* (1998) concluded that for semi arid sites, runoff generation was not exclusively through the infiltration excess process.

Saturation Excess Runoff

Dunne and Black (1970) noted the absence of sheet flow evidence on hillsides and high infiltration rates into permeable vegetated soils; it was concluded that Hortonian flow was not applicable for the vast majority of storms. Dunne and Black found that the importance of hillslope as a producer of storm runoff depended largely on its ability to generate overland flow. It was observed that although surface runoff was generated, the *infiltration capacity* of the soils exceeded rainfall intensity in the vast majority of measured storm events.

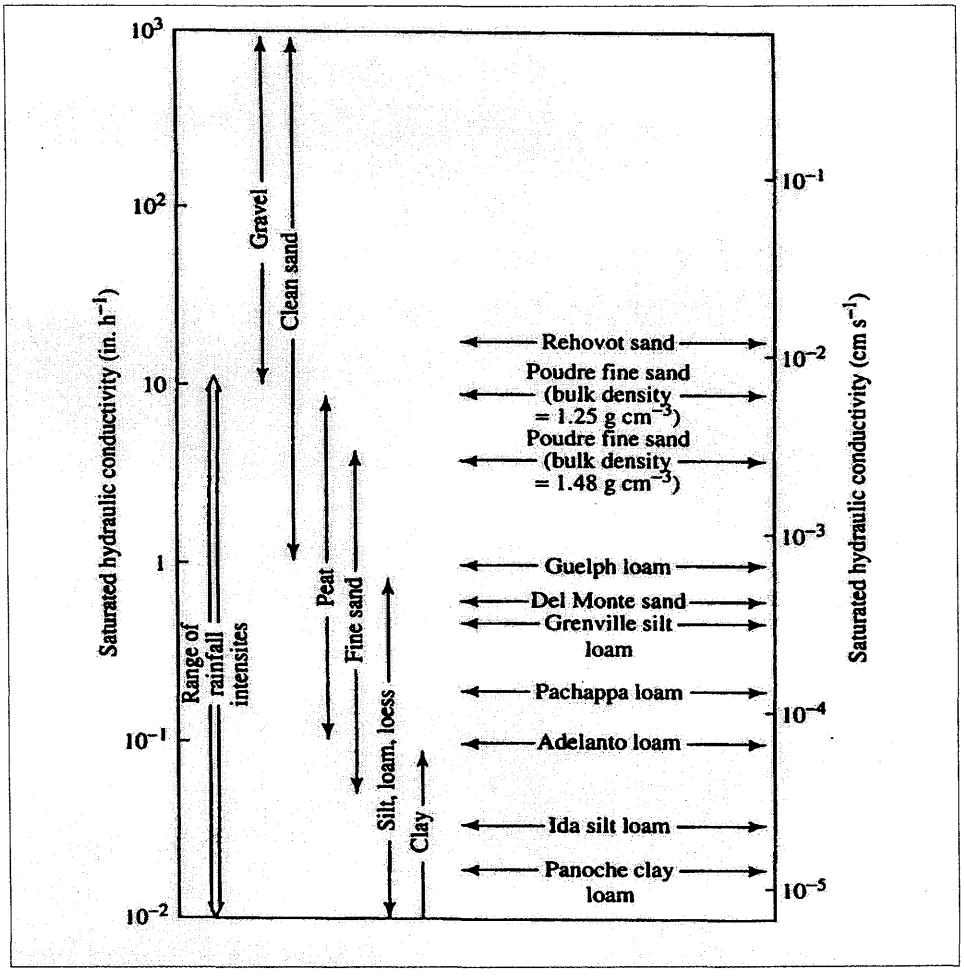

Figure 2.1 Soil hydraulic conductivity versus range of rainfall rates. After Freeze (1972).

Dunne proposed a new runoff process, a *saturation excess runoff*, whereby the soil becomes saturated to the surface from below due to both rainfall inputs and downslope subsurface flow. Saturation excess runoff is generated when rain falls at locations where the entire soil column is saturated, or where a perched water table exists. This scenario occurs for high antecedent soil moisture conditions, or when the accumulated volume of infiltrated water during a storm equals the initial volumetric moisture deficit. The saturation excess mechanism is considered to be the main mechanism for humid and vegetated regions (Mack 1995; Coles *et al.*, 1997).

Throughflow Runoff

Throughflow runoff is water that percolates rapidly through macropores and flows laterally in a temporarily saturated zone. This process commonly occurs above a layer of low hydraulic conductivity material (Maidment 1993). This runoff process differs from other subsurface flow by the rapidity of its response, and relatively large magnitude.

2.5.2 Surface Runoff Controlling Factors

It is alluring to predict the dominant runoff mechanism based on climatic parameters and soil properties. However, field observations have indicated that the runoff process appears variable even under similar climatic and soil conditions (Zollweg *et al.*, 1996).

A general consensus on what controls surface runoff remains ambiguous. However, it is agreed that runoff generation is highly heterogeneous in both space and time (Loague and Gander, 1990; Jordan 1994), and that runoff appears to be governed by spatial variability of soil properties and topography, and by temporal variation in rainfall intensity and duration.

Rainfall intensity and total rainfall are two of the climatic parameters that are identified as having influence over runoff mechanisms (Allan and Roulet, 1994; Coles *et al.*, 1997; Martinez-Mena *et al.*, 1998). Larsen *et al.* (1994) found that the surface hydraulic conductivity and decay in the hydraulic conductivity with depth defined similarities in runoff generation between catchment areas. Conversely, Simanton and Renard (1982) found little correlation between runoff and measured surface or soil parameters. Martinez-Mena *et al.* (1998) deduced that the soil texture defined the dominant runoff mechanism. Digman (1994) found the ratio of excess precipitation contributing to surface runoff over the total precipitation to be 0.63 during a very wet summer (wet anticedent), versus 0.01 during a dry summer (dry antecedent). Allan and Roulet (1994) concluded that runoff depends on antecedent moisture conditions.

2.5.3 Runoff Models

Many models have been proposed to represent the hydrological response to a given rainfall event. There are over 100 rainfall runoff modeling techniques reported (Hromadka and Whitley, 1996) with a large variability in model response (Melone *et al.*, 1998).

Runoff models generally incorporate spatial and temporal variability of the runoff process, and of the runoff producing areas. Watershed runoff models are physically based incorporating a simplified representation of appropriate flow mechanisms. The availability of distributed rainfall data and watershed properties, coupled with increasing computational capabilities, have resulted in the use of distributed rainfall-runoff models.

A new generation of models are emerging to incorporate *saturation overland flow* on variable source areas (Zollweg *et al.*, 1996). For watershed modeling, these models can be coupled with remotely sensed data, such as soil water content estimates from NASA PBMR (push broom microwave radiometer), or an IRE (Institute of Radioengineering and Electronics) multifrequency radiometer (Goodrich *et al.*, 1994).

Of the many distributed watershed runoff models available, TOPMODEL (Beven and Kirby, 1979), KINEROS (Woolhiser *et al.*, 1990; Goodrich *et al.*, 1991), and SmoRMod (Zollweg *et al.*, 1996) are most widely used in North America. TOPMODEL simulates runoff generation by both *infiltration excess* and *saturation excess* mechanisms. KINEROS estimates *infiltration excess* runoff on an event basis, incorporating an event oriented interception, infiltration, surface runoff, and erosion processes. SmoRMod is a cell-based GIS (Geographical Information System) integrated model consisting of soil moisture balance and runoff generation/transport sub-models.

The U.S. Soil Conservation Service (SCS) curve number method is one of the most widely used method for estimating runoff , water recharge, stream flow, infiltration, soil moisture content, and landfill leachate production. It considers soil type, vegetation, and soil

conditions, and it utilizes antecedent precipitation to estimate infiltration characteristics (Mack 1995).

2.5.4 Surface Runoff Measurement and Analysis

Runoff measurement for watershed monitoring and modeling is not central to the scope of this thesis. Of particular interest are small scale runoff measurement techniques; however, literature on small scale runoff measurement and analysis is limited.

Weeks *et al.* (1992) diverted and collected surface runoff from landfill test embankments using asphalt lined ditches. Surface runoff was continuously monitored with two H-flumes and two Stevens water level recorders located at the discharge end of the asphalt lined ditch. Benson *et al.* (1994) diverted runoff to collection tanks where variations in the water level elevation was monitored to estimate runoff. Water elevations were measured using floats attached to Leupold-Stevens Inc. pulse generators. The pulse generators send out voltage pulses on two different channels corresponding to rising or falling of the floats. Blight and Blight used a system of PVC gutters for various surface slope and vegetative conditions with success (Ayres 1998). O'Kane employed a system of PVC gutters and collection reservoirs that were monitored and measured manually on an intermittent basis.

2.6 EVAPORATION

The actual evaporation (*AE*) from a soil surface differs noticeably from evaporation from a free water surface, or potential evaporation (*PE*). However, the physics behind estimating *PE* forms the foundation for various equations and formulations that have been proposed to calculate *AE*. As well, the concept of *PE* is still used widely as a yardstick for classifying and comparing one hydrologic/climatic region from another. The reader is referred to Appendix A for a review of the physics and equations that are used to estimate the *PE*.

2.6.1 Process of Evaporation from a Soil Surface

The *AE* from a soil surface differs from *PE* from a free water surface in that it is characterized by three distinct phases (Wilson *et al.*, 1994): *phase I* evaporation from a saturated or near saturated soil surface; *phase II* drying whereby the rate of *AE* declines rapidly as the surface becomes unsaturated and the supply of water to the surface becomes limited; and *phase III* residual drying. The climatic factors that affect *PE* also influence *AE*; however, there are additional factors that dictate the rate of *AE*.

Holmes (1961) has shown that the ratio of *AE* to *PE* changes as soil dries out, and that the shape of this curve varies significantly depending on water availability, the soil type and drying rate. Gray (1973) suggested that the rate of *AE* is determined by soil moisture content, pore size, shape, and distribution, and fluid properties. Konzelmann *et al.* (1997) postulated that the surface texture and moisture conditions play an important role in determining the *AE*. Gardner (1958) concluded that the rate of *AE* is limited by the rate of water movement to the surface in liquid phase, and that subsurface vapour flow is relative unimportant. Milly (1984, 1986) stated that liquid and vapour transport due to temperature gradients have little effect on the surface fluxes, but that vapour diffusion due to head gradient is significant. Braud *et al.* (1993) found that vapour phase transfer mode is dominant near surface, and that surface evaporation is a function of the soil type, and surface water content and temperature; they also concluded that temperature gradients contributed to a significant downward vapour flux.

Wilson *et al.* (1997) investigated the effects of soil texture, drying time, and water content on the rate *AE*. Their laboratory results using sand, silt, and clay indicated that *AE* is a function of suction at the soil surface (*Figure 2.2)*. They concluded that "*A relationship between the AE rate and total suction was found to exist for all three soil types which appears to be unique and independent of soil texture, drying time, and water content*". They determined that *AE* approximately equals *PE* until the matric suction at the soil surface reaches a suction equivalent to the relative humidity of the surrounding air (*Figure 2.3*). The start of *phase II* drying occurs when the relative humidity in the soil at the surface begins to fall below the relative humidity in the atmosphere.

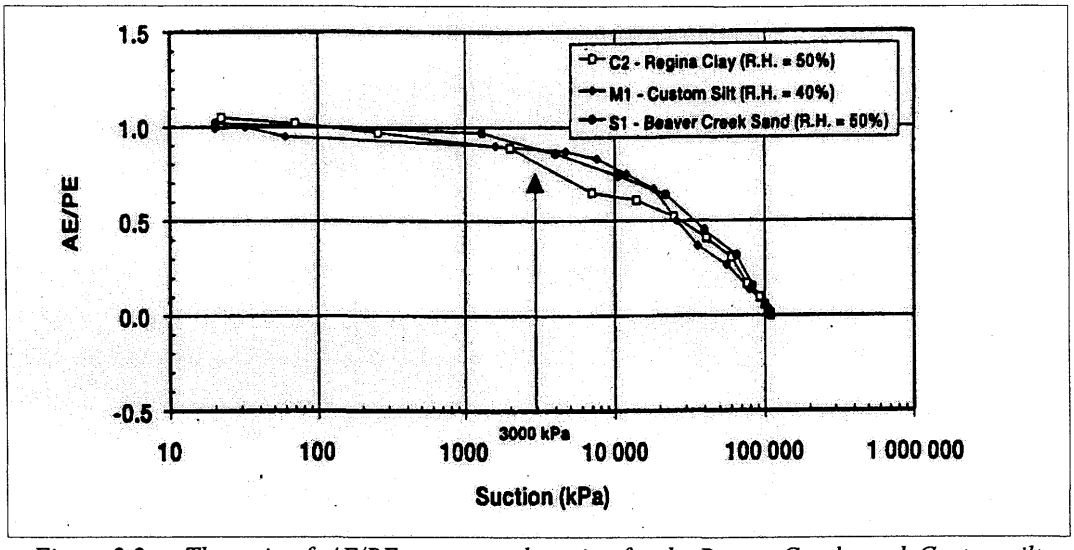

Figure 2.2 The ratio of AE/PE versus total suction for the Beaver Creek sand, Custom silt, and Regina Clay. After Wilson et al., 1997.

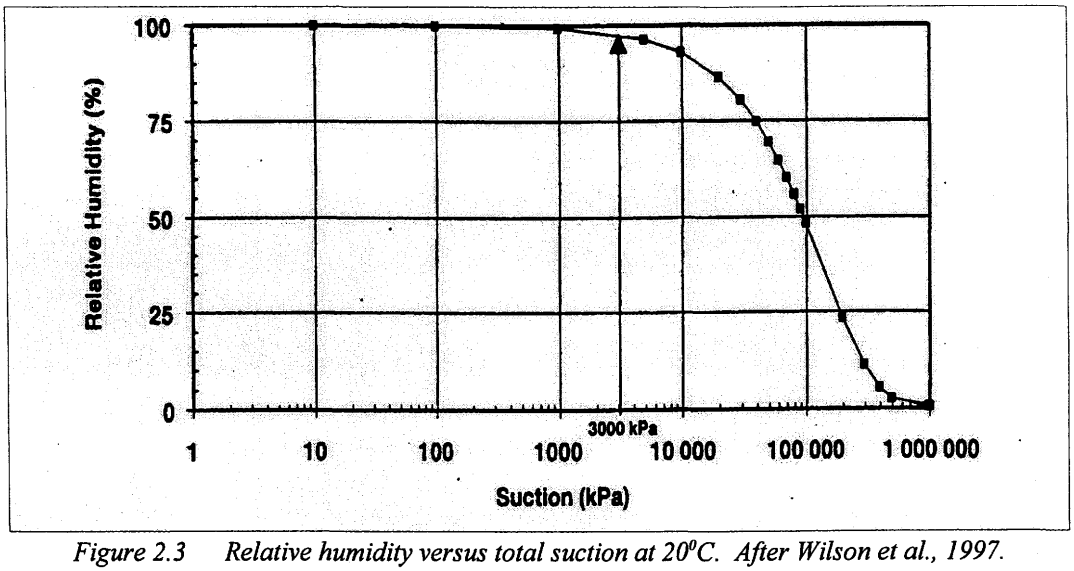

Figure 2.3 Relative humidity versus total suction at 20°C. After Wilson et al., 1997.

2.6.2 Estimating Actual Evaporation: the Energy Balance Method

The use of the energy budget for estimating evaporation from a free water surface can be applied to estimating *AE* from a soil surface. A wet soil surface differs from a free water surface in its ability to absorb radiation and store heat during the day, which subsequently induces evaporation at night. Other factors are roughness of the evaporating surface which affects the turbulent transport of water vapour, and the sensible heat requirement.

The Bowen ratio energy balance (BREB) method, which relates the ratio of sensible heat exchange to latent heat exchange (i.e. energy used for evaporation) as a ratio of surface-air temperature gradient to surface-air vapour pressure gradient, is one of the most widely used method for estimating the rate of evaporation (equations *[A.8]* and *[A.9]* in Appendix A). The BREB method requires specific instrumentation to acquire input parameters: net radiation (Q_n), net conductance to the ground (G), surface-air temperature gradient, and surface-air vapour pressure gradient. This method assumes steady atmospheric conditions and constant energy and mass fluxes with height (Fritschen and Simpson, 1989; Oke 1987). When sensors are mounted close to the surface, these assumptions appear reasonable (Fritschen and Qian, 1990).

The BREB method is subject to error due to resolution limits of the gradient sensors during early morning and late afternoon, during precipitation events, and when the temperature and vapour pressure gradients are small (Ohmura 1982; Maidment 1993). Instability is also attained when the Bowen ratio is in the vicinity of negative one (-1). Xu and Qiu (1997) proposed a *variational method* which uses a vertical wind profile, temperature, and specific humidity for turbulent flow in the surface layer to overcome the Bowen ratio instability.

The subsurface soil heat flux is typically measured at 8 cm in depth. Using uncorrected subsurface soil heat flux (G) measurements can overestimate *AE* by up to 41% (Malek 1993; Malek 1994). Passerat de Silans *et al.* (1997) provides a method for estimating the soil surface heat flux from measured heat flux at depths below the surface.

Tanner (1960) reported a good correlation between evaporation estimated with the Bowen ratio method to what was measured with lysimeters. Malek and Bingham (1993) compared evaporation results from Campbell Scientific Bowen Ratio Instrumentation to evaporation estimated using the water balance method, and found good correlation. Woyshner and St-Arnaud (1994) successfully employed the BREB method to determine evaporation from a bare tailings surface in northern Ontario.

2.6.3 Estimating Actual Evaporation: the Empirical Method

Penman's combination approach has been modified by numerous researchers to account for the rapid decline in the rate of evaporation as the soil surface begins to dry out. Some are solely climate dependant (Monteith 1965; Thom and Oliver, 1977; Stigter 1980; Choudhury and Monteith, 1988), while others are both climate and soil moisture dependent (McCumber and Pielke, 1981; Kondo and Saigusa, 1990; Mahouf and Noilhan, 1991).

Equations that embrace both climatic conditions and soil properties using Philip and de Vries (1957) heat and moisture transport formulation have been proposed in recent years (Schieldge *et al.*, 1982; Camillo *et al.*, 1983; Camillo and Gurney, 1986; Witono and Bruckler, 1989; Passerat De Silans *et al.*, 1989). These models provide good estimates of evaporation, water content profiles, and temperature profiles for drying conditions.

Jackson *et al.* (1974) found that Philip and de Vries' (1957) approach was limited to predicting heat and moisture transport for intermediate soil water content profiles. The application of Philip and de Vries' formulation for prolonged evaporative events has thus been questioned (Wilson *et al.*, 1994). Improvements were made to account for the error in Philip and de Vries' assumption that moisture flow is governed by volumetric water content gradient (Sophocleous 1979, Milly 1982). However, the accuracy of these new models remains to be verified. Wilson (1990) proposed a *modified Penman formulation* to estimate evaporation from a saturated or an unsaturated soil surface. The fundamental assumption made in Wilson's formulation is that the saturation vapour pressure at the soil surface in

Penman's formulation can be replaced with the actual vapour pressure at the soil surface.

Wilson calculates evaporation using routinely available climatic parameters, such as net radiation, air temperature, relative humidity, and wind speed. The actual vapour pressure at the soil surface is calculated as the product of the saturation vapour pressure of water at the temperature of the soil surface, and the relative humidity of the pore air. The relative humidity of the pore air is evaluated on the basis of the total suction at the soil surface. The total suction is dependent on the flow of liquid water and water vapour below the soil surface and evaporative flux to the atmosphere. Wilson's (1990) soil-atmosphere model computes the evaporative flux across the soil-atmosphere interface by solving four equations simultaneously: transient liquid water and water vapour flow; transient heat transfer; partial pressure thermodynamic equation; and the *modified Penman formulation.* Wilson *et al.* (1997) also provides an expression for computing *AE* as a function of suction.

The accuracy of Wilson's *modified Penman formulation* was verified using a controlled laboratory drying tests using two identical columns of fine uniform sands. The test was conducted over a prolonged time to attain *phase III* drying (Wilson *et al.*, 1994). Evaporative flux calculated using above equations also compared favorably with what was measured in the field using the BREB method (Wilson *et al.*, 1993).

2.6.4 Estimating Actual Evaporation: the Water Balance Method

The water balance approach requires accurate measurement of each of the variables in the water budget equation. Weeks *et al.* (1992) and Benson *et al.* (1994) used test plots in which the amount of water added by precipitation and irrigation were measured in conjunction with surface runoff. Changes in subsurface soil moisture were obtained through gravimetric sampling, soil moisture probes, or by weighing-type lysimeters. The success of this approach is dependent on ensuring the accuracy of each of the measured variables.

2.7 MEASUREMENT of SOIL-WATER CONTENT

Temporal variations in subsurface soil-water content are required to assess the performance of a soil cover system. The soil-water content measurement methods can be grouped into: destructive gravimetric soil sampling methods (ASTM D2216-92), and non-destructive volumetric water content measurement methods (TDR probe and neutron moisture probe). The principles of the TDR and neutron moisture probes are briefly reviewed in this section.

2.7.1 Time Domain Reflectometry (TDR)

The TDR probe is a non-destructive measurement technique that estimates *in situ* volumetric soil-water content. The application of the TDR technology for soil-water measurement dates back to 1975. Its reliability, ease of use, and remote and continuous monitoring capability render this method attractive for field monitoring of temporal and spatial variations in soil-water content (Herkelrath *et al.*, 1991; St-Arnaud and Woyshner, 1992; Benson *et al.*, 1994; O'Kane, 1996; Young *et al.*, 1996).

The TDR method translates the change in the dielectric constant of the soil to a change in soil-water content. The dielectric constant of water ($K_{water} \approx 80$) is much greater than that of soil ($K_{soil} \approx 5$) or air ($K_{air} \approx 1$). Therefore, the dielectric constant of the soil medium changes significantly with changes in soil-water content. Topp *et al.* (1980) concluded that the soil dielectric constant is only marginally dependent on soil type, bulk density, ambient temperature, and salt content. Topp *et al.* derived an equation for soils to estimate the volumetric water content of the soil using the TDR method. Although this empirical equation is considered to be applicable for most soils, it could lead to significant errors in organic soils, fine textured heavy clay soils, or soils containing significant amount of frozen water (Zeglin *et al.*, 1992; Kaya *et al.*, 1994; Spaans and Baker, 1995).

The TDR instrumentation consists of a multi-wire probe connected to a TDR device via a coaxial cable. The TDR probes can be a standard laboratory coaxial cell, parallel two-wire

probe, or coaxial emulating three-wire and four-wire probes. The latter yields clearer signals, and are therefore preferred over the two-wire or the standard coaxial cell (Zeglin *et al.*, 1989). The TDR probes may be installed in any direction since the probe yields volumetric water content averaged over the length of the probe regardless of its spatial orientation. Probe installation must result in minimal air gap around the probe wire given that the probe sensitivity is highest in its immediate vicinity.

St-Arnaud and Woyshner (1992), Benson *et al.* (1994), and O'Kane (1996) have successfully monitored the performance of a soil cover system using TDR probes. Young *et al.* (1997) installed TDR probes within a weighing lysimetery to compare the performance of vertically installed TDR probes in estimating evapotranspiration. TDR probes were found to underestimate water that was added. Longer probes (800 mm) were found to yield better results than the shorter probes (200 mm). Richardson *et al.* (1992) found that vertically installed TDR probes in a long soil column measured water contents that were statistically similar to gravimetrically determined water contents.

2.7.2 Neutron Moisture Probe

The neutron moisture probe (neutron probe) has been applied extensively for drainage and irrigation field studies. It also has wide usage in hydrologic modeling and climatological estimates of evapotranspiration (Cuenca, 1988; Carrijo and Cuenca, 1992), environmental monitoring projects (Wong 1985; Kramer *et al.*, 1992); and soil cover evaluations (O'Kane 1996; Ayres 1998). Although its application is wide and extensive with almost fifty years of usage, this popular technique continues to be plagued with controversies associated with the nature of the probe calibration curve, and the interpretation of calibration results.

Mode of Operation

The neutron probe consists of a high energy neutron source and a slow (thermal) neutron detector. The neutron probe takes advantage of the neutron moderation process whereby

high energy fast neutrons emitted from a radioactive source are slowed down (thermalized) by collision with surrounding hydrogen atoms (Kramer et al., 1992; O'Kane 1996). Almost all hydrogen in most soils is in the form of water, thus the measurement of the thermalized neutrons (count rate) is a reflection of the volumetric water content of the soil.

A neutron probe is lowered into a pre-drilled and cased hole, typically 38 mm (1.5 inches) or 55 mm (2 inches) in diameter, and the corresponding thermal neutron count rate is recorded along the depth of the hole. Once an appropriate calibration curve relating the count rate to the soil-water content has been established for a given soil, the soil-water content can be assessed rapidly, accurately, and non-destructively using this technique.

The resolution of a neutron probe is dependant on the water content of the volume sampled. This volume is typically a sphere, and its radius increases from 10 cm at 100% water to more than 24 cm at 4 % water (Marais and Smit, 1960; Chanasyk and Naeth, 1988). The CPN 503 Hydroprobe has an oblong sphere of influence with an axial radius of approximately 15 cm from the center of measurement of the probe, and ranging 7.5 cm on either side (Chanasyk and Naeth, 1988). Within the sphere of influence, or sampled volume, the neutron probe reading integrates the soil-water as a negative exponential function of distance from the neutron source (McGuiness *et al.*, 1961).

Calibration Curve

Gardner and Kirkham (1952) found a definable and reproducible relationship between the thermalized neutron density and the soil-water content when the latter is expressed in terms of unit volume of soil. The relationship, although not entirely linear, appeared to be the same for all five soils tested. As the neutron method developed, universality of this response curve was frequently stated (Stolzy and Cahoon, 1957; Luebs *et al.*, 1968; Rawls and Asmussen, 1973; Babalola, 1978; Silvestri *et al.*, 1991). Conversely, the results of many researchers have also indicated that this curve was affected by soil properties (Marais and Smit, 1960; Holmes 1966; Lal 1974; Greacen and Hignett 1979).

The shape of the calibration curve has also been the topic of many debates. A linear relationship has been proposed by Douglas (1966), Haverkamp *et al.(*1984), Silvestri (1991), and Arslan and Razzouk (1994). Others concluded that the relationship is in general nonlinear with the degree of nonlinearity dependent on soil parameters. Curvilinear relationships with increasing slope at increasing soil-water content has been reported by Olgaard and Haar (19680, Greacen and Schrale (1976), Wilson and Ritchie (1986), and O'Kane (1996). A decrease in slope with increasing soil-water content has also been reported by Stone *et al.* (1955), Stolzy and Cahoon (1957), and Tyler (1988).

The factors that may affect the shape of the calibration curve are: the presence of hydrogen in forms other than free water; absorber elements such as boron, chlorine, iron, potassium; bulk density and soil texture; presence of gravel, rock, and air; high clay content; and the type of access hole casing material and its diameter. The reader is referred to Appendix B for a more detailed discussion. The shape and the universality of the calibration curve remains contentious. It is thus agreed that a site and soil specific calibration must be carried out.

There are two calibration methods for the neutron probe: field calibration and laboratory calibration. The field calibration method consists of *in situ* calibration, correlating concurrent neutron probe readings with moisture content measured by conventional means. The laboratory calibration method typically involves filling a drum with soil at different moisture contents. Due to the many soil factors that may affect the count rate, such as soil texture and soil bulk density, accurate laboratory calibration that reflects actual field conditions is not easily attained. Difficulties associated with field calibration, such as uneven distribution of soil-water and a gradient in bulk density or in chemical composition along the soil profiles, can result in serious calibration errors (Greacen and Schrale, 1976).

The calibration curve often becomes an information filter reducing sensitivity to soil-water content changes (Kramer *et al.*, 1992). The neutron method is a precise and reproducible technique, and thus, raw data is often more sensitive to subtle changes in soil-water content than data processed through a calibration filter.

Near Surface Readings

Due to the geometry of the volume sampled by the neutron probe, readings from the top 10 cm of soil can seriously underestimate moisture content where the sphere of influence extends beyond the soil surface. Several surface "*shields*" have been used to offset errors associated with near surface readings (Pierpont 1966; Black and Mitchell, 1968; Sharma and Tunny, 1972; Hanna and Siam, 1980; Chanasyk and Naeth, 1988). An empirical factor to correct the count rate without shields has also been proposed (Chanasyk and Naeth, 1988).

Sources of Variances

The origin of variances in determining water contents using neutron probe measurements are: the random emission of neutrons as well as the electronic noise in the equipment; the uncertainty associated with the calibration equation; and the spatial variability in soils and access tube installation or site heterogeneity (Haverkamp *et al.*,1984; Grismer *et al.*, 1995). Variances associated with the radioactive decay emissions of neutrons, and limitation of the detectors or instrument errors, are found to be negligible when count rates are recorded in excess of 20 seconds (Grismer *et al.*, 1995). For individual access holes, the primary source of error is the calibration curve. In studies involving multiple access holes, the location, or spatial variance, is the dominant error term. The variances caused by using point estimates to predict field-wide values of soil-water content can sometimes exceed the error stemming from calibration by an order of magnitude (Haverkamp *et al.*, 1984; Vauclin *et al.*, 1984, Vandervaere *et al.*, 1994a and 1994b).

Grismer *et al.* (1995) found that in spite of the relative proximity of study areas, average calibration slopes differed by up to 42.5%. The location or spatial variability variance accounted for more than 90% of the measurement error. Furthermore, it was concluded that when using point estimates to predict field wide values, the number of water content samples necessary to characterize the average water content within an acceptable level of variance was rather large and often impractical.

2.8 MEASUREMENT OF MATRIC SUCTION

Monitoring temporal and spatial variations in soil matric suction provides insight into the infiltrative and evaporative fluxes within the soil cover profile. Changes in soil water content result from changes in soil matric suction in response to infiltration and evaporation.

The measurement of soil matric suction can be achieved using tensiometers or thermal conductivity sensors. The tensiometers provide direct measurement of the soil matric suction when the pore-air pressure is atmospheric (Fredlund and Rahardjo, 1988; Fredlund and Rahardjo 1993). The tensiometers are limited to a maximum suction of 90 kPa and typically require daily servicing, and they are not conducive to continuous and remote monitoring. O'Kane (1996) successfully used a nest of tensiometers as part of a soil cover monitoring program to verify the performance of adjacent thermal conductivity sensors.

A thermal conductivity sensor indirectly measures soil matric suction. Its development dates back to the early 1970s with the Moisture Control System Inc. model MCS600. The thermal conductivity sensors function for a wide range of matric suction measurements for most soil types. These sensors are found to be unaffected by the salt content of the soil, and are relatively insensitive to temperature changes above freezing (Lee and Fredlund, 1984; Fredlund and Rahardjo, 1993). They are easily linked to an automated data acquisition system for remote and continuous monitoring. Fredlund and Rahardjo (1993) provide a thorough discussion on thermal conductivity sensors. A brief overview is presented in this section.

2.8.1 Fundamentals of Thermal Conductivity Sensor Operation

A thermal conductivity sensor consists of a porous ceramic cylinder containing a temperature sensing element and a miniature heater. The porous ceramic cylinder has a wide pore size distribution that allows the water to flow in and out of the sensor until matric suction in the ceramic comes to equilibrium with the matric suction in the soil. The thermal conductivity

of ceramic is much lower than that of water, and therefore, the amount of water in the pores of the ceramic will greatly influence its thermal conductivity. As the soil matric suction increases, the ceramic water content decreases, and the thermal conductivity decreases.

A controlled amount of heat is introduced to the center of the ceramic cylinder, and the temperature in the cylinder is measured after a specified time. The undissipated heat will cause a temperature rise that is inversely proportional to the ceramic water content. The measurement of the temperature rise is thus related to the water content. The sensor is calibrated to yield a relationship between the rate of heat dissipation and matric suction in the ceramic.

2.8.2 Factors that Affect Thermal Conductivity Sensor Measurements

The field application of thermal conductivity sensors to date have had limited success. Their disappointing performances are attributed to: ceramic durability, strength, and pore size distribution; durability and accuracy of the associated electronics; influence of hysteresis on the accuracy of the suction measurements; field installation techniques; and freezing/thawing environment (Fredlund *et al.*, 1998).

The optimum ceramic pore size distribution is that which ensures a linear logarithmic variation in electrical response throughout the majority of the matric suction measurement (Fredlund *et al.*, 1994b). This is required to maintain the accuracy and sensitivity throughout the entire range. The ceramic cylinder must also be durable and strong to withstand installation and freeze/thaw effects. Past sensor mortality has often been attributed to sensor breakage and degradation (Loi *et al.*, 1992).

The accuracy of the measurement depends on the resolution of the data logger system and the quality of the output from the temperature sensor. Earlier generations of thermal conductivity sensors employed a thermocouple temperature sensing device. The new generation of sensors employ an IC (integrated circuit) sensing device which it produces

consistent and accurate measurement over a wide range of temperatures. Sensor failures were experienced when the sensors were subjected to periods of positive pore pressures, and sensor electronics discontinued functioning as water infiltrated due to an inadequate seal (Rahardjo *et al.*, 1989; Fredlund *et al.*, 1992; Loi *et al.*, 1992).

Ceramic hysteresis can result in significant errors for low matric suction ranges (less than 20 kPa) due to sensor calibration that is typically carried out for a drying cycle (Fredlund *et al.*, 1998). See *Figure 2.4.* Air entrapment and poor sensor/soil contact during field installation can also yield unreliable measurements (Fredlund *et al.*, 1992); it results in higher than actual matric suction readings.

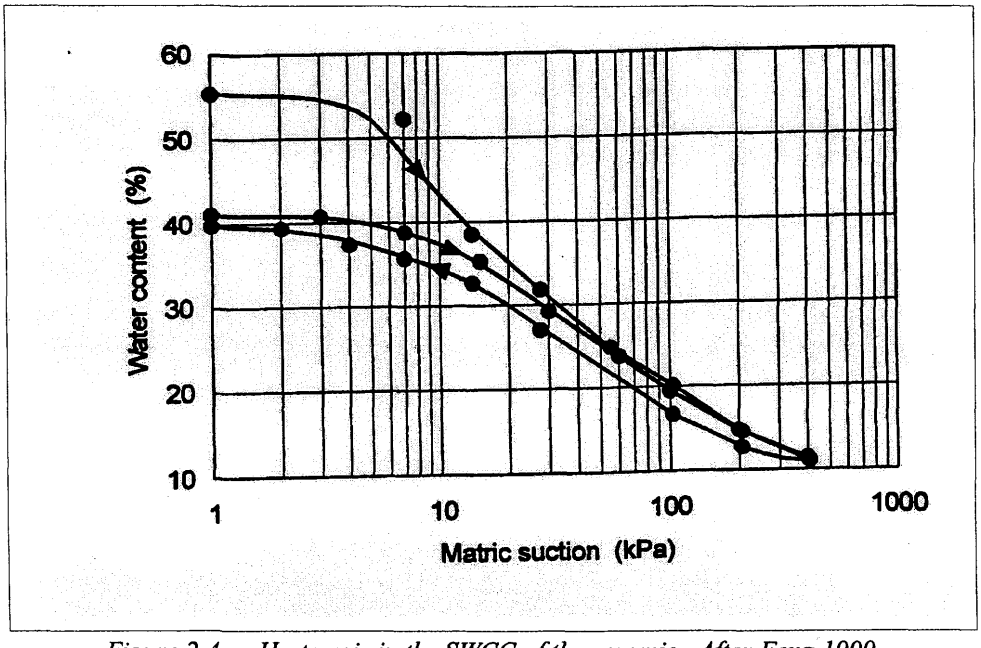

Figure 2.4 Hysteresis in the SWCC of the ceramic. After Feng 1999.

The thermal conductivity of ice is significantly higher than that of water. The formation of ice upon freezing alters the thermal conductivity of the ceramic without any significant change in ceramic water content. Fredlund *et al.* (1991) and Khogali *et al.* (1991) observed that the soil suction readings dropped sharply as the temperature decreased from above freezing to below freezing. As freezing progresses, the sensor readings increased rapidly to approximately the same reading before freezing began. The same behavior was observed as

the temperature was increased from below freezing to above freezing and thawing was initiated. These drops are attributed to the effect of the latent heat of fusion on the thermal conductivity measurements.

2.8.3 Thermal Conductivity Sensor Calibration

A calibration curve correlating the sensor's voltage output to matric suction must be derived for each individual thermal conductivity sensor. The thermal conductivity sensors are typically supplied with a manufacturer's two-point calibration curve that assumes a linear correlation. Although Wong *et al.* (1989) found two-point calibration curves to be adequate, Fredlund and Wong (1989) found the curves to be distinctly bilinear, and O'Kane (1996) and Fredlund *et al.* (1998) concluded the curves to be curvilinear.

The thermal conductivity sensors are typically calibrated in the laboratory using a modified pressure plate apparatus. Earlier calibration procedures involved elaborate systems whereby a sensor was buried within a volume of soil (Fredlund and Wong, 1989; O'Kane 1996). Soil selection had to ensure intimate soil-sensor contact throughout the entire calibration range. Recent research efforts have resulted in a simplified calibration technique whereby a sensor is inserted vertically into a thin layer of slurried bentonite/sand mixture. This mixture provides an intimate contact between the sensor and the high air entry pressure plate. Refer to subsection 4.4 for more details on the current sensor calibration method.

2.8.4 Field Applications

The use of thermal conductivity sensors for geotechnical applications has a relatively a short history. An evaluation of AGWA-II sensors by various researchers have indicated that longterm stable and reliable matric suction readings can be obtained as long as the sensors were not subjected to prolonged positive pore water pressures (van der Raat *et al,*. 1987; Loi *et al.,* 1992; Szafron and Fredlund, 1992). However, they noted the deterioration of sensor tips and sensor electronics failure.

High sensor failure rate among users was not uncommon. Fredlund *et al.* (1992) encountered 25% sensor failure within the first year due to errors in field installation (inadequate backfilling) and sensor electronics deterioration (when exposed to positive pore pressure). O'Kane (1996) experienced 50% sensor failure within the first two years. Although the sensors were found to respond to atmospheric forcing as expected, they also yielded lower suction readings than nearby tensiometers.

2.8.5 University of Saskatchewan Beta-97 Sensors

Numerous shortcomings and difficulties have been associated with commercially available thermal conductivity sensors. Fredlund *et al.* (1994b) identified these difficulties as:high cost of sensors and high cost associated with sensor calibration; inaccuracies for certain matric suction ranges; and low strength and poor durability of the ceramic tip. A collaborative industry-university program was initiated in the fall of 1996 by the Unsaturated Soils Group (USG), Department of Civil Engineering, University of Saskatchewan, to research and develop a reliable thermal conductivity sensor that addressed above shortfalls.

The USG prototype sensors (Beta sensors) have been designed for matric suction ranges from approximately 5 kPa to 500 kPa. The ceramic pore size distribution results in a near-linear logarithmic water content response. The ceramic strength was significantly increased over the existing commercially available sensors. The data accuracy was improved by recording the voltage output over the entire heating curve. This output is analyzed using a best-fit regression analysis to provide the corresponding matric suction value (Shuai *et al.*, 1998). An equation was derived to represent the quasi linear calibration curve as a function of a parameter "*C*" and matric suction. The parameter "*C*" is defined by the thermal properties of the sensor and the heating rate of the heating device (Shuai *et al.*, 1998).

The USG researchers are currently developing a data acquisition system and data analysis software to be used with their sensors. The sensors used for this research are first generation prototype Beta-97 thermal conductivity sensors.

Chapter Three

CAMECO INSTRUMENTATION PROGRAM

This Chapter provides the details of the HLTF test cover and Cameco's instrumentation and monitoring program. The chronology of the site instrumentation and monitoring efforts are summarized in Section 3.1. The details of the test cover configuration are provided in Section 3.2. The particulars of Cameco's instrumentation and monitoring program are discussed in Sections 3.3 to 3.8 (Cameco 1995, 1996, 1997a, 1998a).

3.1 BACKGROUND

In 1992, Cameco initiated a program to evaluate the performance of the engineered cover at Key Lake's HLTF. A soil cover consisting of 60 cm of outwash sand overlain by 60 cm of compacted till was placed over the heavily leached cobble ore. The facility was graded, diversion ditches and berms were constructed, and runoff collection culvert was installed.

In 1993, two *test patches* complete with pan lysimeters were incorporated within the test facility. Two steel culvert manholes were placed adjacent to each of these test patches, and one additional manhole was placed within the main cover area. Manholes were used to install thermal conductivity sensors at various elevations. The weather station and the surface runoff flow measuring station were installed and monitoring instrumentation was connected to two CR10 dataloggers.

Data collection began in earnest in 1994. Two clusters of thermistors were installed, and a cap was built over the cribbed well. In spring, snow melt water infiltrated and flooded all three manholes through small holes that were cut to install thermal conductivity sensors. Extensive damage was incurred to the suction sensor instrumentation and data acquisition system, as well as to the lysimeter collection system. The data acquisition system was relocated and mounted above ground. All sensor lead wires were spliced and reconnected. The small access holes in each manhole were plugged and sealed to prevent future flooding. Lysimeter collection tanks were restored and modified, and the site monitoring program resumed in August, 1994.

In spring of 1996, the thermal conductivity sensor program was discontinued. Modifications were made to the surface runoff flow measuring system to enable low flow measurements. Two neutron probe access holes were installed in November, 1996.

3.2 HLTF and TEST COVER DESCRIPTION

3.2.1 Heap Leach Test Facility

The geometry of the HLTF is an inverted frustum of a pyramid. It is a below ground structure with side slopes of 1:2.5, a bottom surface of about 17 m x 17 m (289 m^2), a top surface of approximately 53 m x 53 m (2,810 m^2), a total storage capacity of approximately 3,750 m^3, and a total depth of approximately 7.5 m (*Figures 3.1* and *3.2*).

The main components of this facility are, from bottom to top, a double liner system consisting of a 40 mils thick secondary HDPE (high density polyethylene) liner, filter sand blanket with drainage piping, 40 mils thick primary HDPE liner, and sand percolation blanket with drainage piping. On the slopes, a double liner system consisting of 40 mils thick HDPE liner, 5 mm thick PE drainage net, 40 mils thick primary HDPE liner, and sand percolation blanket were installed. A square HDPE lined wooden pumping station was

incorporated with a side length of approximately 2.5 m extending from the percolation blanket on the top of the facility to about 1 metre above ground surface.

Foundation materials consist of a low hydraulic conductivity (10^{-6} m/s) till. Cobble ore stored in the facility comprises of sandstone cobbles and boulders in a matrix of fine sand, silt, and clay. The average permeability of the primary liner was found to be in the range of 10^{-9} m/s. It can be assumed that all percolation is either ponding on the primary liner, or intercepted by the secondary seepage recovery system.

3.2.2 Test Soil Cover

The test soil cover consists of 60 cm of outwash sand overlain by 60 cm of till containing 12% to 15% fines. The outwash sand layer (Deilmannn pit stockpiled material) was placed in two 30 cm lifts and was compacted via a dozer. The till layer (materials less than 10 cm) was installed in two 30 cm lifts, with each lift wetted down and compacted by a vibrating roller to 100% Standard Proctor Density. The cover is roof shaped with a 2% gradient from the cribbed well towards the outside embankments where a surface run off collection culvert is installed. Berms and diversion ditches were constructed along the east and west edges to divert extraneous water.

3.2.3 Test Patches

In 1993, two small scale test patches, 4.5 m x 4.5 m in size, were incorporated within the Test Facility (*Figures 3.1* and *3.2*). One test section consisted of 60 cm of outwash sand overlain by 60 cm of till with 15% to 20% fines. The second test section consisted of, from bottom to top, 40 cm of outwash sand, 20 cm of till/bentonite (5% by weight), and 60 cm of till with 15% to 20% fines.

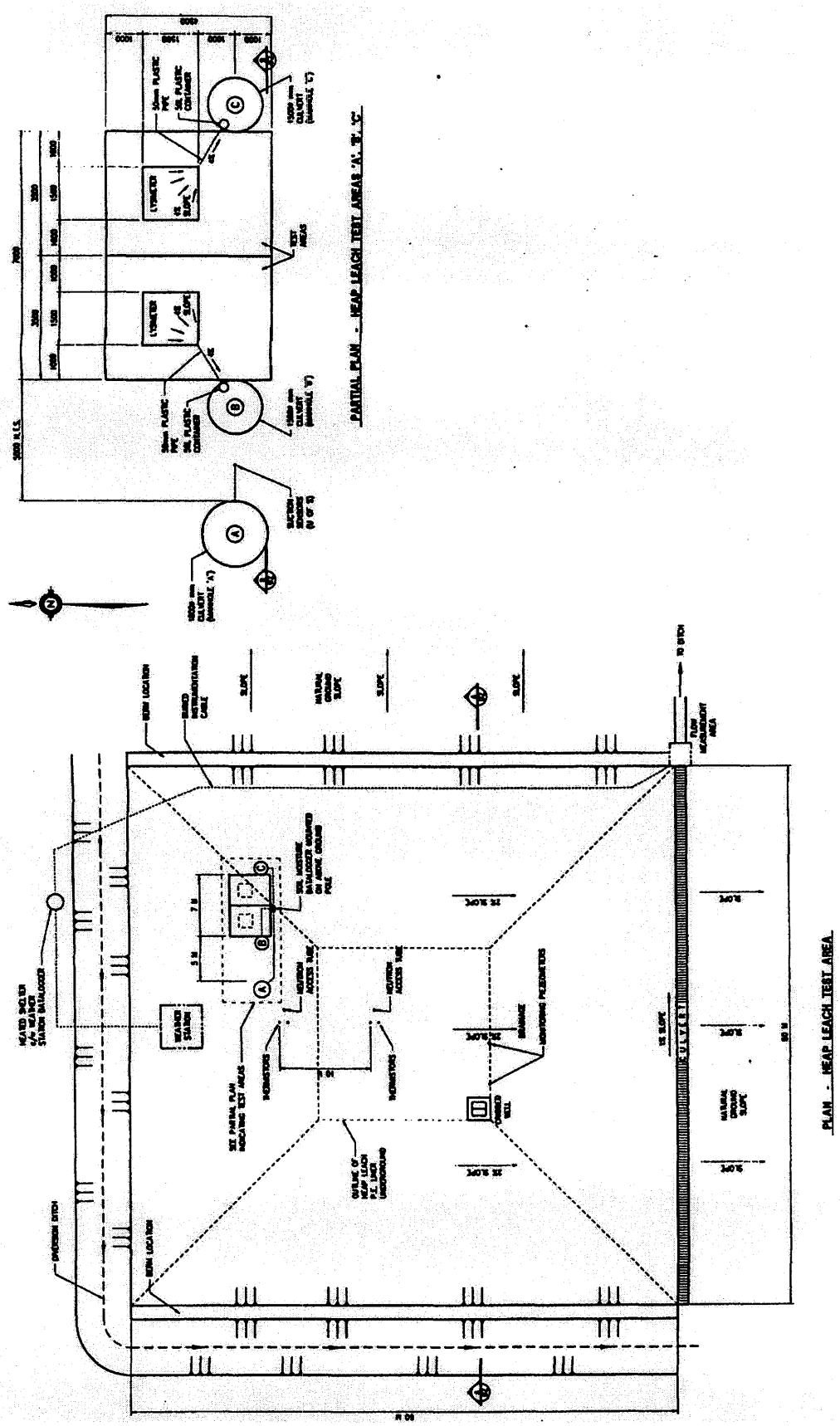

Figure 3.1 Plan view of the Heap Leach Test Facility (Cameco).

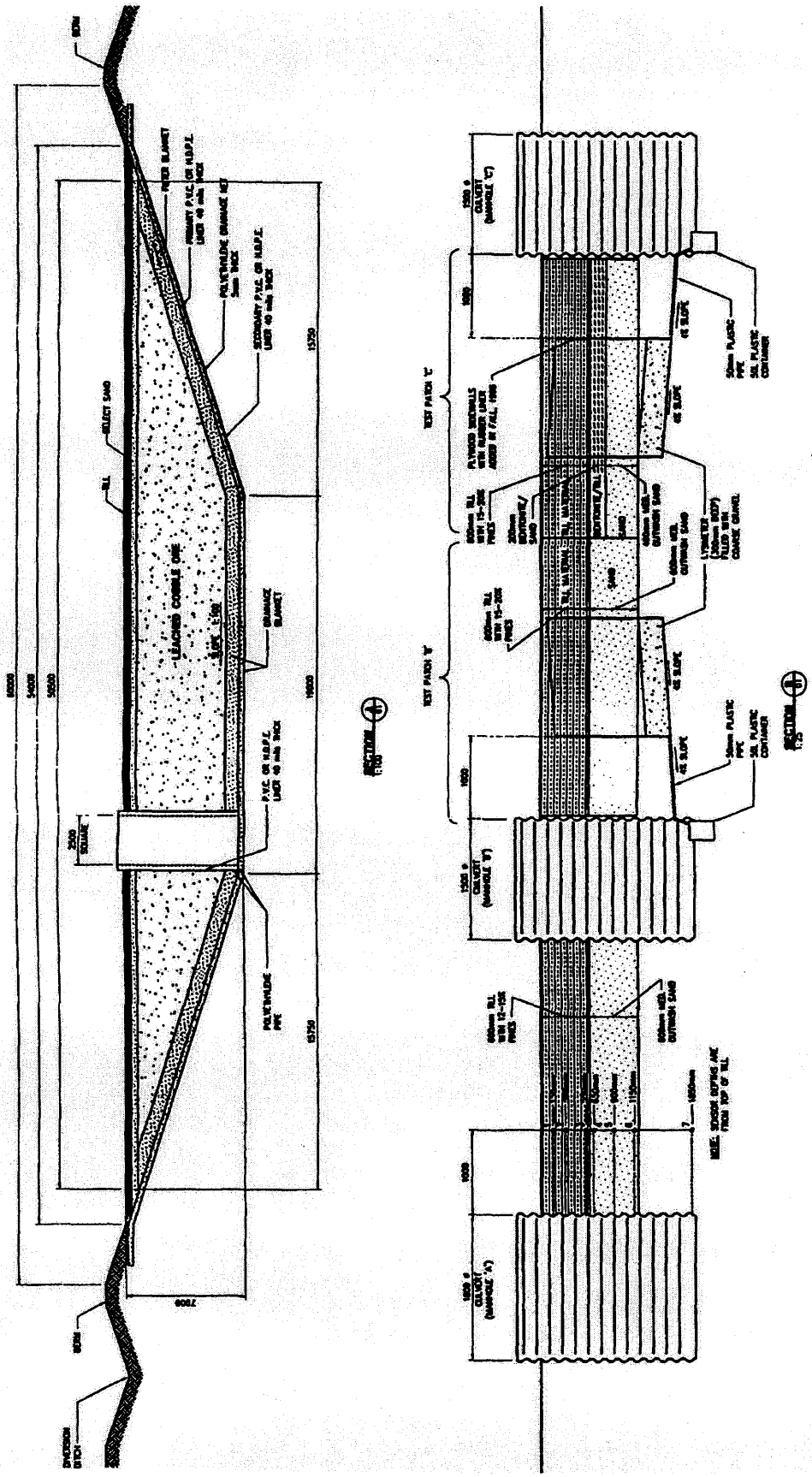

Figure 3.2 Sectional view of the Heap Leach Test Facility (Cameco).

3.3 WEATHER MONITORING PROGRAM

The weather monitoring program was initiated in 1993 and consists of an automated weather station that records precipitation, air temperature, relative humidity, wind speed and direction, net and incoming radiation, snow depth, and pan evaporation. The weather sensors, excluding the rain gauge and the evaporation pan, are mounted on a 3 m high tripod (*Figure 3.3*), and are linked to a datalogger that monitors each parameter at specified time intervals.

3.3.1 Weather Station

Precipitation was initially recorded using a *standard storage rain gauge* (Model FS-100). It consisted of a cylindrical steel tank mounted on a steel stand approximately one meter

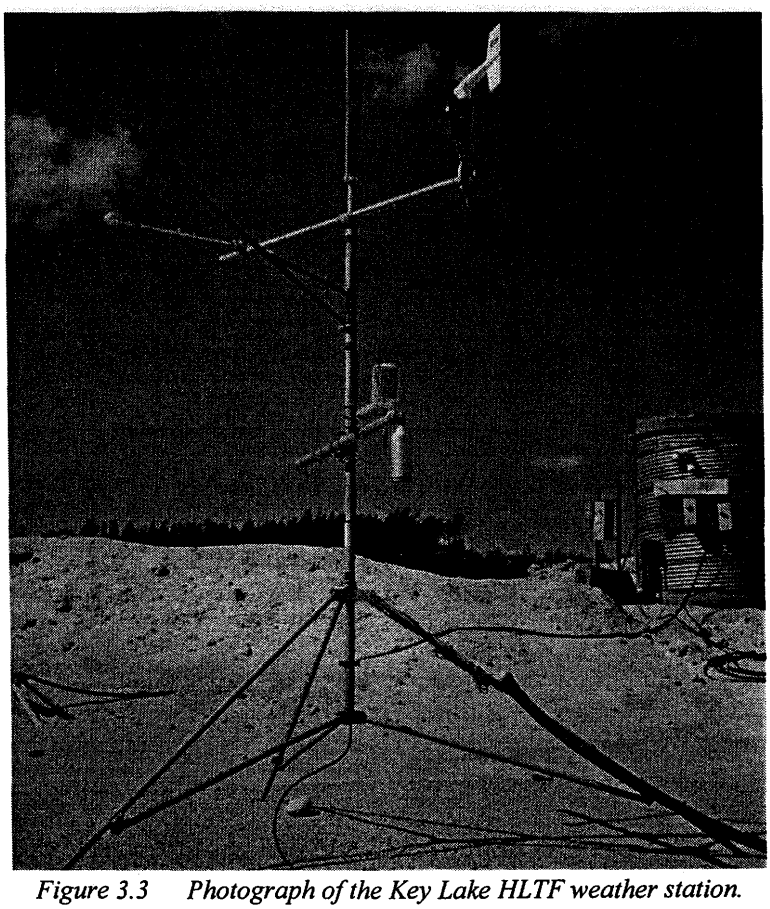

Figure 3.3 Photograph of the Key Lake HLTF weather station.

above the ground. The tank was initially filled with a mixture of antifreeze and oil. The antifreeze was used to prevent freezing, and the oil was added to prevent evaporation. An electric pump was incorporated to mix the antifreeze/oil mixture once every hour. An electric transducer was installed to record the fluid level at the end of each day.

Numerous difficulties were experienced with the FS-100 rain gauge. The gauge eventually failed completely on July, 1995. It was replaced with a *tipping bucket rain gauge* in spring, 1996. The tipping bucket rain gauge is mounted on the steel stand that previously supported the FS-100 rain gauge. The gauge is linked to a datalogger to record precipitation every 15 minutes during rainfall events.

The *air temperature* and *relative humidity* are monitored on an hourly basis with a Vaisala (Model HMP35CF) probe. It is housed in a white radiation shield device and mounted on the tripod approximately 2 m above the ground.

The *wind speed* and direction are recorded using a high resolution wind sensor (RM Young Model 05103) mounted on the tripod approximately 3 m above the ground. The recorded wind parameters are: total mileage for the month, greatest mileage in 24 hours, greatest distance and prevailing direction in one hour, longest continued distance, prevailing direction by distance, prevailing direction by hours, and average wind speed for the month. Wind speed and direction are monitored hourly.

The *net radiation* is monitored with a net radiometer (Radiation and Energy Balance Systems Inc. Q*6.1). Incoming radiation is monitored with a pyranometer (LI-COR LI-200SZ). Radiation sensors are mounted on the tripod with the net radiometer located approximately 3 m above the ground, and the pyronometer mounted approximately 2.5 m above the ground. The net and incoming radiation are recorded once every hour.

The site pan *evaporation* is monitored using a Class A evaporation pan situated above ground. The pan water level is measured using floats attached to sensors that send out

signals corresponding to the rise and the fall of the pan water level. The evaporation pan is also equipped with a wind run gauge and pan water temperature sensor (thermistor). These parameters are used to estimate the pan coefficient (Kohler *et al.*, 1955). The pan parameters are monitored once a day.

A sonic *snow depth* sensor (UDG01) is attached to the tripod approximately 2 m above the ground to measure snow depth below the sensor. Accumulated snow depth is calculated based on the difference between a reference distance (bare surface) and shorter distances measured as snow is accumulated. UDG01 is a sonic sensor that sends out a sonic pulse and records the corresponding reflection time. This sensor is monitored once a day.

3.3.2 Weather Station Data Acquisition System

The fluid level in the storage rain gauge was recorded daily while the tipping bucket rain gauge was monitored every 15 minutes when raining. Snow depth and pan evaporation were monitored once a day, and the remainder of the weather parameters are monitored once every hour (i.e., air temperature, relative humidity, wind speed and direction, net and incoming radiation).

A Campbell Scientific Inc. (CSI) *CR10 measurement and control module* (CR10) was used to access and store data from weather sensors. The CR10 is a fully programmable datalogger and controller. A lap top computer and CSI PC208 software package were used to communicate with CR10 (O'Kane 1996). The stored data was downloaded monthly.

3.4 SURFACE RUNOFF COLLECTION AND MONITORING

The surface runoff collection and monitoring system was installed in stages. In 1992, the surface of the soil cover facility (HLTF) was graded at approximately a 2% slope towards the south where the runoff collection culvert is installed (*Figure 3.4*). Ditching and grading

along the north, east, and west boundaries diverted extraneous runoff around the facility. Berms were constructed along the east and west edges to contain runoff originating from the facility.

The surface runoff flow measuring station was installed at the downstream end of the collection culvert in 1993. A length of smooth-walled steel pipe was installed at the end of the corrugated culvert (*Figure 3.5*). A containment area was constructed at the discharge point with a free drop of approximately 50 cm. A half culvert was trenched to carry the water down the embankment and away from the HLTF. A UDG01 sonic sensor was installed directly above the discharge point to measure the brink depth.

The UDG01 was connected to a CR10 to record the brink depth every 30 seconds. This resulted in large amount of redundant data that was stored during periods without precipitation. The instantaneous water flow rate was calculated using the "*Brink depth method for circular sections*" (Smith 1962). An air temperature sensor was mounted in the vicinity of the runoff flow measuring station to calculate corresponding sonic wave speed.

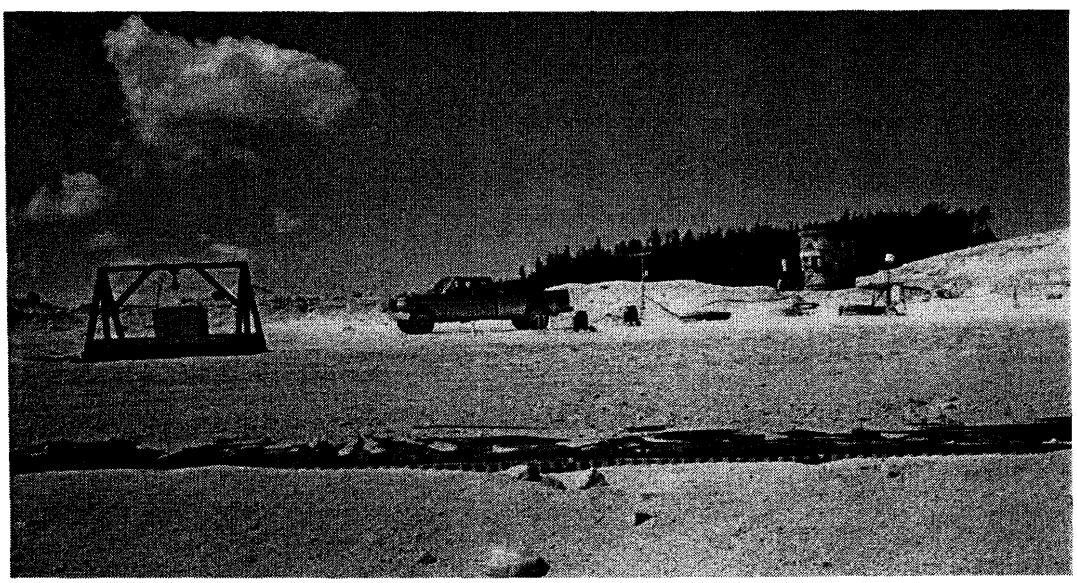

Figure 3.4 Photograph of the surface runoff collection culvert at HLTF. Looking north.

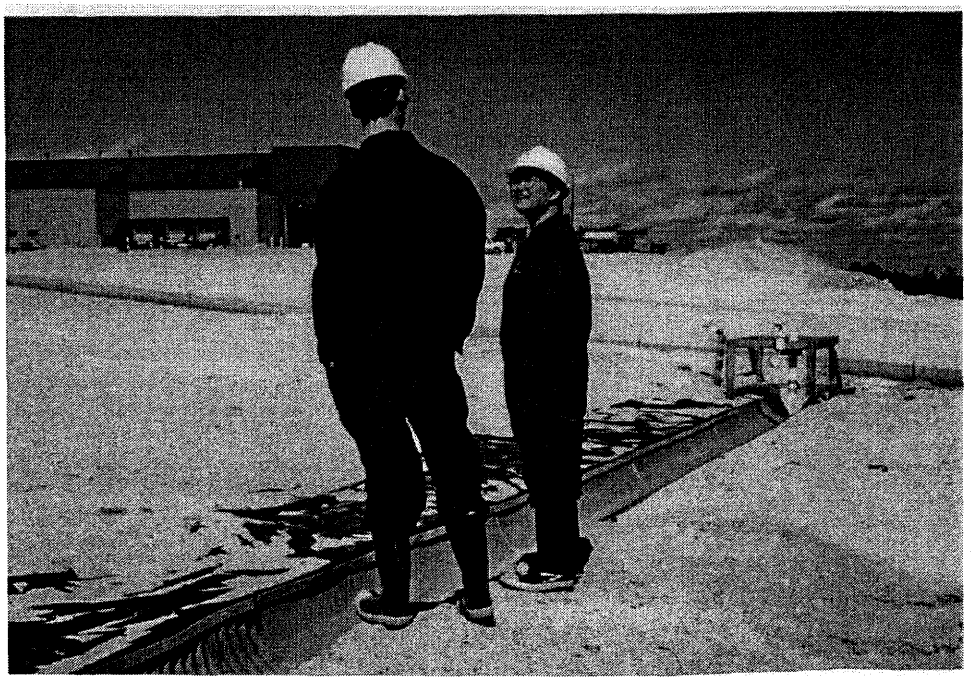

Figure 3.5 Photograph of the runoff collection and measuring station. Looking east.

Difficulties in estimating low flow conditions resulted in further changes. In May 1996, a V-notch weir with a 60° angle was installed at the open end of the runoff collection culvert. This modification enabled measurement of low flow conditions and improved overall flow measurement accuracy. With the installation of the tipping bucket rain gauge, the data acquisition program was modified to record surface runoff data only during rainfall events, and for a short duration following the event. The UDG01 sensor was activated by the tipping of the first filled tipping vessel, and continued to record for one hour after the last rainfall.

3.5 THERMAL CONDUCTIVITY SENSORS

A total of thirty nine (39) Agwatronics Incorporated AGWA-II thermal conductivity sensors were installed within the HLTF in 1993. The thermal conductivity sensors were installed in pairs along the soil profile. 27 thermal conductivity sensors were installed at seven different depths within the main cover area and the *test patch "B"* area. The remaining 12 sensors were installed at six different depths within the *test patch "C"* area (*Figure 3.1).* The

sensors were connected to a dedicated CR10 data acquisition system. AGWA-II sensors were individually calibrated at the University of Saskatchewan over 0 kPa to 300 kPa range using 8 calibration points. Calibration curves were found to be bi-linear with a break point at approximately 150 kPa to 175 kPa (Wong *et al.*, 1989).

3.5.1 AGWA-II Sensor Field Installation

The thermal conductivity sensors were installed horizontally along the soil profile from corrugated steel culverts that were installed adjacent to each of the cover areas. This method was successfully employed for a till soil cover system (O'Kane 1996). The sensors were installed according to installation procedures outlined in O'Kane (1996).

Two 1.5 m diameter steel culverts (manholes *"B"* and *"C"*) were installed adjacent to the two test patches. One 1.8 m diameter steel culvert (manhole *"A"*) was installed in the main cover area in the vicinity of the two test patches. The culverts were pre-drilled with installation holes at pre-determined elevations. One meter long holes were excavated horizontally into the soil. Sensors were carefully positioned, two per hole, and carefully backfilled. Sensor installation elevations were determined based on the soil profile, that is, near the surface, mid point, and on sand/till interface (*Figure 3.1*). In the main cover area and within the *test patch "B"* , the sensors were installed at following depths from surface: 5 cm, 30 cm, 55 cm, 65 cm, 90 cm, 115 cm, and 150 cm. In the *test patch "C"*, the sensors were installed at: 5 cm, 30 cm, 55 cm, 70 cm, 75 cm, and 115 cm from surface.

3.5.2 AGWA-II Sensor Data Acquisition System

The sensors were connected to a data acquisition system mounted inside manhole "*A*". The data acquisition system consisted of a CR10 measurement and control module, two relay multiplexers (AM416), one relay driver (A21REL), one precision voltage regulator, one power supply, and one CSI SM192 storage module (SM192). A lap top computer and CSI PC208 software package are used to communicate with CR10 datalogger and SM192.

3.6 INFILTRATION MEASUREMENT

The HLTF was constructed with a pumping station consisting of a HDPE lined wooden structure (cribbed well) approximately 2.5 m x 2.5 m. The pumping station was used to recirculate leachate during the cobble ore leaching program. The rise and fall of the water level in the cribbed well indicates infiltration and/or evaporation from the facility. The total annual percolation, or net infiltration, is approximated by monitoring the volume of water pumped out of the cribbed well during summer months. A cap was built over the cribbed well in 1994 to prevent ingress of surface runoff water (*Figure 3.6*).

Square pan lysimeters, 1.5 m x 1.5 m, were installed beneath each of the *test patches* in 1993. The lysimeters were 0.5 m in height and filled to a depth of 0.35 m with coarse sand. The top of the coarse sand was at same elevation as the bottom of the outwash sand cover layer. The lysimeters each drain to a 50 litre cylindrical plastic container located in the manhole. In 1996, the lysimeters were excavated and the side walls were extended to surface using plywood and impermeable liner fabric. The lysimeters were carefully backfilled with excavated material. Infiltration was measured periodically by measuring the volume of collected water. In 1998, the plastic container was replaced with a tipping bucket rain gauge.

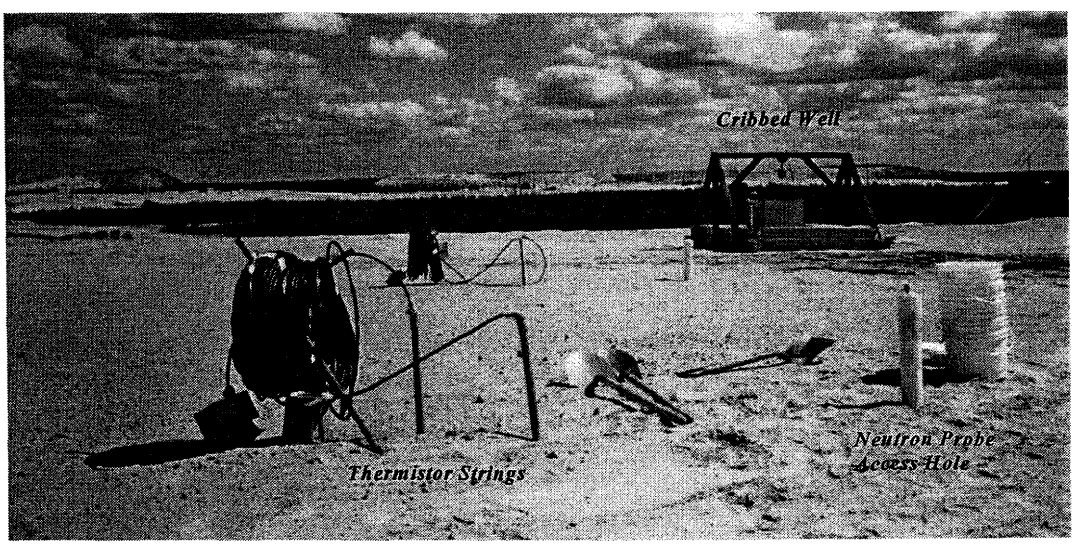

Figure 3.6 Photograph of the HLTF. The photo shows two nests of thermistor strings, two neutron probe access holes, and capped cribbed well (looking south).

3.7 THERMISTORS and NEUTRON PROBE ACCESS HOLES

Two clusters of thermistor strings were installed in 1994 (*Figure 3.6*). The thermistors are installed to measure subsurface soil temperature at 50 cm intervals from surface to approximately 6.5 metres in depth. They are read manually using a read-out gauge.

Two neutron moisture probe access holes, HL-101N and HL-102N, were installed in November 1996 adjacent to existing thermistor strings (*Figure 3.6*). The size of the access hole was dictated by the availability of the installation equipment. Access holes, 3 $^{15}/_{16}$" (100 mm) diameter, were drilled to approximately 2.1 m in depth. Three gravimetric samples were taken from each hole to estimate gravimetric water content. A 3" diameter Schedule 40 PVC tube (90 mm outside diameter) was placed into each of the bored holes. Access tubes are capped and sealed at the base to prevent water infiltration through the base of the tubing. Following access tube installation, neutron probe readings were taken in 30 cm increments from approximately 0.5 m to 2.1 m from surface.

3.8 SPRING SNOW SURVEY

The UDG01 sonic sensor provided an estimate of snow depth at one location. Snow surveys were undertaken during the spring of 1996 and 1997 in order to obtain larger samples of snow depth and snow densities. A total of nine equidistance survey points were used. *MSC Type I* snow survey equipment was acquired from Environment Canada to carry out the snow survey program following the procedures outlined in "*Snow Surveying - Manual of standards, Snow surveying procedures*" (Environment Canada, 1973).

Chapter Four

LABORATORY AND FIELD PROGRAM

A quantitative assessment of a soil cover system involves determining the parameters in the water balance equation including precipitation, surface runoff, infiltration, evaporation, percolation, and subsurface storage. Cameco's instrumentation and monitoring program yielded reliable precipitation and surface runoff data. However, the infiltration and subsurface soil moisture data were infrequent, and the pan evaporation data was unreliable.

To complement the existing data, additional laboratory and field program was undertaken. The laboratory program endeavored to identify pertinent soil properties such as grain size distribution, specific gravity, SWCC, and hydraulic conductivity. The field program included an evaluation of *in situ* soil density and hydraulic conductivity. New thermal conductivity sensors were installed, and neutron probe calibration was carried out to better define changes in soil suction and moisture along the soil profile. Bowen Ratio Instrumentation was installed to estimate actual evaporation.

4.1 LABORATORY TEST PROGRAM

Soil samples that were required for laboratory testing were obtained from the HLTF, where possible. Three brown till samples, approximately 17 kg each, and two outwash sand samples, approximately 8 kg each, were taken from respective layers within the main cover area. One 13 kg pink till sample was acquired from the stockpile. Two filter sand samples,

approximately 8 kg each, were taken along the boundary of the HLTF. Two cobble ore samples, approximately 16 kg and 6 kg, were sampled with a drill from the main cover area.

Soil samples were placed into 20 litre plastic containers and transported to the University of Saskatchewan *Geotechnical and Environmental Laboratory*. Tests were carried out to define the grain size distribution, the specific gravity, the saturated hydraulic conductivity, the soil-water characteristic curves (SWCC), and moisture-density relationships. A summary of tests performed on the HLTF soil samples is presented in *Table 4.1*.

Table 4.1 Number of laboratory tests performed on the soil samples.

Soil Type	No. of Samples	Grain Size	Specific Gravity	Hydraulic Conductivity	Compaction Test	SWCC
Brown Till	3	4	1	1	5	3
Outwash Sand	2	3	1	1	Nil	4
Cobble Ore	2	1	1	1	Nil	1
Pink Till	1	1	1	1	Nil	1
Filter Sand	2	2	Nil	Nil	Nil	Nil

4.1.1 Grain Size Distribution

The distribution of particle sizes larger than 75 μm (No.200 sieve) was determined by mechanical sieving (sieve test) while those smaller than 75 μm was determined by a sedimentation process (hydrometers test) as outlined in ASTM D422-63 (reapproved 1990) "*Standard Test Method for Particle-size Analysis of Soils*".

ASTM provides a schedule of "approximate minimum mass of portion" as a function of the largest particle size (*Table 4.2*). For example, the minimum sample portion required for testing sandy soils is approximately 150 g passing No. 10 sieve. The test sample portion was thus determined on the basis of the ASTM guidelines, where possible.

A portion of the sample prepared for sieve analysis was set aside for hydrometer tests. Hydrometer analysis was performed on 50 g of oven dried material passing No. 10 sieve. One hydrometer test was performed for each soil type.

Table 4.2 Approximate actual mass of portion for particle size analysis.

Soil Type	Nominal Diameter of Largest Particles (mm)	Approximate Minimum Mass of Portion Retained on No.10 Sieve (g)	Approximate Actual Mass of Portion Used (g)
Brown Till	160	>5000	2000
Outwash Sand	9.5	500	1000
Cobble Ore	50.8	4000	4000
Pink Till	9.5	500	2200
Filter Sand	4.75	500	1000

4.1.2 Specific Gravity

The specific gravity test was performed on 50 g of oven dried samples passing the 4.75 mm (No. 4) sieve according to the ASTM D854-92 "*Standard Test Method for Specific Gravity of Soils*".

4.1.3 Hydraulic Conductivity

The soil hydraulic conductivity was determined using the constant head permeability test, and the falling head permeability test. The hydraulic conductivity test procedures are outlined in the ASTM D2434-68 (reapproved 1994) "*Standard Test Method for Permeability of Granular Soils (Constant Head)*" and the ASTM D5856-95 "*Standard Test Method for Measurement of Hydraulic Conductivity of Porous Material Using a Rigid-wall, Compaction-mold Permeameter*".

The ASTM D2434-68 (1994) is applicable for granular soils with a hydraulic conductivity

greater than 10^{-5} m/s. The ASTM D5856-95 is appropriate for soils with a hydraulic conductivity less than or equal to 10^{-5} m/s. Both standards are used for testing disturbed granular soils which are laboratory compacted into rigid-wall compaction-molds (permeameters) either by using a specified compactive effort, or by compacting to a certain density.

The outwash sand sample was tested using the ASTM D2434-68 (1994) *Constant head test* standard. The brown till, pink till, and cobble ore samples were tested using the ASTM D5856-95 Test Method B "*Falling head test with constant tailwater level*" standard. The soil samples were prepared by passing air dried samples through a 4.75 mm sieve. They were wetted to respective optimum water contents (as listed in HBT, 1992), and compacted into 100 mm diameter compaction-molds to standard proctor density as outlined in the ASTM D698-91 "*Standard Test Method for Laboratory Compaction Characteristics of Soil Using Standard Effort*". The permeameters were assembled to function with no restraint against swelling at the top of test specimens. The specimens were allowed to slowly saturate from the bottom up by flooding with tap water. The saturated specimens were assembled either for the constant head or falling head test with a constant tailwater level.

4.1.4 Soil-Water Characteristic Curve

The soil-water characteristic curve was determined following the modified pressure plate testing and vapour equilibrium testing procedures outlined in O'Kane (1996) and Ayres (1998). Material passing the 4.75 mm sieve was prepared at optimum water content. It was carefully compacted into oedometer rings to approximately represent actual field densities. The prepared specimen was placed into a modified pressure plate apparatus. The apparatus was assembled, and the sample was saturated and tested from 0 kPa to 300 kPa suction. Upon completion of modified pressure plate testing, 5 to 10 samples, approximately 5 g each, were prepared for vapour equilibrium testing. Vapour equilibrium testing was carried out for five different equivalent total suction values ranging from 1.9 MPa to 292 MPa.

4.1.5 Compaction Testing

Standard proctor compaction test was carried out for the brown till soil sample only. A sample of approximately 2500 g air dried material passing the 4.75 mm sieve was used to prepare each specimen for the laboratory compaction testing using 100 mm diameter compaction-molds. A total of five specimens at varying water contents were prepared following the ASTM D698-91 "*Standard Test Method for Laboratory Compaction Characteristics of Soil Using Standard Effort*" Method A.

4.2 FIELD TEST PROGRAM

A field test program was carried out to define *in situ* density and hydraulic conductivity. The *in situ* density tests were performed for brown till and pink till surficial layers, as well as the underlying outwash sand layer. The *in situ* hydraulic conductivity tests were carried out using a *Guelph Permeameter* on the brown till, pink till, and outwash sand layer.

4.2.1 *In Situ* Density

The ASTM D2167-94 "*Standard Method for Density and Unit Weight of Soil in Place by the Rubber Balloon Method*" is appropriate for materials containing particles smaller than 37.5 mm, such as outwash sand. For materials containing appreciable amounts of large particle sizes, the ASTM D4914-89 (reapproved 1994) "*Standard Test Methods for Density of Soil and Rock in Place by the Sand Replacement Method in a Test Pit*" or the ASTM D5030-89 (reapproved 1994) "*Standard Test Methods for Density of Soil and Rock in Place by the Water Replacement Method in a Test Pit*" are generally recommended.

Till, by nature, consists of significant quantity of large particle sizes. Although larger particles (>165 mm) were removed prior to placement, the till cover contained a significant amount, approximately 12%, of gravel/cobble size particles (*Figure 4.1*). The rubber balloon

Figure 4.1 Photograph of the brown till cover material.

method, used for the outwash sand, was deemed inappropriate for till. The test methods D4914 and D5030 involves careful excavation of test pits and construction of test pit frames. In its place, a modified water replacement method was employed, yielding reasonable estimates of *in situ* density.

The *in situ* density test was carried out on June 1997. The *in situ* density in till was estimated by removing the upper 10 cm layer of weathered material. The surface was carefully leveled, and a test pit approximately 8 000 cm^3 in volume was carefully excavated. The excavated material was placed into 20 litre plastic containers for a laboratory assessment of gravimetric water content and weight of soil excavated. The excavated test pit volume was determined by lining the pit with plastic, and measuring the volume of water required to refill the hole with water using a graduated cylinder (*Figure 4.2*). Three test pits were excavated in brown till and one in pink till.

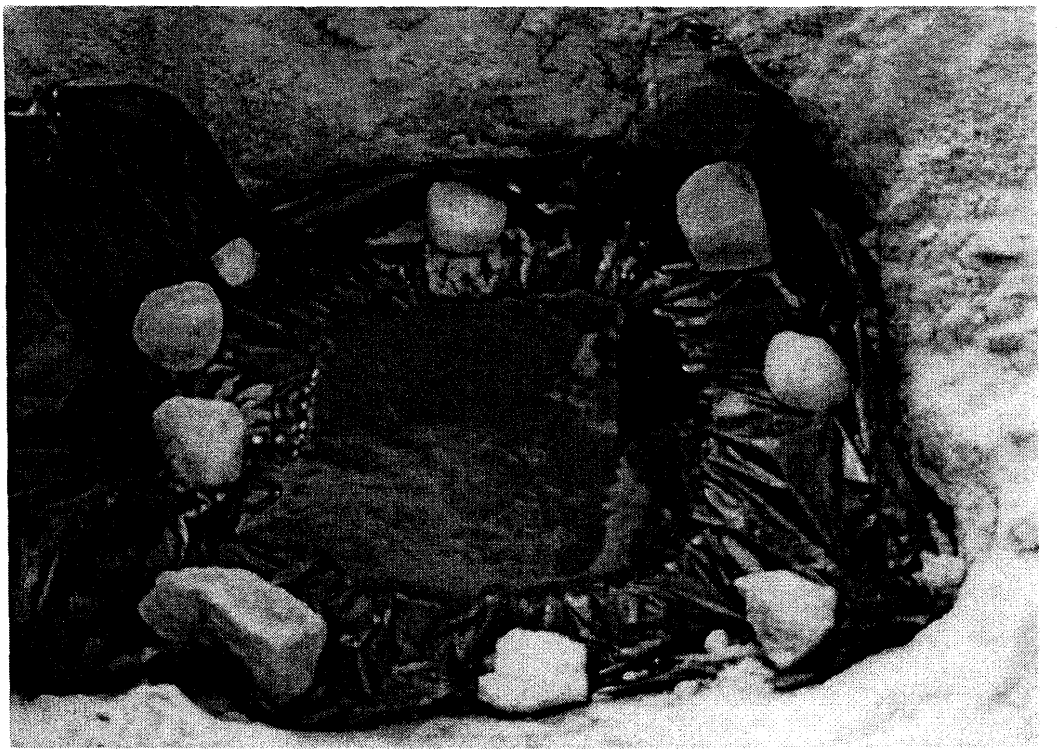

Figure 4.2 Photograph of the in situ density test. A modified water replacement technique was used. The test pit is lined with plastic and refilled with water.

4.2.2 *In Situ* Hydraulic Conductivity

Estimates of *in situ* hydraulic conductivity was performed using a *Guelph Permeameter* (Soil Moisture Equipment Corp., 1986) in October 1997. The Guelph Permeameter method involves measuring the steady state rate of water recharge into unsaturated soil from a small cylindrical well hole in which a constant depth of water is maintained. The flow rate out of the well declines to a steady value within a short period of time. The rate of constant outflow of water, the diameter of the well, and the height of water in the well are used to determine the field saturated hydraulic conductivity (Reynolds and Elrick, 1985).

This method is portable, fast, and simple to use. Its practical measurement range is limited to soils with the field saturated hydraulic conductivity ranging from 10^{-4} m/s to 10^{-8} m/s. It is designed for uncased wells ranging in radius from 20 cm to 50 cm.

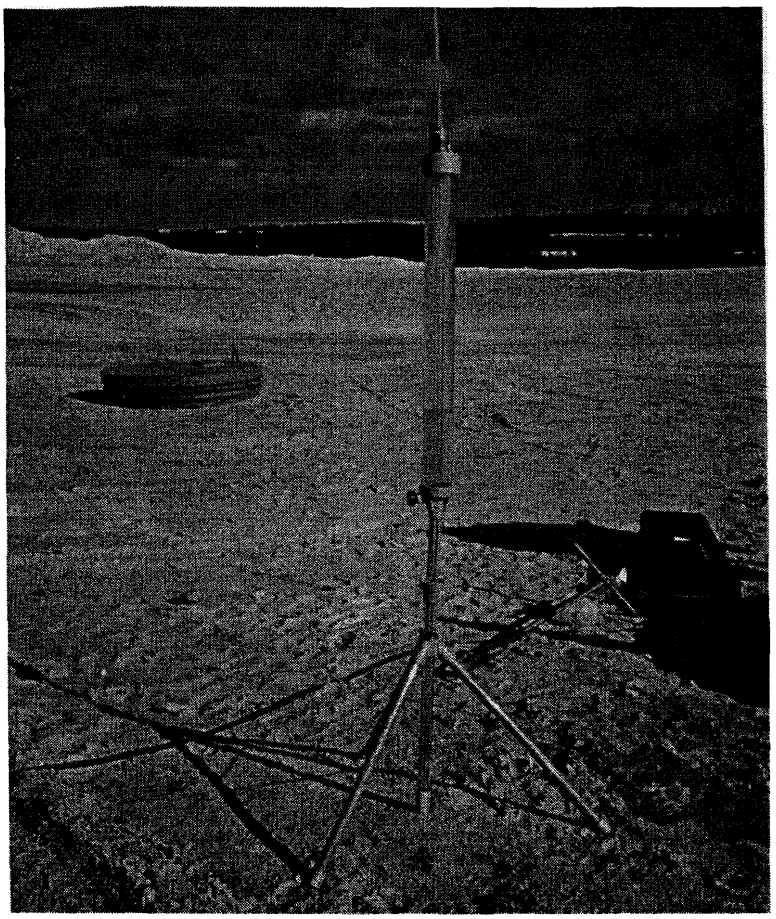

Figure 4.3 Photograph of a Guelph Permeameter.

The Guelph Permeameter is essentially an in-hole Mariotte bottle constructed of two concentric transparent plastic tubes (*Figure 4.3*). A cylindrical well is excavated to a desired depth. The Guelph Permeameter is filled with water and placed carefully into the excavated hole. The permeameter is started and the water level is maintained in the well at a constant depth (typically 5 cm). The rate of fall of water in the reservoir needed to maintain a constant well water depth is monitored (i.e. flow rate out of the permeameter) until a steady rate is attained. This procedure is repeated for a second well water depth (typically 10 cm).

4.2.3 Soil Profile Sampling

The main purpose of the soil profile sampling program was to obtain cobble ore soil samples

for laboratory testing. In October 1997, a sonic drill was employed to access cobble ore approximately 1.2 m below surface. Two 76 mm diameter holes were drilled to approximately 3.0 m and 4.5 m in depth. Cobble ore from the 3.0 m hole was extracted and placed into a 20 litre plastic container for laboratory testing. The entire length of the 4.5 m hole was carefully logged, divided, and sampled for laboratory assessment of water contents.

The sonic drill is used in sandy soils and in frozen/thawed tailings to secure relatively intact soil samples. The drill sample undergoes some lateral distortion as it is placed into larger diameter plastic sleeves (92 mm). The sample maintains more or less its shape with minimal mixing, thus preserving the sequencing of soil layers.

The 4.5 m hole sample was extruded into three plastic sleeves of equal lengths. Each plastic sleeve was carefully and evenly divided into approximately 10 cm lengths. They were logged and individually placed into small plastic sampling bags. The gravimetric water content was measured in the laboratory for each of the samples. The *in situ* density was calculated based on the drill sample diameter and sample length. A constant lateral distortion along the length of each plastic sleeve sample length was assumed. The *in situ* density estimates using the sonic drill sampling procedure represent a reasonable approximation of the expected soil density along the soil profile.

4.3 NEUTRON PROBE CALIBRATION

Neutron moisture probes are supplied with a factory calibration curve. Although a factory calibration curve has been known to be adequate for some applications (Silvestri 1991), it has generally been found to underestimate the soil moisture content (Grismer *et al.*, 1995). The neutron probe is factory calibrated using a barrel of clean sand, and therefore, it is applicable for sandy soils with no significant absorber elements or organic compounds. A site and soil specific calibration is required in order to obtain meaningful quantitative data.

The neutron probe used in this project is a CPN 503DR hydroprobe manufactured by Campbell Pacific Nuclear Corporation.

4.3.1 Neutron Probe Field Calibration

A field calibration is typically carried out by sampling within the access hole at the time of the access tube installation. Three gravimetric soil samples were taken at varying depths from each access hole during excavation in November 1996. Neutron probe readings were logged at 30 cm increments, and gravimetric water content analysis was carried out on the samples. Cameco concluded that the sampling procedure employed resulted in lower than expected water contents. Due to the lack of confidence associated with this field calibration attempt, an additional calibration program was deemed necessary.

Neutron probe readings were taken at 30 cm increments along the length of one soil profile sampling hole in October 1997.

4.3.2 Neutron Probe Laboratory Calibration

A laboratory calibration was carried out for the brown till and outwash sand samples taken from the stockpiles. A CPN 503 Hydroprobe employed at Key Lake was used for this calibration work.

A laboratory calibration is generally performed using a 45 gallon drum fitted with a centered access tube, and packed with soil at different known water contents and densities. This method results in an even moisture distribution within the drum, however, it is difficult to accurately reproduce actual field densities and pore-size distributions. Another common laboratory technique is to pack the drum with dry soil, and then saturate it to obtain a two point (dry and saturated) calibration curve.

Two sets of laboratory calibration measurements were taken using 0.2 m^3 (45 gallon) metal

drum containers that were fitted with a centered 3" Schedule 40 PVC access tubes. The access tubes were 1 meter in height, and each access tube was capped and sealed at the bottom to keep it dry during calibration. The soil was carefully compacted in 5 cm layers into the drum by tamping with a 4' length of 4" x 4" wooden post. Two 32 second probe count readings were taken at 5 cm increments along the soil profile. The soil was subsequently saturated from the bottom up employing two hoses that were placed along the side wall of the drum. The soil was considered saturated when surface ponding due to saturation from below was noted. Two 32 second readings were taken again at 5 cm increments along the soil profile under saturated conditions (*Figure 4.4*).

The first set of calibration measurement was taken using approximately 190 kg of sand and approximately 220 kg of till. The soil samples were compacted to their respective *in situ* field densities. The sand and brown till were compacted at 3.8% and 6.7% water content, respectively. The resulting dry bulk densities were 1.69 g/cm^3 for sand (versus 1.76 g/cm^3 average *in situ*) and 1.99 g/cm^3 for till (versus 2.02 g/cm^3 average *in situ*). The final heights after packing were 36 cm for the sand sample, and 43 cm for the till sample.

The sphere of influence of a CPN 503 Hydroprobe is oblong in shape with an axial radius of approximately 15 cm from the center of measurement of the probe, and ranging 7.5 cm on either side of the center of measurement (Chanasyk and Naeth, 1988). It was postulated that the sphere of influence may actually extend further than the thickness of the compacted soil under dry conditions. Additional soil samples were brought in from site to fill the drums to the top. A second calibration was undertaken using the larger samples.

The second set of calibration measurement was obtained using approximately 290 kg of sand and 320 kg of till. The soils samples were compacted to 75 cm in height. They were compacted at air dried water content representing a wider range of soil moisture contents. Consequently, the resulting bulk densities were lower than the average *in situ* field densities: 1.58 g/cm^3 for sand and 1.80 g/cm^3 for till.

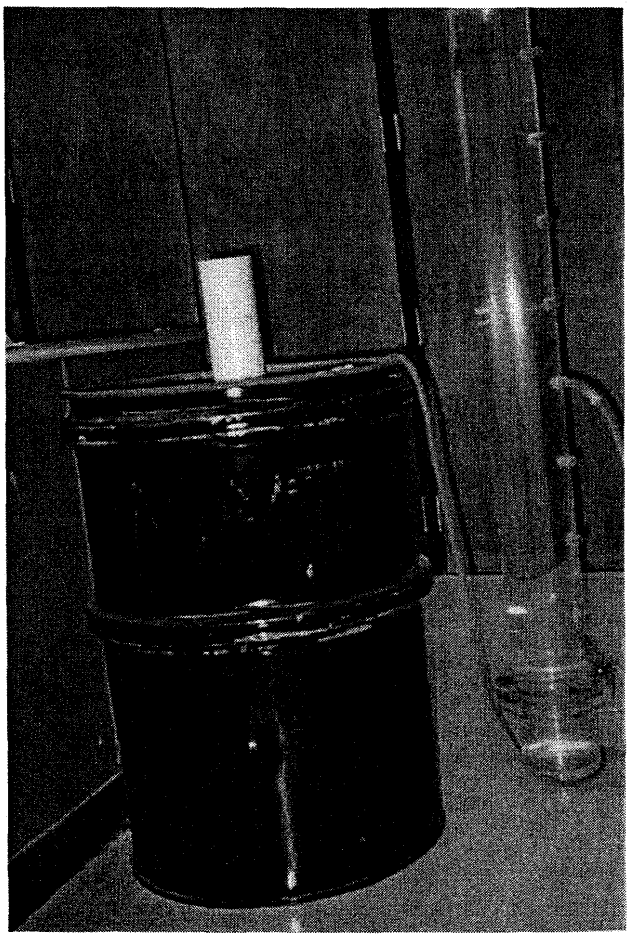

Figure 4.4 Neutron Probe laboratory calibration. A 0.2 m^3 (45 gallon) metal drum and a 3" diameter PVC access tube was used.

4.4 THERMAL CONDUCTIVITY SENSORS

The AGWA-II thermal conductivity sensors did not function as expected. The cover materials used at the HLTF possess very low air entry values (1kPa to 2 kPa) and reach a residual water content at very low matric suction values (10kPa to 20 kPa). During the summer of 1997, the Unsaturated Soils Group (USG) at the University of Saskatchewan was developing new thermal conductivity sensors under the direction of Dr. D.G. Fredlund. The sensors appeared to exhibit the necessary sensitivity in the low matric suction range, i.e., less than 20 kPa. It was thus proposed that these prototype Beta-97 sensors (*Figure 4.5*) be installed at the HLTF.

Figure 4.5 Beta-97 thermal conductivity sensors.

4.4.1 Beta-97 Sensors

The USG produced 22 Beta-97 sensors for a field evaluation at the HLTF. The sensors were calibrated at the University of Saskatchewan, and installed at the HLTF in August, 1997. The Beta-97 sensor consists of a ceramic tip that is 28 mm in diameter and 38 mm in height. An integrated circuit is used as a temperature sensing device, and a resistor as a heating unit. Difficulties were encountered with the epoxy that was employed for sealing and backing. The epoxy underwent high volume change upon saturation causing many of the ceramic tips to sustain both lateral and longitudinal cracks during the calibration process. The sensor electronics were not affected by the crack formation.

4.4.2 Beta-97 Sensor Data Acquisition System

The data acquisition system consists of one CSI CR10, two power supply units, two 16-port multiplexers (AM416), one relay driver (A21REL), one constant voltage source, and one CSI SM192 storage module. The CR10 is a fully programmable measurement and control module (i.e. a datalogger). The mulitplexers are used to increase the number of sensors that can be monitored and controlled by the CR10. The relay driver and the constant voltage

source form a *"heating control unit"* which supplies a constant voltage (10V) across the sensor heater. One power supply unit supplies power to the heating control unit, and the second power supply supplies power to the temperature sensing unit. The SM192 storage module increases the data storage capacity, and stores data in the event of a power loss to the CR10. A portable lap top computer and a CSI *PC208* program are used to communicate with the CR10 and the SM192 units. The 22 sensors are monitored once every 6 hours. Due to the large amount of data that was generated by each sensor (100 data points per sensor per reading), sensor data was downloaded once a week.

4.4.3 Beta-97 Sensor Calibration

Sensor calibration was carried out using a modified pressure plate apparatus. Modifications were made to the calibration procedure that is described by Fredlund and Rahardjo (1993). The continuity between the water phase in the ceramic cylinder and the high air entry plate was provided by a thin layer of sand/bentonite soil slurry mixture (approximately 20 mm) placed on top of the high air entry disk. The sensors were embedded vertically into the soil mixture. The modified pressure plate apparatus was equipped with four sensor wire ports to allow calibration of four sensors simultaneously. The sensor calibration was carried out for 7 suction values, of which four were within the range of 2 kPa to 20 kPa. This was needed to assure required accuracy and sensitivity in the 0 kPa to 20 kPa matric suction range.

4.4.4 Beta-97 Field Installation

The 22 sensors were installed in the main cover area. The sensor installation elevations were determined based on the soil profile and included depths at 5 cm, 30 cm, 55 cm, 65 cm, 90 cm, 115 cm, and 150 cm from surface. The sensor installation into the till layer was carried out by excavating a pit from surface. The method of installing the sensors horizontally from an access manhole was deemed inappropriate for the till soil layer due to the significant inclusion of gravel/cobble size particles. The sensor installation holes were

carefully augured horizontally into the excavated face at predetermined elevations using a drill bit. The drill bit was smaller in diameter than the sensor tips. The sensors were installed into undisturbed soil (*Figure 4.6*). The excavated pit was subsequently filled and carefully compacted.

The sensor installation into the sand layer was carried out from the manhole "A". Horizontal holes, 0.5 m in length, were carefully excavated into the undisturbed sand layer using a combination of auguring and drilling tools *(Figure 4.7)*. Good sensor/sand contact was insured by coring a hole smaller in diameter than the sensor, approximately 50 mm long, at the end of each installation hole. A tamper was used to carefully tamp sand behind and around it. The entire length of the excavated hole was then backfilled with sand. Metal plates were bolted to the steel culvert, and caulking was used to seal the plate to prevent ingress of water into the manhole.

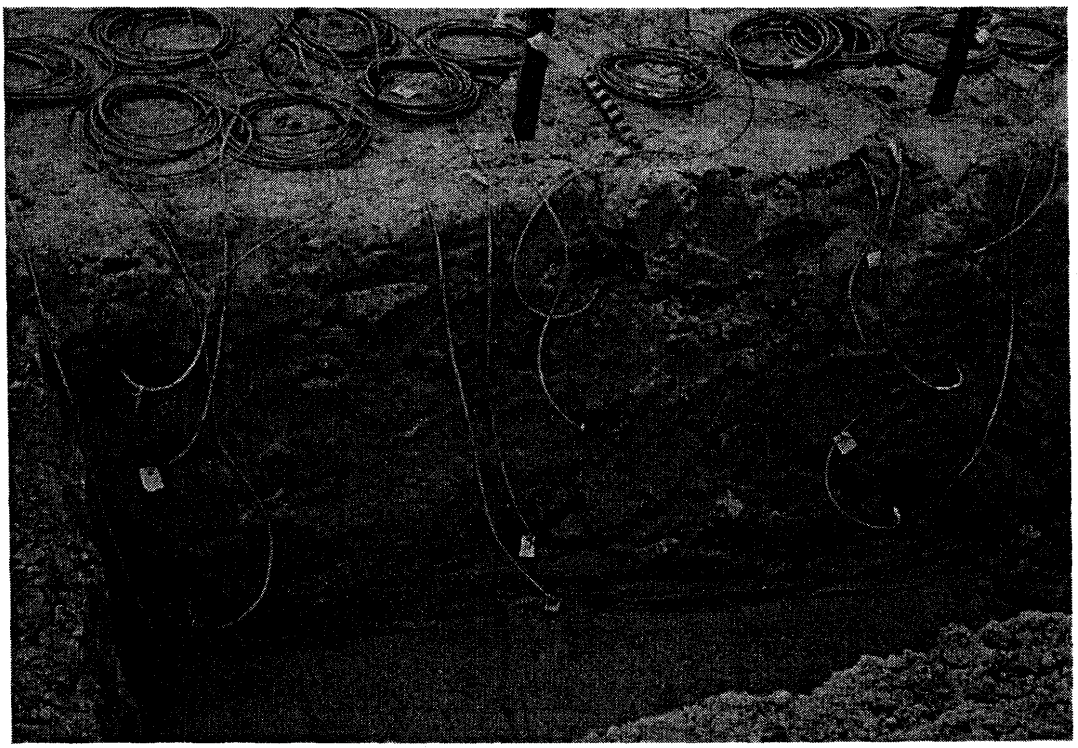

Figure 4.6 Photograph of Beta-97 sensors installed in brown till.

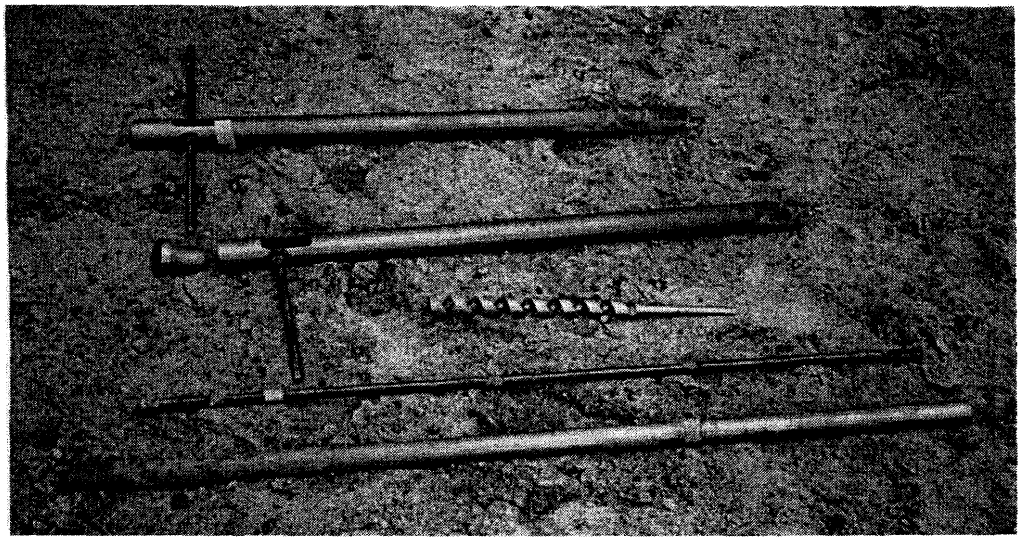

Figure 4.7 Photograph of sensor installation tools.

4.5 BOWEN RATIO INSTRUMENTATION

The Bowen Ratio Energy Balance approach is the most practical method for continuous recording of evaporation. The Bowen ratio system employed for this project site was a CSI Bowen Ratio Instrumentation initially designed by Bingham *et al.* (1987). Bingham *et al.* developed a system using a single cooled-mirror dew point hygrometer and physical sample integration to provide dew point temperature measurements at 1 meter and 2 meter heights, at 2 minute intervals. Two fine thermocouples are used to measure air temperature and temperature differences at these heights. The system is built with a minimum number of moving parts. It is solar powered and includes remote data collection capabilities. Therefore, it is suitable for longterm continuous monitoring at remote sites.

4.5.1 Bowen Ratio Instrumentation Field Installation

A CSI Bowen Ratio Instrumentation was installed at the HLTF on June 1998, and it operated for one month following the installation.

The Bowen Ratio Instrumentation was installed following the procedures outlined in the CSI "*Bowen ratio instrumentation instruction manual*" (Campbell Scientific 1998). The lower and upper support arms for air intakes and thermocouples were mounted approximately 0.5 m and 2.5 m above the ground, respectively (*Figure 4.8*). The heat flux plate was installed 8 cm below the soil surface. The soil heat flux thermocouples were installed 2 cm and 6 cm below the soil surface. The net radiometer was mounted approximately 0.5 m above the ground.

The data acquisition system consisted of a CSI CR21X datalogger and a SM716 storage module, a MSX30 solar panel, and a 12 volt deep cycle battery. Data was recorded every twenty minutes. A lap top computer and a CSI PC208 program are used to communicate and to program the CR10 and the SM176.

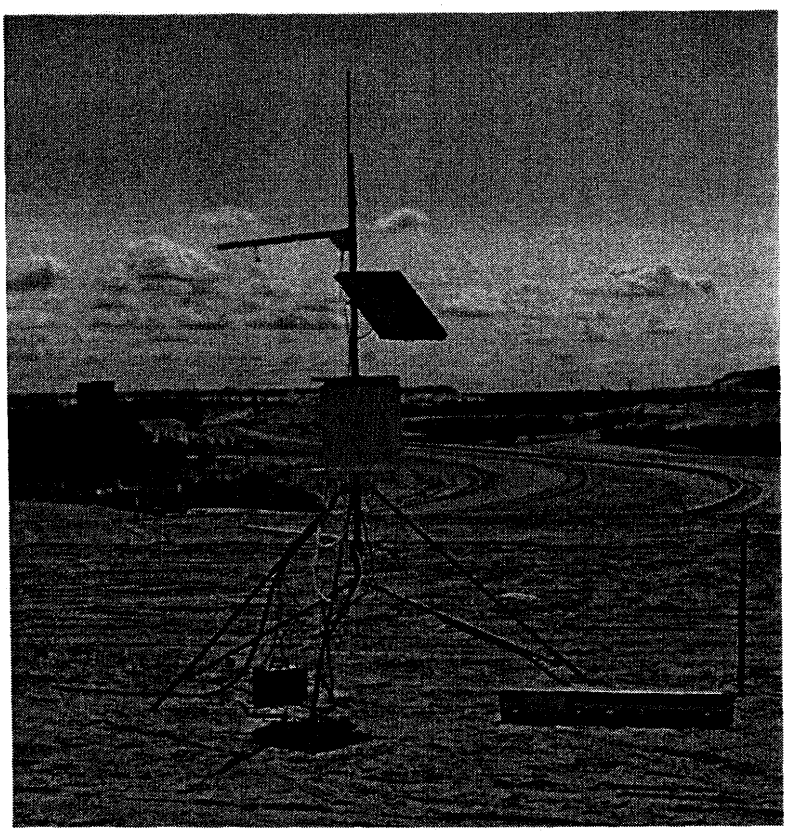

Figure 4.8 Photograph of the Bowen Ratio Instrumentation.

Chapter Five
PRESENTATION OF RESULTS

This chapter presents the results of the laboratory and field programs outlined in Chapters Three and Four. The laboratory and field test results that characterize the soil cover materials are presented in sections 5.1 and 5.2, and the detailed supporting data are found in Appendix C. The climatological data is presented in section 5.3, and the detailed climate data is included in Appendix D. The surface runoff, infiltration, and evaporation monitoring results are presented in sections 5.4, 5.5, and 5.6 respectively. The supporting runoff data are provided in a graphical format in Appendix E. The subsurface soil moisture monitoring results are found in section 5.7, and the corresponding data are provided in Appendix F.

5.1 LABORATORY TEST RESULTS

A summary of the laboratory test results is presented in this section, and the detailed data which supports the presentation of the results are found in Appendix C.

HBT AGRA Limited was contracted to carry out laboratory particle size analyses and soil moisture-density relationship tests on potential HLTF soil cover materials in July 1992. The Geotechnical Group of the University of Saskatchewan (U of S) was employed to establish soil-water characteristic curves for select soil cover materials in 1993. The current laboratory test results are therefore compared to the existing HBT AGRA Limited (1992) and U of S (1993) test results. Cluff Lake till properties are also presented for comparison (Ayres 1998)

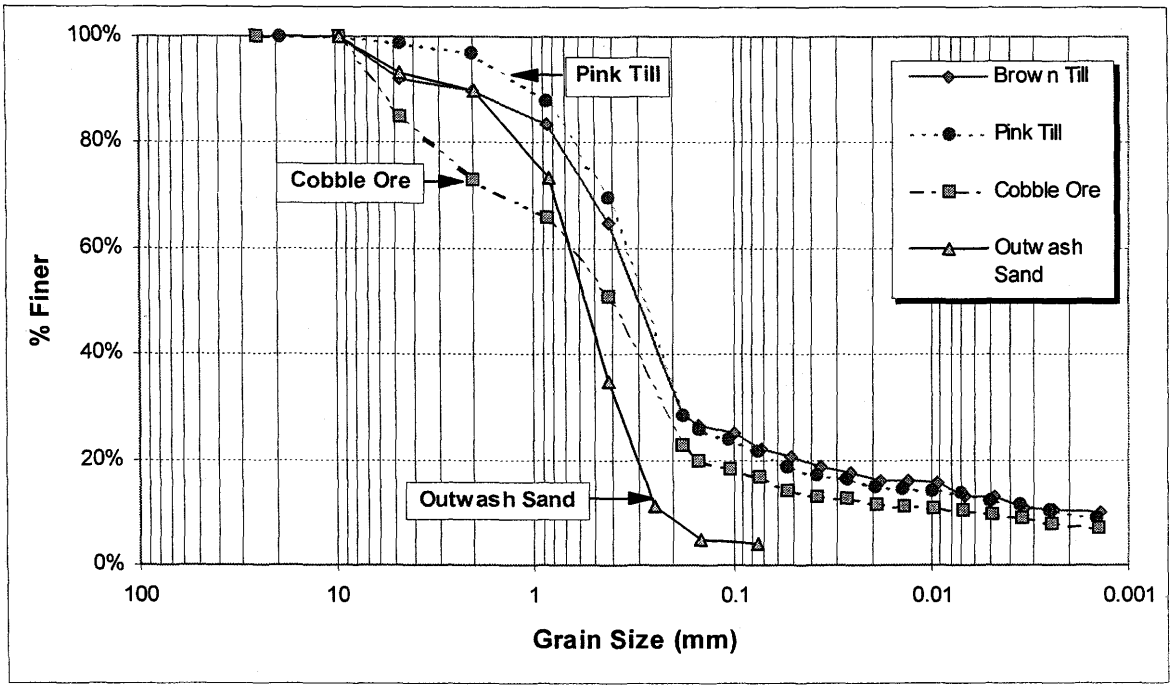

Figure 5.1 *Grain size distribution for Key Lake soils. Hydrometer test results for the brown till, pink till, and cobble ore and mechanical sieve test results for the outwash sand.*

5.1.1 Grain Size Distribution

The results of the particle size analysis using mechanical sieving and hydrometer test procedures are shown in *Figure 5.1*. *Table 5.1* provides a summary of grain size distribution based on standard particle size categories. In general, the grain size distribution test results compare well with those reported by HBT AGRA Limited (Appendix C.1). The hydrometer test results are also comparable to sieve test results.

The results of the laboratory particle size analysis indicates that the brown till has 20% to 23% fines (<75μm) content. This is higher than the expected 12% to 15% based on Cameco's report (Cameco 1995). The pink till was found have a fines content within the reported 15% to 20% range. There appears to be an insignificant difference in the grain size distribution between the brown till and the pink till.

A comparison of the Key Lake tills with the Cluff Lake till indicates that they both contain similar portion of fines (<75μm) with the Key Lake tills containing significantly higher clay contents (4% to 8% for the Cluff Lake till versus 13% for the Key Lake tills). The surficial Cluff Lake till that was sampled at 0.1 m depth has similar sand/gravel size particle distribution as the Key Lake tills. The Cluff Lake till samples at depths greater than 0.1 m is generally well graded with higher portions of coarse sand and gravel (*Figure 5.2*).

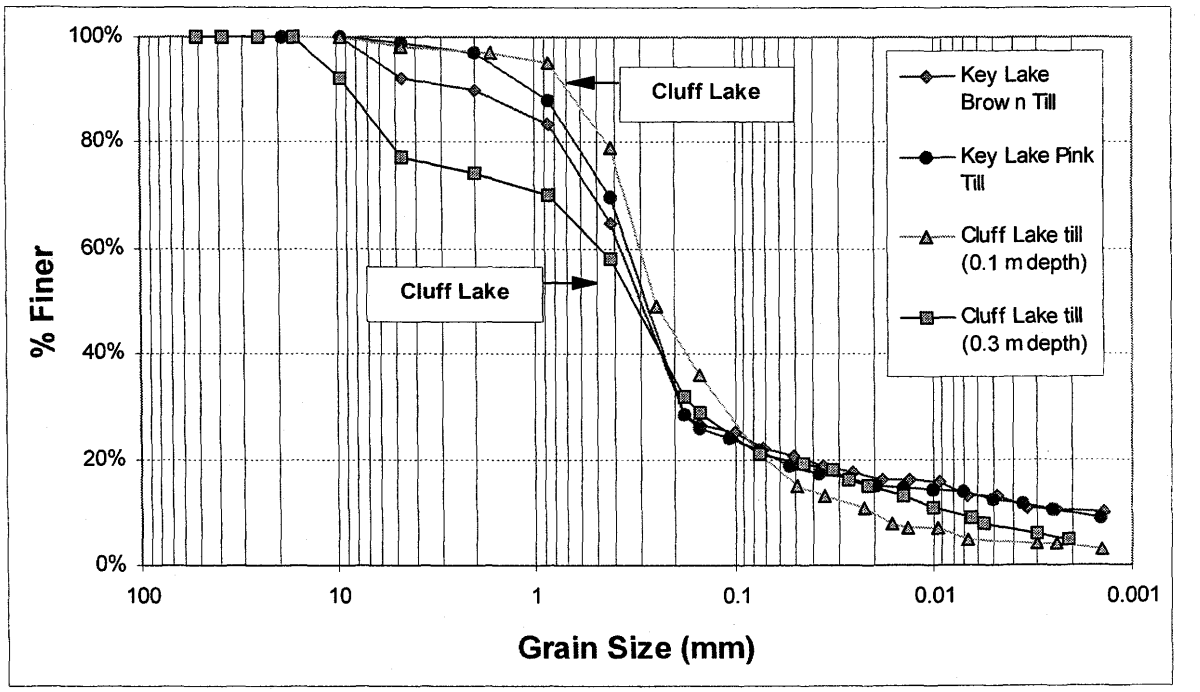

Figure 5.2 Key Lake till and Cluff Lake till grain size distribution.

5.1.2 Specific Gravity

The specific gravity tests results were as follows: 2.65 for outwash sand, 2.61 for brown till, 2.60 for pink till, and 2.62 for cobble ore. The test results are based on one test per soil type, and they are comparable to Cluff Lake till samples which ranged from 2.63 to 2.68 (Ayres 1998).

Table 5.1 Table of grain size distributions.

Soil Type	*Particle Size*	*Sieve Test*	*Hydrometer*	*HBT AGRA*
Outwash Sand	Gravel/Cobble (>4.75 mm)	7%		2%
	Sand (<4.75 mm)	89%		96%
	Silt (<75μm)	4%		2%
	Clay (<5μm)			
Brown Till	Gravel/Cobble (>4.75 mm)	12%	8%	10%
	Sand (<4.75 mm)	68%	70%	74%
	Silt (<75μm)	20%	9%	14%
	Clay (<5μm)		13%	
Pink Till	Gravel/Cobble (>4.75 mm)	3%	1%	7%
	Sand (<4.75 mm)	79%	77%	88%
	Silt (<75μm)	18%	9%	11%
	Clay (<5μm)		13%	4%
Cobble Ore	Gravel/ Cobble (>4.75 mm)	25%	15%	
	Sand (<4.75 mm)	62%	68%	
	Silt (<75μm)	13%	7%	
	Clay (<5μm)	n/a	10%	

5.1.3 Hydraulic Conductivity

The laboratory hydraulic conductivity test results are summarized in *Table 5.2* and are presented graphically in Appendix C.2. The tests were performed on specimens that were molded to approximate *in situ* field densities. The Cluff Lake till corresponds to a sample taken at 0.3 m depth; the hydraulic conductivity was determined based on laboratory consolidation test results (Ayres 1998).

Table 5.2 Hydraulic conductivity test results.

Soil Type	**Average Field Density**	**Test Density**	**Test Method**	**Hydraulic Conductivity (k_{sat})**
Outwash sand	1.79 g/cm^3	1.73 g/cm^3	Constant head	1.3 x 10^{-4} m/sec
Brown Till	2.02 g/cm^3	1.91 g/cm^3	Falling head	2.0 x 10^{-7} m/sec
Pink Till	1.78 g/cm^3	2.00 g/cm^3	Falling head	8.5 x10^{-8} m/sec
Cobble Ore	1.90 g/cm^3	1.90 g/cm^3	Falling head	2.6 x 10^{-8} m/sec
Cluff Lake Till	1.62 g/cm^3	1.88 g/cm^3	Consolidation	3 x 10^{-7} m/sec

5.1.4 Soil-water Characteristic Curves

The soil-water characteristic curves (SWCC) for four Key Lake soils is shown in *Figure 5.3.* It is apparent that all Key Lake soils tested possess very low air entry values (1 kPa to 2 kPa). They also reach residual water contents at low matric suction values (10 kPa to 30 kPa). The Cluff Lake till displays a noticeably higher air entry value (5 kPa).

The cobble ore exhibits a bi-modal behaviour. The cobble ore drains very much like a till material over the range of 0 kPa to 10 kPa and has a distinct air entry value. The curve subsequently flattens out, and the cobble ore begins to behave more like a clay material. The SWCC of the cobble ore attains a second air entry value starting at approximately 250 kPa. The cobble ore continues to drain gradually to a low residual water content, in a similar manner as the tills.

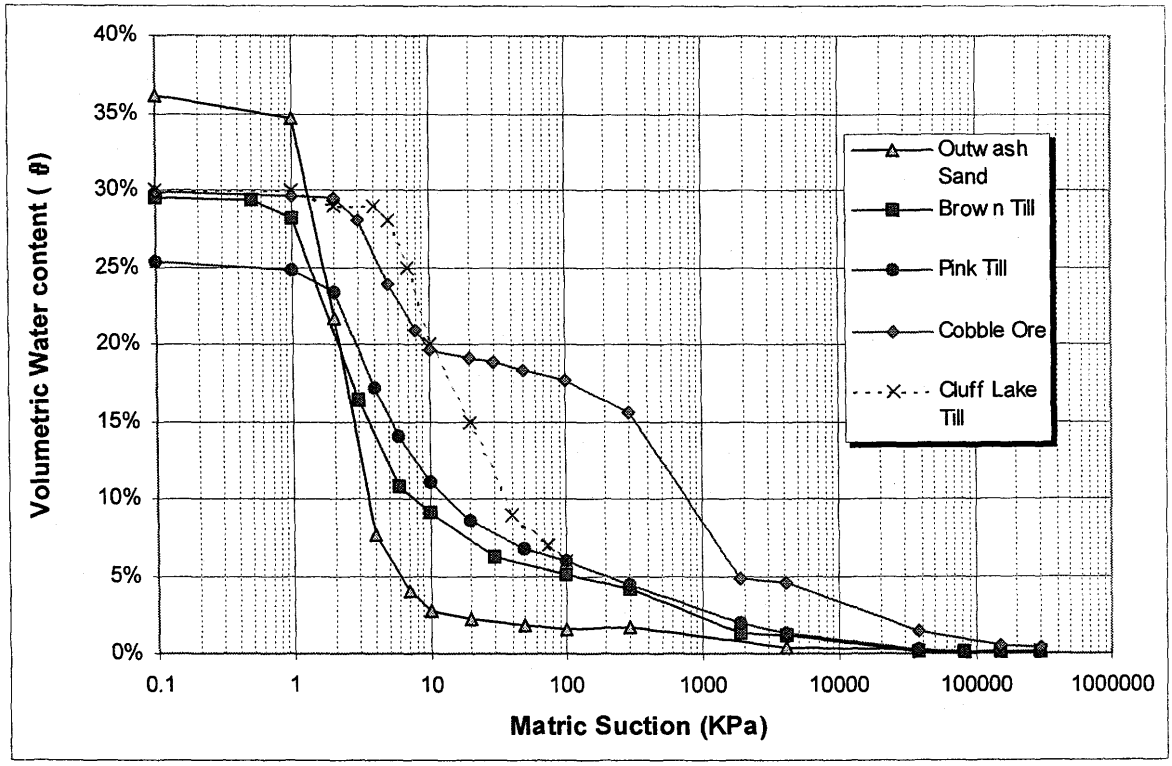

Figure 5.3 Soil-water characteristic curves for the Key Lake HLTF soil cover materials, and the Cluff Lake till @0.3 m depth.

The Effect of Initial Dry Bulk Density

The SWCC test specimens were carefully molded to represent actual field soil densities, however, the resulting specimen densities were found to be variable. The SWCCs for the outwash sand and brown till molded at different dry densities are shown in *Figures 5.4* and *5.5*. Swanson (1995) and O'Kane (1996) stated that as the soil density decreases, the soil porosity increases, and the air entry value of the soil decreases. O'Kane (1996) noted that compacting the till cover material increased the air entry valued from 10 kPa to 90 kPa.

The decrease in the air entry value with a decrease in soil density is not as apparent for the outwash sand samples (*Figure 5.4)*. The brown till samples, on the other hand, indicate a decrease in the air entry value with a decrease in soil density (*Figure 5.5)*.

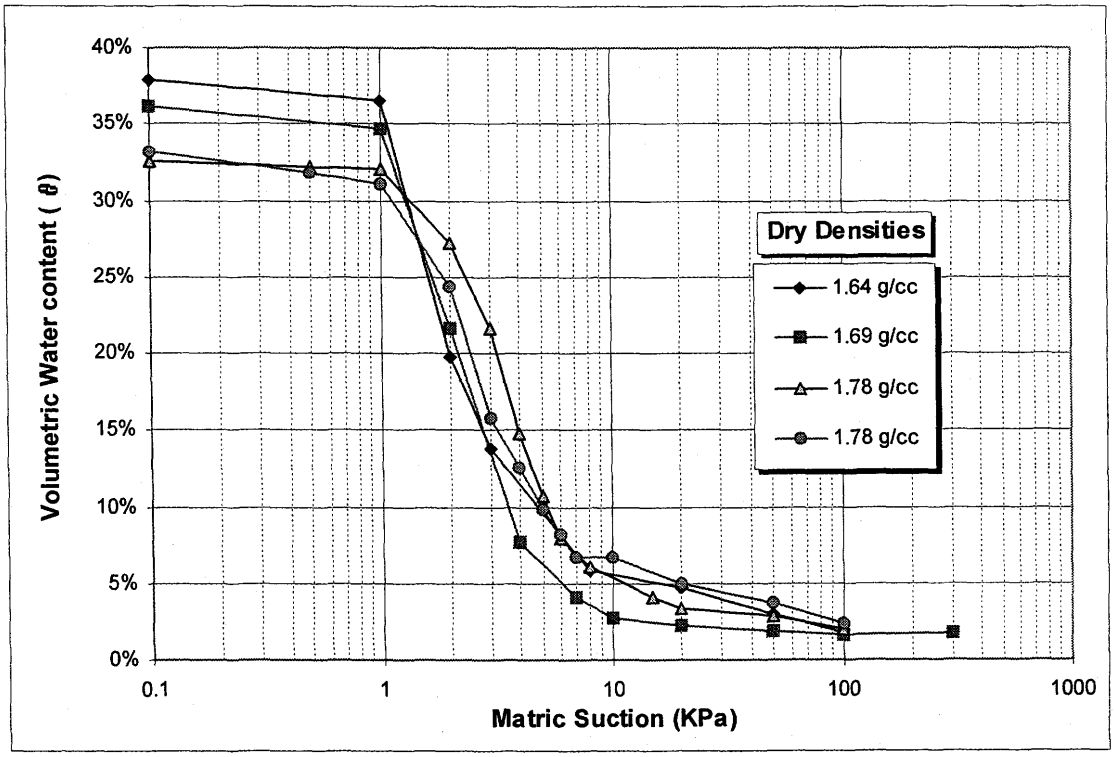

Figure 5.4 Outwash sand SWCCs at different molding densities.

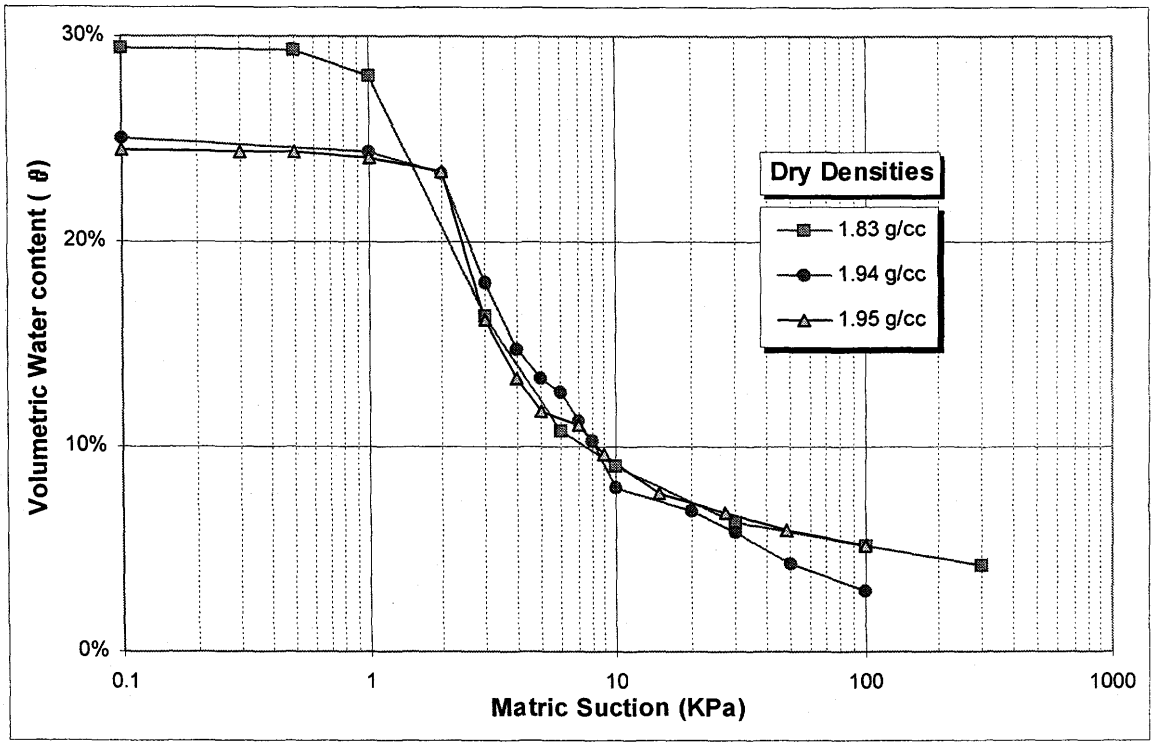

Figure 5.5 Brown till SWCCs at different molding densities.

The Effect of Coarse Gravel and Cobble Size Particles

The laboratory SWCC is determined using soil samples passing No. 4 sieve (4.75 mm). The significance of removing larger particles on the resulting SWCC was evaluated by Yazdani (1995). He determined the SWCC for soils containing various portions (15% to 65%) of gravel and cobble size particles. He subsequently refined the soils by passing the samples through a No. 4 sieve, and removing the gravel/cobble size portion. He established the SWCC for the fine portion, and compared the results against the SWCC for the unprocessed soil samples.

Yazdani (1995) concluded that the gravel/cobble size particles did not have a significant effect on the air entry value or the residual water content when the gravel/cobble size fraction constituted less than 65% of the total soil volume. All soils tested within the scope of this

research contain less than 65% volumetric coarse fraction. The cobble ore with the highest gravel/cobble portion contained 18%. Thus, it can be concluded that the SWCCs of tested soil specimens using material passing No. 4 sieve is representative of the unprocessed soil samples that contain gravel/cobble size particles.

It was previously noted that the molding density did not affect the air entry value or the shape of the SWCC. Therefore, a laboratory determined SWCC can be applied to actual field conditions. The saturated volumetric water content must be adjusted to reflect actual *in situ* densities.

The Effect of Hysteresis

The effect of hysteresis on the SWCC was not investigated. O'Kane (1996) provides a thorough discussion on the effect of hysteresis on the SWCC of compacted till cover material. He concluded that the effect of hysteresis can be ignored since the covers maintained high degree of saturation throughout the monitoring period with very little evidence of hysteresis. O'Kane observed that the compacted till cover did not experience the full extent of its hysteretic loop.

The HLTF compacted till cover, on the other hand, remained mostly under gravity drained moisture conditions. Although the effects of hysteresis was not investigated, it may be of some significance for this cover design.

5.1.5 Compaction Testing

The results of the standard laboratory compaction tests for brown till are shown in *Figure 5.6*. The results obtained by HBT AGRA Limited (1992) yield a higher value of maximum dry density than what was determined in the laboratory: 2.01 g/cm^3 versus 1.95 g/cm^3. The difference between the two results is within 3%.

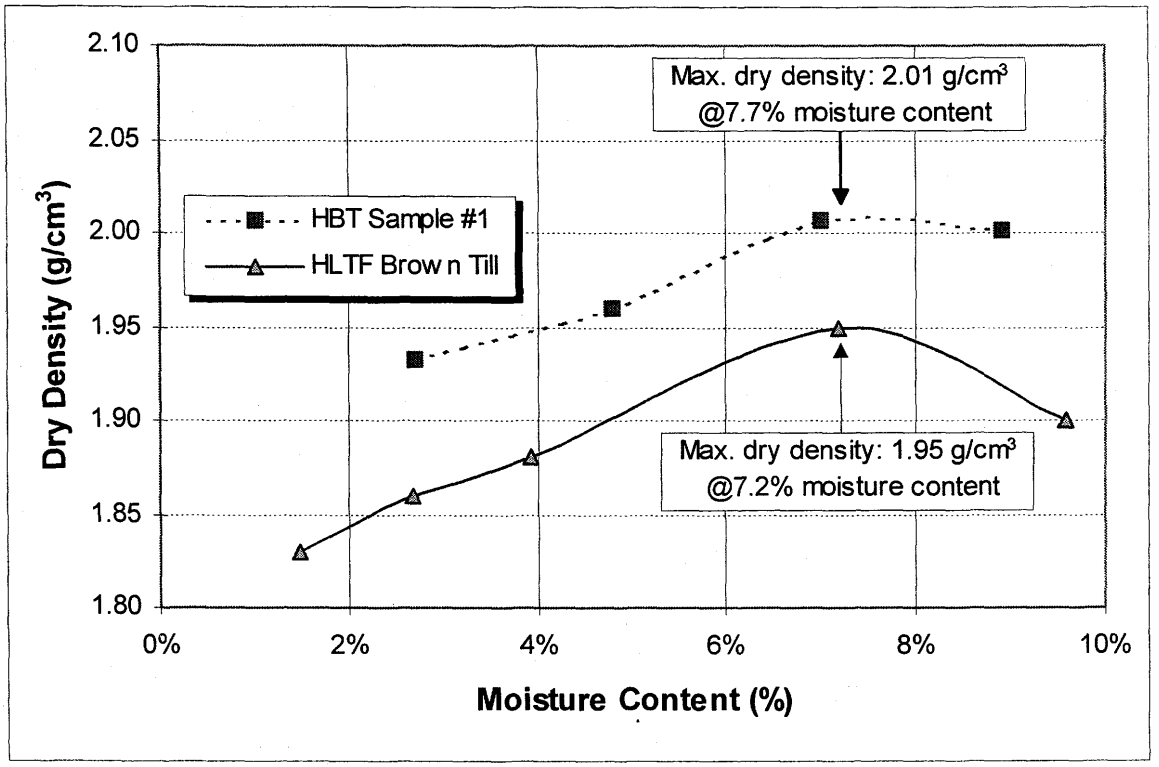

Figure 5.6 Laboratory compaction test results for the Key Lake brown till. HBT AGRA Limited results indicate slightly higher maximum dry density.

5.2 FIELD TEST RESULTS

5.2.1 *In Situ* Density

The *in situ* density tests were carried out using a modified water replacement technique. The results are tabulated in *Table 5.3*. *Table 5.4* provides a comparison of the *in situ* density test results with estimates of *in situ* densities measured on samples taken during the sonic drill sampling program, and the maximum dry density results from the moisture-density relationship tests (HBT AGRA Limited 1992). The modified water replacement technique and the sonic drill sampling methods provided a reasonable estimate of the *in situ* soil densities when compared to the HBT AGRA Limited moisture density relationship results. The pink till *in situ* density was found to be significantly lower; this cover material was not compacted to the design density after it had been excavated to make modifications to the underlying lysimeter.

Table 5.3 In situ density test results.

Soil Type	Test Pit Volume (cm^3)	*In Situ* Density (g/cm^3)
Brown Till	8,000 cm^3	2.13
Brown Till	8,220 cm^3	2.16
Brown Till	8,300 cm^3	2.07
Outwash Sand	4,000 cm^3	1.79

Table 5.4 In situ density of cover materials determined using various methods.

Soil Type	*In Situ* Density Test (g/cm^3)	Sonic Drill Sampling Density (g/cm^3)	HBT Maximum Dry Density (g/cm^3)
Brown Till	2.12	1.93	2.04
Outwash Sand	1.79	1.82	1.75
Pink Till	1.78	n/a	1.90
Cobble Ore	n/a	1.90	n/a

5.2.2 *In Situ* Hydraulic Conductivity

The *in situ* hydraulic conductivity was estimated using the Guelph Permeameter. The Guelph Permeameter method provides a measurement of a *field-saturated hydraulic conductivity*. The field-saturated hydraulic conductivity is defined as the hydraulic conductivity of a porous medium containing entrapped air, and it can be a factor of two or more below the saturated hydraulic conductivity (Reynolds and Elrick, 1985). For flow in most unsaturated soils, the field-saturated hydraulic conductivity is considered to be more representative given that positive pore pressures do not persist long enough for the entrapped air to dissolve. Reynolds and Zebchuk (1996) and Joshi (1997) concluded that the Guelph Permeameter method yielded reliable estimates of field-saturated hydraulic conductivity in fine grained soils, uniform silty clay, and glacio-lacustrine silty clay soils.

The Guelph Permeameter was used to estimate the field-saturated hydraulic conductivity of the brown till, pink till, and outwash sand layers. The expected hydraulic conductivity was within the measurement limits for the Guelph Permeameter (10^{-4} m/s to 10^{-8} m/s). One attempt in the outwash sand layer and over twenty attempts in the brown till and pink till layers found this method to be inadequate for the type of soils tested at the HLTF.

In the outwash sand layer, the water level in the reservoir dropped too rapidly to enable any reasonable measurements. The anticipated hydraulic conductivity of the outwash sand layer was at the upper limit of the measurement range. In the brown till and pink till layers, the water coming out of the *water outlet tube* eroded the walls of the well. This erosion caused the hole to slowly collapse around the water outlet tube, and eventually, the water flow out of the tube was completed blocked off.

A *well stabilizer cylinder* was constructed of fine stainless steel mesh by the staff at the University of Saskatchewan Geotechnical Laboratory. The well stabilizer cylinder was inserted into augured holes to prevent erosion. This modification resulted in limited success. The accumulation of fines at the bottom of the meshed cylinder caused uncertainties in the

results. Three reasonable test results were achieved in the brown till layer yielding a field-saturated hydraulic conductivity values of 2.3×10^{-7} m/s, 3.4×10^{-6} m/s, and 6.5×10^{-6} m/s with an arithmetic mean of 3.3×10^{-6} m/s. The laboratory determined hydraulic conductivity for the brown till is 2.0×10^{-7} m/s.

5.2.3 Soil Profile Sampling

Sonic drill was used to drill and sample a 4.5 m deep test hole. The hole was drilled in the vicinity of a thermistor string installation and a neutron probe access hole. The results are tabulated in *Table 5.5*. The soil profile through the soil cover system constructed above the leached cobble ore was found to consist of more than 60 cm of outwash sand layer overlain by 60 cm of compacted brown till layer. The facility was graded at 2% sloping towards the collection ditch. The extraneous material underlying the outwash sand layer may have been additional soil placed to achieve the needed surface gradient.

Table 5.5 HLTF soil profile sampling results.

Soil Type	Depth from Surface	Soil Profile Thickness	Average dry density
Brown Till	0 to 60 cm	60 cm	1.93 g/cm^3
Outwash Sand	60 to 137 cm	77 cm	1.82 g/cm^3
Sand (green in colour)	137 to 187 cm	50 cm	1.69 g/cm^3
Brown till	187 to 259 cm	72 cm	1.85 g/cm^3
Sand (visually determined))	259 to 295 cm	36 cm	1.90 g/cm^3
Cobble Ore	295 to 450 cm	155 cm	1.90 g/cm^3

5.3 WEATHER PARAMETER MONITORING RESULTS

The climatological data reliability was established by comparing results with neighboring weather stations: the Environment Canada *Key Lake weather station* located approximately 10 km from the HLTF (Cameco 1997b, 1998b); and the *Cluff Lake weather station* located approximately 265 km north-west of the HLTF (Ayres 1998). The reliability of the Cluff Lake weather station data was evaluated by Ayres (1998) through comparison with historical regional data from Fort Chipewyan, Alberta (110 km west-northwest of Cluff Lake), and Fort Smith, Northwest Territories (190 km north-northwest of Cluff Lake). A monthly and daily summary of the HLTF climatological data for 1996 and 1997 are found in Appendix D.

5.3.1 Precipitation

The monthly precipitation statistics from 1977 to 1997 for the *Key Lake weather station* is provided in *Figure 5.7*. The monthly maximum, monthly minimum, and monthly average precipitation statistics are plotted to illustrate the variability of summer precipitation. Precipitation occurs mainly as snow during the months of October to April, and as rain from May to September. The average annual precipitation is 456 mm, of which 166 mm is winter precipitation (i.e. October to April), and 293 mm is summer precipitation (i.e. May to September). Approximately 65% of annual precipitation is attributed to rainfall.

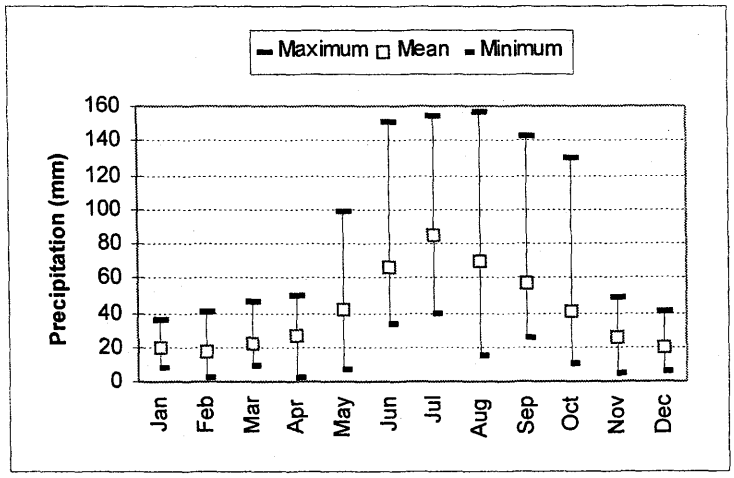

Figure 5.7 Key Lake precipitation statistics from 1977 to 1997.

The mean monthly precipitation statistics from 1981 to 1996 for Key Lake and Cluff Lake are shown in *Figure 5.8.* Key Lake and Cluff Lake received similar mean monthly precipitation during this fifteen year period. The Key Lake 1996 monthly precipitation plot shows 1996 to have received an average amount of precipitation throughout the year. In contrast, the precipitation recorded for 1997 had higher than average summer precipitation, and new monthly records were set for July and September during this year.

A comparison of the 1996 precipitation statistics for Key Lake and Cluff Lake illustrates the highly variable nature of summer precipitation typical of this region (*Figures 5.9* and *5.10*). In 1996, Cluff Lake recorded 402 mm of summer precipitation compared to 276 mm for Key Lake. Approximately 60 mm of this discrepancy is attributed to two heavy rain storms in the region that occurred on September 22nd and 23rd. Another source of discrepancy is the loss of the *Key Lake weather station* precipitation data over a 9 day period in August when Cluff Lake recorded 45 mm of precipitation. In 1997, both locations recorded similar amounts of summer precipitation. Cluff Lake recorded 491 mm versus 503 mm at Key Lake.

A comparison of the *Key Lake weather station* and the HLTF weather station data also indicates site variability due to high intensity summer rainfalls. The discrepancy for August 1996 is mainly due to the loss of the *Key Lake weather station* precipitation data when approximately 50% of the monthly total rainfall occurred in the region. A close examination of the daily precipitation data for July 1997 attributes the variance to two high intensity rainfall events.

It should also be noted that in general, the *Key Lake weather station* records higher rainfall than the HLTF weather station (478 mm versus 435 mm respectively for 1997). This is due to a *standard storage rain gauge* in use at Key Lake versus a *tipping bucket rain gauge* employed at the HLTF. It has been noted that tipping bucket rain gauges generally under-record during heavy rainfall events (Dingman 1994). Some daily and monthly variations are also attributed to the time of observation. At the *Key Lake weather station*, the total daily precipitation is recorded at 8:00 a.m. versus midnight at the HLTF weather station.

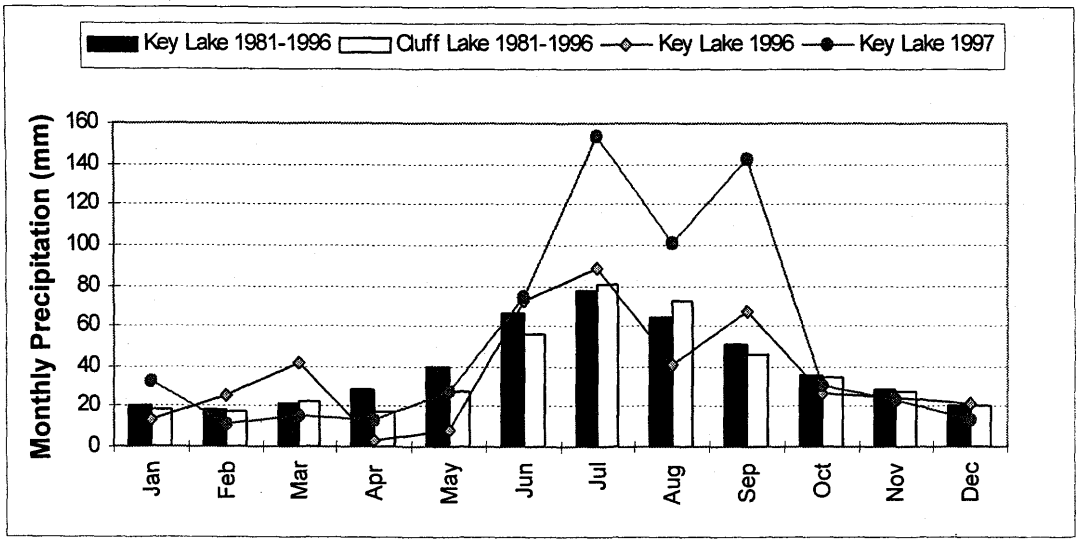

Figure 5.8 15 year monthly precipitation statistics.

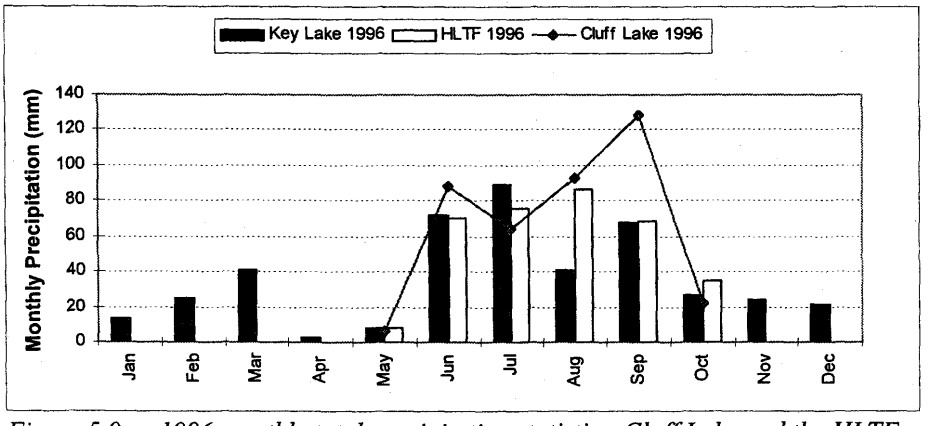

Figure 5.9 1996 monthly total precipitation statistics. Cluff Lake and the HLTF only recorded summer precipitation.

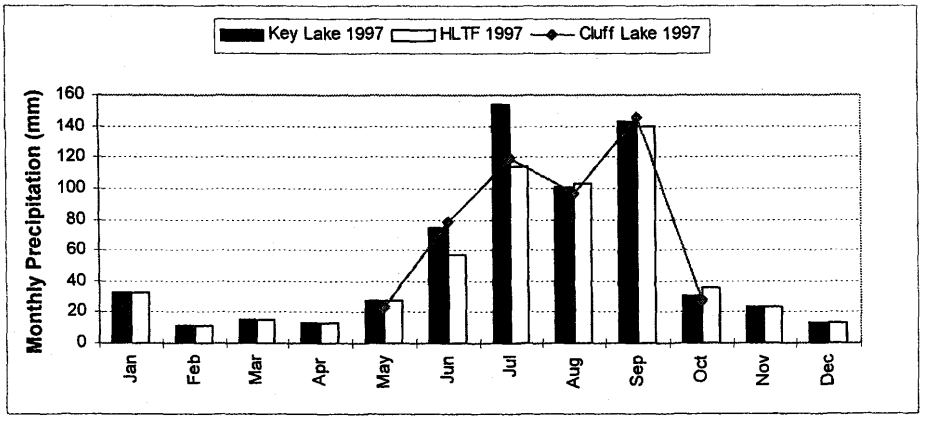

Figure 5.10 1997 monthly total precipitation statistics. Cluff Lake and the HLTF only recorded summer precipitation.

5.3.2 Air Temperature

The *Key Lake weather station* mean monthly air temperature statistics from 1981 to 1996 are shown in *Figure 5.11.* The minimum mean temperature occurs in January (-22.8^{0}C), while the maximum mean temperature occurs in July (15.6^{0}C). The average mean annual air temperature for the period 1981 to 1996 is -2.7^{0}C, versus -0.6^{0}C for Cluff Lake. Although Cluff Lake is located north-west of Key Lake, fifteen year climate data indicates Cluff Lake to be consistently warmer throughout the year. The air temperature at Cluff Lake is on average 2.8^{0}C higher during winter months and 1.5^{0}C higher during summer months than in the Key Lake region.

The mean annual air temperatures at Key Lake for 1996 and 1997 are -3.9^{0}C and -1.6^{0}C, respectively. Lower than average temperatures were recorded for January, March, November, and December, 1997. *Figure 5.12* provides 1997 monthly mean air temperature comparisons for Key Lake, Cluff Lake, and the HLTF. In general, these three sites appear to have similar mean monthly air temperature trends with Cluff Lake recording consistently higher mean monthly air temperatures.

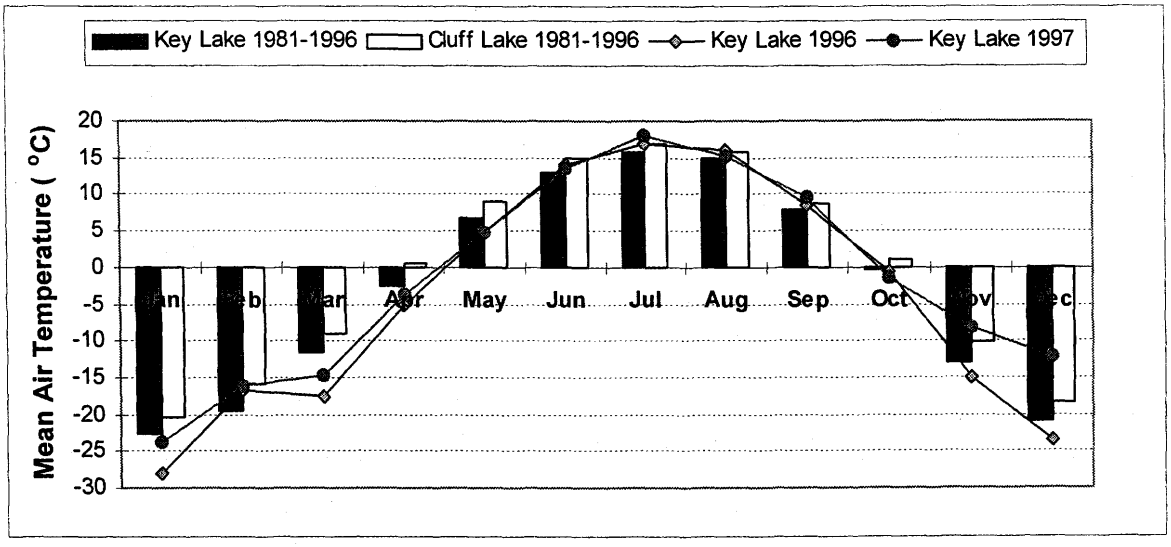

Figure 5.11 Monthly mean air temperature statistics.

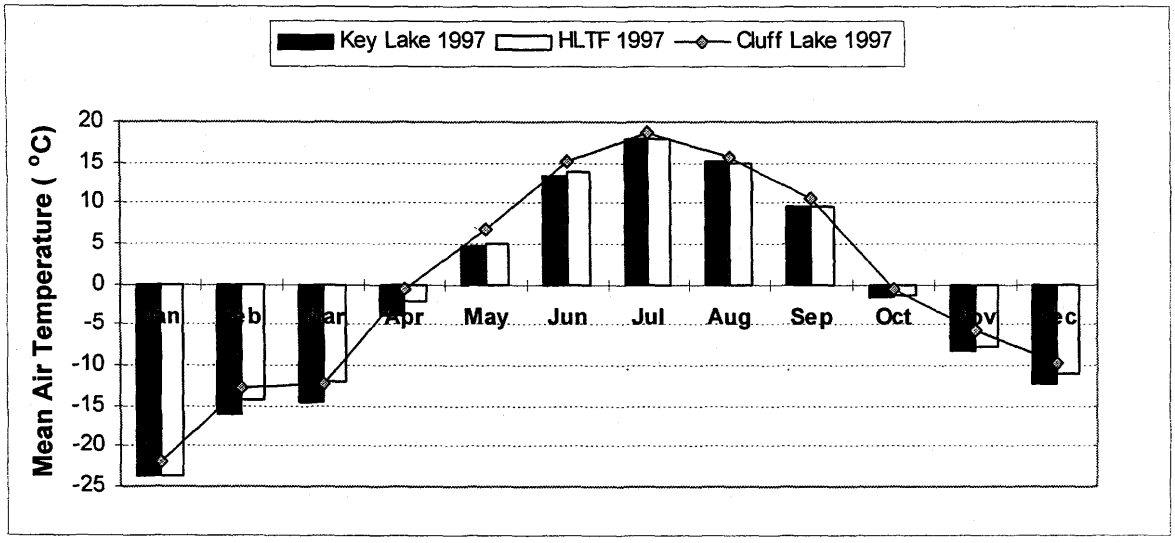

Figure 5.12 1997 monthly mean air temperature statistics.

5.3.3 Relative Humidity

The HLTF 1996 and 1997 relative humidity data indicated instrument error during the 1997 monitoring year. Higher than actual relative humidity levels were recorded due to the drifting of the instrument. Relative humidity values greater than 100% were noted from April to December, 1997. *Figure 5.13* provides a comparison of Cluff Lake and the HLTF relative humidity data. The relative humidity data was corrected to normalize higher than 100% relative humidity, and to adjust to levels that are comparable to what was recorded at Cluff Lake for the same monitoring period. A correction factor of 0.925 was assumed from April to August, and December; a correction factor of 0.95 was assumed from September to November.

The daily mean relative humidity for the HLTF and Cluff Lake follow similar trends (*Figure 5.14*). The mean monthly relative humidity is lowest during April and May (59% at the HLTF and 56% at Cluff Lake), and highest during October and November (87% at the HLTF and 89% at Cluff Lake) with the annual mean relative humidity of approximately 73% at both sites.

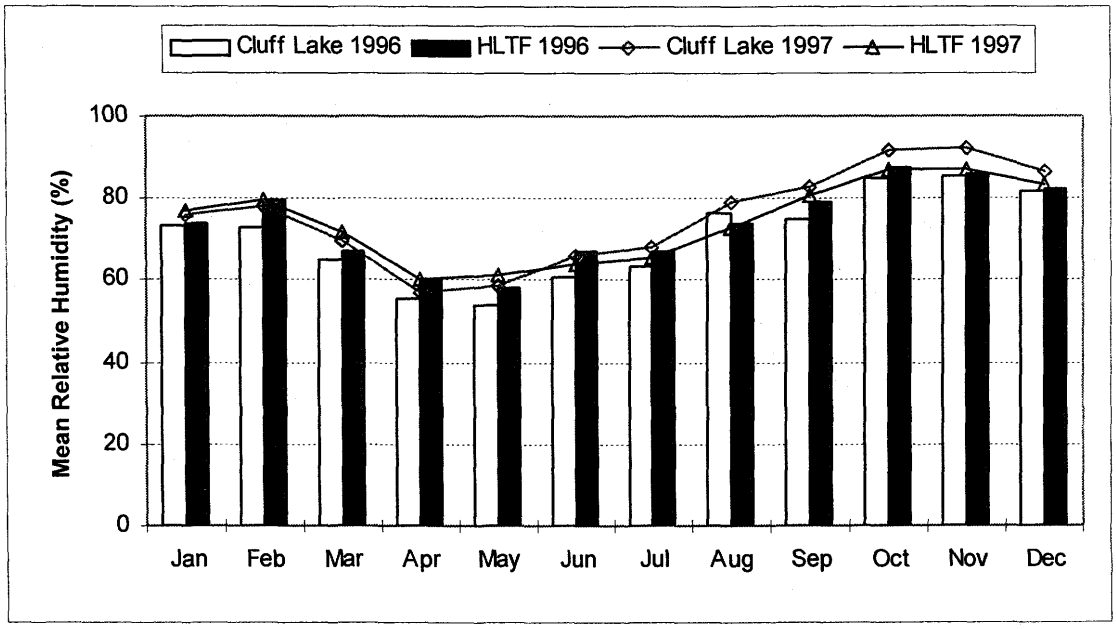

Figure 5.13 1996 and 1997 monthly mean relative humidity.

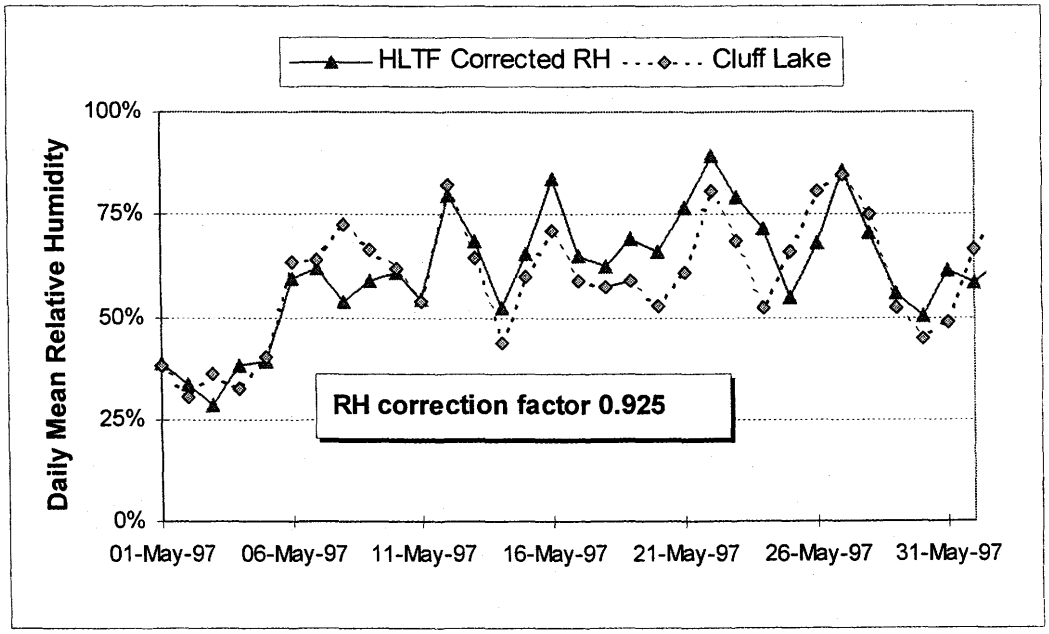

Figure 5.14 Corrected daily mean relative humidity for May 1997.

5.3.4 Wind Speed

Wind speed is highly dependant on the height of the instrument installation and the surrounding topography. *Figure 5.15* provides a comparison of mean daily wind speed for four summer months at three sites. The Key Lake weather station monitors wind speed 10 m above ground, as well as at the evaporation pan located within a small clearing in a sheltered treed area. The HLTF weather station monitors wind speed at approximately 3 m above ground, and at less than 1 m above the ground at the evaporation pan. The HLTF weather station and the evaporation pan are located in an open approach to a local topographic high. The Cluff Lake station monitors wind 3 m above ground in the middle of a cleared area.

The Key Lake weather station annual mean wind speed for the period 1993 to 1997 is 12.2 km/hr versus 9.7 km/hr at the HLTF weather station, and 8.6 km/hr at the HLTF evaporation pan. The 1996 and 1997 annual mean wind speed is 6.4 km/hr for Cluff Lake and 3.4 km/hr for Key Lake evaporation pan wind data. Ayres (1998) stated that the Cluff Lake wind speed data was significantly lower than the reported regional wind speed due to the difference in the height of the wind monitoring installation. The historical annual mean wind speed is reported to be 11 km/hr for Fort Chipewyan and Fort Smith (Ayres 1998).

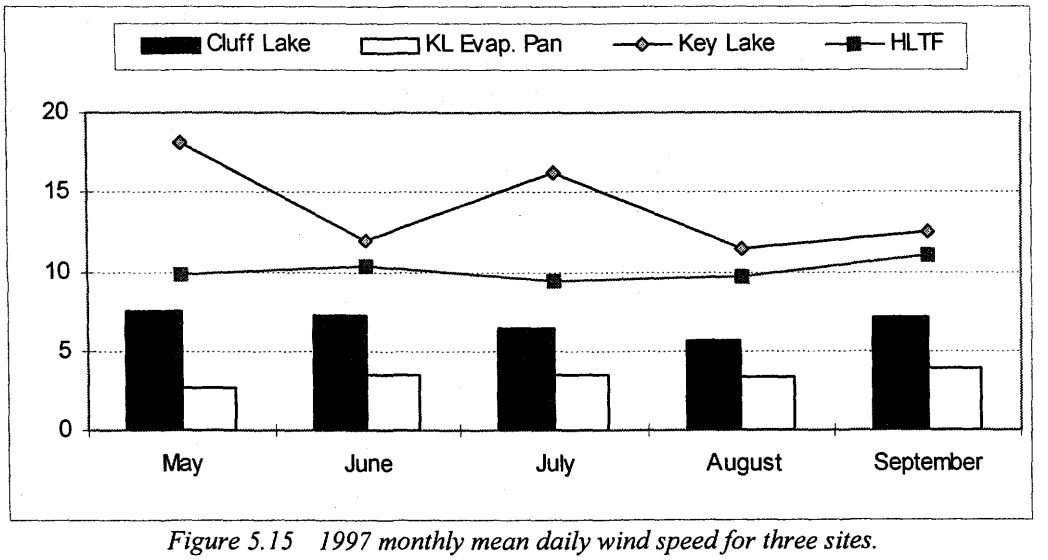

Figure 5.15 1997 monthly mean daily wind speed for three sites.

5.3.5 Net Radiation

The recorded net radiation data indicated that Cluff Lake receives a significantly higher level of net radiation than Key Lake, particularly during summer months (*Figure 5.16*). The annual average mean net radiation is 3.9 MJ/m^2 per day at Cluff Lake versus 2.2 MJ/m^2 per day at the HLTF. A comparison of the Cluff Lake net radiation data to the regional historical net radiation data found it to be representative (Ayres 1998). An analysis of the *Key Lake weather station* pan evaporation data has suggested that the HLTF net radiation is seriously underestimated (section 5.6.3). The radiometers have since been sent to the manufacturer for maintenance and calibration.

A correction factor of 1.58 was applied to the HLTF daily net radiation data from mid April to mid October to adjust the levels to the levels recorded at Cluff Lake over the same period. The adjusted net radiation data resulted in an annual average mean of 3.4 MJ/m^2 per day. The corrected net radiation data better reflects the recorded regional net radiation levels.

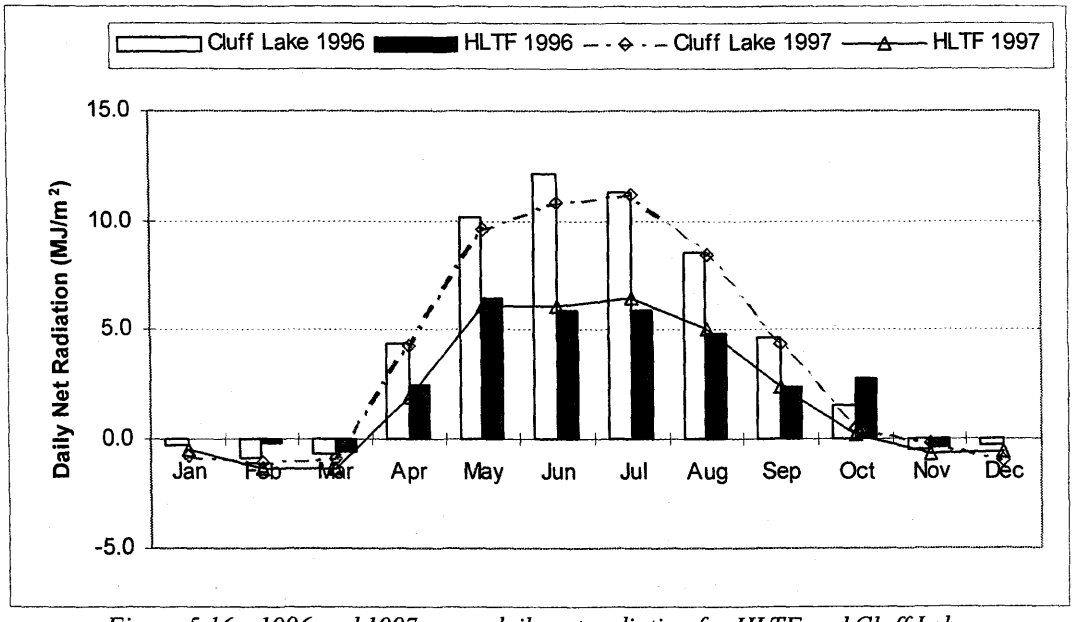

Figure 5.16 1996 and 1997 mean daily net radiation for HLTF and Cluff Lake.

5.3.6 Snow Survey

The results of the 1996 and 1997 spring snow surveys at the HLTF are summarized in *Table 5.6*. The snow surveys were carried out on March 20th, 1996 and March 27th, 1997.

The measured snow depths for March 1996 ranged from 241 mm to 432 mm with an arithmetic mean depth of 326 mm. The snow densities ranged from 210 kg/m^3 to 400 kg/m^3, with an arithmetic mean density of 290 kg/m^3.

The measured snow depths for March 1997 ranged from 178 mm to 305 mm with an arithmetic mean depth of 247 mm. Snow densities ranged from 200 kg/m^3 to 270 kg/m^3 with an arithmetic mean density of 240 kg/m^3. A heavy rain two days prior to carrying out the snow survey resulted in numerous ice lenses throughout the area making coring and core retrieval difficult. The actual snow densities may have been higher than the results indicate.

The Cluff Lake snow surveys resulted in an average snow density of 255 kg/m^3 for 1996 (versus 290 kg/m^3 for the HLTF), and 210 kg/m^3 for 1997 (versus 240 kg/m^3 for the HLTF). The estimated snow densities are within the expected range for northern Manitoba and southern Saskatchewan (Gray 1973; Ayres 1998).

Table 5.6 1996 and 1997 snow survey results.

	HLTF	**Cluff Lake**	**HLTF**	**Cluff Lake**
Survey dates	March 20th, 1996	March 20th and 28th, 1996	March 27th, 1997	March 18th and April 1st, 1997
Measured snow depths	241 to 432 mm	230 to 580 mm	178 to 305 mm	400 to 490 mm
Mean snow depth	326 mm	460 mm	247 mm	445 mm
Measured snow densities	210 to 400 kg/m^3	208 to 339 kg/m^3	200 to 270 kg/m^3	187 to 234 kg/m^3
Mean snow density	290 kg/m^3	255 kg/m^3	240 kg/m^3	210 kg/m^3

Snowfall Partitioning

Table 5.7 provides a summary of snowfall partitioning for 1996 and 1997. The total snowfall precipitation is derived from the Key Lake weather station precipitation records from October of the previous year to April of the reported year. The snow survey results have been converted to equivalent millimeters of rain.

The spring snow survey results have indicated that approximately 40% to 50% of the snowfall is lost to sublimation and drifting throughout the winter.

Table 5.7 Spring snow survey results for the HLTF.

	Spring 1996	***Spring 1997***
Total snowfall at Key Lake weather station	**160 mm**	**120 mm**
HLTF spring snow survey results		
Mean snow pack depth	326 mm	247 mm
Mean snow pack density	290 kg/m^3	240 kg/m^3
mm rain equivalent	**95 mm**	**59 mm**
% of total snowfall	59%	49%

5.4 SURFACE RUNOFF

The surface runoff monitoring results are presented in this section. The surface runoff monitoring system consists of a single point distance measuring system which estimates the flow depth across the collection culvert every 30 seconds. The measured flow depths are converted into instantaneous flow volumes. A 15-minute intensity precipitation hyetograph and the corresponding surface runoff hydrograph for two high intensity short duration rainfall events are illustrated in *Figure 5.17*. A plot of precipitation and surface runoff for three low intensity long duration rainfall events are shown in *Figure 5.18*. *Figures 5.17* and *5.18* illustrate the sensitivity of the HLTF surface runoff monitoring system which is capable of detecting small changes in the flow depth. The scatter in the runoff hydrograph indicates that the turbulent nature of the water flow along the length of the open culvert is being detected by the flow depth sensor.

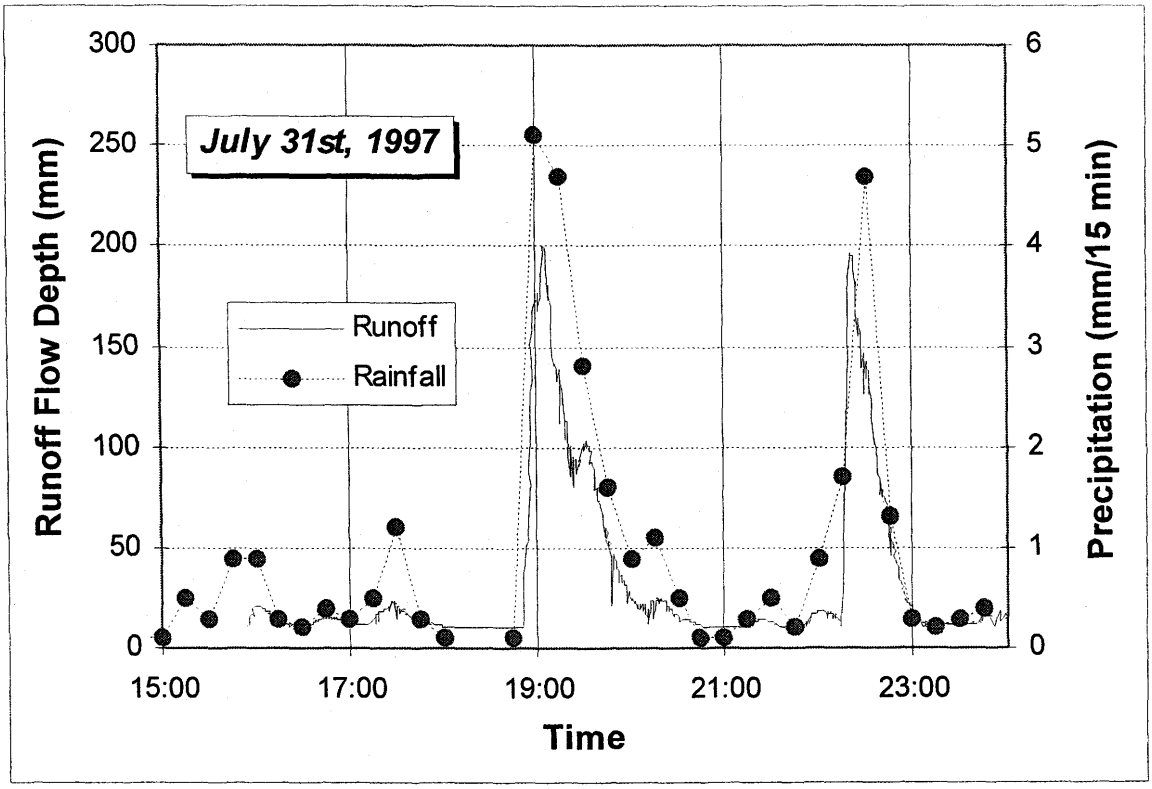

Figure 5.17 Surface runoff hydrograph for high intensity rainfall events. The surface runoff is measured every 30 seconds. Precipitation is recorded in 15 minute intensities.

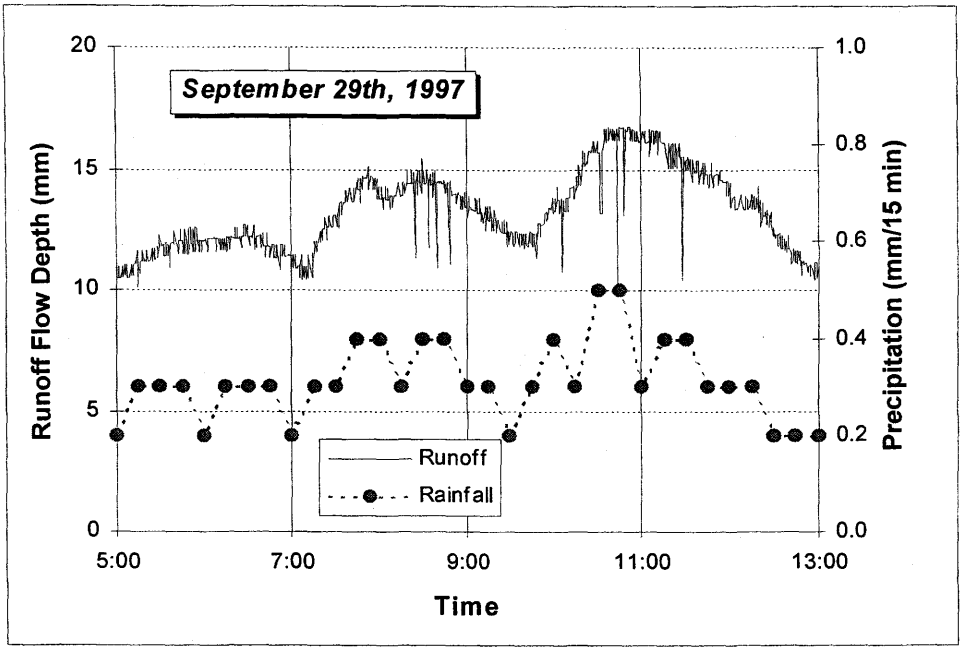

Figure 5.18 Surface runoff hydrograph for low intensity rainfall events.

Figure 5.19 provides a comparison of the monthly total precipitation versus the monthly total surface runoff. 8.1% (32 mm) of the recorded 1997 summer precipitation (i.e. 387 mm for June to mid-October) partitioned into surface runoff. Surface runoff was not monitored during May. *Figure 5.19* also indicates that surface runoff is governed by factors other than the total precipitation. For the months of July and September with similar precipitation totals, 15.8 mm (14%) of runoff was generated in July, versus 8.3 mm in September.

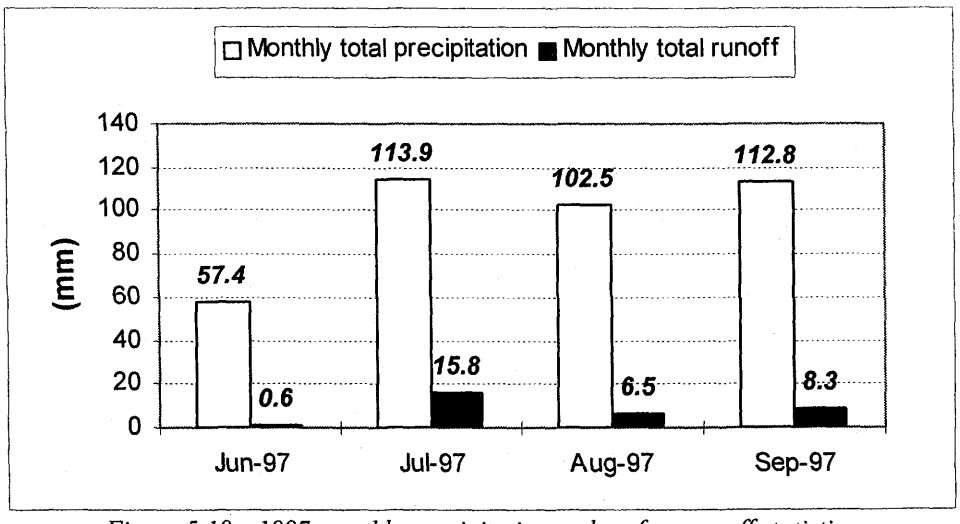

Figure 5.19 1997 monthly precipitation and surface runoff statistics.

5.4.1 Surface Runoff Characteristics

The surface runoff is thought to be governed by surface soil properties, surface topography, precipitation intensity and duration, and antecedent soil moisture conditions. For the HLTF with unchanging soil properties and topography, the generation of surface runoff is therefore governed solely by the variation in the precipitation intensity and duration, and antecedent soil moisture conditions.

The surface runoff data analysis and interpretation along with a discussion on the surface runoff characteristics is provided in Section 6.3.

5.4.2 Surface Runoff during Spring Snow Melt

The surface runoff that was generated during spring snow melt was monitored in April, 1997. The spring snow pack survey indicated that there was 59 mm (rain equivalent) of snow at the end of March, just prior to the onset of spring snow melt. The snow pack melted over a six day period in mid April. 2.2 mm of surface runoff was recorded during this period (*Table 5.8*). The actual snow melt runoff, however, ws expected to be higher than the recorded values. The collection culvert was leaking at one location during this period, and therefore, not all the snow melt runoff was detected by the sensor.

Table 5.8 Summary of snowfall partitioning.

	mm rain equivalent
Total snowfall at the Key Lake weather station (October 1996 to March 1997)	120 mm
Snow cover at the HLTF prior to snow melt	59 mm (49% of total snowfall)
Recorded snow melt runoff (lower than actual due to a leakage in the collection culvert)	2.2 mm (3.7% of spring snow pack)
Snow melt infiltration into the facility (higher than actual since runoff is underestimated)	<56.8 mm (47% of total snowfall)

5.5 INFILTRATION

The net infiltration into the Heap Leach Test Facility (HLTF) is monitored via a cribbed well located approximately at the center of the facility. The infiltrated, or the percolated water is pumped out regularly during summer months by a "super-sucker" truck (6.8 m^3 capacity). The well typically remains frozen until late July, and therefore, the infiltrated water is removed only after thawing has occurred. The annual total net infiltration is calculated on the basis of the water truck capacity, and the total number of truck loads that were pumped and hauled to draw the watertable level down to a predetermined elevation.

The net infiltration data from 1994 and 1995 are deemed unreliable because the quantity of water removed was not carefully measured (Cameco 1997). In 1996, 644 m^3 of water (45% of the total annual precipitation) was pumped from the cribbed well. In 1997, 810 m^3 of water (52% of the total annual precipitation) was removed from the cribbed well. *Table 5.9* provides a summary of the annual net infiltration for the HLTF. Ayres (1998) estimated the annual total net infiltration for the Cluff Lake till to be approximately 36% of the total annual precipitation for 1996, and 42% for 1997.

The two lysimeters that were installed beneath the test patches continued to experience operational difficulties even though they were excavated and modified in 1996. There is no reliable lysimeter data that can be presented in this section.

Table 5.9 Summary of annual net infiltration.

	1996	**1997**
Annual total net infiltration (water removed from the HLTF)	645 m^3 (228 mm rain equivalent)	810 m^3 (287 mm rain equivalent)
Total snowfall (October to April)	160 mm (rain equivalent)	120 mm (rain equivalent)
Total rainfall (May to September)	347 mm	435 mm
Net infiltration	**45% of total precipitation**	**52% of total precipitation**
Cluff Lake net infiltration (Ayres 1998)	36% of total precipitation	42% of total precipitation

5.6 EVAPORATION

The free water evaporation at the Heap Leach Test Facility (HLTF) was monitored using a Class A evaporation pan. The actual evaporation at the HLTF was monitored using a Bowen Ratio Instrumentation. The HLTF evaporation data was compared against Key Lake and Cluff Lake evaporation data for 1996 and 1997.

This section presents site evaporation monitoring results. The HLTF pan evaporation and actual evaporation data were rejected due to instrumentation malfunctions. As a result, the HLTF actual evaporation was estimated based on calculated potential evaporation, SoilCover predictions (SoilCover 1997), and Cluff Lake reported evaporation levels (Ayres 1998). The details of site evaporation estimates and analysis are provided in sub-section 6.1.3.

5.6.1 Historical Regional Evaporation Statistics

The pan evaporation statistics from 1979 to 1997 for the *Key Lake weather station* is shown in *Figure 5.20*. The average historical annual pan evaporation is approximately 652 mm. A close inspection of the pan evaporation data for 1996 and 1997 indicated numerous manual addition and manual data recording errors.

A conspicuously lower than average annual total for 1996 (457 mm) was due to the fact that pan evaporation was recorded for four months (June to September) versus five months in 1997 (May to September). Approximately 90 mm of pan evaporation was recorded for May 1997. In addition, climatic data was unavailable for a 9 day period in August 1996 during which approximately 40 mm of evaporation would have been recorded.

The 1997 annual total evaporation (651 mm) is higher than actual due to recording and addition errors totaling approximately 64 mm. A careful inspection of other extreme years, such as 1988 and 1992, might result in similar findings.

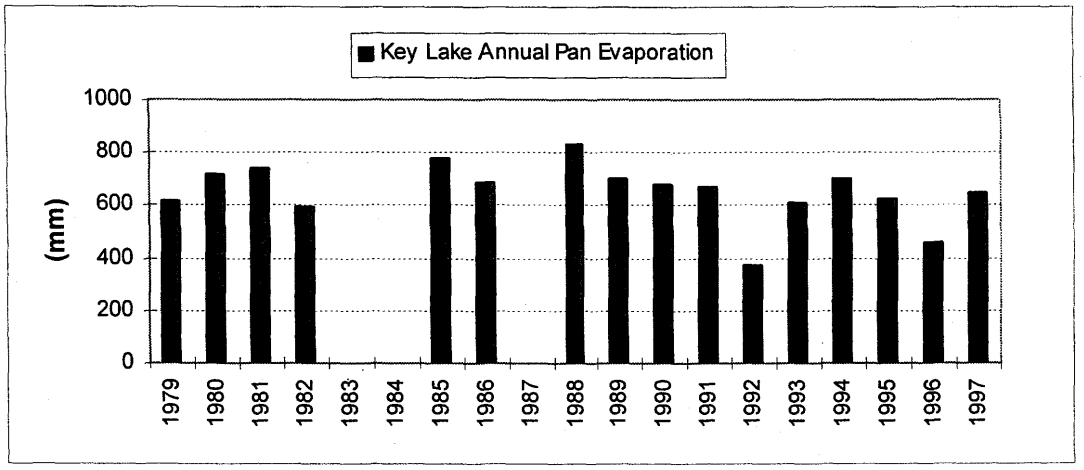

Figure 5.20 Historical pan evaporation statistics for Key Lake.

5.6.2 Heap Leach Test Facility Pan Evaporation Results

The pan evaporation data for the HLTF was found to be unreliable. The data error is due to the inappropriate mechanics of the water level monitoring instrumentation. The pan water level monitoring system was not responsive to the daily fluctuations in the pan water level. *Figure 5.21* shows that the pan evaporation data reflects precipitation rather than daily evaporation. The water level monitoring instrumentation appears to respond well to quick rises in water level due to heavy rainfalls; however, it did not record slow changes in water level due to evaporation.

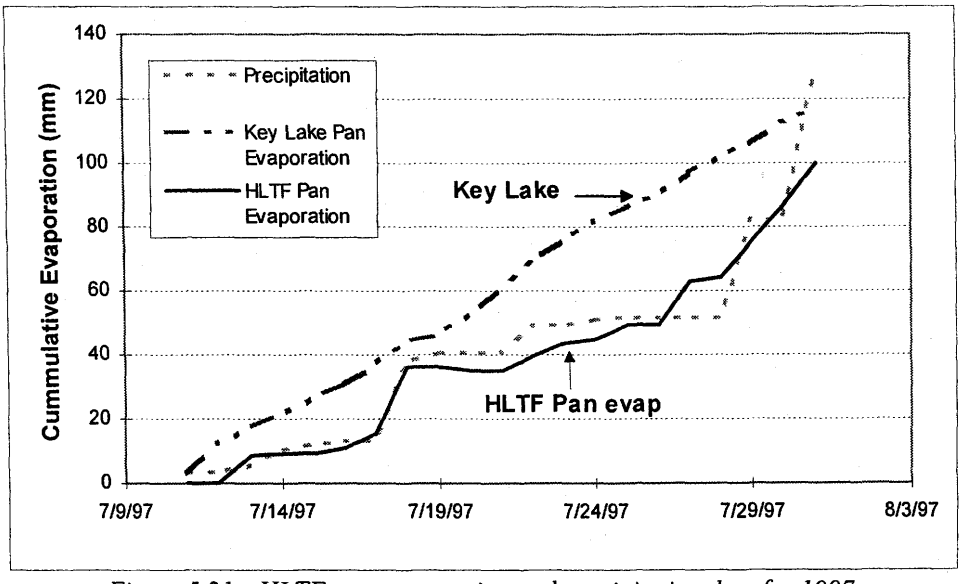

Figure 5.21 HLTF pan evaporation and precipitation data for 1997.

5.6.3 Key Lake Weather Station Pan Evaporation Results

The *Key Lake weather station* pan evaporation data was closely examined to evaluate the possibility of utilizing this data for the HLTF. The reliability of the Key Lake evaporation data was established by comparing pan coefficient estimates (a ratio of potential evaporation over recorded pan evaporation) that were derived using the Kohler *et al.* (1955) empirical formula, and the Penman formulation (Maidment 1993).

The Kohler *et al.* empirical formula calculates the free water evaporation (i.e., potential evaporation) using the following parameters (see Appendix A): daily pan evaporation, daily mean pan water temperature, daily mean air temperature, and daily mean wind speed 15 cm above the rim of the pan. A plot of the 1997 Key Lake cumulative pan evaporation and the cumulative Kohler *et al.* free water evaporation from May to July, inclusively, is shown in *Figure 5.22.* The Key Lake pan water temperature was not available for August 1997 to calculate free water evaporation during this period. A pan coefficient of 0.76 was estimated using the Kohler *et al.* empirical method. This is within the expected pan coefficient values for the region (Gray 1973; Ayres 1998).

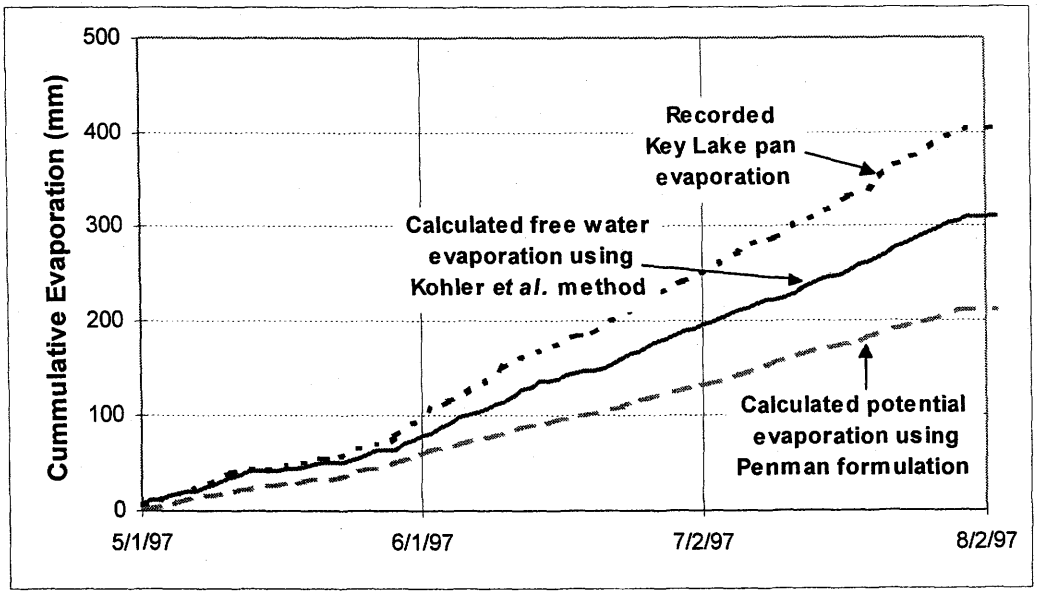

Figure 5.22 Cumulative evaporation at the Key Lake weather station.

The Penman formulation (Maidment 1993) calculates the potential evaporation using the following parameters (Appendix A): mean air temperature, mean wind speed, mean relative humidity, and daily net radiation. The mean air temperature and mean wind speed were recorded in the vicinity of the Key Lake evaporation pan. The relative humidity and net radiation levels were recorded at the HLTF. The relative humidity and net radiation climatic parameters typically display small spatial variation, and thus, the HLTF data was used in combination with the Key Lake data. The recorded HLTF relative humidity data was adjusted to normalize greater than 100% relative humidity levels (see subsection 5.3.3).

The estimated potential evaporation using the Penman formulation resulted in a pan coefficient of 0.53. The resulting pan coefficient is unreasonably low for this region, and significantly different from what was calculated using the Kohler *et al.* empirical formula (*Figure 5.22*). It has been noted that the recorded net radiation at the HLTF was significantly lower than the reported regional net radiation statistics (subsection 5.3.5). The HLTF net radiation data was thus adjusted using a correction factor of 1.58 to arrive at radiation levels that were more representative of the region. The Key Lake potential evaporation (Penman formulation) was recalculated using the adjusted net radiation data from the HLTF resulting in a pan coefficient of 0.73 versus 0.76 using the Kohler *et al.* empirical formula.

The calculated potential evaporation using the Kohler *et al.* empirical formula indicated that the Key Lake pan evaporation data was reliable; the calculated potential evaporation using the Penman formulation indicated that the HLTF net radiation instrument was under-recording actual net radiation levels.

5.6.4 Estimating HLTF Potential Evaporation

The potential evaporation at the HLTF is expected to differ from the Key Lake pan evaporation levels. The recorded mean wind speed at the HLTF is significantly higher than what was measured in the vicinity of the Key Lake evaporation pan (section 5.3.4). The HLTF potential evaporation was thus estimated using the Penman formulation and the

recorded HLTF weather data (i.e., mean wind speed, mean air temperature, corrected relative humidity, and corrected net radiation). The total cumulative potential evaporation at the HLTF was calculated to be 18% higher than what was estimated for the Key Lake over the same three month period (*Figure 5.23*). *Table 5.10* provides a summary of evaporation estimates that have been presented in this section.

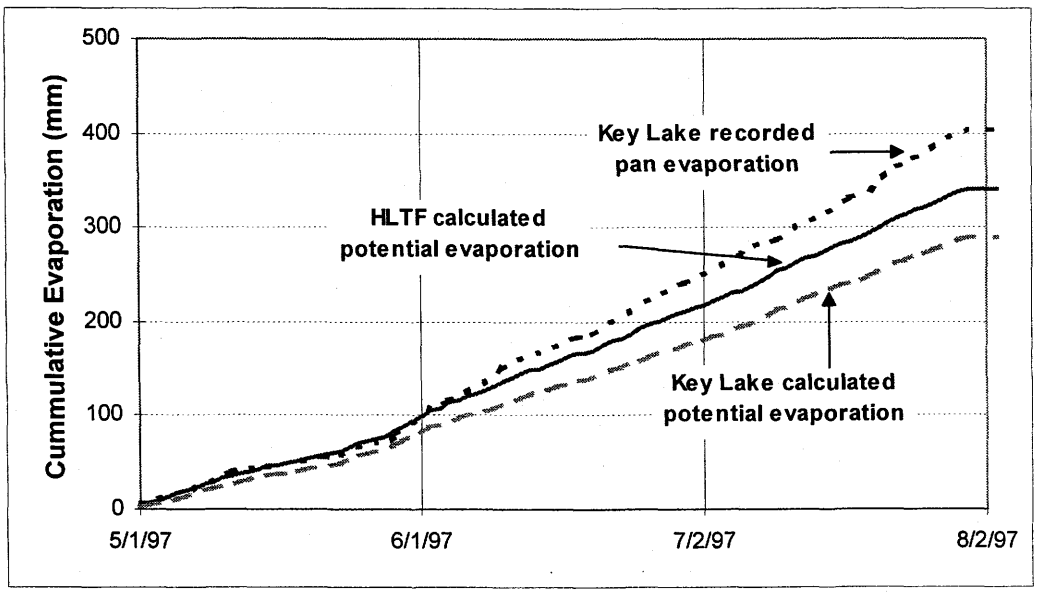

Figure 5.23 A comparison of potential evaporation estimates.

Table 5.10 Summary of potential evaporation estimates.

	Cumulative Evaporation (May 1997 to July 1997)
Key Lake weather station recorded pan evaporation.	**397 mm**
Key Lake weather station calculated free water evaporation using the Kohler *et al.* (1955) empirical method.	**300 mm**
Key Lake weather station calculated potential evaporation using the Penman formulation.	**289 mm**
HLTF calculated potential evaporation using the Penman formulation with HLTF corrected weather data.	**341 mm**

5.6.5 Actual Evaporation Monitoring Results

The actual evaporation at the HLTF was monitored using a Bowen Ratio Instrumentation during June 24th to July 22nd, 1998. Most of the actual evaporation data was rejected due to instrumentation malfunction (dew point hygrometer) 3 ½ days after the monitoring program began. The analysis of the Bowen Ratio data showed irregularities prior to failure, and thus, there is no reliable actual evaporation data.

The Bowen Ratio Instrumentation was previously installed at Cluff Lake (Ayres 1998). Ayres noted that the dew point hygrometer was functioning intermittently towards the end of the monitoring season. Therefore, the actual evaporation and transpiration data collected at Cluff Lake after July 21st, 1997, was rejected. The irregularities in the collected data were attributed to the malfunction in the hygrometer pump. A new pump was installed, and regular maintenance was performed on the instrumentation, prior to installation at Key Lake. However, based on the HLTF Bowen ratio results, the hygrometer pump was not the only problem with the instrumentation.

5.6.6 Estimating HLTF Actual Evaporation

The actual evaporation for the HLTF was estimated based on calculated potential evaporation, and estimated daily actual evaporation (AE) to potential evaporation (PE) ratios. AE is a function of total suction at the soil surface, and as the soil surface dries out (i.e., total suction increases), the AE/PE ratio decreases (Wilson *et al.*, 1997).

The AE/PE ratios for the HLTF was estimated on a day to day basis using SoilCover predicted AE/PE ratios, and reported Cluff Lake AET/PE ratios (Ayres 1998). A detailed discussion and analysis of the HLTF actual evaporation estimates are found in subsection 6.1.3.

5.7 SUBSURFACE SOIL MOISTURE

The subsurface soil moisture monitoring instrumentation program consisted of two types of thermal conductivity sensors, and two neutron probe access holes. The AGWA-II thermal conductivity sensors underwent serious degradation over the three years (1993 to 1996) that they were being monitored. The neutron probe access holes were installed at the end of 1996 to replace the AGWA-II sensors. Twenty-two Beta-97 soil suction sensors were installed in 1997.

5.7.1 AGWA-II Thermal Conductivity Sensors

Thirty-nine AGWA-II thermal conductivity sensors were installed at the HLTF in 1993. In spring of 1994, all three manholes were flooded due to the ingress of snow melt water. The flooding resulted in serious damage to the AGWA-II instrumentation. The summer was spent relocating the datalogger, and rewiring and repairing all the sensor lead wires. Consequently, soil suction data was not collected during the summer of 1994.

Approximately one-third of the sensors were damaged as a result of flooding. Loi *et al.* (1992) noted that AGWA-II sensors are prone to failure due to inadequate isolation of sensor electronics from water penetration. Fredlund *et al.* (1992) experienced 25% sensor failure within the first monitoring year.

In May, 1995, only 15 of the 39 sensors were functioning, 4 sensors had failed completely, and 20 sensors were producing erratic and meaningless results. By the end of September 1995, 6 more sensors had failed, bringing the total number of failure to 30 out of 39 sensors (85%). O'Kane (1996) reported 50% mortality rate after two years of field monitoring.

By June, 1996, only 2 sensors were responding as expected, 7 sensors had ceased to function, and 30 were producing erratic responses. The AGWA-II sensors were thus abandoned in 1996. In addition to high sensor failure rate, these sensors were found to be inappropriate

for the type of soil cover material that was used. The sensors needed to be responsive and accurate to within ±1 kPa in the 0 kPa to 20 kPa suction range. The AGWA-II sensors were accurate to within ±10 kPa. The results of the AGWA-II sensor monitoring program is not presented in this thesis.

5.7.2 Beta-97 Thermal Conductivity Sensors

The Beta-97 thermal conductivity suction sensor calibration and field monitoring results are presented in this subsection. The corresponding detailed data is found in Appendix F.

5.7.2.1 Sensor Calibration Results

Twenty two Beta-97 soil suction sensors were calibrated in the laboratory over 2 kPa to 300 kPa range using a modified pressure plate apparatus (subsection 4.4.3). The calibration process consisted of introducing a controlled amount of heat to the sensor, and recording the resulting voltage output. A typical sensor heating curve for sensor #2 is shown in *Figure 5.24.* The difference in the voltage output at rest, and the peak voltage output upon heating, is then plotted against the corresponding matric suction value. Each sensor was calibrated at seven specific matric suction values: 2 kPa, 5 kPa, 10 kPa, 20 kPa, 50 kPa, 100 kPa, and 300 kPa.

Shuai *et al.* (1998) derived a curve fitting parameter "*C*" by best fitting the measured heating curve at each matric suction value. This parameter is a function of the sensor matric suction. The relationship between "*C*" and matric suction is used to define the calibration curve. The parameter "*C*" is given by (Shuai *et al.*, 1998):

$$C = \frac{Q}{4\pi\lambda}\left(\frac{1}{\sqrt{\pi D}} + \frac{1}{r}\right) \qquad [5.1]$$

where, Q = heating rate of the heating device

$\lambda =$ thermal conductivity of the porous ceramic (W/mK)

$D =$ thermal diffusivity of the porous ceramic (m^2/s)

$r =$ radius of inner epoxy column containing the temperature sensor and the heating device (m)

The relationship between the curve fitting parameters and matric suction is given by:

$$\psi = \left[\frac{(a-\Delta V)b}{\Delta V - c}\right]^d \qquad [5.2]$$

where a,b,c,d are calibration curve fitting parameters, and ψ is soil matric suction. A minimum of five calibration points are required to establish the calibration curve that consists of four curve fitting parameters. The sensor calibration curve is given by:

$$C = \frac{ab + c\psi^d}{b + \psi^d} \qquad [5.3]$$

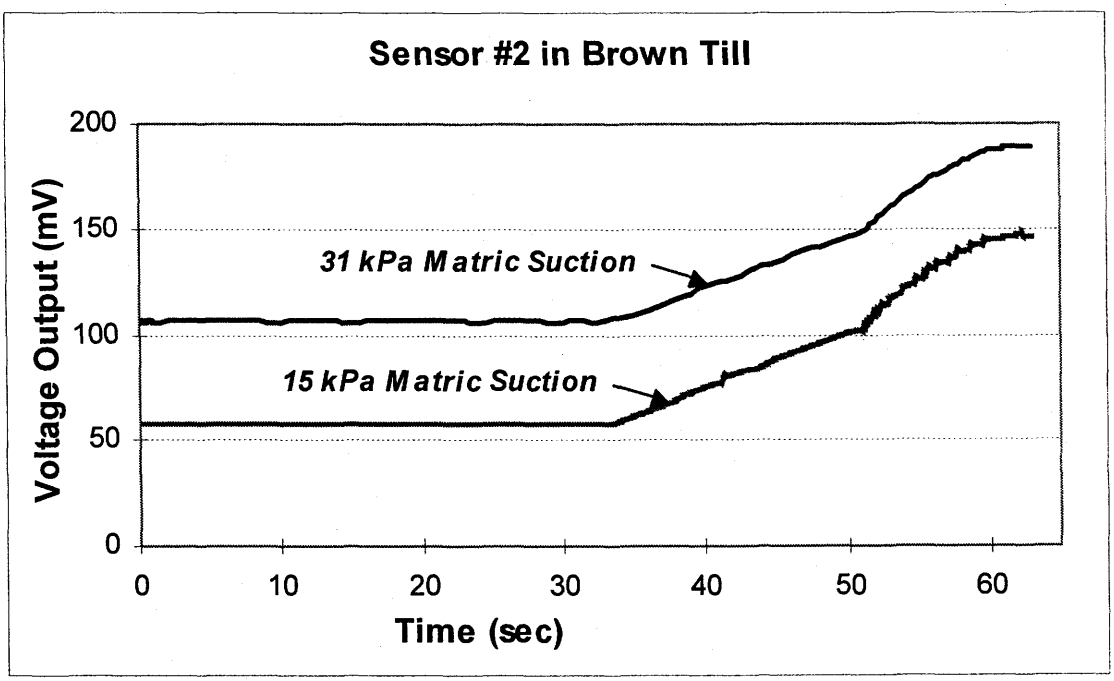

Figure 5.24 Beta-97 suction sensor #2 heating curves.

The calibration parameters *a, b, c,* and *d* for twenty sensors employed at the HLTF are listed in Appendix F. Twenty out of twenty-two sensors (91% of total sensors) exhibited an anomalous behaviour at 10 kPa reading. The voltage output dropped significantly (*Figure 5.25*) or leveled off (*Figure 5.26*) at 10 kPa. Therefore, the sensor accuracy in the suction range less than 20 kPa is uncertain for the majority of these sensors. The newer generation of Beta sensors do not display this behavior.

Individual sensor calibration curves can be found in Appendix F. A total of five sensors resulted in unreliable calibration curves (sensors #1, #3, #9, #18, and #20). In general, the sensors were very responsive from 20 kPa to 100 kPa matric suction range.

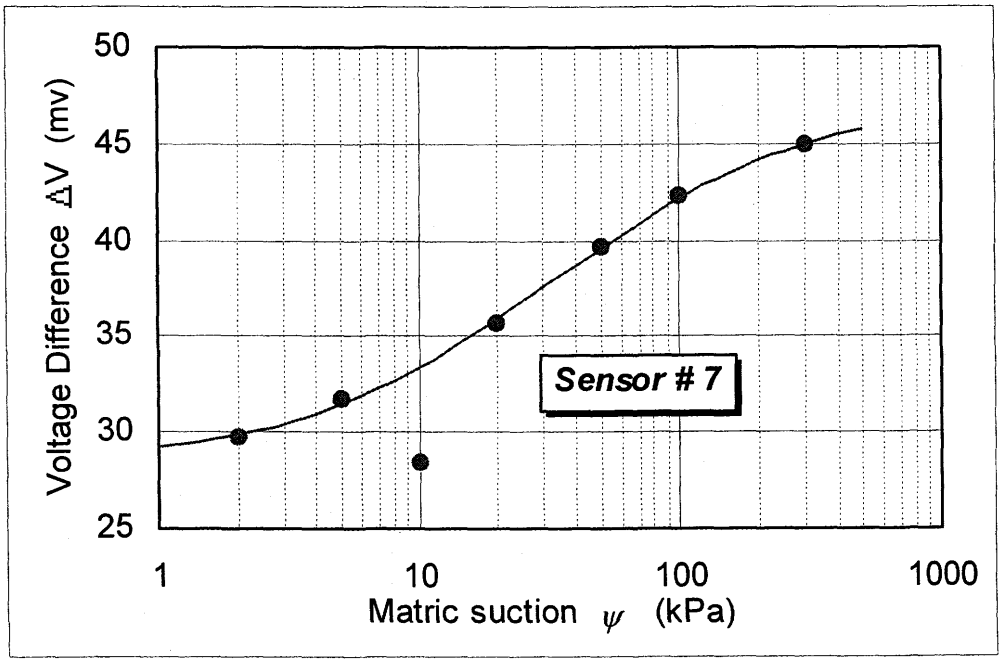

Figure 5.25 Beta-97 sensor #7 calibration curve. The drop in voltage at 10 kPa has been noted for 91% of the sensors.

5.7.2.2 Sensor Field Monitoring Results

The Beta-97 sensors were installed over two days in August 1997 (August 13th to 14th). The first set of field data was collected 16 days later, on August 30th. The delay was due to

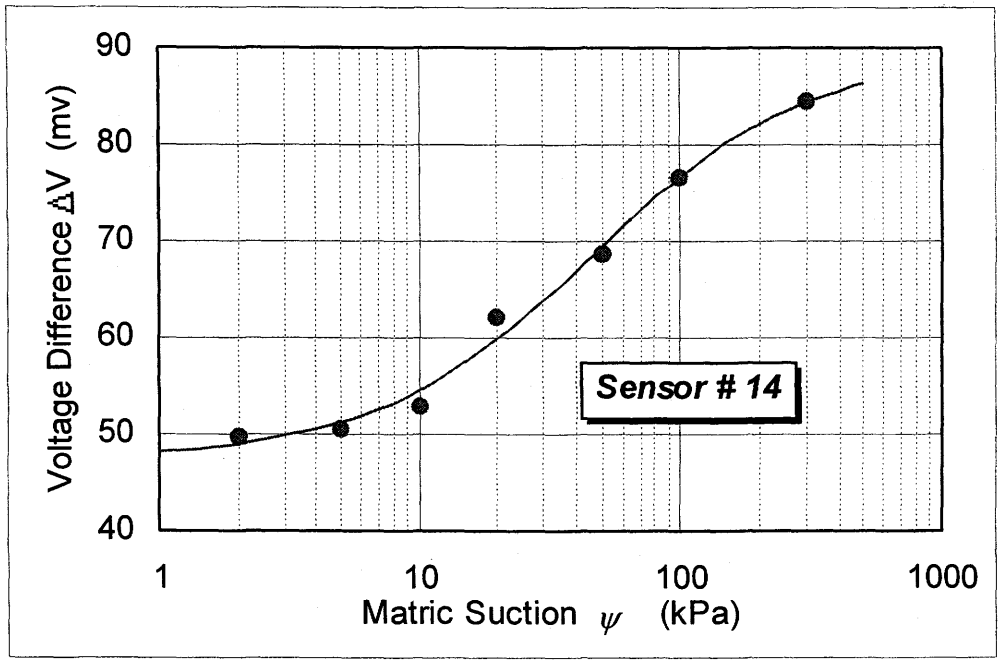

Figure 5.26 Beta-97 sensor #14 calibration curve. This calibration curve lacks sensitivity in the matric suction range less than 10 kPa (i.e. very flat curve).

programming difficulties. The data collection continued till October 31st, 1997. The datalogger was programed to record 100 data points along the heating curve for each sensor, and the 22 sensors were recorded every six hours. This created a very large database in short period of time. The datalogger had to be downloaded weekly to avoid data loss. Data was lost from 12:00 p.m., September 10th to 12:00 p.m., September 12th due to data being overwritten. The data was also lost between September 17th and October 1st due to instrumentation failure caused by flooding of manholes.

Criteria for Sensor Rejection

The sensors were installed in groups of three to provide verification of their reliability and performance. A close examination of sensor performance in conjunction with their calibration results has suggested that nine sensors are unreliable (*Table 5.11*). Two sensors, #1 and #3, were deemed unreliable due to the dubious nature of their calibration curves (*Figures F.1* and *F.3*). Although sensors #1 and #2 were found to yield similar soil suction

results (*Figure F.23*), the resulting suction levels were unreasonably low. It was thus concluded that all three sensors, #1, #2, and #3, at 15 cm depth were yielding erroneous values. *Figure 5.27* provides a suction profile for September 13th, 1997, and highlights the sensors that were rejected on the basis of this analysis.

Sensor #4 lacked sensitivity in comparison to sensors #5 and #6. It consistently yielded lower than average highs and higher than average lows (*Figure 5.28*). Sensor #19 became erratic after the manholes were flooded at the end of September, 1997. Water infiltration into the sensor electronics is most likely the cause for this erratic behaviour. Sensors, #18, #20, and #22 were damaged during installation. Sensor #21, produced higher than expected suction values (*Figure 5.27*). It is postulated that this is a result of poor sensor/soil contact. Cobbles and gravels were encountered in holes #20, #21, and #22.

The high rate of sensor rejection is attributed to the epoxy that was used to isolate the heating unit and the temperature sensor within the ceramic tip. The epoxy underwent significant swelling when the sensors were saturated during the laboratory calibration process. Radial and longitudinal micro-fracture formation was prevalent in all the sensors. The new generation of Beta sensors are constructed using a different epoxy with significantly lower swell factor.

Table 5.11 Thermal conductivity Beta-97 sensor failure status.

Sensor #	Reason for Rejection
#1, #3	Unreliable calibration curve
#2	Suction values obtained are unreasonably low
#4	Sensor's not very responsive
#18, #20, #22	Failed immediately after installation
#19	Became erratic after flooding
#21	Suction values obtained are unreasonably high

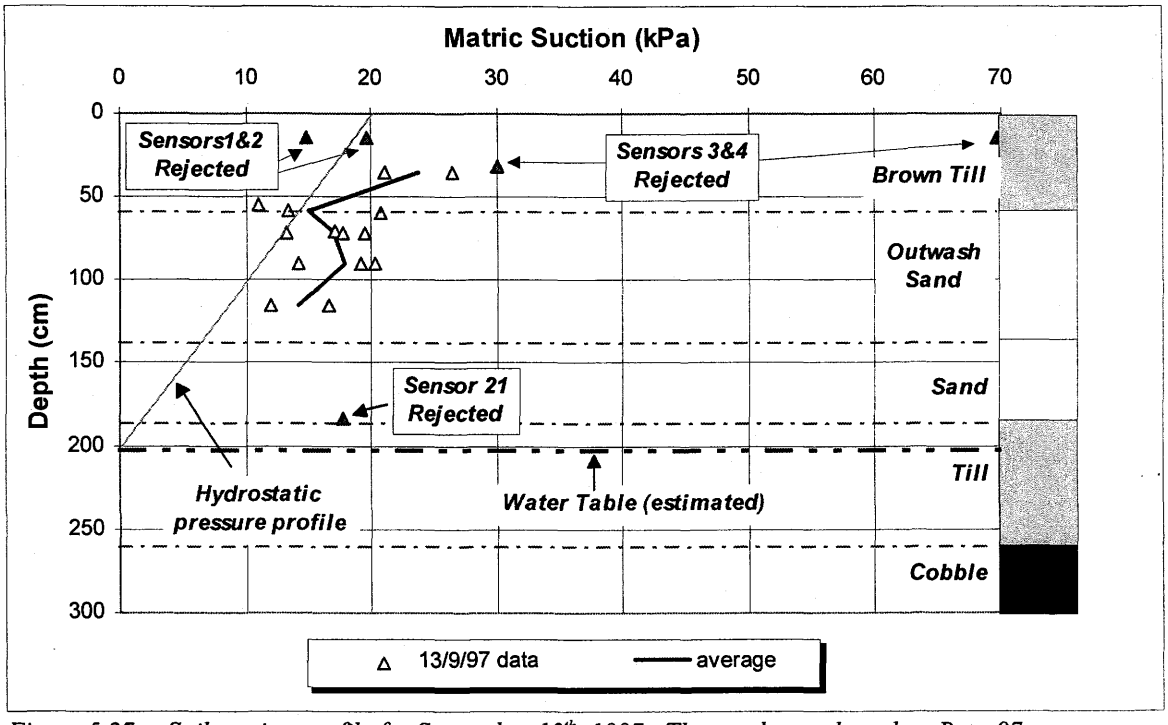

Figure 5.27 Soil suction profile for September 13th, 1997. The results are based on Beta-97 sensor monitoring results. The water table elevation is an approximation.

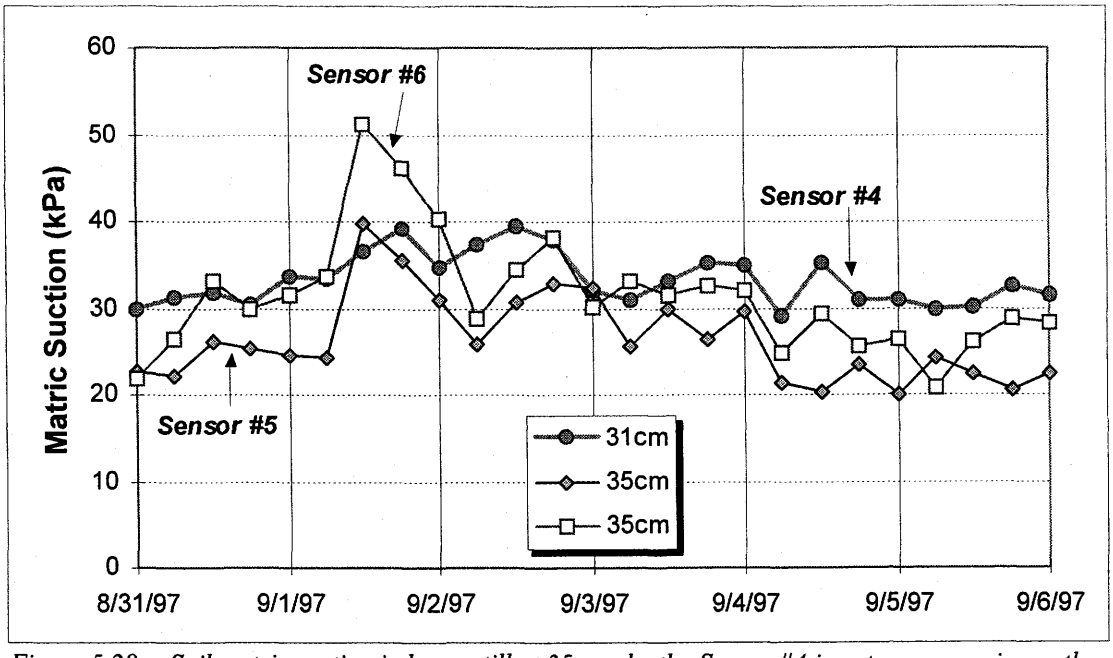

Figure 5.28 Soil matric suction in brown till at 35 cm depth. Sensor #4 is not as responsive as the other two sensors.

Assessment of Sensor Reliability

The sensors were installed in groups of three to verify their reliability and reproducibility. The statistical analysis on 140 sets of readings (each set corresponding to a group of sensors installed at same depth) has indicated the following. The maximum *range* (i.e. the difference between the largest and the smallest reading) is 21.7 kPa, and the average *range* is 7.0 kPa. The maximum *standard deviation* is 8.9 kPa, and the average *standard deviation* of 3.7 kPa.

This analysis indicates that although the sensors were found to be responsive to changes in atmospheric and soil suction conditions, they did not have the required reproducibility for application in the types of soils that were used for this study. For soils with low air entry values (1 kPa to 2 kPa) that attain residual water content at low matric suction levels (20 kPa), the sensors must provide accuracies within ±1 kPa over the 0 to 20 kPa measurement range.

Sensor Response to Atmospheric Forcing

The Beta-97 sensors were found to be highly responsive to changes in atmospheric conditions. *Figure 5.29* illustrates the change in matric suction as a function of potential evaporation. The sensors at 35 cm depth (nearest to the surface) are most responsive.

The sensors that are installed in till at 35 cm depth (*Figure 5.30)* indicate small change in soil suction levels as precipitation infiltrates through the soil profile. However, *Figure 5.31* shows that the change in soil suction recorded by the sensors corresponds to insignificant changes in soil moisture content. The suction values were translated into volumetric water contents using the laboratory soil-water characteristic curves (SWCCs). According to suction sensor monitoring results, a significant precipitation events on September 13th (22 mm rainfall) and September 16th (28 mm rainfall) resulted in a small increase in soil moisture level. The increase in the volumetric water content with depth are: <0.4% at 35 cm depth and <0.3% at 55 cm depth. This is indicative of a well drained soil profile.

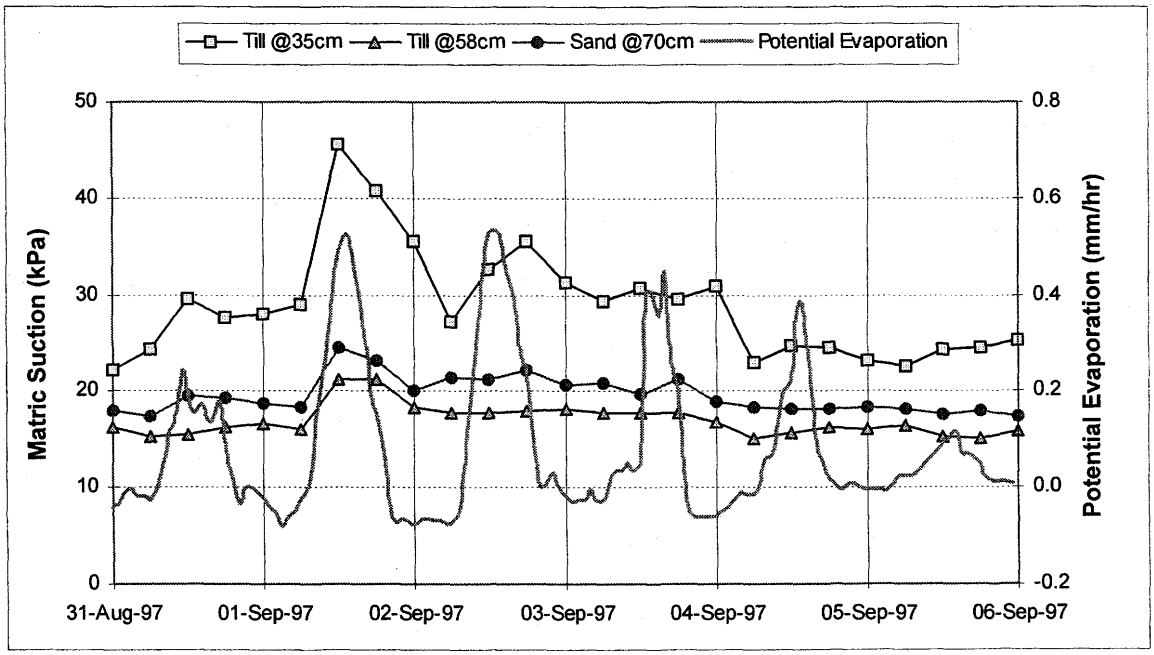

Figure 5.29 Temporal variation in soil suction versus potential evaporation.

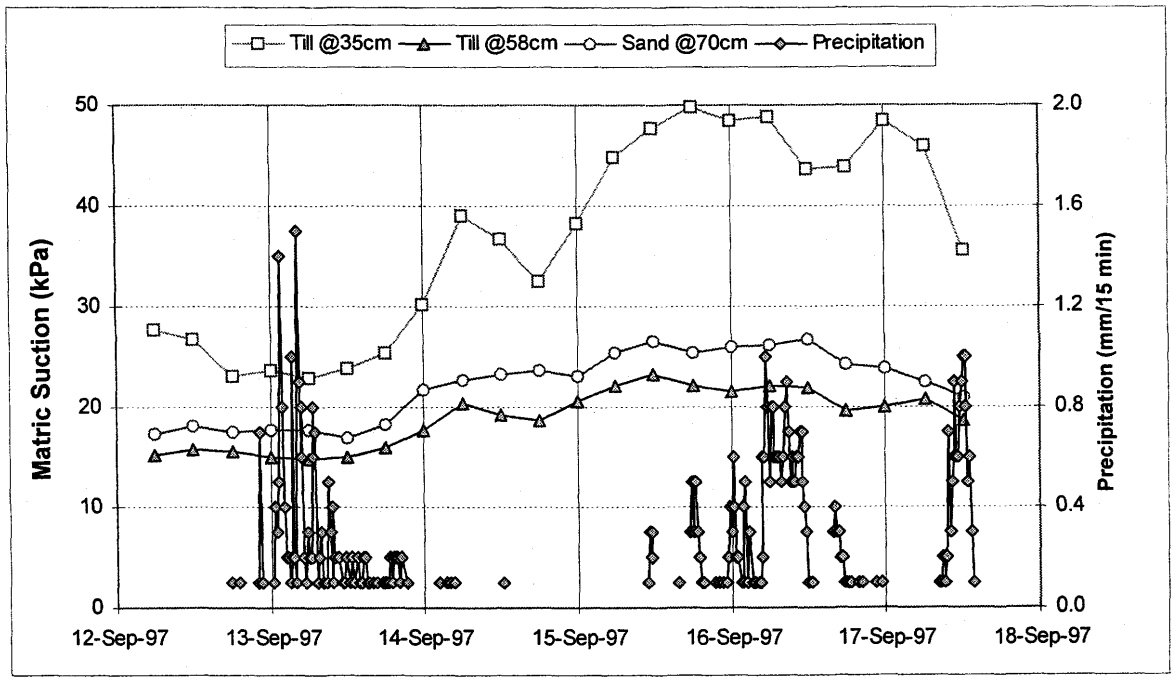

Figure 5.30 Fluctuation in soil matric suction in response to precipitation.

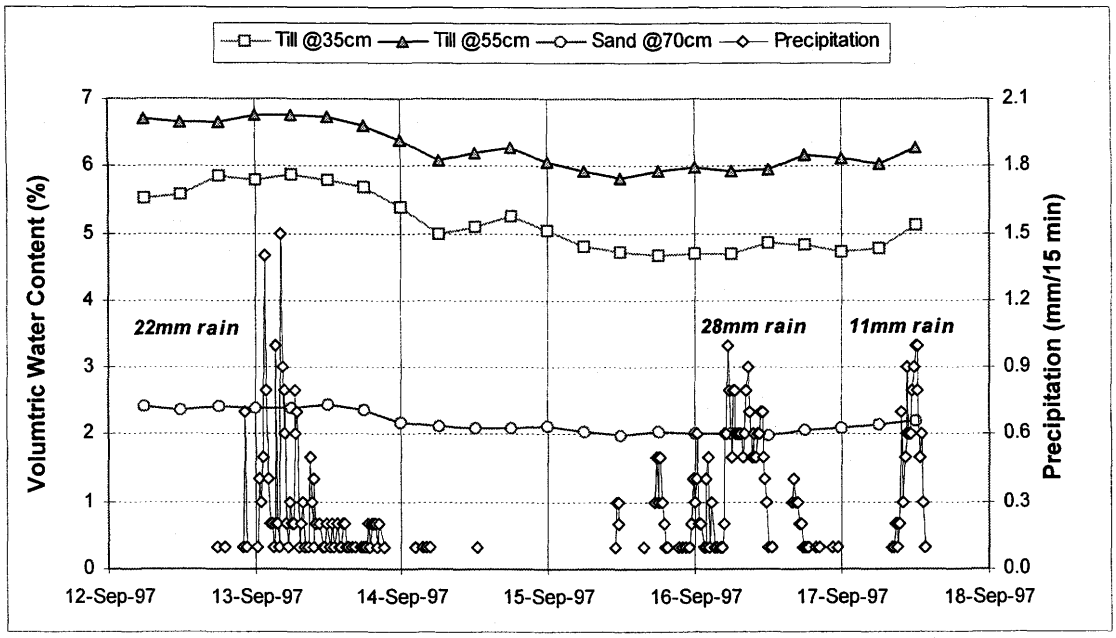

Figure 5.31 Soil moisture trends for September 13th to 17th, 1997.

Effects of Freezing

Figure 5.32 indicates that when the air temperature dips below freezing, the sensor readings become unreliable. The sharp decrease in suction on October 15th and 20th, 1997 are due to the effects of freezing. This phenomenon is thought to be attributed to the phase transformation of water within the ceramic tip (Khogali *et al.*, 1991).

Soil Suction Profile

The soil suction profile for September 13th to 17th are shown in *Figure 5.33*. The laboratory SWCCs were used to construct the soil moisture profiles shown in *Figure 5.34*. 39 mm total rainfall was recorded from September 15th to 17th, 1997. Based on runoff observations, 32 mm ended up as infiltration; however, due to lack of storage capacity (12 mm), much of it would have infiltrated to the cobble layer below (subsection 6.1.6). *Figure 5.33* indicates a decrease in soil suction throughout the soil profile from September 16th to 17th. The decrease in suction is greatest near the surface (8 kPa at 35 cm depth) with an overall average decrease in soil suction of 5.8 kPa.

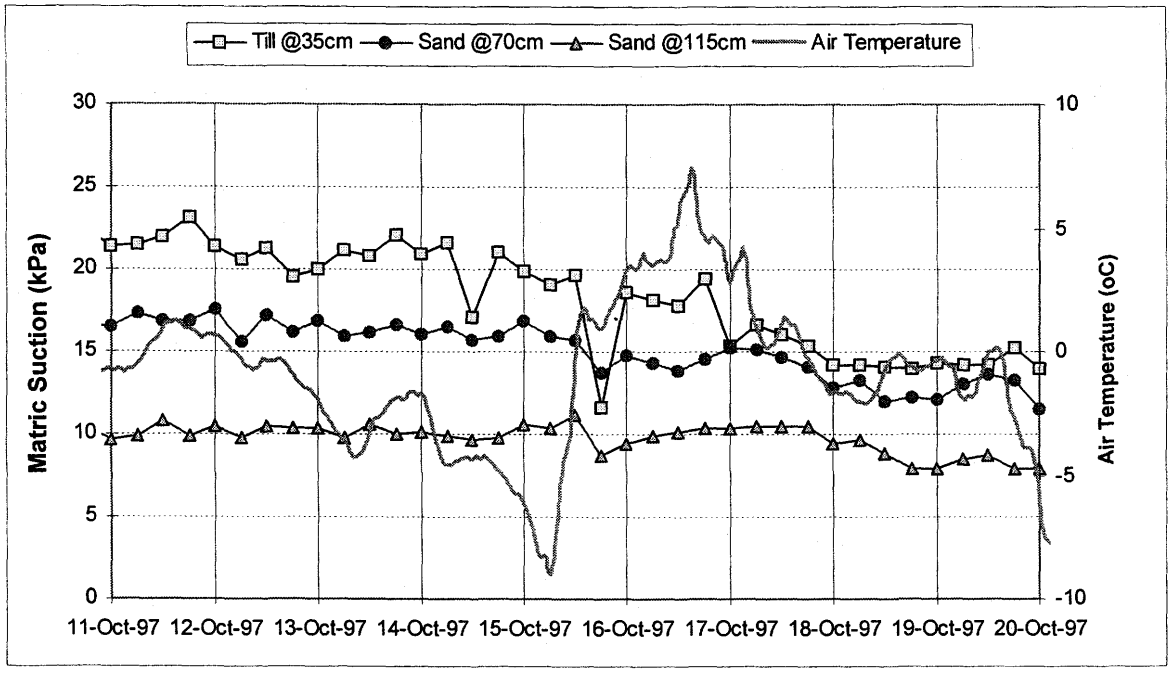

Figure 5.32 Temporal variation in soil suction and air temperature.

A sharp decrease in soil suction is noted at the sand/till interface at approximately 60 cm from surface. A very sharp suction gradient indicating an upward flow (evaporation), is evident in the uppermost till layer. It should be noted that the suction profile in the till layer throughout the monitoring period never yielded an infiltrating suction profile. Beneath the sand/till interface, there appears to be a gentler suction gradient indicating a downward flow (infiltration). The suction profile below 95 cm depth parallels the hydrostatic line.

The soil moisture profile shown in *Figure 5.34* indicates a low volumetric water content profile, with the water content in the till layer (5% to 6%) noticeably higher than in the sand layer (2% to 3%). The actual water content in the soil profile, however, is expected to be higher. Field soil sampling results have indicated that the *in situ* volumetric water contents under gravity drained conditions are 7% to 9% for till, and 5% to 7% for sand. The variance between the *in situ* and the sensor determined water contents can be attributed to erroneous SWCCs, or to inaccuracies in the suction sensor results.

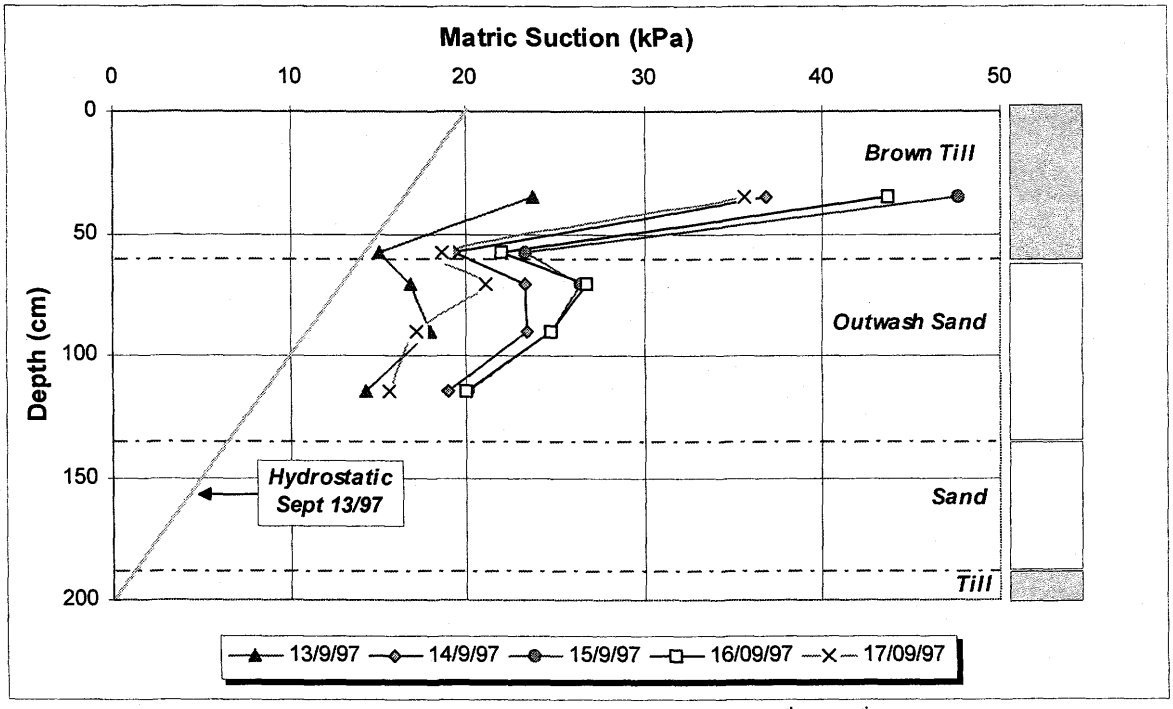

Figure 5.33 Soil suction profile for September 13th to 17th, 1997.

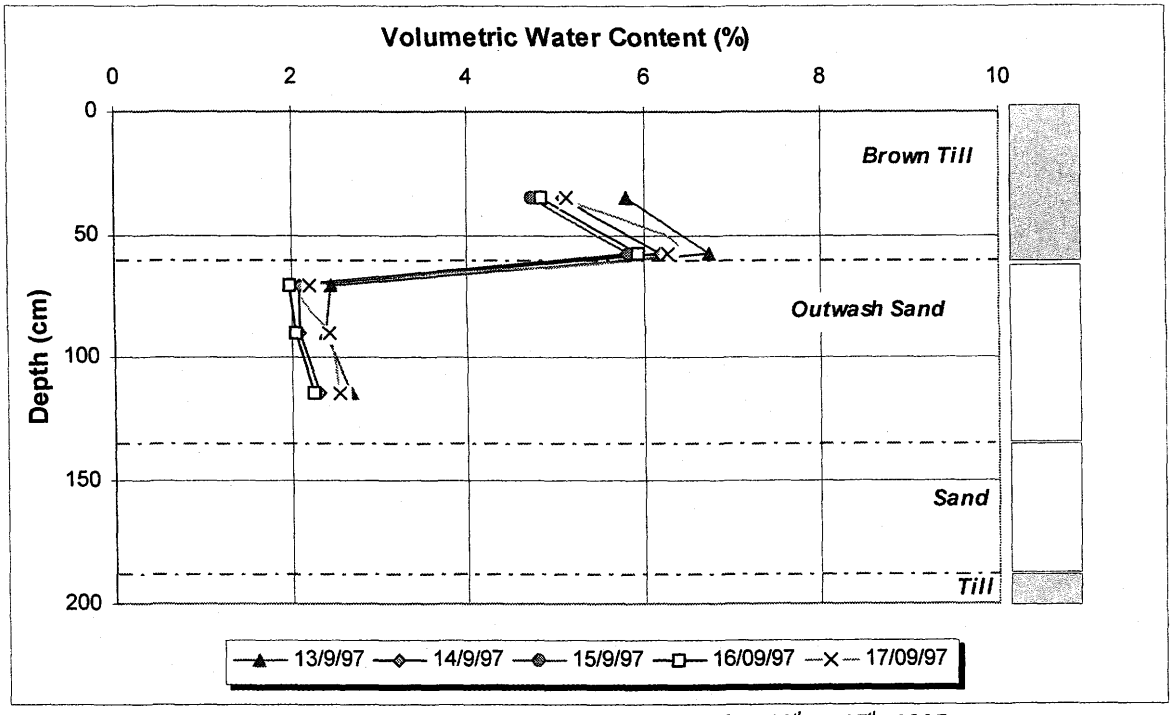

Figure 5.34 Soil moisture profile for September 13th to 17th, 1997.

Figure 5.35 shows a comparison of the outwash sand SWCCs. The SWCC that was determined as part of this thesis is compared against the curves that were determined by Julian Gan (University of Saskatchwan 1993). The University of Saskatchewan samples were not consolidated.

Figure 5.35 indicates that the outwash sand SWCC that was used to construct the soil moisture profile shown in *Figure 5.34* is consistent with what was previously reported (University of Saskatchewan 1993). A comparison of brown till SWCCs have also indicated that the brown till curve is similar to the previously reported value (University of Saskatchewan 1993). It can thus be concluded that the suction sensors are reporting higher than actual suction levels. This error can be due to the hysteresis of the ceramic tip, or the inherent variability in sensor response.

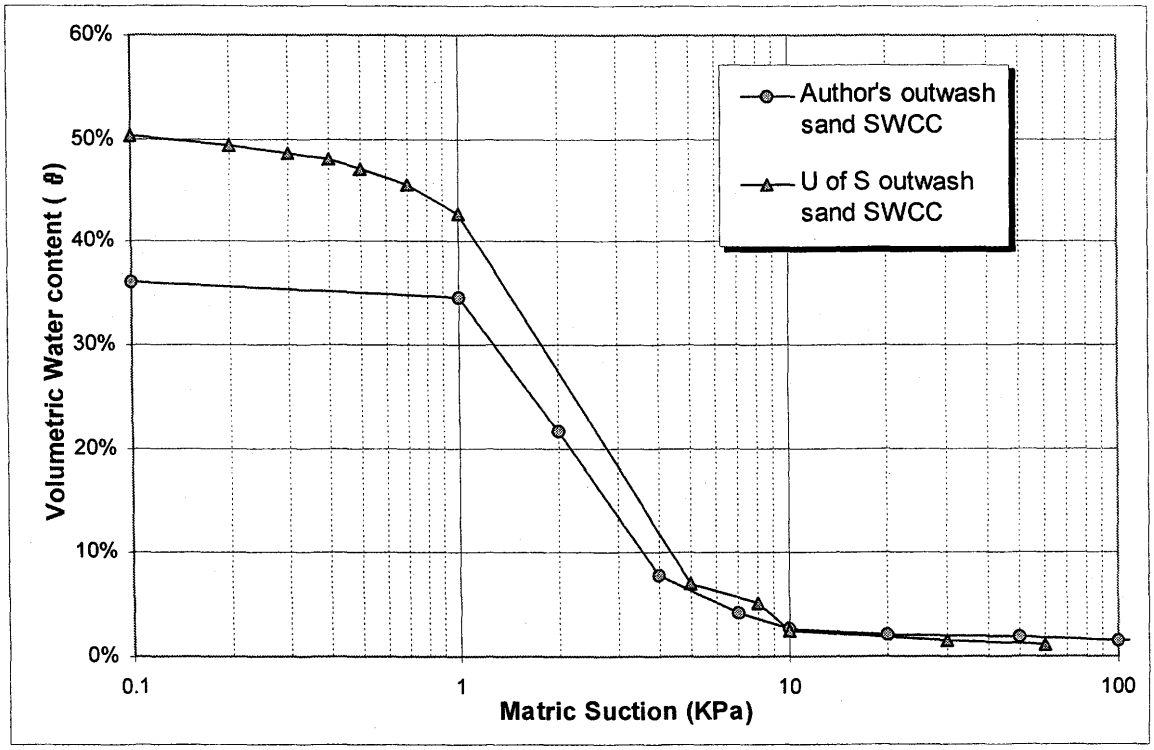

Figure 5.35 A comparison of outwash sand SWCCs.

Comparison of Various Soil Moisture Content Assessment Methods

Figure 5.36 provides a comparison of different soil moisture content assessment methods. The soil moisture profile in this figure was determined using the neutron probe and Beta-97 thermal conductivity sensor results. As well, soil samples were taken using a sonic soil sampling drill, and manual sampling procedures using shovels. The plot of hydrostatic water contents reflect soil-water contents under a hydrostatic condition for each soil horizon using the laboratory determined SWCCs. There was no precipitation four days prior to this date and insignificant evaporation is anticipated during this period due to the climatic conditions.

When compared to soil sampling results, the neutron probe appears to overestimates soil moisture conditions, while the Beta-97 sensors underestimate soil moisture conditions. The residual water contents are approximately 8% in till layers (0 to 0.6 m and 1.9 to 2.6 m) and approximately 6% in sand layers (0.6 to 1.4 m and 1.4 to 1.9 m).

According to Nicholson (1989), Akindunni *et al.* (1991), and Barbour and Yanful (1994), the lower layers under drainage conditions should be at their residual water content. The soil-water content in the surficial layer, on the other hand, will decrease below its residual water content in response to evaporative demand. The soil sampling results in *Figure 5.36* confirms these findings. The soil moisture profiles in the lower till layer (1.9 to 2.6 m) and the surficial till layer (0 to 0.6 m) are at the residual water content of the brown till of approximately 8%. The soil moisture profiles in the sand layers are at outwash sand residual water content of approximately 6%..

The Beta-97 soil suction sensors were installed to 1.8 m in depth. The recorded temporal variation in soil moisture content within the instrumentation horizon is very small. This is expected given the depth of the water table (typically greater than 1.8 m), the thickness of the soil cover (2.6 m total), and the water storage/release characteristic of the soil materials used. The soil moisture conditions were at residual water content throughout the monitoring profile during the Beta-97 sensor instrumentation and monitoring time period.

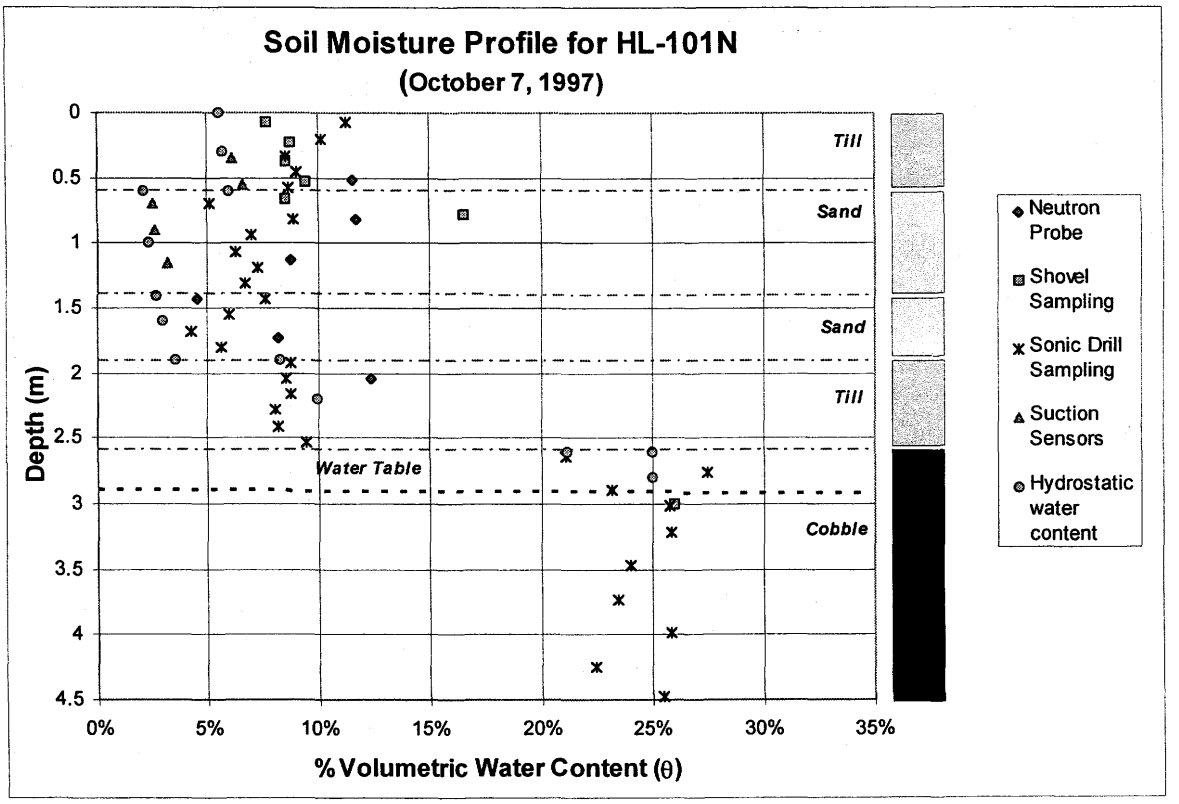

Figure 5.36 Soil moisture profile for October 7th, 1997. A comparison of various soil moisture content assessment techniques is provided.

Summary

In summary, the Beta-97 sensors were responsive to climatic changes. They provided a reliable insight into the temporal and spatial variation in soil suction. However, the soil suction levels that were recorded by the sensors resulted in soil moisture conditions that were lower than anticipated. This may be attributed to the hysteresis of the ceramic tip, or the variability in the sensor results.

The Beta-97 sensor data from August 30th to September 16th, and from October 1st to 31st, has indicated that the soil cover maintained a gravity drained (residual) water content profile throughout the monitoring period.

5.7.3 Neutron Moisture Probe

In November 1996, two 3 $^{15}/_{16}$" diameter (100 mm) access holes were drilled and lined with a 3" diameter (90 mm outside diameter) Schedule 40 PVC tubing. The laboratory calibration program was carried out using the same tubing material in October 1997. The results of the neutron probe field calibration and laboratory calibration programs are presented in this sub-section. The detailed supporting data can be found in Appendix F.

5.7.3.1 Field Installation Technique

The selection of access tube diameter and material, and correct installation procedures impact the sensitivity of this method. In general, a 38 mm or a 50 mm diameter aluminum tubing is preferred. A larger diameter tube reduces the sensitivity of the installation and often results in a non-linear calibration curve (Marais and Smit, 1960), while PVC tubing is found to decrease the count rate through neutron absorption (Hanson and Dickey, 1993). The reduction in sensitivity for the large diameter PVC tubing that was employed is clearly evident in the resulting steep calibration curves (see subsection 5.7.3.4).

Drilling a hole that is significantly larger than the access tube will create a space along the length of the hole that can act as a preferential flow path for surface infiltration. Drilling a hole that is too small may compress and distort soil along the sides of the tubing during installation, thus inadvertently creating a density gradient. A 90 mm outside diameter tubing inserted into a 100 mm diameter hole was found to be practical and workable. The PVC tubing was found to fit snug without undue lateral movement.

5.7.3.2 Field Calibration Results

Field calibration errors result from uneven distribution of soil water and bulk density gradient within the sphere of influence of the neutron probe. This is further exacerbated by inherent errors associated with gravimetric and volumetric soil sampling techniques. Field calibration

errors are minimized when water content sampling is carried out within the access hole at the time of hole excavation, however, this approach often does not provide a wide enough range of soil moisture data (Grismer *et al.*, 1995, Ayres 1998). As a result, field calibration generally requires additional sampling and concurrent probe readings before, during, and after a significant saturation event.

At the HLTF, three gravimetric samples were procured from each access hole during hole excavation. Soil profile sampling was also undertaken on October 7th, 1997 adjacent to the access hole HL-101N. The gravimetric water content results and their respective neutron count readings are presented in *Figure 5.37.* The volumetric water contents were calculated using field in situ density measurement results.

The field calibration data is clustered along the factory calibration curve. However, it is difficult to arrive at a conclusive correlation due to the narrow water content range encountered during the calibration process (5% to 13% water content). A reliable regression is achieved only when the water content is varied from near dry to near saturated conditions.

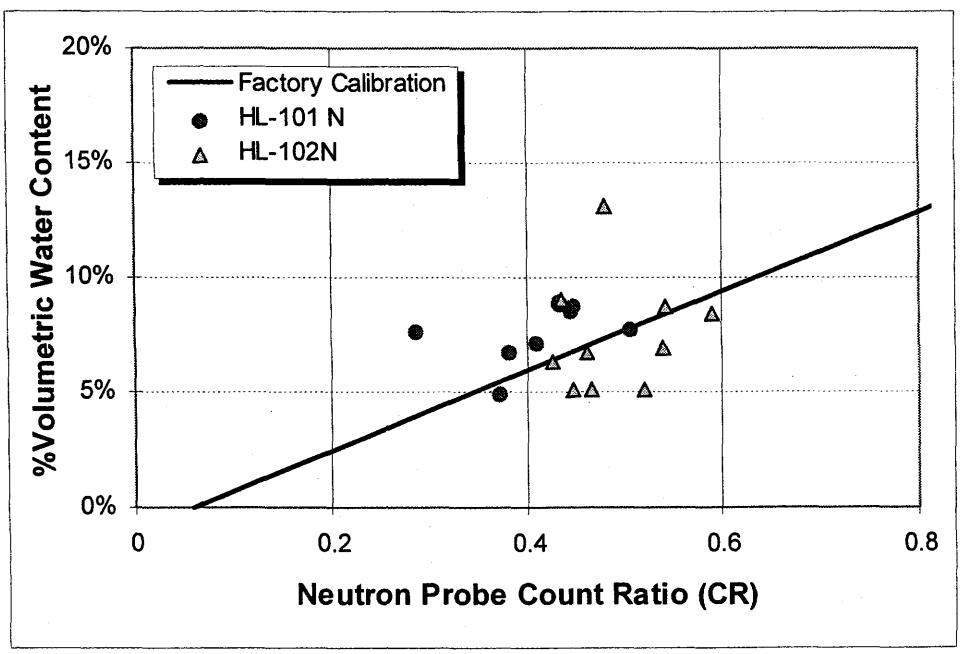

Figure 5.37 Neutron probe field calibration results.

Sources of Field Calibration Error

Field calibration method commonly produces poor calibration results. For example, Ayres'(1998) calibration curves had a coefficient of determination of $r^2 = 0.17$ based on 41 soil moisture data points in till, and a coefficient of determination of $r^2 = 0.19$ with 18 soil moisture data points in the tailings material. The narrow range of soil moisture conditions that were encountered during soil sampling is the main reason for the lack of correlation.

Calibration errors due to spatial variability has been shown to constitute a large portion of the total error (Haverkamp *et al.*, 1984). In *Figure 5.37*, the spatial variability between the two access holes is evident. In general, HL-102N yielded higher count ratio for a given water content than HL-101N. Therefore, using a common calibration curve for the two access holes will have a filtering, or an averaging effect. The difficulty associated with spatial variability is further emphasized in the neutron count profiles shown in *Figure 5.38*. The neutron count ratio profile along the two access holes are different on the same day indicating inter hole variability in soil moisture profiles.

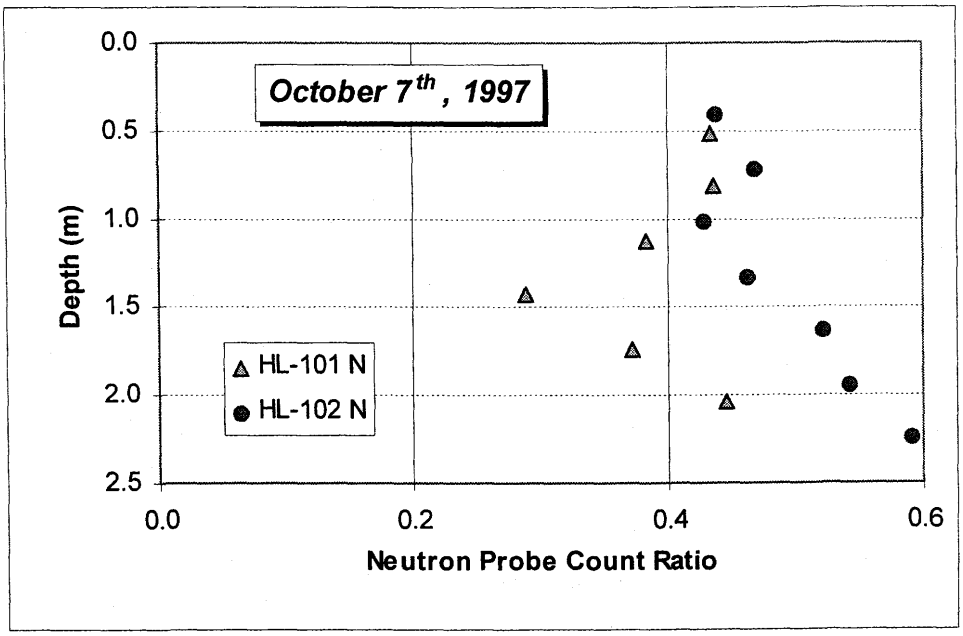

Figure 5.38 Comparison of neutron probe count ratios for two access holes.

The field calibration efforts did not result in a reliable calibration curve. This was due to the narrow range of water contents that were encountered during the calibration process. The spatial variation was noted to be significant, and errors associated with the gravimetric soil sampling procedures have been noted. A laboratory calibration program was undertaken to overcome these field calibration difficulties.

5.7.3.3 Laboratory Calibration Results

Laboratory calibration errors result from difficulties associated with attaining a soil volume that reflects actual field soil density and texture conditions. In addition, non-random differences in bulk density commonly arise when packing. Although the laboratory drum calibration method has limitations on sample size and uniformity of packing, they are considered manageable when compared with the possible error and variability associated with field calibration procedures (Greacen and Schrale, 1976).

The laboratory calibration method that was employed is described in detail in subsection 4.3.2. A laboratory calibration is commonly obtained using a two-point, or a two-standard calibration technique. A linear relationship is assumed *a priori* and a calibration curve of the following general equation is obtained:

$$\theta = a\,(CR) + b \qquad [5.4]$$

where,

θ = volumetric water content

CR = count ratio

a = slope of CR vs θ curve

b = θ - intercept when $CR = 0$

The results of the laboratory calibration program are tabulated in *Table 5.12.* Two sets of two point calibration were carried out for each soil type at varying dry densities. The results are also illustrated in *Figure 5.39.*

Table 5.12 Neutron probe laboratory calibration results.

Soil Medium	Dry Density	Slope (a)	θ -intercept (b)
Sand (#1)	1.69 g/cm^3	0.684	-12.1
Sand (#2)	1.58 g/cm^3	0.614	-3.3
Till (#1)	1.99 g/cm^3	0.680	-18.1
Till (#2)	1.80 g/cm^3	0.596	-3.9

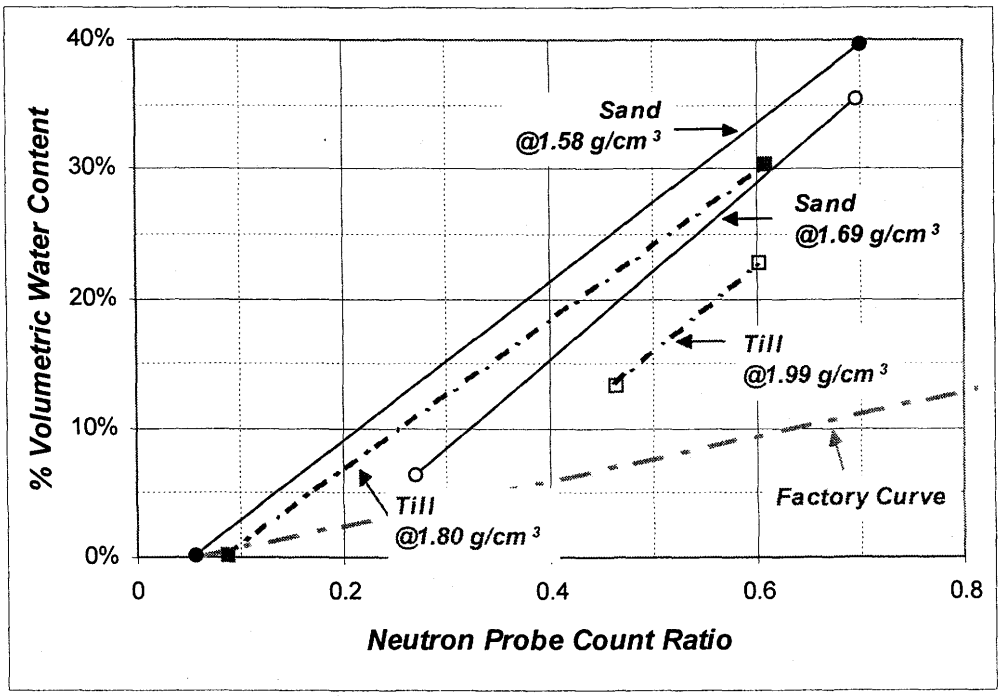

Figure 5.39 Laboratory NP calibration results using a two-standard technique.

The laboratory calibration results exhibit numerous trends consistent with findings by many researchers. As the soil bulk density increases, the count ratio for a given volumetric water content increases (Jensen and Somer, 1967; Damagnez 1967; Nagy and Verites, 1968; Greacen and Schrale, 1976). A change in the soil bulk density results in a significant parallel shift of the calibration curve (Marais and Smit, 1962). As the bulk density increases, the y-intercept becomes more negative (Chanasyk and McKenzie, 1986). The slope of the laboratory calibration curves are three to four times the factory calibration curve (i.e. less

sensitive) due to the application of a large diameter PVC tubing material (Grismer *et al.*, 1995). The factory calibration curve underestimates soil water content by 65% to 75%. The presence of large size particles in the brown till results in lower count ratio when compared to the outwash sand.

5.7.3.4 Estimation of the Calibration Curve

The results of the laboratory calibration tests were used to assess the effects of soil type and dry density on the resulting curve, as well as the shape of the curve. Many researchers have concluded that the neutron probe calibration curve was independent of the soil type (Babalola 1978; Silvestri *et al.*, 1991). Conversely, other researchers have indicated that the curve was very much dependent on soil property (Greacen and Highett, 1979). The effects of the soil type on the nature of the calibration curve was evaluated by analyzing the data based on soil type, as well as grouping all data irrespective of the soil type.

The significance of bulk density effects was evaluated by applying a bulk density correction factor (Greacen and Schrale, 1976). Raw data was normalized to the average field density for each soil type (1.76 g/cm^3 for sand and 2.02 g/cm^3 for till). In addition, all data was normalized to an arbitrary standard density of 1.80 g/cm^3. The density corrected data was compared to uncorrected raw data to assess the effects of soil density.

It has been concluded by many researchers that the calibration curve becomes more and more non-linear as the diameter of the access tube increases (Marais and Smit (1960); Tyler 1988). The shape of the calibration curve was evaluated by performing a series of linear and power regression analysis of the calibration data by soil type, and for all combined data.

A total of sixteen regression analysis were carried out to determine the best fit curve. The regression results are presented in detail in Appendix F. The best fit analysis has indicated that an insignificant improvement in data correlation was achieved by grouping data based on soil type and/or by applying a bulk density correction factor. As well, a power regression

resulted in the best fit calibration equation (*Figure 5.40*). It is thus concluded that a laboratory calibration equation using a power regression on uncorrected and combined data best represents the overall calibration equation. Combining all data points irrespective of the soil type, dry density, or calibration method, has an averaging or a filtering effect. However, given the lack of information on soil density and soil type along the length of each neutron probe access hole, this averaging may best estimate field soil moisture conditions.

The subsequent regression analysis consisted of combining the laboratory calibration data with the field calibration data. The laboratory calibration data consisted of eight uncorrected data points. Field calibration data consisted of nine HL-101N data points that were grouped and reduced to four data points based on water content values. Field data sorting and grouping was necessary due to the narrow range in the water content values in the data set which would imposes too much significance to the lower water content range.

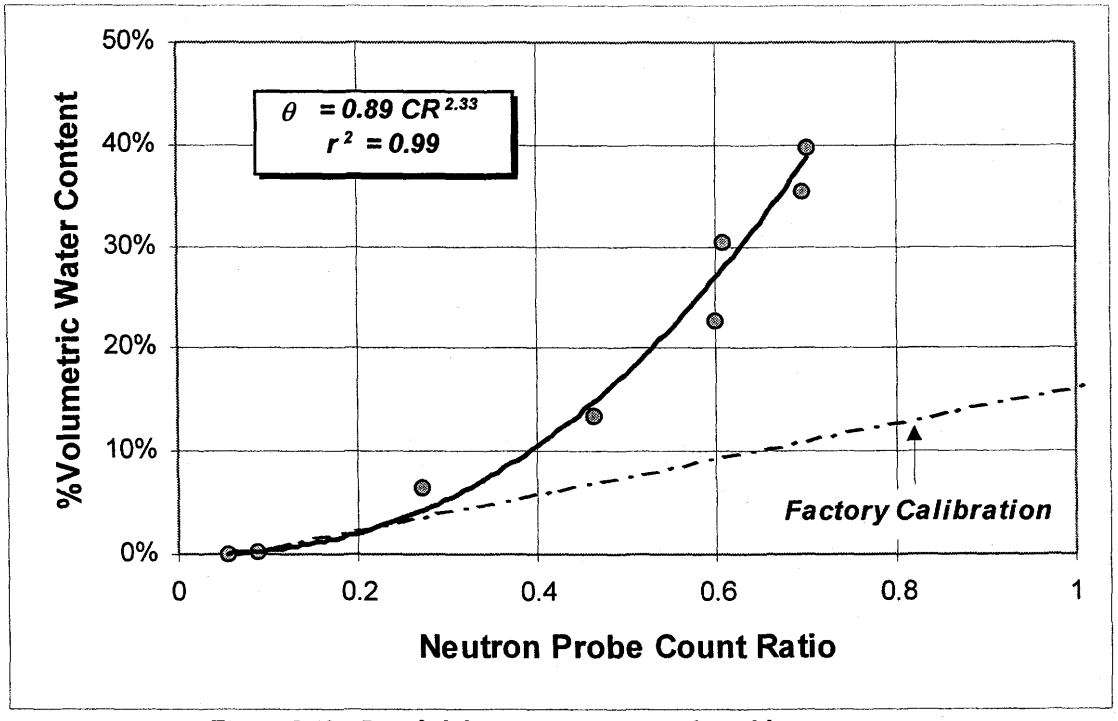

Figure 5.40 Best fit laboratory neutron probe calibration curve.

Figure 5.41 provides a comparison of the resulting laboratory calibration curve versus the

combined laboratory and field data calibration curve. The combined calibration equation yields a coefficient of determination $r^2 = 0.923$ versus $r^2 = 0.993$ for the laboratory calibration curve. It estimates lower water content at higher count ratios. The neutron probe calibration equation employed to convert field monitored count ratio to field soil moisture content is based on the combined field and laboratory calibration data. The calibration equation is represented as:

$$\theta = 0.78\ (CR)^{2.28} \qquad [5.5]$$

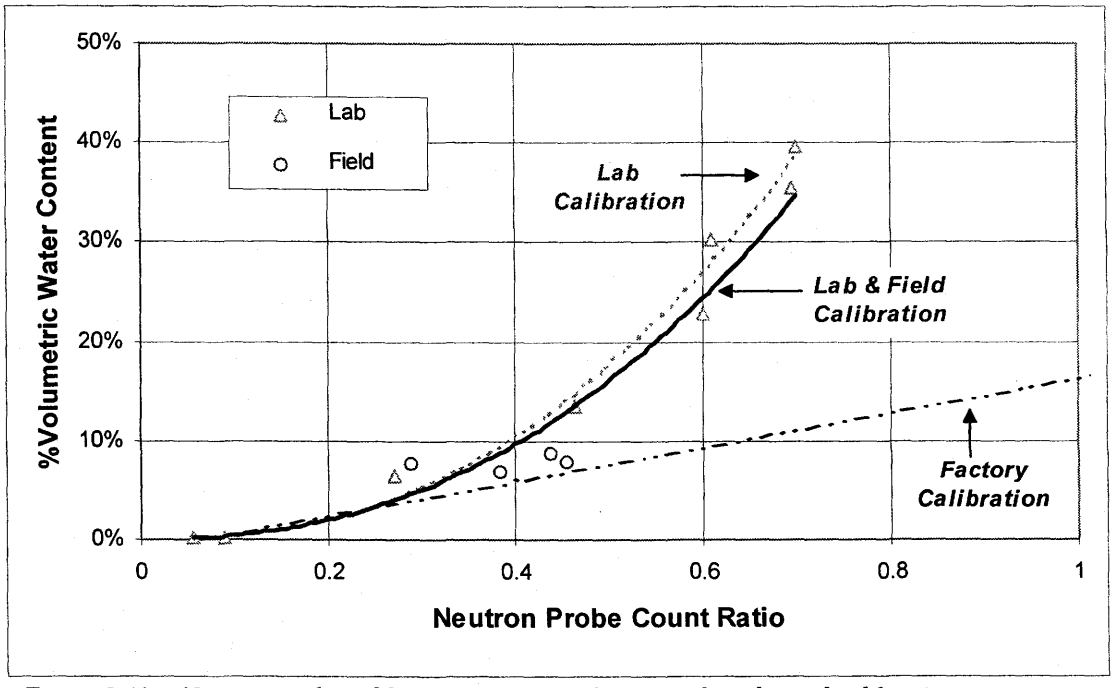

Figure 5.41 *Neutron probe calibration curves. Laboratory data derived calibration curve versus combined laboratory and field data derived calibration curve.*

5.7.3.4 Verification of the Calibration Equation

The estimated neutron probe calibration curve requires verification to establish confidence in the equation. The soil moisture profile for the access hole HL-101N on October 7th, 1997 is shown in *Figure 5.42*. This profile was compiled using the results of the sonic drill soil sampling near the access hole HL-101N, hand excavation sampling results, and neutron probe count ratios that were converted to soil moisture contents using the calibration equation. In general, the calibration equation appears to overestimate the soil moisture content when compared to other measurement techniques.

The temporal changes in the soil moisture profile for the access hole HL-101N is shown in *Figure 5.43*. As surface infiltration percolates downward, the water table rises from approximately 2.9 m from surface in April to approximately 2.4 m in August. The high moisture content at 2 m depth on August 22nd, 1997 reflects the high water table. The moisture content of the subsurface materials, sand and till, fluctuate significantly near the water table with its rise and fall. However, there is very little change in the soil moisture profile within the upper 1.5 m (*Figure 5.43*).

Figure 5.44 shows an accumulation of snow melt infiltration at the frost line where the frozen soil/water medium provides an impermeable barrier to the infiltration water. As the facility warms up and thaws out with the advent of warmer weather, the accumulated water infiltrates to the water table below.

Figure 5.45 shows temporal variation in the soil moisture profile for the access hole HL-102N. This profile clearly illustrates the effect of rise and fall of the water table. The drastic change in the soil water content at the cobble ore/sand interface is clearly evident. This reflects the vastly differing soil water characteristic of these two materials. The accumulation of the snow melt water in May is also evident at 1.6 m depth.

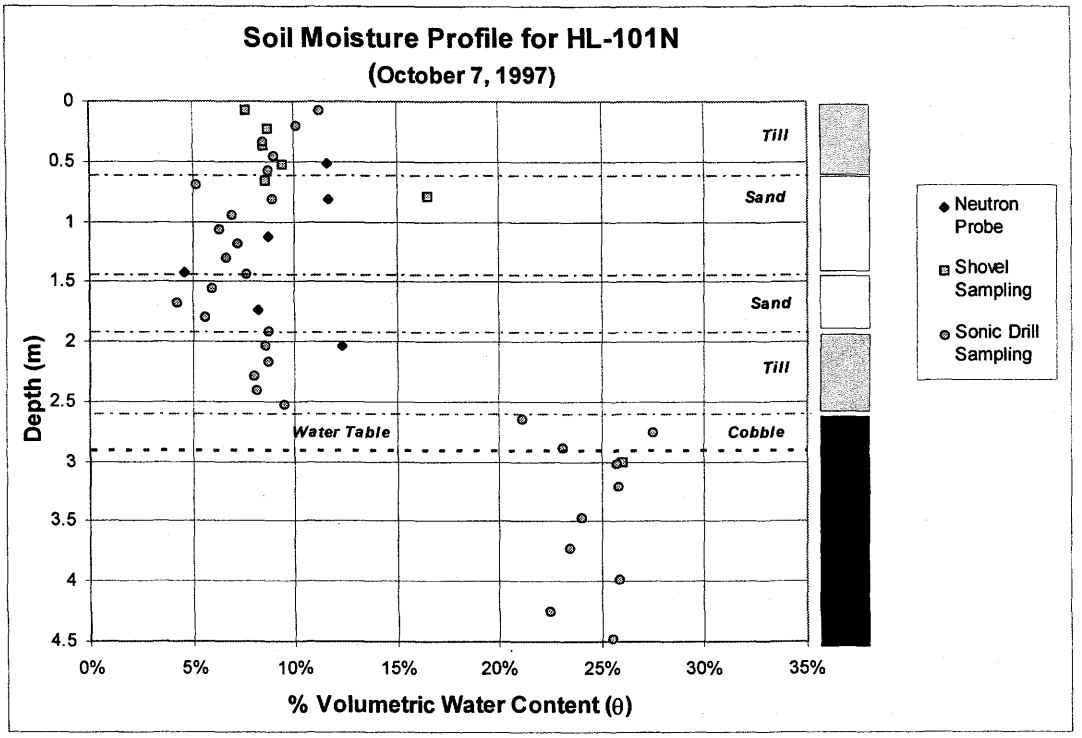

Figure 5.42 HL-101N soil moisture profile for October 7th, 1997.

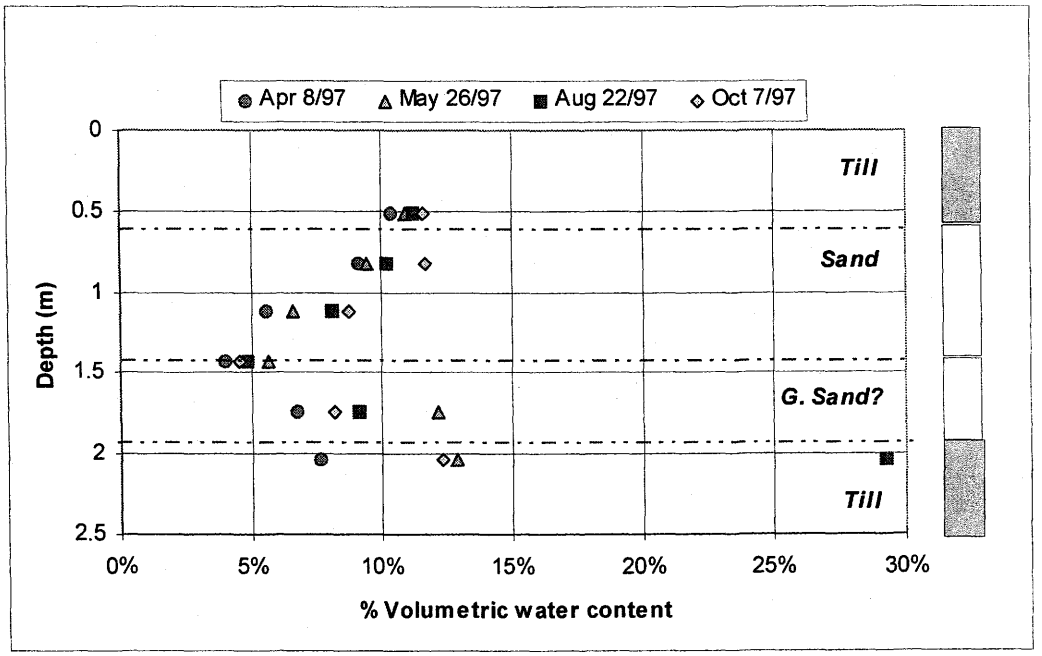

Figure 5.43 Temporal variation in the soil moisture profile for HL-101N.

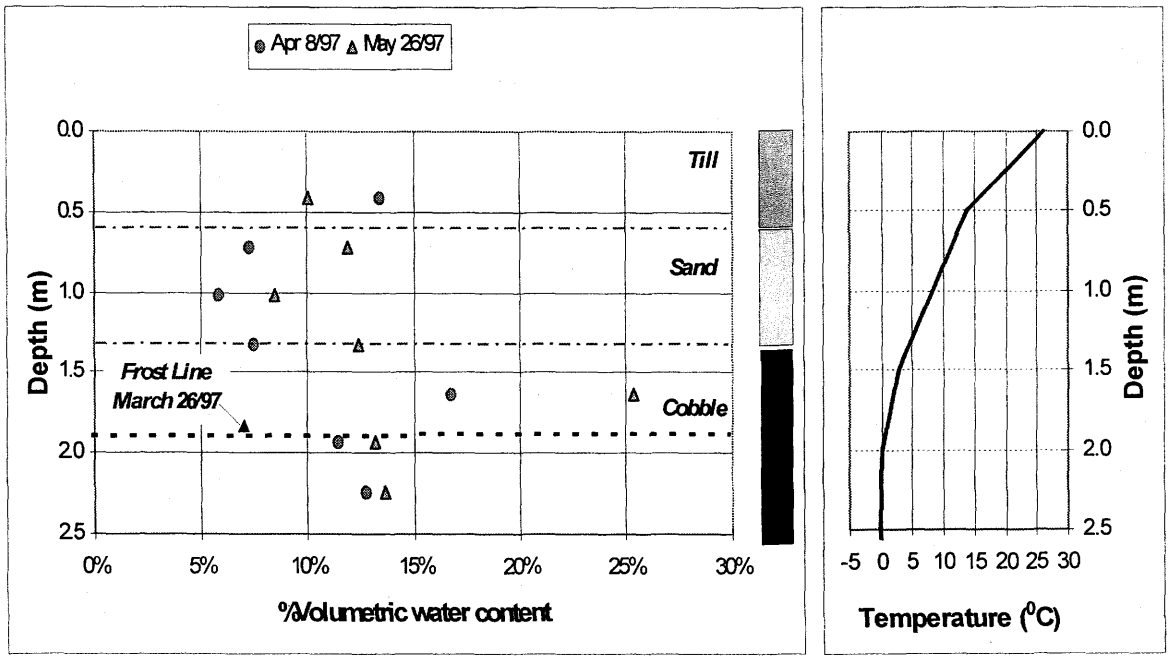

Figure 5.44 April snow melt infiltration accumulates at the frost line.

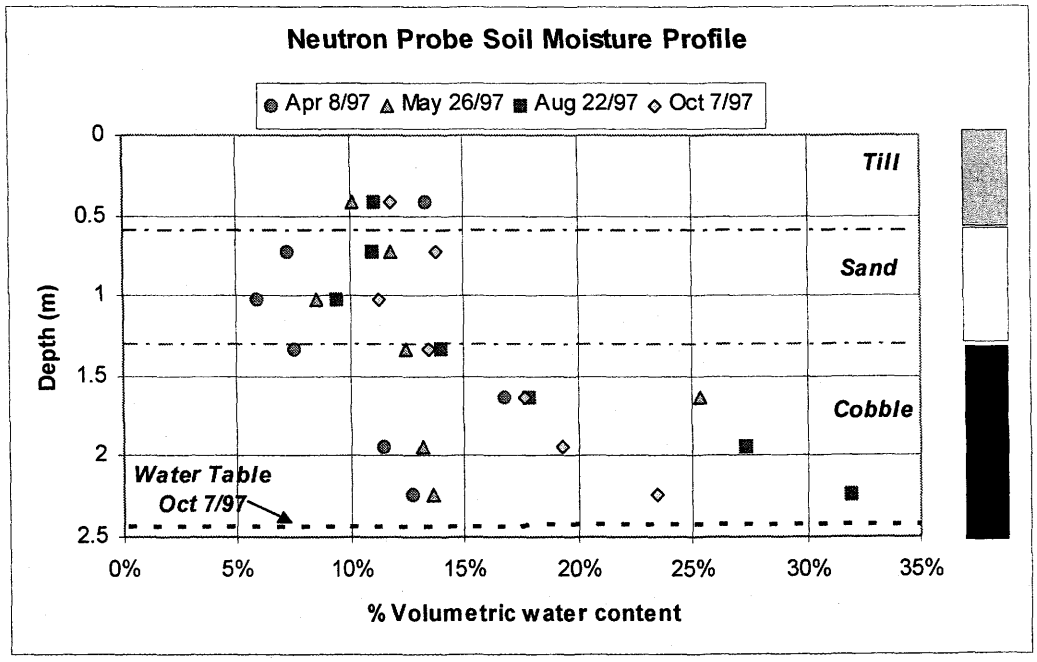

Figure 5.45 Soil moisture profile for access hole HL-102N.

5.7.3.5 Verification of Access Hole HL-102N Soil Profile

A detailed soil sampling program was undertaken in the vicinity of the access hole HL-101N, and the results were used to construct the soil profile found in *Figures 5.42* and *5.43*. At the time the field investigation was undertaken, it was believed that the soil profile was consistent throughout the facility, and therefore, one profile sampling was considered adequate. However, the neutron probe results for access hole HL-102N have indicated that the soil profile along the length of this hole differs significantly from access hole HL-101N.

Using an estimated water table depth, and assuming a hydrostatic condition, a plot of neutron probe estimated soil moisture content versus soil suction was generated (*Figure 5.46*). This field estimated soil water characteristic curve (SWCC) was compared to laboratory estimated brown till and cobble ore SWCCs. Along the access hole HL-101N, sand and till was present at 1.35 m to 2.5 m depth. However, the plot of field estimated SWCC for the access hole HL-102N has identified the material found in depths greater than 1.35 m to be cobble ore. This conclusion was used to generate the soil profile found in *Figures 5.44* and *5.45*.

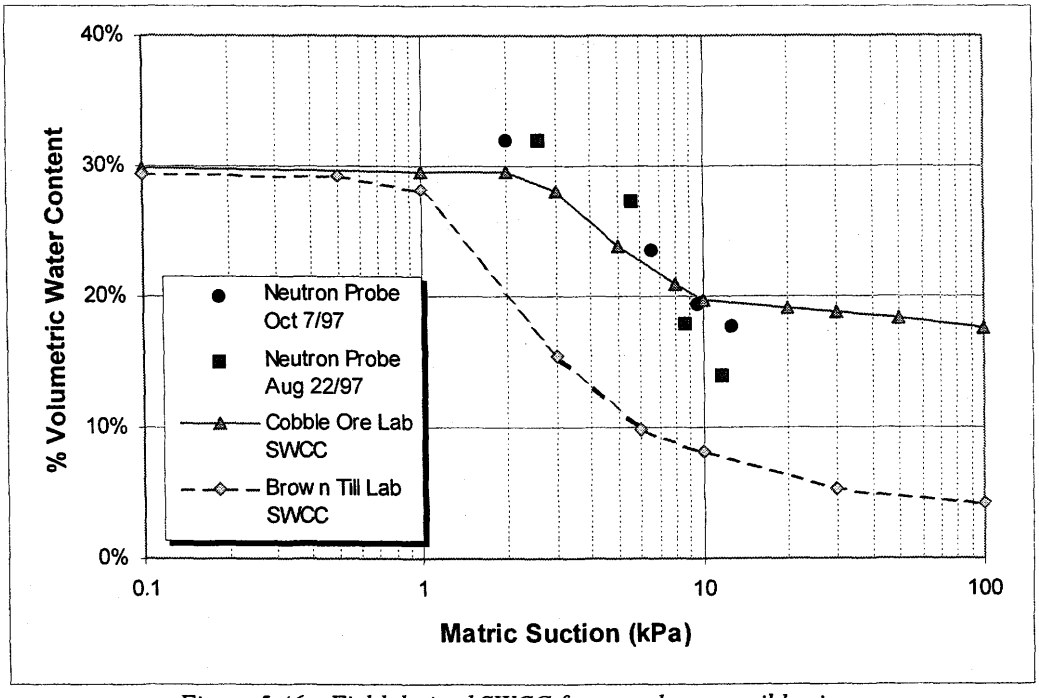

Figure 5.46 Field derived SWCC for an unknown soil horizon.

Chapter Six

ANALYSIS AND INTERPRETATION

This chapter provides the basis for the analysis and the evaluation of the Key Lake HLTF prototype test cover performance. The field performance of a cover system is assessed by monitoring and verifying net water infiltration into the system. The required overall facility water balance calculation and analysis are found in section 6.1. Section 6.2 presents a discussion on the suitability of utilizing local tills and sands for cover materials based on the evaluation of the test cover performance. Section 6.3 presents an analysis of runoff and infiltration characteristics based on actual precipitation and runoff data.

6.1 WATER BALANCE

The main objective of this research project was to evaluate the field performance of the HLTF test cover as designed and constructed. The primary function of a soil cover system is to minimize net water infiltration into the waste containment facility. Thus, an assessment of a soil cover system is achieved by monitoring the net infiltrative flux.

The net infiltration through a non-vegetated soil cover system is given by:

$$I_n = P - R - E - D \pm \Delta S \qquad [6.1]$$

where, I_n = net infiltration

P = precipitation

R = surface runoff

E = actual evaporation

D = deep percolation or water removed from the facility, and

ΔS = change in subsurface soil-water storage.

An effective soil cover monitoring system strives to accurately identify each of the above parameters. *Table 6.1* provides a summary of the HLTF cover monitoring program. The 1997 water balance calculation is carried out from mid-April to mid-October, 1997. This is because winter precipitation doesn't contribute to infiltration until the onset of spring snow melt. Moreover, the surface snow cover effectively shuts down evaporation during the winter months.

Table 6.1 HLTF water balance for 1997 monitoring season.

Parameter	**Measurement Method**	**Data Reliability**	**Total mm**
Net Infiltration(I_n)	Indirect (estimated by recording the volume of water removed from the facility)	Reasonable (based on the assumption of constant water table height at the end of each pumping season)	287 mm
Precipitation (P)	Direct measurement (tipping bucket rain gauge)	Reliable (tipping bucket rain gauges typically under-estimate 1% to 5% for heavy intensity rainfalls)	494 mm (59 mm snow pack and 435 mm rainfall)
Actual evaporation (E)	Indirect estimation (calculated using weather parameters and AE/PE estimates)	Evaporation estimate is used to verify the accuracy of infiltration measurements	167 mm
Surface runoff (R)	Direct measurement (measured every 30 seconds)	Reliable	35 mm
Water removed (D)	Direct measurement (water removed from the facility is metered)	Reliable	287 mm
Change in subsurface soil-water storage (ΔS)	Indirect measurement (soil-water content profile is determined using the neutron method)	Reasonable (the method reliability is highly dependent on the calibration curve)	Insignificant

6.1.1 Net Infiltration

The net infiltration represents the net change in subsurface water storage for a given period of time. The net infiltration can be directly determined by using weighing lysimeters, or indirectly by monitoring the change in soil suction or soil-water content with depth (subsection 2.4.5). Typically, the net change in the subsurface water storage is dependent on water input (*P-R*) and water output (*E+D*). For a containment system that incorporates water removal through drainage and/or pumping, the net infiltration is given by the quantity of water removed (*E+D*) and the net change in the subsurface water storage.

The HLTF is a double lined containment system (section 3.2). It is essentially a very large lysimeter, whereby the net infiltration is determined by monitoring the temporal variation in soil-water content profile, the changes in water table depth, and the quantity of water removed from the containment facility. During the summer of 1997, 287 mm of water was pumped from the facility (section 5.5). This quantity represents water that was removed to re-establish the water table depth to the previous year's depth of 2.4 m in October, 1996. The neutron probe results indicate insignificant changes in subsurface soil-water content between November 27th, 1996 and October 7th, 1997 from 0.6 to 2.1 m depth (*Figure 6.1*).

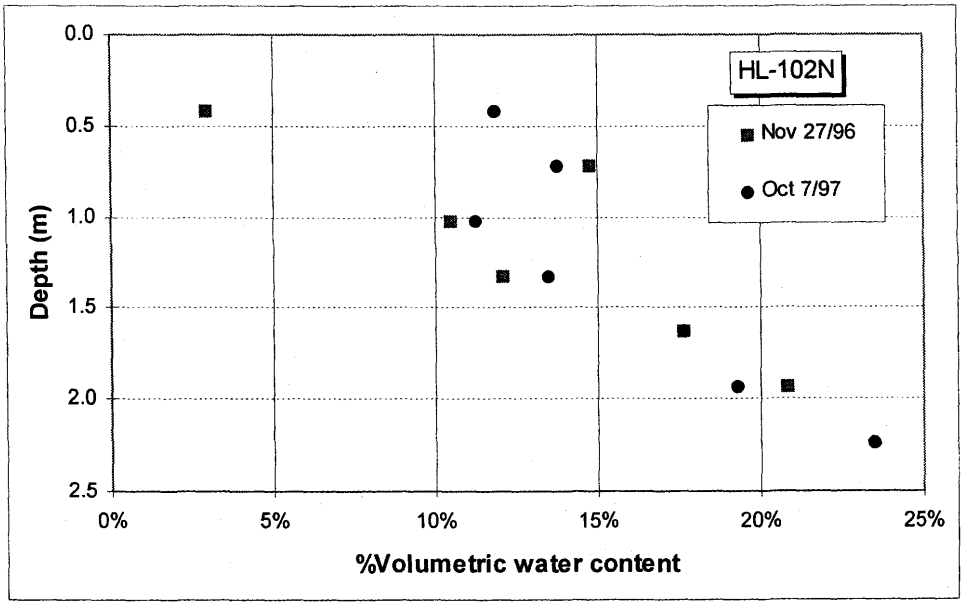

Figure 6.1 Neutron Probe access hole HL-102N monitoring results.

The neutron probe reading at 0.4 m depth shows higher subsurface soil-water storage on October 7th (12% versus 3% on November 27th, 1996). The difference in the volumetric water content between the two dates is 9%. However, the subsurface water in the surficial till layer would have drained to the residual water content of approximately 7 to 8%, and surficial freezing would have further lowered the soil-water content.

The net change in the subsurface water storage between November 1996 and November 1997 is considered to be insignificant. Therefore, the net infiltration from April 1997 to October 1997, inclusive, is approximately equal to 287 mm of water removed from the facility. This represents 52% of the annual precipitation (1997 summer rainfall plus 1996-1997 winter snowfall), or 58% of the total precipitation available for infiltration (snow pack prior to spring snow melt plus rainfall).

The 52% annual net infiltration for this study site is comparable to results obtained by Ayres (1998), and Meneley and Cherry (1986) at Cluff Lake. For a vegetated natural till study site at Cluff Lake, Ayres estimated 36% net infiltration for 1996, and 42% net infiltration for 1997. Meneley and Cherry estimated 40% net infiltration for a watershed adjacent to Ayres' study site. Both research sites at Cluff Lake sustain natural vegetation, and therefore, the annual total evapotranspiration at Cluff Lake is expected to be higher than the annual total evaporation at the non-vegetated HLTF.

6.1.2 Precipitation

The precipitation parameter is relatively easily quantified. Winter precipitation does not contribute to infiltration until the commencement of spring snow melt in April. The quantity of the accumulated snowfall that partitions into runoff and infiltration in spring is estimated directly by carrying out a field snow survey just prior to the onset of spring snow melt (subsection 5.3.6). The runoff monitoring results have indicated that a spring snow melt event typically occurs over a short period of time. In spring 1997, an average accumulated snow depth of 247 mm, or 59 mm rain equivalent, melted over a five day period.

The summer rainfall was monitored using a tipping bucket rain gauge (subsection 5.3.1). The 1997 weather monitoring program yielded 435 mm of rainfall during the months of May to October. The total precipitation for 1997 is estimated to be 494 mm, of which 435 mm is summer rainfall and 59 mm is snow pack prior to the commencement of spring snow melt.

6.1.3 Actual Evaporation

The actual evaporation (AE) is typically monitored using a Bowen Ratio Instrumentation. The Bowen Ratio Instrumentation program at the HLTF was not successful due to equipment failure (subsection 5.6.5). As a result, the site AE was estimated using the calculated daily PE, and estimated daily AE/PE ratios.

The AE at the soil surface approximately equals PE (i.e., AE/PE = 1) when the soil surface is near saturated (i.e., when the matric suction at the soil surface is at a suction level equivalent to the relative humidity of the surrounding air). As the soil surface dries out (i.e., as relative humidity in the soil at the surface begins to fall below the relative humidity in the atmosphere), the rate of AE declines rapidly (i.e., AE/PE < 1). That is to say, the AE can equal to PE during and immediately after a significant rainfall event when the soil surface becomes saturated. As the soil surface begins to dry out in response to atmospheric demands, the AE/PE ratio begins to decline to a residual AE/PE ratio.

The AE/PE ratios were assigned on a day to day basis as a function of Cluff Lake AET/PE ratios (Ayres 1998), SoilCover (1997) modeling results, and the daily site weather data.

Estimating Site Potential Evaporation

The daily PE were calculated using the Penman formulation and the HLTF weather data: mean wind speed, mean air temperature, adjusted mean relative humidity, and adjusted net radiation. An analysis of site air temperature and wind speed data have suggested they are reliable (subsections 5.3.2 and 5.3.4). However, the humidity probe was found to record

higher than 100% relative humidity (subsection 5.3.3); net radiation was substantially lower than the recorded regional net radiation (subsections 5.3.5). Data correction was carried out to adjust the relative humidity and net radiation data to recorded regional levels.

The calculated PE was compared to the *Key Lake weather station* pan evaporation data to validate the required data adjustment. The uncorrected weather data yielded a pan coefficient of 0.53 versus 0.76 using the Kohler *et al.* (1955) empirical method (subsection 5.6.3). The corrected weather data resulted in a pan coefficient of 0.73, which is within the expected values for the region (Gray 1973, Ayres 1998). Therefore, the estimated daily PE values for 1997 using adjusted weather data are deemed representative.

Estimating AE/PE Ratios

Th AE is characterized by three distinct phases. The first phase represents evaporation after a significant rainfall event when the soil surface is saturated or near saturated. During this initial phase, the AE approximately equals PE. The second phase describes the subsequent drying out period when the rate of AE declines rapidly as the soil surface becomes unsaturated. The last phase is the residual drying phase.

SoilCover (1997) modeling was carried out to establish the shape of the AE/PE curve with time following a rainfall event. The slope of the curve during phase II drying, as well as the residual AE/PE ratios during phase III drying, were investigated. The SoilCover modeling exercise attempted to better define factors that affect the shape of the AE/PE curve.

The antecedent soil-water content conditions and precipitation characteristics were varied to assess their impact on the magnitude of the initial, or the maximum AE/PE ratio. The seasonal changes in climatic conditions were also investigated to evaluate their effects on the slope of the curve during phase II drying, and the magnitude of the residual phase III AE/PE ratio. Using SoilCover modeling results and actual AET/PE ratios that were recorded at Cluff Lake, daily AE/PE ratios were allocated for the HLTF from April to October, 1997.

Figure 6.2 illustrates the effects of antecedent soil-water content on the resulting AE/PE using actual weather data (July 18th to 27th, 1997). *Table 6.2* summarizes the initial conditions that were used in the model: a hydrostatic profile with water table at 2.4 m depth (i.e., dry); a residual soil-water content profile with water table at 2.4 m depth (i.e., gravity drained); and an infiltrating soil-water content profile with water table at 0.6 m depth (i.e., wet). An equal amount of precipitation (20 mm) was applied over a 6 ½ hour period (17:30 to 24:00) on July 18th, and the soil profile was allowed to dry out for 9 subsequent days.

The hydrostatic and near residual antecedent conditions yielded almost identical AE/PE curves. The wet antecedent condition also resulted in a similar AE/PE curve. For the conditions that were evaluated, SoilCover does not appear to differentiate the changes in antecedent moisture conditions.

Table 6.2 Comparison of antecedent soil-water content profile.

Soil Type	***Elevations***	***Hydrostatic profile***	***Residual profile***	***Wet profile***
Till	70 - 64 cm	5% to 3%	12% to 14%	25% to 30%
Sand	64 - 57 cm	3% to 1%	8% to 8%	35% to 35%
Cobble	57 - 46 cm	10% to 18%	18% to 30%	30% to 30%
Cobble	46 - 0 cm	18% to 30%	30%	30%

Figure 6.3 illustrates the effects of climatic parameters on the AE/PE ratios. The initial soil-water content profile (gravity drained) and the precipitation input was maintained identical for all three seasonal scenarios (20 mm). Actual climate data was used for each of the three months. The slopes of the AE/PE curves for spring (April) and summer (July) conditions appear to be similar. However, during spring, the rainfall input results in an AE/PE ratio of one (1) on the first day, whereas during summer, the AE/PE ratio becomes one (1) on the following day. The residual AE/PE ratio is the lowest for the summer scenario (July).

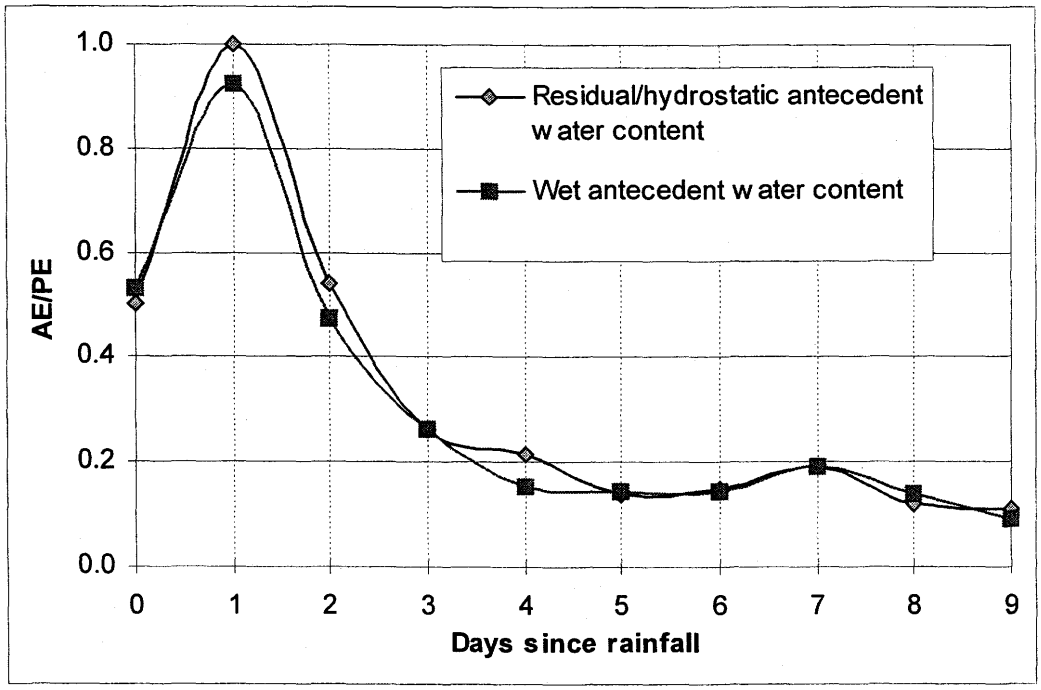

Figure 6.2 Effects of antecedent soil-water conditions on the AE/PE ratio.

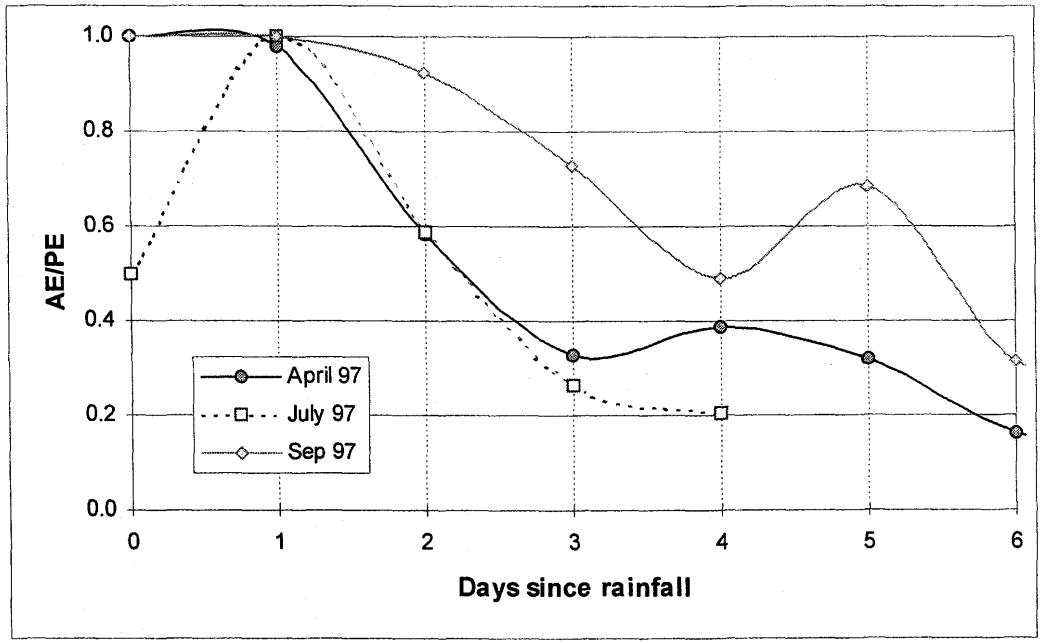

Figure 6.3 Effects of climatic conditions on the resulting AE/PE ratios.

Figure 6.4 provides a comparison of SoilCover predicted AE/PE ratios at the HLTF versus the actual AET/PE ratios at Cluff Lake (Ayres 1998). The illustrated Cluff Lake AET/PE curve is for June 1997 following two days of moderate precipitation (11 mm total) when site vegetation was insignificant. The slope of the Cluff Lake AET/PE curve is shallower, and the minimum AET/PE ratio is higher than what was predicted by SoilCover for the HLTF.

In general, SoilCover predicted an AE/PE ratio of one (1) for most rainfall events that were modeled. However, during May 10th to July 7th, 1996, the Bowen Ratio monitoring program for the Cluff Lake till only recorded one day when the AET/PE ratio was close to one (0.97). This occurred after 2 ½ days of heavy rainfall (June 16th to 19th) totaling 52.6 mm.

SoilCover was also used to predict the HLTF AE/PE ratios for June, July, and August, 1997 by partitioning each modeling period by major rainfall events. SoilCover predicted an average AE/PE ratio of 0.54. The AET/PE ratio at Cluff Lake till monitoring site for the same period was reported to be 0.46 (Ayres 1998). It appears that SoilCover over-predicts evaporation levels for the soil and climatic conditions at the HLTF.

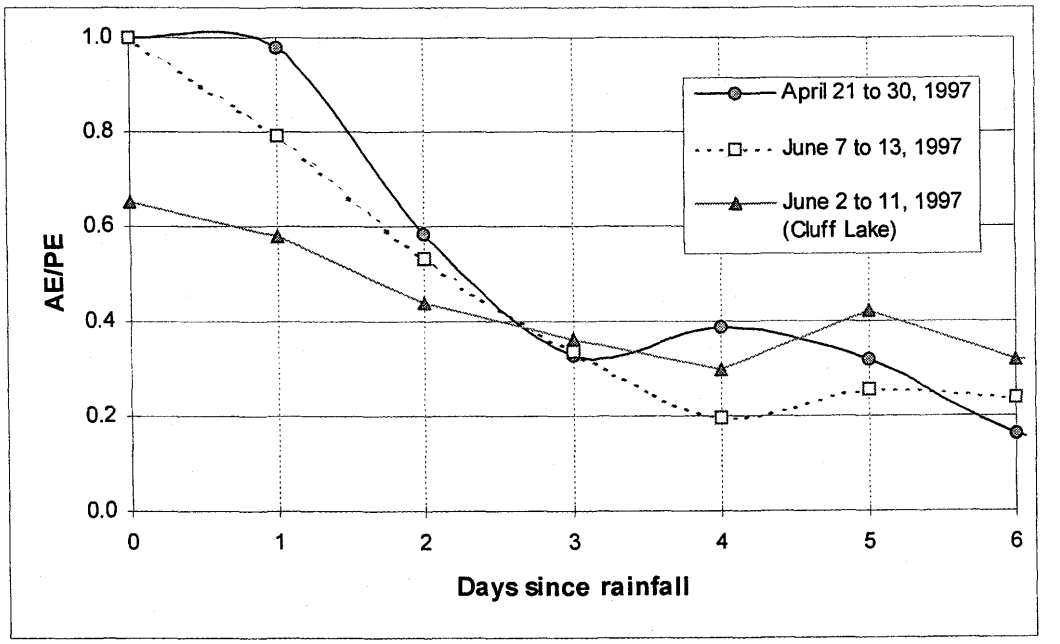

Figure 6.4 AE/PE ratios for the HLTF versus AET/PE ratios as Cluff Lake.

The daily AE/PE ratios were assigned based on SoilCover modeling results, Cluff Lake till monitoring site AET/PE ratios (Ayres 1998), and daily weather conditions. The resulting average AE/PE ratio for the HLTF is 0.31. *Table 6.2* provides a summary of AE/PE ratio comparisons. The total estimated AE for April to October, 1997, is 167 mm.

Table 6.3 Comparison of 1997 AE/PE ratios.

	Estimated HLTF AE/PE	**SoilCover Predicted AE/PE for HLTF**	**Cluff Lake AET/PE for 1996 (Ayres 1998)**	**Cluff Lake AET/PE for 1997 (Ayres 1998)**
April	**0.23**		0.50	0.50
May	**0.23**		0.24	0.30
June	**0.29**	0.48	0.54	0.73
July	**0.39**	0.47	0.60	0.70
August	**0.41**	0.63	0.70	0.70
September	**0.40**	0.68	0.70	0.70
October	**0.22**		0.50	0.60
Average AE/PE	***0.31***	***0.56***	***0.54***	***0.60***

6.1.4 Surface Runoff

The partitioning of precipitation into runoff and infiltration has been successfully and accurately measured on a real time basis at the HLTF from June to mid-October, 1997 (section 5.4). Although the partitioning of rainfall into runoff was not monitored for May, actual runoff for this months is anticipated to be insignificant. For June, less than 1% runoff was recorded for 64 mm of monthly total rainfall, versus 28 mm of rainfall in May.

The recorded surface runoff during 1997 spring snow melt is 2.2 mm. However, the actual snow melt runoff is expected to be higher; the runoff collection culvert was leaking during

this time, and therefore, not all the surface runoff was detected by the sensor. Based on the recorded runoff hydrograph and the extent of soil erosion due to leakage from the culvert, the actual snow melt surface runoff was estimated at 4.2 mm. The recorded 1997 summer runoff was 31.8 mm. The total runoff for the 1997 water balance is 35 mm, or 7.3% of the recorded rainfall from June to October, 1997, inclusive, and 7.1% of the surveyed snow pack in April, 1997.

6.1.5 Drainage

The HLTF is a contained system that collects and isolates all infiltration. The facility was periodically pumped to remove infiltrated water during the summer months. The quantity of water removed was metered to maintain an accurate account of the volume of water pumped from the facility. At the end of the monitoring season in late October, the facility is typically pumped to re-establish the water table to a predetermined depth of 2.4 m.

The total volume of water pumped from the facility is therefore a reasonable estimate of the annual net infiltration: i.e., $D = I_n$. The total volume of water removed during 1997 pumping season is 810 m^3, or 287 mm.

6.1.6 Subsurface Storage

The net change in subsurface soil-water content is considered to be insignificant since the water table was drawn down to the same depth at the end of each monitoring season. The neutron probe results have indicated little change in the soil-water content profile (subsection 6.1.1.). Furthermore, the storage capacity of the HLTF cover system is nominal (12 mm).

The Stormant and Morris (1998) method of estimating the water storage capacity of a capillary barrier system was used to calculate the water storage capacity of the HLTF soil cover system. Stormant and Morris determine the storage capacity of a layered system by estimating the suction head profile in the upper fine layer when water first enters into the

underlying coarse layer (i.e., at its air entry value). Then using the soil-water characteristic curve (SWCC) of the overlying fine layer, the corresponding water content profile is derived. Integrating the water content over the depth of the upper soil layer indicates the total water storage capacity of the capillary barrier system. The net storage capacity, for a non-vegetated system, is the total capacity less the storage capacity under gravity drained soil moisture conditions (i.e., field capacity). The field capacity is the maximum water content that a soil can hold against gravity before it drains downward.

Both the surficial till and the underlying sand layers at the HLTF have similar air entry values (approximately 1 kPa), and therefore, the underlying sand layer will not form a capillary barrier. The sand and till layers will drain together when suction at the cobble ore/sand interface drops below the cobble ore air entry value (AEV). Using the cobble ore AEV lower boundary condition (3 kPa) at the cobble ore/sand interface, a water content profile was constructed (*Figure 6.5*). The water content profile was generated using laboratory determined sand and till SWCCs under hydrostatic conditions. The water content in each of the layers was not allowed to drop below respective gravity drained water content levels.

The net storage capacity of each soil layer is graphically presented in *Figure 6.6.* The estimated net storage capacity is approximately 9 mm in the sand layer, and 3 mm in the till layer. The total net storage capacity of the HLTF soil cover system is 12 mm. The storage capacity in each of the layers is also illustrated in *Figures 6.7* and *6.8*. The net storage capacity is the area bounded by the SWCC and the gravity drained water content along the y-axis (5% for sand and 7% for till), and the suction at the underlying soil layer interface along the x-axis (3 kPa for sand and 9 kPa for till).

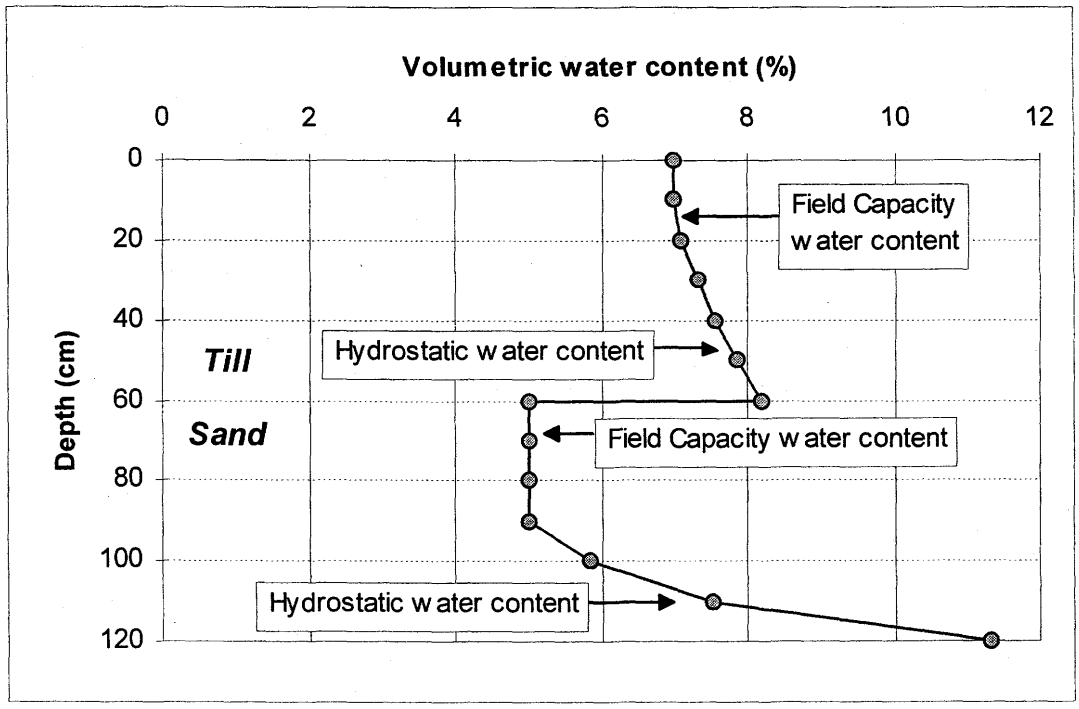

Figure 6.5 HLTF soil cover water content profile.

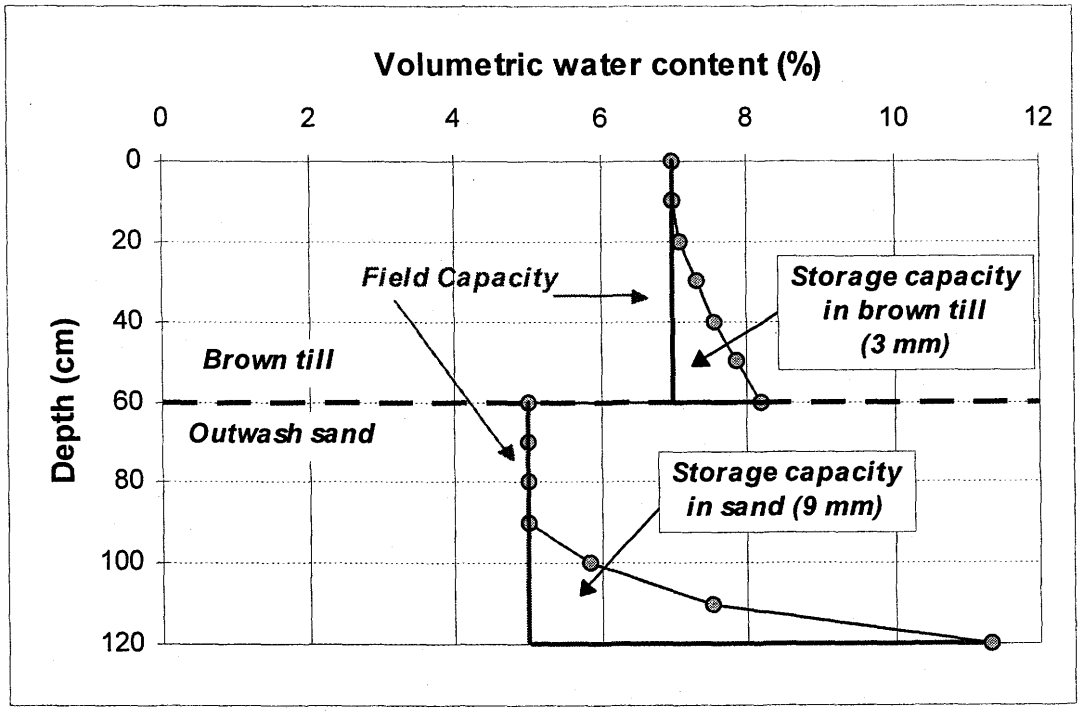

Figure 6.6 HLTF soil cover water storage capacity profile.

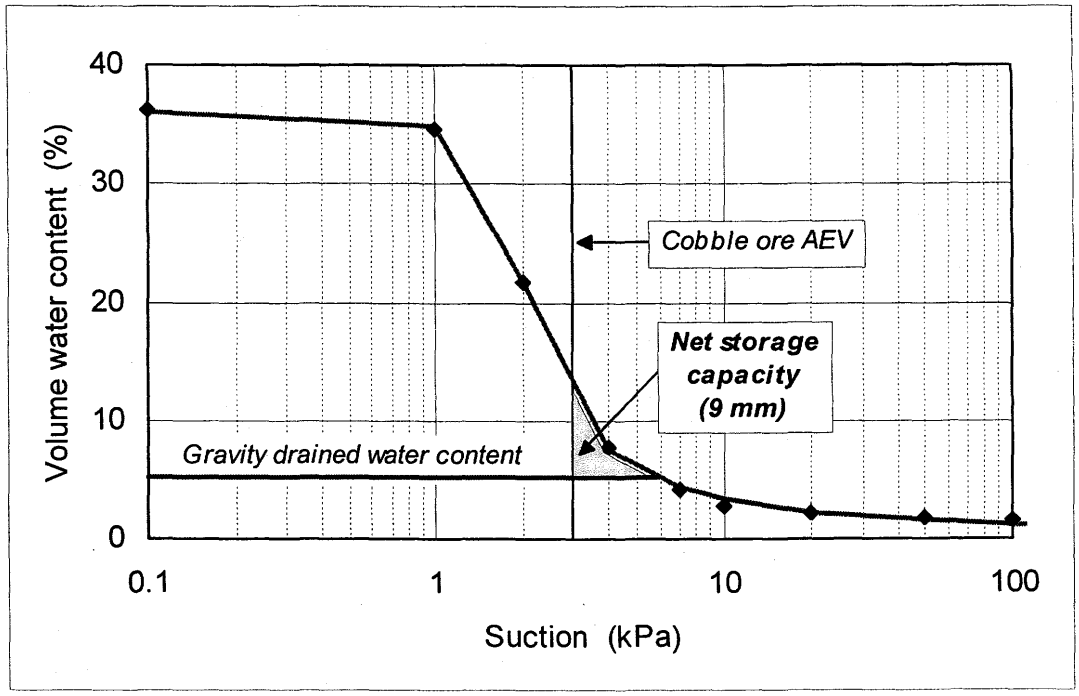

Figure 6.7 Net water storage capacity in the sand layer.

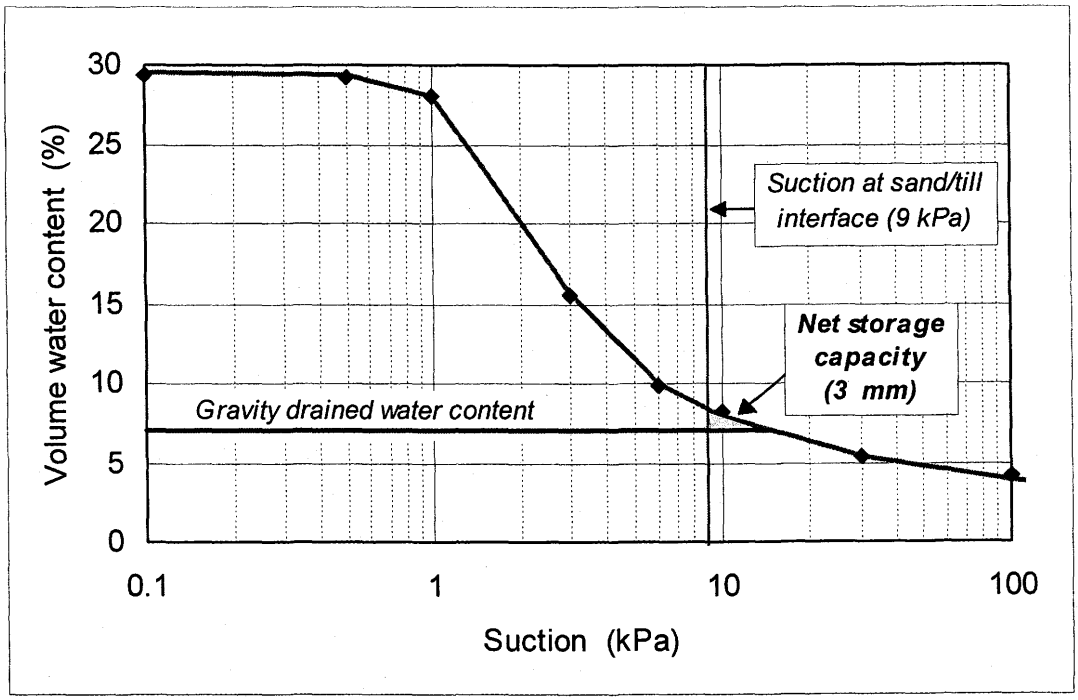

Figure 6.8 Net water storage capacity in the till layer.

6.1.7 1997 Water Balance

The 1997 water balance is graphically presented in *Figure 6.9,* and tabulated in *Table 6.3.* Based on the water balance calculation, the net infiltration for the HLTF is estimated at 292 mm versus 287 mm of measured net infiltration. This is based on the estimated AE using the AE/PE ratios that are approximately half of those reported for Cluff Lake till monitoring site (Ayres 1998).

A 20 year (1977 to 1997) high summer precipitation was recorded for 1997. As well, a 20 year high monthly records were set for July and September (subsection 5.3.1). The three month average rainfall for July, August, and September, 1997, is 110 mm. The three month average runoff for the same period was 9.3%. However, during June, 1997, 64 mm monthly total rainfall resulted in less than 1% runoff. The recorded 20 year average monthly total rainfall is approximately 60 mm. It is therefore postulated that 1997 recorded higher than average total surface runoff.

Accordingly, 1997 should have experienced lower than average summer evaporation due to an increased number of rainy days. Ayres (1998) estimated the net infiltration for 1996 and 1997 to be 36% and 42% respectively. It is therefore anticipated that the average annual net infiltration will be similar to what was recorded for 1997. During wet years, the increase in runoff will typically be offset by a decrease in evaporation as a result of a decrease in the number of high evaporation, sunny days.

Table 6.4 1997 water balance for the HLTF.

	1997 Total	% Precipitation
Precipitation (*P*)	494 mm contributing to infiltration	
Runoff (R)	35 mm	7%
Evaporation (*E*)	167 mm	34%
Net subsurface storage (ΔS)	0 mm	0 %
Drainage/pumping (*D*)	287 mm	58%
Net Infiltration (I_n)	**287 mm estimated**	**58%**
		Note: or 52% total annual precipitation
Cluff Lake Net Infiltration		**42%**

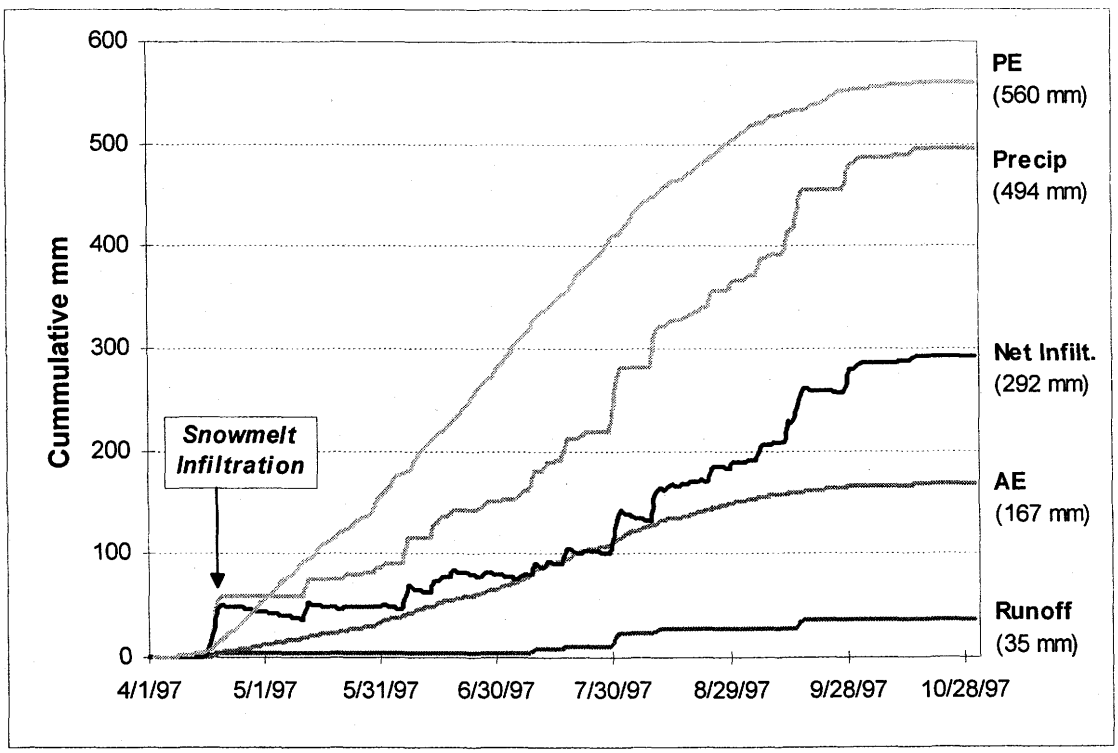

Figure 6.9 1997 water balance for the HLTF.

6.2 SUITABILITY OF LOCAL TILLS and SANDS

The water balance calculation in Section 6.1 has indicated the HLTF test cover experienced higher levels of infiltration when compared to a non layered natural till system at Cluff Lake (Ayres 1998; Meneley and Cherry, 1986). The test cover was designed and constructed as a capillary barrier system with storage and release characteristics that would minimize net infiltration into the underlying cobble ore. However, the soil cover did not perform as anticipated.

The main function of a capillary barrier soil cover is to minimize water infiltration into the underlying waste management system. This is achieved by incorporating a design that:

1. minimizes net infiltration by providing a subsurface moisture barrier,
2. maximizes surface runoff while providing surface stability,
3. increases evapotranspiration by storing infiltrated water close to the surface for subsequent evaporation, and by providing support for vegetation, and
4. provides longterm cover integrity.

6.2.1 Providing Subsurface Moisture Barrier

A capillary barrier soil cover typically consists of two or more layers of soils that differ significantly in their ability to store and transmit water. This difference creates a barrier to subsurface moisture flow and gas migration. The HLTF test cover was designed on the basis of the capillary barrier concept whereby the fine textured till was underlain by the coarse textured outwash sand. The ability of a layered system to function as a capillary barrier, however, does not depend on the textural differences between the two soil types. A capillary barrier is formed only when the overlying fine material has an air entry value much greater than the matric suction attained in the underlying coarse layer at its residual water content (subsection 2.2.1).

The soil-water characteristic curves (SWCC) for the two cover materials that were used to construct the HLTF soil cover system can be found in *Figure 6.10*. The air entry value of the overlying brown till is essentially the same as the underlying coarse sand. In other words, as the underlying sand layer begins to drain, the overlying till layer will also drain. As precipitation infiltrates into the subsurface layer, the infiltrated water continues downward instead of ponding at the sand/till layer interface.

The grain size distribution analysis of the Cluff Lake till and the Key Lake till indicates the two materials to be similar (*Figure 5.2*). However, their SWCCs are noticeably different from each other. A soil cover system consisting of the Cluff Lake till and the Key Lake outwash sand has a potential to perform as a moderate moisture barrier. When the Cluff Lake till begins to drain at about 5 kPa matric suction, the sand is at its near residual soil-water content of 6%. The corresponding unsaturated hydraulic conductivity of the sand layer at this water content is so low that the water in the overlying till layer will not readily drain.

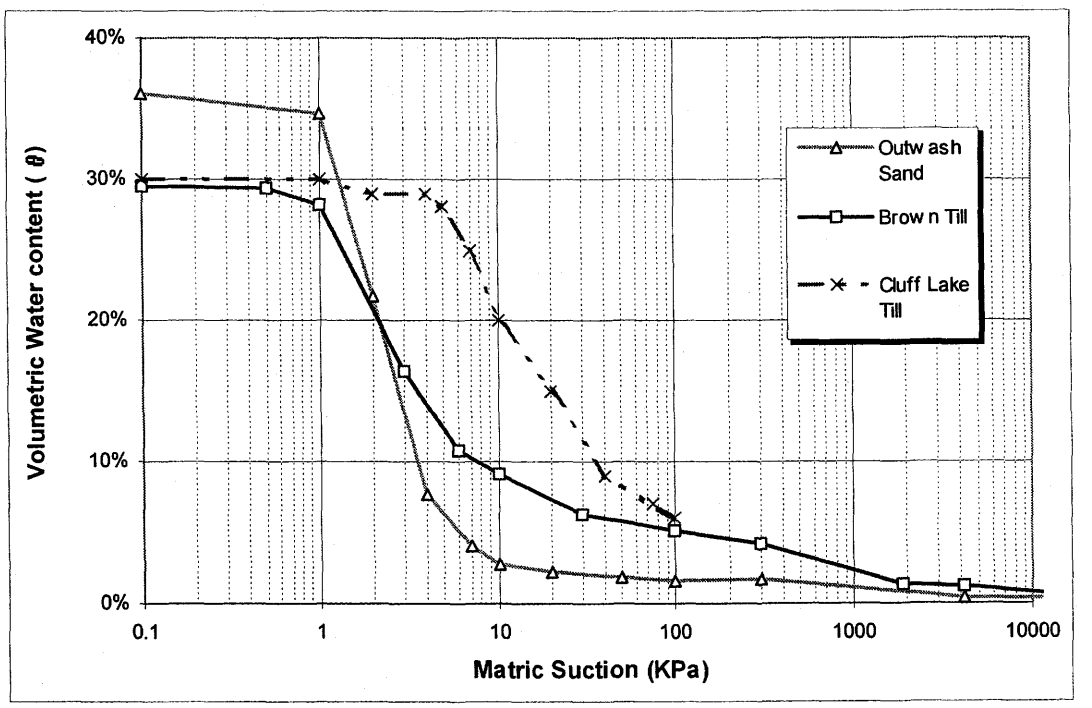

Figure 6.10 SWCCs of Key Lake till and sand, and Cluff Lake till.

6.2.2 Maximizing Surface Runoff

The surface runoff characteristics can be affected by the surface gradient, the presence of hills and depressions, and vegetation. The production of surface runoff can be increased by increasing the surface gradient. However, the gradient must be selected to provide protection against severe surface erosion that may result in cover degradation. The surface erosion can be stabilized by incorporating vegetation, but surface vegetation, in turn, will effectively decrease surface runoff. Surface depressions can provide temporary storage for surface runoff, which subsequently becomes delayed infiltration under ponded conditions. The net infiltration from numerous minor depressions can represent a significant percentage of the total infiltration.

The HLTF has been graded at 2%. Although it provides runoff erosion protection, it does not readily promote surface runoff. Furthermore, vehicle traffic over the years has created surface depressions on top of the cover that entrap runoff and result in delayed infiltration.

6.2.3 Maximizing Evapotranspiration

The HLTF was designed as a non-vegetated cover system. However, it is worth noting that vegetation is an effective method of decreasing net infiltration. The main benefit of surface vegetation for regions of high intensity rainfalls on sandy tills is its ability to extract moisture from depths greater than the soils' inherent evaporative zone depth. The evaporative zone depth is the maximum depth from which water may be removed by evapotranspiration.

In sandy soils, the evaporative zone depth is limited to 10 cm to 20 cm from the surface; in silty soils, the evaporative zone depth is 20 cm to 45 cm (Schroeder *et al.*, 1994). Therefore, evaporation alone cannot extract moisture from a till layer that is 60 cm in thickness.

Surface vegetation will extend the evaporative zone depth as a function of rooting depth. The surficial storage layer thickness is thus determined by the required water storage

capacity, and the vegetation rooting depth. Vegetation increases evapotranspiration, as well extending the evaporative zone depth. The average AE/PE ratio that was used for the water balance calculation in Section 6.1 was approximately ½ of the average AET/PE ratio that was reported for Cluff Lake (Ayres 1998). Incorporating surface vegetation can potentially increase the annual evapotranspiration by a factor of two. However, this increase in evapotranspiration will be partially offset by a decrease in runoff.

Vegetation also increases the net storage capacity of a cover system. In *Figure 6.8* (subsection 6.1.5), the net storage capacity of the non-vegetated till layer is shown to be 3 mm. Incorporating vegetation will lower the "residual" soil-water content from the gravity drained soil-water content of 7%, to a soil-water content corresponding to the permanent wilting point. The permanent wilting point is typically defined as the soil-water content at 1,500 kPa (Cassel and Nielsen, 1986). In the case of the HLTF till, the permanent wilting point is approximately 2%. *Figure 6.11* illustrates the significance of lowering the "residual" soil-water content from 7% to 2%. The net storage capacity is increased from 3 mm to 33 mm (area under the SWCC). Incorporating vegetation will increase the net storage capacity of the surficial till layer. Larger amount of water will be stored in the till layer for evapotranspiration, and consequently, less water will percolate to the layers below.

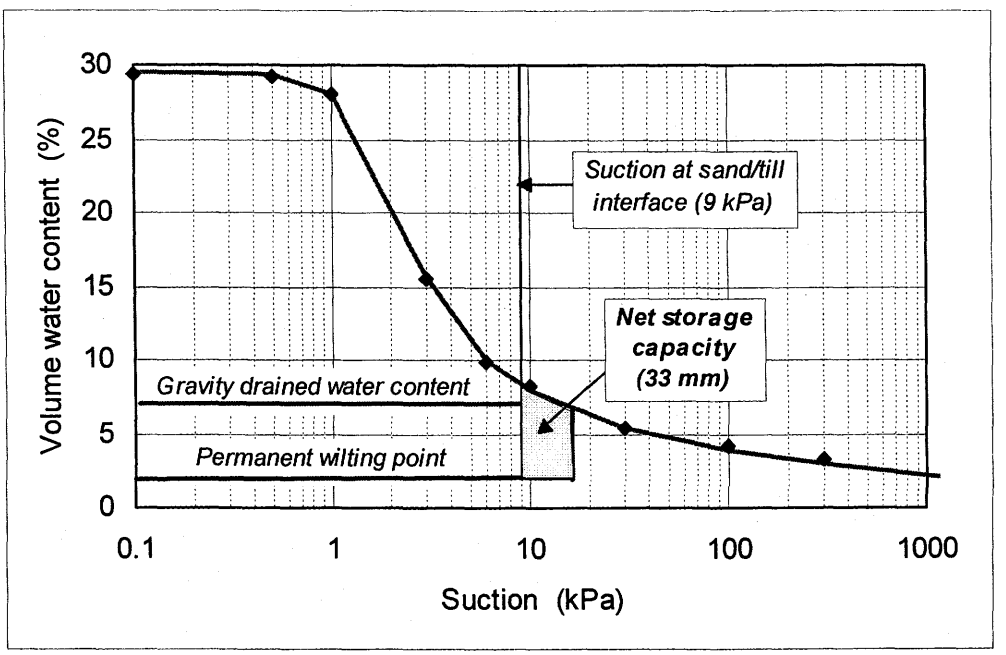

Figure 6.11 *HLTF net water storage capacity for a vegetated layer.*

In 1997, there were 13 recorded precipitation events, when the total precipitation exceeded the storage capacity of the HLTF soil cover (12 mm). The rainfall in excess of cover storage capacity amounts to 90 mm of infiltration into the underlying cobble ore. A vegetated soil cover system with increased storage capacity (42 mm) could have stored these large rainfall events. Interestingly, if we reduce the total annual infiltration (287 mm) by the reduction in net infiltration due to increased storage capacity of a vegetated system (90 mm), the resulting annual net infiltration is 40%. This compares well with the reported Cluff Lake net infiltration of 42% for a vegetated natural till site.

Surface vegetation also provides some secondary benefit through its ability to intercepts low intensity rainfalls, thus decreasing the amount of water that reaches the soil surface. Surface vegetation also provides protection against surface erosion, and effectively decreases surface runoff and soil evaporation. However, the benefits of increased evapotranspiration is more significant than the disadvantages associated with incorporating surface vegetation.

6.2.4 Providing Longterm Cover Integrity

A soil cover must provide longterm integrity. Soil covers are typically designed for reclaiming waste management facilities that require containment for hundreds and thousands of years with minimum maintenance. The surficial till material displayed some degree of wind and water erosion. The high intensity summer rainfalls, in particular, are threatening to the longterm integrity of the HLTF till cover system. Incorporating surface vegetation will decrease the potential for wind and water erosion.

6.3 RUNOFF and INFILTRATION CHARACTERISTICS

Precipitation falling onto the soil surface partitions into surface runoff and infiltration. Understanding the runoff and infiltration mechanisms is therefore essential for a soil cover system.

Water infiltrates due to the combined effects of gravity and soil matric suction. For a given precipitation event, Horton (1933) stated that infiltration is typified by high infiltration rate at the start followed by a rapid decline as the surface layer becomes saturated. Eventually, the rate of infiltration approaches to a near-constant residual value approximately equal to the hydraulic conductivity of the surface soil.

The process of infiltration, albeit highly variable, is relatively well understood. There are many theoretical, and theory based empirical models, that predict infiltration within acceptable level of accuracy (section 2.4). Surface runoff, on the other hand, has been commonly estimated as the quantity that exceeded infiltration during a water input event.

Small scale field studies and laboratory investigation into runoff mechanism are limited, and their results are generally inconclusive (section 2.5). The existing surface runoff models tend to be semi-analytical, and they are based on empirical relations that appear to provide reasonable results.

The surface runoff and infiltration analysis was carried out on 1997 summer precipitation data which was partitioned into individual rainfall events. The precipitation hyetograph shown in *Figure 6.*12 was separated into two rainfall events: the first event from 18:45 to 21:00 hours; and the second event from 21:00 to 23:15 hours. A total of 100 distinct rainfall events with corresponding runoff data was used to analyze surface runoff characteristics, and to verify the factors that are deemed to control the surface runoff mechanism.

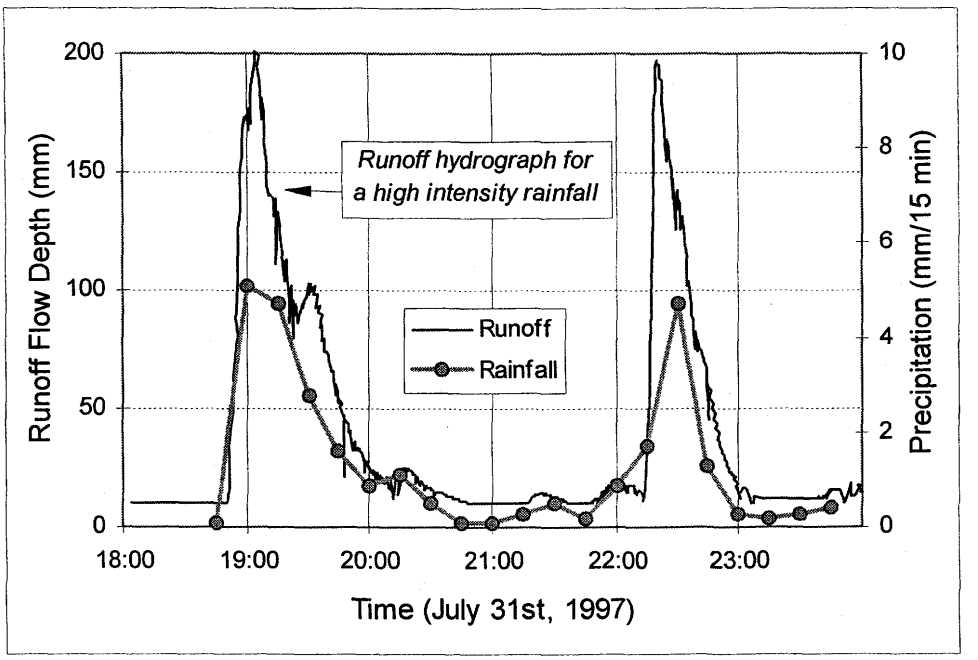

Figure 6.12 Precipitation hyetograph for July 31st, 1997.

6.3.1 Runoff and Rainfall Intensity

A plot of surface runoff versus the *maximum* 15-minute precipitation intensity for each rainfall event is shown in *Figure 6.13.* The analysis of 100 rainfall events has indicated that runoff is generated regardless of antecedent soil moisture conditions when the maximum 15-minute precipitation intensity exceeds 1.4 mm. The 1,025 15-minute rainfall intensities and the corresponding surface runoff data also indicate that runoff is generated when the 15-minute rainfall intensity exceeds 1.4 mm (*Figure 6.14*). Of the 1,025 15-minute rainfall intensities that were recorded, there were only four incidences (shaded in data points) where the 15-minute rainfall intensities greater than 1.4 mm did not generate surface runoff.

The 15-minute intensity of 1.4 mm corresponds to a surface hydraulic conductivity of 1.5×10^{-6} m/sec, which is higher than the laboratory estimated hydraulic conductivity for brown till (2.0×10^{-7} m/sec). It is, however, within the range of *in situ* hydraulic conductivities that were obtained with the Guelph Permeameter (2.3×10^{-7} m/sec to 6.5×10^{-6} m/sec).

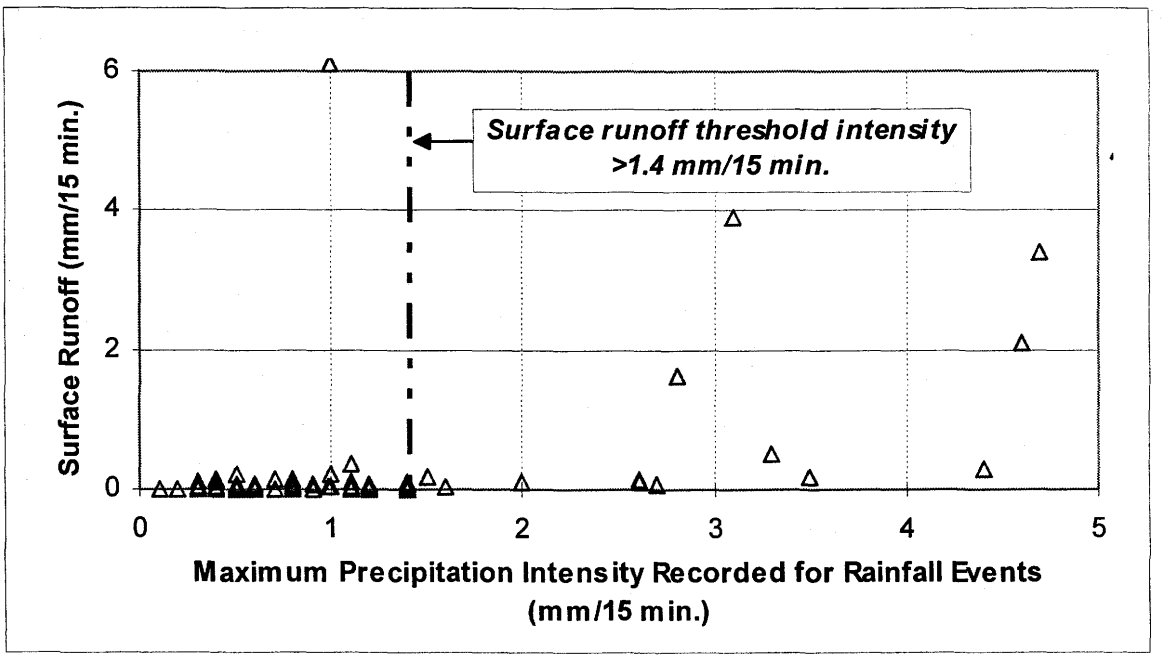

Figure 6.13 The maximum 15-minute rainfall intensities versus surface runoff. It is based on precipitation data from 100 individual rainfall events.

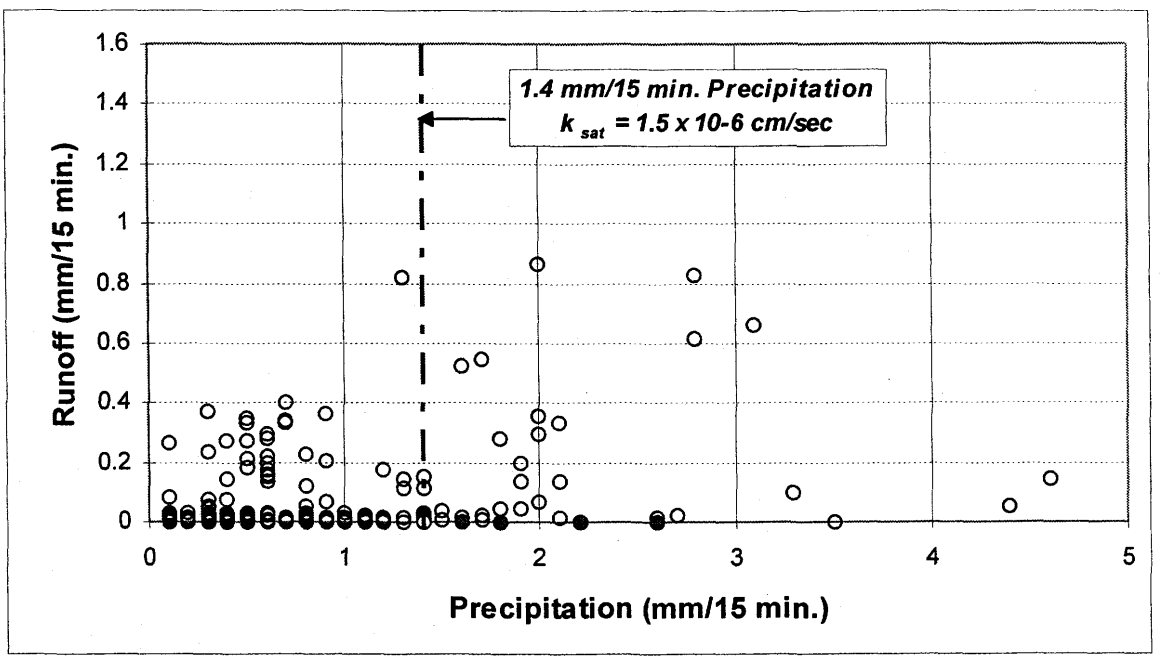

Figure 6.14 Recorded 1,025 15-minute rainfall intensities and runoff quantities.

Based on 1 025 15-minute rainfall intensities and corresponding runoff quantities, it can be concluded that runoff is generated regardless of soil moisture conditions when the precipitation intensity exceeds the near surface hydraulic conductivity of 1.5 x 10^{-6} m/s. When runoff occurs as a result of the rainfall intensity exceeding the *infiltration capacity*, or the saturated hydraulic conductivity, of the surficial soil, it is described as an *infiltration excess* runoff.

Freeze (1972) concluded that the occurrence of rainfall intensities greater than the hydraulic conductivity of the vast majority of naturally occurring soils was generally uncommon. For this region, where high intensity short duration rainfall events are considered frequent, less than 5% of the 1 025 recorded 15-minute rainfall intensities were found to be greater than the surface hydraulic conductivity of 1.5 x 10^{-6} cm/sec, or 1.4 mm/15-minutes. The *infiltration excess* runoff process is nevertheless quite significant. Although only less than 5% of the recorded intensities were higher than 1.4 mm, these events account for 30% of the total summer precipitation, and 63% of the total summer runoff.

The 100 individual rainfall events were further grouped into wet and dry antecedent soil moisture conditions. It was considered dry when rainfall occurred after the facility was allowed to dry out over the previous day. A plot of surface runoff versus the *maximum* 15-minute precipitation intensity for wet antecedent conditions are shown in *Figure 6.15.*

Under wet antecedent conditions, runoff was generated when the *maximum* 15-minute precipitation intensity exceeded 0.5 mm, or 3.5 x 10^{-7} m/sec. This decrease in runoff threshold intensity indicates decrease in hydraulic conductivity with depth; from surface hydraulic conductivity of 1.5 x 10^{-6} m/sec to subsurface hydraulic conductivity of 2.0 x 10^{-7} m/sec.

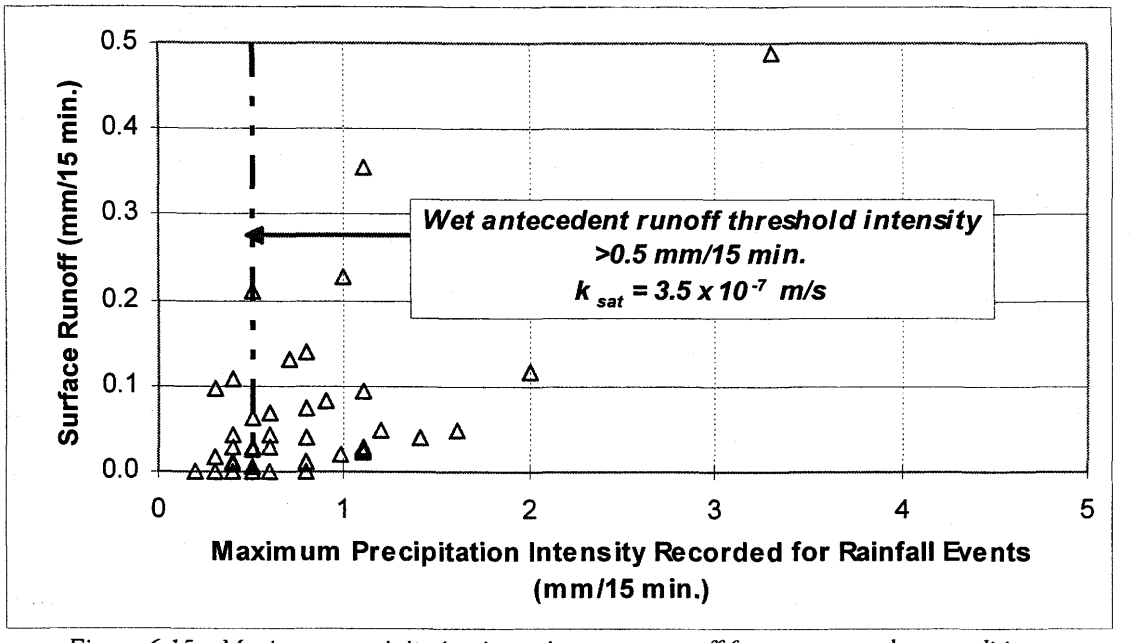

Figure 6.15 Maximum precipitation intensity versus runoff for wet antecedent conditions.

6.3.2 Infiltration and Rainfall Intensity

Figure 6.16 shows a plot of 15-minute rainfall intensities against the corresponding 15-minute infiltration rate for a very high intensity rainfall event. The infiltration rate is calculated based on rainfall intensities and the corresponding runoff volumes. This rainfall event recorded 27.6 mm total rainfall over a 5 hour duration. Based on Horton's infiltration theory, all rainfall in excess of surface hydraulic conductivity should partition into surface runoff. However, the infiltration rate does not appear to approach to a near constant value. This observation may represent higher surface hydraulic conductivity, or surface depression storage and delayed runoff mechanism.

Figure 6.17 illustrates 15-minute rainfall intensities versus the resulting runoff for a low intensity rainfall event. Based on Horton's (1933) infiltration theory, all precipitation at rates less than the *infiltration capacity* are expected to infiltrate. However, *Figure 6.17* indicates that surface runoff is generated even when the rainfall intensities are significantly less than the infiltration capacity. In fact, the surface runoff that was generated at these low intensities account for 43% of the total recorded summer runoff.

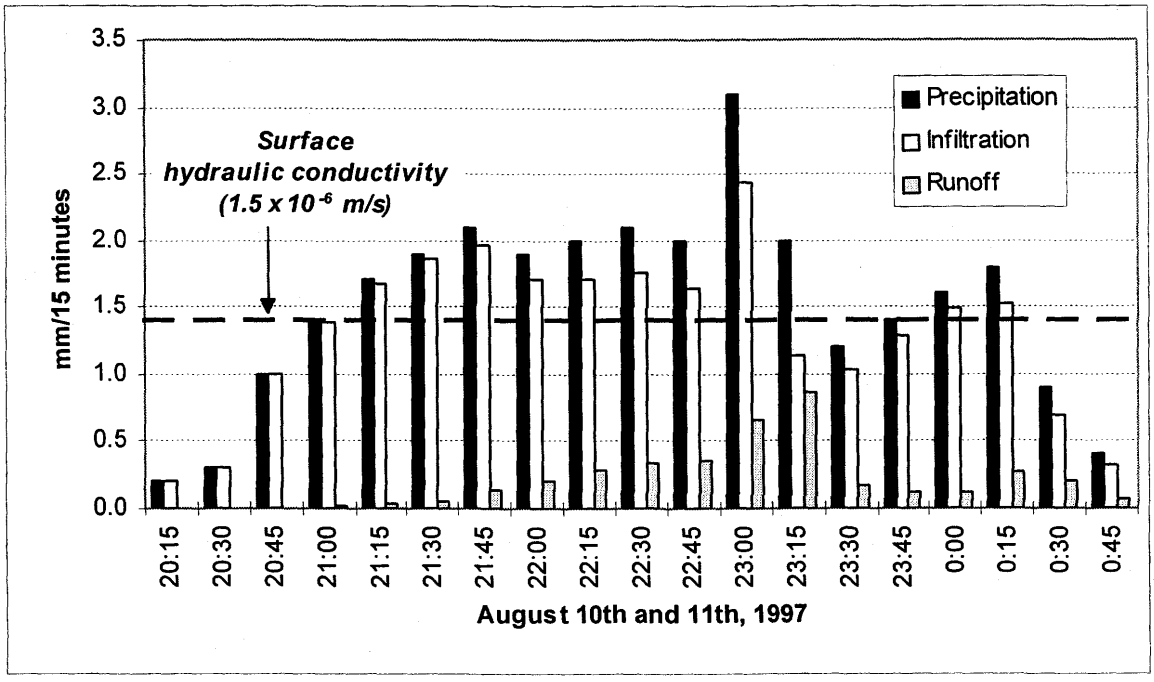

Figure 6.16 Rainfall intensity versus infiltration for high intensity rainfall event.

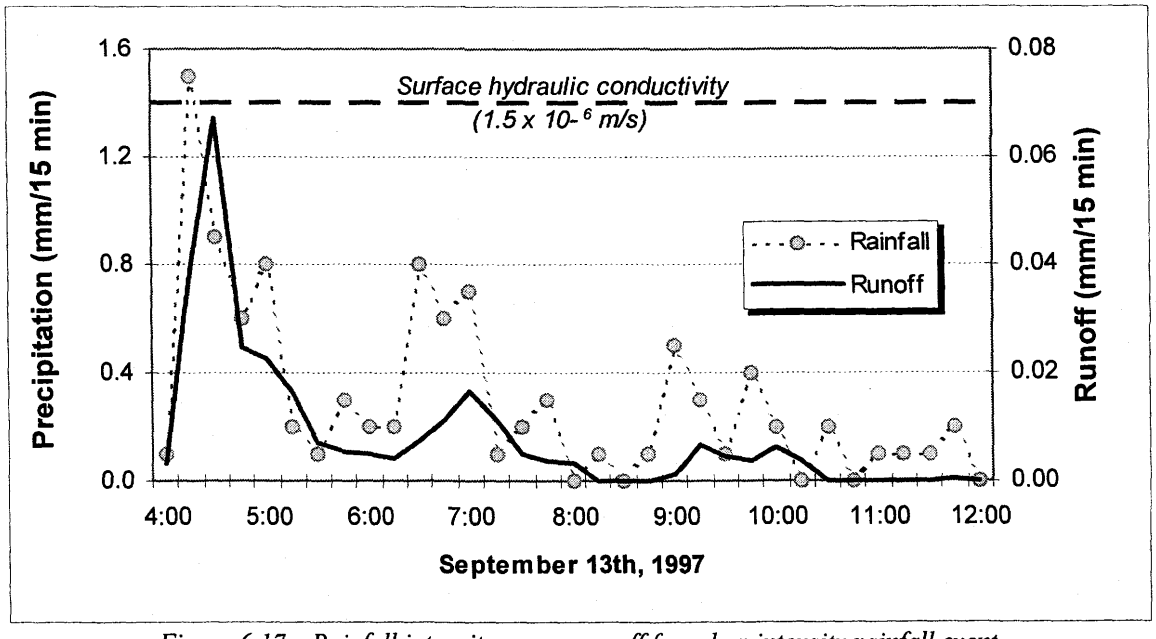

Figure 6.17 Rainfall intensity versus runoff for a low intensity rainfall event.

6.3.3 Runoff and Soil Moisture Conditions

Figure 6.18 suggests that the runoff is dependent on soil moisture conditions throughout the rainfall event. For example, 0.8 mm rainfall between 6:00 a.m. and 6:15 a.m. resulted in 0.02 runoff/rainfall ratio. The same precipitation intensity between 8:00 a.m. and 8:30 a.m. produced 0.23 runoff/rainfall ratio. The runoff/rainfall ratio increased as the soil surface and the subsurface layer became more and more saturated.

Figure 6.19 provides a relationship between runoff and rainfall intensity for two antecedent soil moisture conditions (wet and dry). The wet antecedent conditions generated a higher percentage runoff than the dry antecedent conditions. The coefficient of determination (r^2) for the wet curve is lower (0.72 for wet versus 0.91 for dry) due to one anomalous long duration medium intensity rainfall event that generated significantly higher than average runoff. When this one event is ignored, the coefficient of determination is improved to 0.95.

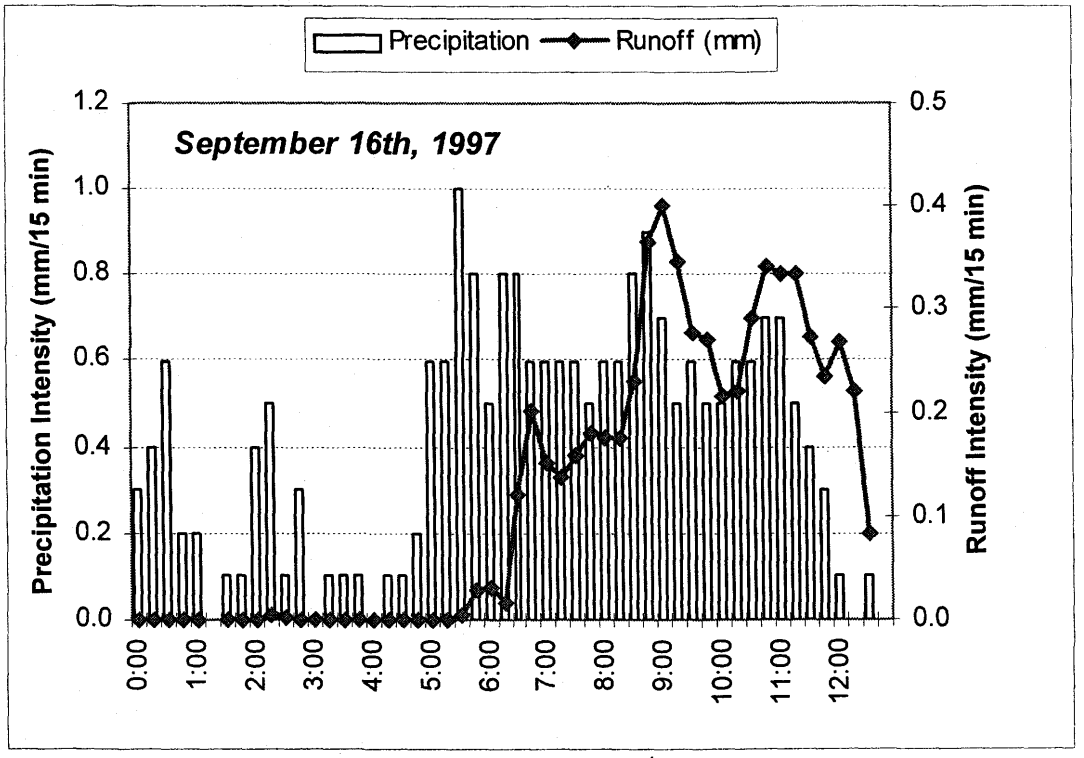

Figure 6.18 Precipitation versus runoff for September 16th, 1997. The rainfall event is a long duration moderate intensity rainfall, uncommon for this region.

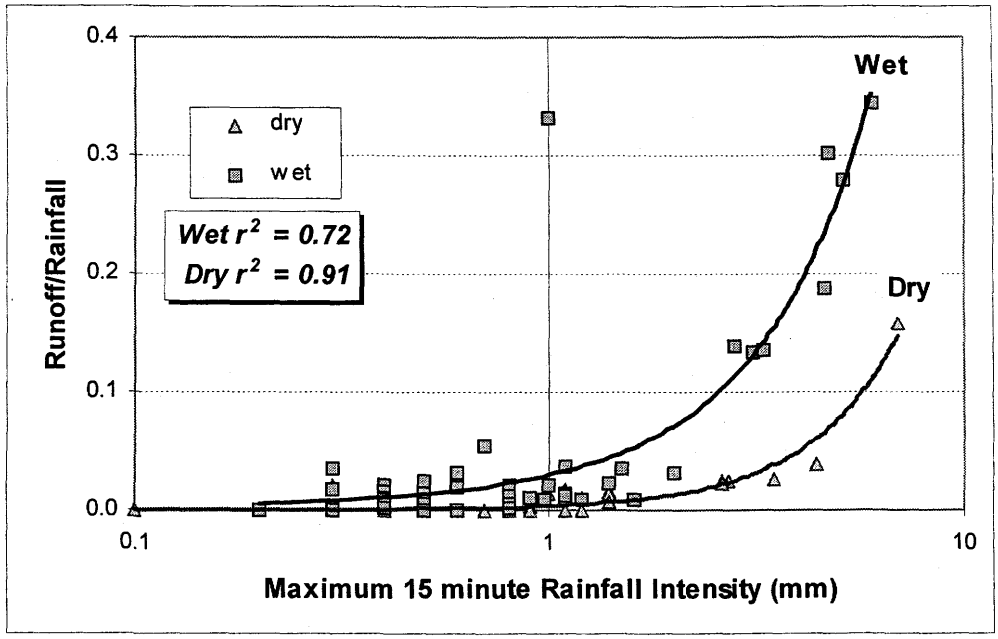

Figure 6.19 Runoff versus antecedent soil moisture conditions. A plot of 100 individual rainfall events grouped based on antecedent moisture conditions.

6.3.4 Summary of Surface Runoff and Infiltration Characteristics

The process of surface runoff and infiltration are closely inter-related. An analysis of runoff data indicates that these two processes are most affected by maximum intensity of the precipitation event, and by antecedent soil moisture conditions. The total precipitation and precipitation duration did not greatly influence the partitioning of rainfall into infiltration and runoff. The factors such as surface soil properties and surface topography were not evaluated because they were constant parameters for this test site.

Chapter Seven
SUMMARY AND CONCLUSIONS

Engineered soil cover desings are generally faced with a unique engineering requirement in that these designs must function for hundreds and thousands of years with minimal maintenance. Significant progress has been made in recent years towards better understanding the parameters that control the performance of a soil cover system. And concurrently, many waste management operators are incorporating weather and/or soil cover monitoring program in preparation for outlining decommissioning plans.

Key Lake commenced the HLTF soil cover monitoring program in 1993 to evaluate the performance of the HLTF soil cover, and to assess the suitability of using local tills and sands for future decommissioning of various waste management facilities. The summary and conclusions arising from this project are presented in this chapter.

7.1 EVALUATION OF EXISTING DATA

The main conclusions and recommendations pertaining to the evaluation of the Cameco HLTF monitoring data are outlined below.

1. The HLTF weather monitoring program was fraught with numerous difficulties. The assessment of the 1993 to 1997 weather data has indicated various instrumentation malfunctions for each of the monitoring year.

2. Remote and automatic monitoring capabilities have simplified the weather monitoring tasks, and minimized the human error component. However, instrumentation failure can be common, even for standard equipment. Frequent data collection and verification is essential, as well as data comparison with regional and historical data.

3. Some of the climatic parameters, such as precipitation and wind speed, displayed significant spatial and temporal variability. The accuracy of a soil cover monitoring program will depend considerably on the availability of site specific weather data.

4. Standard recording gauges do not provide reliable snowfall measurements. In cold regions where insignificant snow melt occurs throughout the winter, a snow survey just prior to the onset of spring snow melt is generally adequate.

5. Site pan evaporation was recorded automatically using a Class A evaporation pan and a system of floats and sensing units. The pan water level was left to rise and fall in response to rainfall and evaporation, and water was added or removed only on an intermittent basis. However, the standard evaporation pan operating procedure specifies that the water level in the pan be maintained at a standard depth from the rim by removing or adding measured amounts of water on a daily basis. This is needed to provide a constant heat storage capacity.

6. Wind speed is dependent on the height of the instrument installation. The wind gauge at an environment Canada weather station is typically mounted 10 m above the ground, however, the wind speed near the surface is significantly less.

7. The evaluation of the AGWA-II thermal conductivity sensors has indicated that the sensors were inappropriate for the Key Lake soils due to lack of sensor sensitivity in the low matric suction range (1 kPa to 20 kPa). It is thus important to ensure that sensors are suitable for their intended application.

8. The surface runoff was monitored on a real time basis every 30 seconds, while precipitation was summarized to provide a standard 15-minute intensities. At times, the 15-minute precipitation intensity was inadequate for runoff analysis. A 5-minute precipitation intensities would have been useful.

7.2 SUMMARY OF LABORATORY PROGRAM

The conclusions and recommendations arising from the laboratory program are listed below.

1. The grain size distribution curve is typically used to identify and categorize a soil type. When designing a soil cover system, the soil water characteristic curve (SWCC) provides a better insight on how the soil will behave when subjected to water and vapour flux under unsaturated conditions.

2. The two materials that were used to construct the HLTF soil cover were outwash sand and till. The SWCCs indicate that they will behave in a similar manner when subjected to infiltration and evaporation, and that there is no significant difference between the two soil types.

3. Although the Cluff Lake till and the Key Lake till have similar grain size curves, the Cluff Lake till has a higher air entry value (5 kPa) than the Key Lake till (1 kPa).

4. Neutron probe factory calibration curve cannot be used without carrying out a site and soil specific calibration. The laboratory calibration resulted in a single curvilinear calibration curve for the two soil types. The calibration curve has been found to be significantly less sensitive than the factory curve.

5. The Beta-97 thermal conductivity sensor calibration curve is curvilinear with a decreased sensitivity in the lower suction range (0 to 20 kPa).

7.3 SUMMARY OF FIELD INSTRUMENTATION PROGRAM

The highlights of the field instrumentation program are presented below.

1. The Guelph Permeameter was not suitable for determining the field saturated hydraulic conductivity of the outwash sand and the till found at Key Lake. In the till layer, the water flowing out of the water outlet tube eroded the walls of the well causing the well to collapse around the outlet tube.

2. The sonic drill soil profile sampling has indicated that the cover is considerably different from the design. In the vicinity of the manholes, there was an additional 140 cm of sand and till material beneath the soil cover. It is postulated that this excess material was used to grade the facility prior to placing the soil cover.

3. The Bowen Ratio instrumentation for monitoring actual evaporation was not successful due to instrumentation malfunction. The actual evaporation was estimated based on Cluff Lake evaporation levels and SoilCover modeling results.

4. The neutron probe calibration curve overestimates the actual soil-water content. The neutron probe method is accurate and reproducible. Errors arise from the calibration process and the calibration curve.

5. The neutron probe data suggests that the cover system maintains a residual water content profile throughout the season. The soil moisture content only increases at depths immediately above the water table.

6. The Beta-97 thermal conductivity sensors were found to be responsive to the changes in atmospheric conditions. The inter-sensor variability was too large to be used for the HLTF cover materials. In general, the sensors underestimated soil moisture conditions.

7. The subsurface soil moisture content instrumentation (neutron probe and Beta-97 sensors) did not record any significant changes in the water content due to the nature of the cover material and the depth of the water table.

8. The depth to the water table was monitored infrequently. The change in the water table depth throughout the monitoring season is an effective means of verifying the water balance calculation.

7.4 HLTF SOIL COVER PERFORMANCE

The assessment of the HLTF soil cover has revealed that the cover did not function as a capillary barrier system. The net infiltration through the cover was 52% of the total annual precipitation (October 1996 to September 1997), or 58% of the precipitation available for infiltration (spring snow pack and summer precipitation).

The suitability of using local tills and sands, as well as a summary of cover design criteria are discussed below.

1. The local till underlain by sand did not form a barrier to water and moisture flow. The sand and the till had similar SWCCs (air entry values of approximately 1 kPa), and as a result, they behaved in a similar manner to infiltration. The air entry value of the overlying fine material must be high enough for the sand layer to remain at residual water content.

2. Cluff Lake till underlain by Key Lake sands would have performed as a moderate capillary barrier (Cluff Lake till had an air entry value of 5 kPa).

3. The sand layer did not form a capillary barrier, and as a result, the net storage capacity of the two layers is only approximately 12 mm.

4. The thickness of the upper brown till layer exceeds the soil's inherent evaporative zone depth. Infiltrated water cannot be extracted by evaporation from this depth. The soil cover would have recorded high net infiltration even if the sand layer had performed as a capillary barrier layer.

5. Surface vegetation will increase the storage capacity of the soil significantly (42 mm versus 12 mm for a non-vegetated cover). Surface vegetation has the potential to increase actual evapotranspiration by a factor of two. It also extends the evaporative zone depth (the depth from which water can be extracted) and decreases the residual water content. Surface vegetation provides surface erosion protection, however, it will also affect surface runoff generation.

6. The surface of the facility was graded at 2%. Vehicle traffic over the years has created depressions throughout the cover that entrap runoff water and increases infiltration.

7.5 RUNOFF AND INFILTRATION CHARACTERISTICS

The real time runoff data enabled a detailed analysis of runoff and infiltration characteristics. The 1997 summer precipitation and runoff data has indicated that surface runoff is generated regardless of antecedent soil moisture conditions when the 15-minute rainfall intensity exceeded 1.4 mm. This is equivalent to a surface hydraulic conductivity of 1.5×10^{-6} m/s, higher than what was estimated in the laboratory. However, it is still within the range of *in situ* hydraulic conductivity values that were obtained using the Guelph Permeameter.

Surface runoff was also noted for rainfall intensities less than the surface hydraulic conductivity. Surface runoff was found to be most responsive to the changes in antecedent soil moisture conditions and the maximum precipitation intensity.

7.6 FUTURE RESEARCH

The following recommendations and comments are put forth for future research.

1. The Beta-97 thermal conductivity sensor results have demonstrated large variability between adjacent sensors. The sensors provide an indirect measurement of soil suction, and therefore, the source of sensor variability may be the calibration curve. The accuracy of the calibration curve and sensor variability should be evaluated in the laboratory to identify the source of error. This can be done by subjecting sensors to various suction levels, and verifying the curve's ability to predict actual suction.

2. The Beta-97 sensor calibration curve is a drying curve whereby a saturated sensor is eventually desaturated throughout the testing procedure. Incorporating a wetting and a drying calibration curve will improve the sensor's ability to estimate actual field suction conditions.

3. A remote and automated instrumentation system provides a wealth of information with minimal human intervention. However, instrumentation malfunction was not uncommon, and thus, frequent data downloading for verification is imperative.

REFERENCES

Abeele, W.V. 1979. The influence of access hole parameters on neutron moisture probe readings. LA-8094-MS. Los Alamos Scientific Laboratory, Los Alamos, New Mexico. (From Keller *et al.*, 1990).

Ahuja, L.R. 1983. Modeling infiltration into crusted soils by the Green-Ampt approach. *Soil Science Society of America Journal* 47:412-418.

Akindunni, F.F., R.W. Gillham, and R.V. Nicholson. 1991. Numerical simulations to investigate moisture-retention characteristics in the design of oxygen-limiting covers for reactive mine tailings. *Canadian Geotechnical Journal* 28:446-454.

Allan, C.J., and N.T. Roulet. 1994. Runoff generation in zero-order Precambrian Shield catchments: the stormflow response of a heterogeneous landscape. *Hydrological Processes* 8:369-388.

ASTM Standards D422-63 (reapproved 1990). 1990. Standard test method for particle size analysis of soils. *American Society for Testing and Materials*, Philadelphia, Pa.

ASTM Standards D698-91. 1991. Standard test method for laboratory compaction characteristics of soil using standard effort. *American Society for Testing and Materials*, Philadelphia, Pa.

ASTM Standards D854-92. 1992. Standard test method for specific gravity of soils. *American Society for Testing and Materials*, Philadelphia, Pa.

ASTM Standards D2167-94. 1994. Standard test method for density and unit weight of soil in place by the rubber balloon method. *American Society for Testing and Materials*, Philadelphia, Pa.

ASTM Standards D2216-92. 1992. Standard test method for laboratory determination of water (moisture) content of soil and rock. *American Society for Testing and Materials*, Philadelphia, Pa.

ASTM Standards D2434-68 (reapproved 1994). 1994. Standard test method for permeability of granular soils (constant head). *American Society for Testing and Materials*, Philadelphia, Pa.

ASTM Standards D4914-89 (reapproved 1994). 1994. Standard test method for density of soil and rock in place by the sand replacement method in a test pit. *American Society for Testing and Materials*, Philadelphia, Pa.

ASTM Standards D5030-89 (reapproved 1994). 1994. Standard test method for density of soil and rock in place by the water replacement method in a test pit. *American Society for Testing and Materials*, Philadelphia, Pa.

ASTM Standards D5220-92. 1992. Standard test method for water content of soil and rock in-place by the neutron depth probe method. *American Society for Testing and Materials*, Philadelphia, Pa.

ASTM Standards D5856-95. 1995. Standard test method for measurement of hydraulic conductivity of porous material using rigid-wall, compaction-mold permeameter. *American Society for Testing and Materials*, Philadelphia, Pa.

Anderson, J.E., R.S. Nowak, Ratzlaff, and O.D. Markham. 1993. Managing soil moisture on waste burial sites in arid regions. *Journal on Environmental Quality*, 22:62-69.

Arslan, A., and A.K. Razzouk. 1994. Effects of gypsum on the neutron probe calibration curve. *Soil Science* 158:174-180.

Ayres, B.K. 1998. Field monitoring of soil-atmosphere fluxes through uranium mill tailings and natural surface soils at Cluff Lake, Saskatchewan. M.Sc. Thesis, Department of Civil Engineering, *University of Saskatchewan*, Saskatoon, Saskatchewan.

Babalola, O. 1978. Field calibration and use of the neutron moisture meter on Nigerian soils. *Soil Science* 126:118-124.

Barbour, S.L. 1990. Reduction of acid generation in mine tailings through the use of moisture retaining cover layers as oxygen barriers: Discussion. *Canadian Geotechnical Journal* 27:398-401.

Barbour, S.L., and A.K. Canful. 1994. A column study of static equilibrium fluid pressures in sand during prolonged drainage. *Canadian Geotechnical Journal* 31:299-303.

Bell, A.V., M.D. Riley, and A.K. Canful. 1995. Evaluation of a composite soil cover to control acid waste rock pile drainage. *CIM Bulletin* 88:41-46.

Bell, J.P. and J.S.G. McCulloch. 1966. Soil moisture estimation by the neutron scattering method in Britain. *Journal of Hydrology* 4:259-263.

Bennet J.W., A.I.M. Ritchie. 1991. Measurements of the transport of oxygen into two rehabilitated waste rock dumps. *Second International Conference on the Abatement of Acidic Drainage*, Montreal, Quebec. 3:289-298.

Benson, C.H., P.J. Bosscher, D.T. Lane, and R.J. Pliska. 1994. Monitoring system for hydrologic evaluation of landfill covers. *Geotechnical Testing Journal* 17:138-149.

Berndtsson, R. 1987. Application of infiltration equations to a catchment with large spatial variability in infiltration. *Hydrological Sciences Journal* 32:399-413.

Beven, K., and M.J. Kirkby. 1979. A physically based variable contributing area model of basin hydrology. *Hydrological Science Bulletin* 24:43-49.

Beven, K., and P. Germann. 1981. Water flow in soil macropores: 2. A combined flow model. *Journal of Soil Science* 32:15-29.

Beven, K., and P. Germann. 1982. Macropores and water flow in soils. *Water Resources Research* 18:1311-1325.

Bews, B.E., M. O'Kane, G.W. Wilson, and D. Williams. 1997. The design of a low flux cover system, including lysimeters, for acid generating waste rock in semi-arid environments. In, *Proceedings of the Fourth International Conference on Acid Mine Drainage*, Volume II, Vancouver, B.C. pp. 747-762.

Bingham, G.E., B.D. Tanner, J. Greene, and M. Tanner. 1987. A Bowen Ratio system for long term remote measurement of evapotranspiration. Preprint, 18th Conf. Agric. For. Meteor., W. Lafayetter, IN, 15-18 September 1987, American Meteorological Society, Boston, MA, USA, pp. 63-66. (From Malek and Bingham, 1993).

Black, J.D.F., and P.D. Mitchell. 1968. Near-surface soil moisture measurement with a neutron probe. *Journal of Australian Institute of Agricultural Science* 34:181-182.

Blight, G.E., and J.J. Blight. 1993. Runoff and infiltration into capped landfills. *Joint CSCE/ASCE National Conference on Environmental Engineering.* Montreal, Quebec, Canada. pp. 877-884.

Boulet, G, I. Braud, and M. Vauclin. 1997. Study of the mechanisms of evaporation under arid conditions using detailed model of the soil atmosphere continuum. Application to the EFEDA I experiment. *Journal of Hydrology* 193:114-141.

Brakensiek, D.L., and W.J. Rawls. 1983. Agricultural management effects on soil water processes. Part II: Green and Ampt parameters for crusting soils. *Transactions of the ASAE* 26(6):1753-1757.

Braud, I., J. Noilhan, P. Bessemoulin, P. Mascart, R. Haverkamp, and M. Vauclin. 1993. Bare ground surface heat and waste exchanges under dry conditions: observations and parameterization. *Boundary-Layer Meteorology* 66:173-199.

Bronswijk, J.J.B. 1988. Modeling of water balance, cracking, and subsidence of clay. *Journal of Hydrology Netherlands* 97:199-212. (From Swanson 1995).

Brutsaert, W.H. 1982. *Evaporation into the atmosphere*. D. Reidel Publishing Company, Dordrecht, Holland.

Cameco Corporation. 1994. Deilmann In-Pit Tailings Management Facility Environmental Impact Statement Volume I. *Cameco Corporation*, Saskatoon, Saskatchewan.

Cameco Corporation. 1995. Performance Report - Tailings Management Facility at Key Lake, April 1994 to April 1995. *Cameco Corporation*, Saskatoon, Saskatchewan.

Cameco Corporation. 1996. Performance Report - Tailings Management Facility at Key Lake, April 1995 to April 1996. *Cameco Corporation*, Saskatoon, Saskatchewan.

Cameco Corporation. 1997a. Performance Report - Tailings Management Facility at Key Lake, April 1996 to April 1997. *Cameco Corporation*, Saskatoon, Saskatchewan.

Cameco Corporation. 1997b. Key Lake Operation Annual Environmental Report. *Cameco Corporation*, Saskatoon, Saskatchewan

Cameco Corporation. 1998a. Performance Report - Tailings Management Facility at Key Lake, April 1997 to April 1998. *Cameco Corporation*, Saskatoon, Saskatchewan.

Cameco Corporation. 1998b. Key Lake Operation Annual Environmental Report. *Cameco Corporation*, Saskatoon, Saskatchewan

Camillo, P.J., R.J. Gurney, and T.J. Schmugge. 1983. A soil and atmospheric boundary layer model for evapo-transpiration and soil moisture studies. *Water Resources Research* 19:371-380.

Camillo, P.J., and R.J. Gurney. 1986. A resistance parameter for bare soil evaporation models. *Soil Science* 141:95-105.

Campbell Scientific Inc. 1998. Bowen ration instrumentation instruction manual. Revision 4/98. Campbell Scientific (Canada) Corp., Edmonton, Alberta.

Carrijo, O.A, and R.H. Cuenca. 1992. Precision of evapotranspiration estimates using neutron probe. *ASCE Journal of Irrigation and Drainage Engineering* 118:943-953.

Cassel, D.K., and D.R. Nielsen. 1986. Field capacity and available water capacity. Methods of soil analysis: part I. Physical and Mineralogical Methods, Agronomy Monograph No.9, 2nd Ed., *Soil Science Society of America*, Madison, Wis. (From Stormont and Morris, 1998).

Chanasyk, D.S. and R.H. McKenzie. 1986. Field calibration of a neutron probe. *Canadian Journal of Soil Science* 66:173-176.

Chanasyk, D.S., and M.A. Naeth. 1988. Measurement of near-surface soil moisture with a hydrogenously shielded neutron probe. *Canadian Journal of Soil Science* 68:171-176.

Choudhury, B.J., and J. L. Monteith. 1988. A four layer model for the heat budget of homogeneous land surfaces. *Quarterly Journal of the Royal Meteorological Society* 114:373-398.

Chu, S.T. 1978. Infiltration during an unsteady rain. *Water Resources Research* 14(3):461-466.

Chu, S.T. 1985. Modeling infiltration into tilled soil during non-uniform rainfall. *Transactions of the ASAE* 28:1226-1229.

Chu, S.T. 1995. Effect of initial water content on Green-Ampt parameters. *Transactions of the ASAE* 38:839-841.

Church, G.R., and D.B. Smith. 1955. An instrument for the measurement of hydrogen content of soil and bulk material. Re. A.E.R.E. Harwell No. 1/R 1687. (From Marais and Smit, 1962).

Coles, N.A., M. Sivapalan, J.E. Larsen, P.E. Linnet, and C.K. Fahrner. 1997. Modeling runoff generation on small agricultural catchments: can real world runoff responses be captured? *Hydrological Processes* 114:644-663.

Cuenca, RH. 1988. Model for evapotranspiration using neutron probe data. *ASCE Journal of Irrigation and Drainage Engineering* 114:644-663 .

Damagnez, J. 1967. Problem of the calibration of neutron probe: Application to the determination of soil evapo-transpiration or crops. Soil moisture and irrigation studies Proceedings Pane *FAO/IAFA, Vienna*, Austria, pp21-37. (From Arslan and Razzouk, 1994).

De Boodt, M. and P. Demeester. 1968. A comparative study on the accuracy of the radio-active method for soil moisture determination using thermal and epi-thermal neutrons. *Trans. 9th Int. Congr. Soil Science* 3:555-564.

Dickey, G.L., R.G. Allen, J.H. Barclay, J.L. Wright, J.F. Stone, and B.W. Draper. 1993. Neutron gauge calibration comparison of methods. *Proceedings of 1993 National Conference on Irrigation and Drainage Engineering*, ASCE, New York, N.Y. pp.1136-1144. (From Grismer *et al.*, 1995).

Dingman, S.L. 1994. *Physical Hydrology*. Prentice Hall, Englewood Cliffs, New Jersey.

Douglass, J.E. 1966. Volumetric calibration of neutron moisture probes. *Soil Science Society of America Journal* 30:541-544.

Dunne, T., and R.D. Black. 1970. Partial area contribution to storm runoff in a small New England watershed. *Water Resources Research* 6:1296-1311.

Environment Canada. 1973. Snow Surveying. Manual of standards; snow surveying procedures. Second Edition. *Atmospheric Environment, Environment Canada*, Toronto, Ontario.

Essen I.I.. 1989. Estimation of Green-Ampt parameters from infiltrometer data. *Soil Science* 147:231-239.

Fayer, M.J., M.L. Rockhold, and M.D. Cambell. 1992. Hydrologic modeling of protective barriers: comparison of detailed data and simulation results. *Soil Science Society of America Journal* 56:690-700.

Feng, M. 1999. The Effects of capillary hysteresis on the measurement of matric suction using thermal conductivity sensors. M.Sc. Thesis, Department of Civil Engineering, *University of Saskatchewan*, Saskatoon, Saskatchewan.

Fredlund, D.G., and H. Rahardjo. 1988. State-of-development in the measurement of soil suction. Proceedings of the *First International Conference on Engineering Problems on Regional Soils.* August 11-15, Beijing, China, pp. 582-588.

Fredlund, D.G., and D.K.H. Wong. 1989. Calibration of thermal conductivity sensors for measuring soil suction. *ASTM Geotechnical Testing Journal* 12(3):188-194.

Fredlund, D.G., J.K-M. Gan, and H. Rahardjo. 1991. Measuring negative pore-wate pressures in a freezing environment. *Transportation Research Record* 1307:291-299.

Fredlund, D.G., P.J. Sattler, and J.K-M. Gan. 1992. *In situ* suction measurements using thermal sensors. 7th International Conference on Expansive Soils, Dallas, Texas, pp.325-330.

Fredlund, D.G., and H. Rahardjo. 1993. *Soil Mechanics for Unsaturated Soils*. John Wiley & Sons, Inc., New York, NY.

Fredlund, D.G., A. Xing, and H. Shangyan. 1994a. Predicting the permeability function for unsaturated soils using the soil-water characteristic curve. *Canadian Geotechnical Journal* 31:533-546.

Fredlund, D.G., J.K-M. Gan, and W-X. Li. 1994b. Thermal conductivity suction sensors - design consideration. Proceedings of the *13th International Conference on Soil Mechanical Foundation Engineering*, New Delhi, India, pp. 291-296.

Fredlund, D.G., and A. Xing. 1994. Equations for the soil-water characteristic curve. *Canadian Geotechnical Journal* 31:521-532.

Fredlund, D.G., F. Shuai, J. Yazdani, and M. Feng. 1998. Recent developments on a sensor for the insitu measurement of matric suction. Proceedings of the *51st Canadian Geotechnical Conference*, Edmonton, Alberta, pp. 81-86.

Freeze, R.A. 1972. Role of subsurface flow in generating surface runoff 2. Upstream source areas. *Water Resources Research* 8:1271-1283.

Freeze, R.A. 1974. Stormflow generation. *Review Geophysics* 12:627-647. (From Moore and Grayson, 1991).

Freyberg, D.L., J.W. Reeder, J.B. Franzini, and J. Remson. 1980. Application of the Green-Ampt model to infiltration under time-dependent surface water depths. *Water Resources Research* 16:517-528.

Fritschen, L.J., and J. R. Simpson. 1989. Surface energy and radiation balance systems: general description and improvements. *Journal of applied Meteorology* 28:680-689.

Fritschen, L.J., and P. Qian. 1990. Net radiation, sensible and latent heat flux densities on slopes computed by the energy balance method. *Boundary Layer Meteorology* 53:163-171.

Gardner, W.R., and D. Kirkham. 1952. Determination of soil moisture by neutron scattering. *Soil Science* 73:391-401.

Gardner, W.R. 1958. Some steady-state solutions of the unsaturated moisture flow equation with application to evaporation from a water table. *Soil Science* 85:228-232.

Goodison, B.E., H.L. Ferguson, and G.A. McKay. 1981. Measurement and data analysis. In *Handbook of snow*: principles, process, management, and use. Edited by D.M. Gray and D.H. Male. Pergamaon Press, Toronto, pp.191-274.

Goodrich, D.C, L.B. Bach, M.A. Weltz, T.J Jackson, T.J. Schmugge, T.O. Keefer, S.A. Amer, and C.L Unkrich. 1991. Preliminary runoff simulation sensitivity to various measures of initial soil water content. p.170-173. *Proceedings of American Meteorological Society 20th Conference* on Agriculture and Forest Meteorology, Salt Lake City, UT.

Goodrich, D.C, T.J. Schmugge, T.J Jackson, C.L Unkrich, T.O. Keefer, R. Parry, L.B. Bach, and S.A. Amer. 1994. Runoff simulation sensitivity to remotely sensed initial soil water content. *Water Resources Research* 30:1393-1405.

Gornat, B. and D. Goldberg. 1972. The relationship between moisture measurements with a neutron probe and soil texture. *Soil Science* 114:254-258.

Gray, D.M. 1973. Handbook on the Principles of Hydrology. Water Information Center, Inc., Water Research Building, Manhasset Isle, Port Washington, N.Y.

Greacen, E.L. and G. Schrale. 1976. The effect of bulk density on neutron meter calibration. *Australian Journal of Soil Research* 14:159-169.

Greacen, E.L. and C.T. Hignett. 1979. Sources of bias in the field calibration of a neutron meter. *Australian Journal of Soil Research* 17:405-415.

Greacen, E.L. 1981. Soil and water assessment by the neutron method. CSIRO Publication, East Melbourne, Victoria, Australia, 140 pp.

Green, W.H., and G.A. Ampt. 1911. Studies on soil physics. Part 1. The flow of air and water through soils. *Journal of Agricultural Science* 4:1-24.

Grismer, M.E., K.M. Bali, and F.E. Robinson. 1995. Field-scale neutron probe calibration and variance analysis for clay soil. *ASCE Journal of Irrigation and Drainage Engineering* 121:354-362.

Hajdukovic, M., M. Jokovljevic, and V. Vajgand. 1967. Comparison of three methods of measuring soil moisture. Isotopes and radiation techniques in soil physics and irrigation studies. IAFA/FAO Symposium, Istanbul, pp. 117-124. (From Arslan and Razzouk, 1994).

Hanna, L.W., and N. Siam. 1980. The estimation of moisture content in the top 10 cm of soil using a neutron probe. *Journal of Agricultural Science* 94:251-253.

Hanson, B.R. and G.L. Dickey. 1993. Field practices affect neutron moisture meter accuracy. *California Agr.* 47:29-31. (From Grismer *et al.*, 1995).

Haug, M.D., L.C. Wong, K. Johnston. 1991. Design and construction of a compacted earth test cover for a potash tail pile. *Proceedings of the First Canadian Conference on Environmental Geotechnics*, May 1991, Montreal, Quebec.

Haverkamp, R., M. Vauclin, and G. Vachaud. 1984. Error analysis in estimating soil water content from neutron probe measurements: 1. Local standpoint. *Soil Science* 137:78-90.

HBT AGRA Limited. 1992. Heap Leach cover design sampling and testing, Key Lake Mine Site. Project Report SX-01822. HBT AGRA Limited, Saskatoon, SK, 16 pp.

Herkelraath, W.M., S.P. Hamburg, and F. Murphy. 1991. Automatic real-time monitoring of soil mositure in a remote field area with time domain reflectometry. *Water Resources Research* 27:857-864.

Hills, R.C. 1971. Lateral flow under cylinder infiltrometers: A graphical correction procedure. *Journal of Hydrology* 13:153-162.

Holmes, J.W. and A.F. Jenkinson. 1959. Techniques for using the neutron moisture meter. *Journal of Agricultural Engineering Research* 4:100-109.

Holmes, J.W. 1966. Influence of bulk density of the soil on neutron moisture meter calibration. *Soil Science* 102:355-360.

Holmes, R.M. 1961. Estimation of soil moisture content using evaporation data. *Proceedings of Hydrology Symposium*, No. 2 Evaporation, Queen's Printer, Ottawa, Ontario, pp. 184-196. (From Wilson *et al.*, 1997).

Horton, R.E. 1933. The role of infiltration in the hydrological cycle. *Transactions of the American Geophysical Union* 14:446-460.

Horton, R., and P.J. Wierenga. 1983. Estimating the soil heat flux from observations of soil temperature near the surface. *Soil Science Society of America Journal* 47:14-20.

Hromadka, T.V. and R.J. Whitley. 1996. Approximating Rainfall-runoff Modelling Response Using Stochastic Integral Equation. *Hydrological Processes* 10:1003-1019.

Jackson, R.D., R.J. Reginato, B.A. Kimcall, and F.S. Nakayama. 1974. Diurnal soil-water evaporation: comparison of measured and calculated soil-water fluxes. *Soil Science Society of America Journal* 38:861-866.

Jensen, P.A., and E. Somer. 1967. Scintillation techniques in soil moisture and density measurements. Isotopes and radiation techniques in soil physics and irrigation studies. *IAEA/FAO Symposium, Istanbul*, pp.31-46. (From Arslan and Razzouk, 1994).

Jordan, J.P. 1994. Spatial and temporal variability of stormflow generation processes on a Swill catchment. *Journal of Hydrology* 149:9-25.

Joshi, B. 1997. Estimation of diffuse vadose zone soil- water flux in a semi-arid region. Ph.D. Thesis, Department of Agricultural and Bioresource Engineering, *University of Saskatchewan*, Saskatoon, Saskatchewan.

Kaya, A., and C.W. Lovell, and A.G. Altschaeffl. 1994. The effective use of time domain reflectometry (TDR) in geotechnical engineering. In *Time Domain Reflectometry in Environmental, Infrastructure and Mining Applications*. Unites Sates Bureau of Mines special Publication No. 19-94, pp. 96-100. (From Ayres 1998).

Keller, B.R., L.G. Evertt, and R.J. Marks. 1990. Effects of access tube material and grout on neutron probe measurements in the vadose zone. *Groundwater Monitoring Review*, Winter: 96-100.

Khogali, W.E.I., K.O. Anderson, J.K-M. Gan, and D.G. Fredlund. 1991. Installation and monitoring of moisture suction sensors in a fine-grained sub-grade soil subjected to seasonal frost. Presented to the second *International Symposium, "state-of-the-art" in pavement Response-Monitoring Systems for Roads and Airfields*. Sponsored by U.S. Army Cold Regions, Research and Engineering Laboratory, Hanover, New Hampshire and Federal Aviation Administration, Washington, D.C., West Levanon, N.H.

Kim, S.J. and H.W. Chung. 1994. Field evaluation of layered Green-Ampt infiltration model considering temporal variation of physical properties. *Transactions of the ASAE* 37:1845-1852.

Kirkham, R.R., G.W. Gee, and T.L. Jones. 1984. Weighing lysimeters for long-term water balance investigations ar remote sites. *Soil Science Society of America Journal* 48:1203-1205.

Klock, G.O. 1972. Snowmelt temperature influence on infiltration and soil water retention. *Journal of Soil and Water Conservation* 27:12-14.

Kohler, M.A., T.J. Nordenson, and W.E. Fox. 1955. Evaporation from pans and lakes. *U.S. Weather Bureau* Research Paper 38, Washington, DC. (From Dingman 1994).

Kondo, J., and N. Saigusa. 1990. A parameterization of evaporation from bare soil surfaces. *Journal of Applied Meteorology* 29:385-389.

Konzelmann T., P. Calanca, G. Muller, L. Menzel, and H. Lang. 1997. Energy balance and evapotranspiration in a high mountain area during summer. *Journal of Applied Meteorology* 36:966-973.

Kramer, J.H., S.J. Cullen, and L.G. Everett. 1992. Vadose zone monitoring with the neutron moisture probe. *Groundwater Monitoring Review* Summer: 177-187.

Lal, R. 1974. The effect of soil texture and density on the neutron and density probe calibration for same tropical soils. *Soil Science* 117:183-190.

Larsen, J.E., M. Sivapalan, N.A. Coles, and P.E. Linnet. 1994. Similarity analysis of runoff generation processes in real-world catchments. *Water Resources Research* 30:1641-1652.

Lee, R.K.C., and D.G. Fredlund. 1984. Measurement of soil suction using the MCS 600 gauge. In Proceedings of the 5th International Conference on Expansive Soils, Adelaide, Australia, pp.50-54. (From Szafron and Fredlund, 1992).

Link, S.O., N.R. Wing, G.W. Gee. 1995. The development of permanent isolation barriers for buried wastes in cool deserts: Hanford, Washington. *Journal of Arid Land Studies* 4:215-224. (From Vanapalli *et al.*, 1997).

Loague, K.M., and G.A. Gander. 1990. R-5 revisited. 1. Spatial variability of infiltration on a small range land catchment. *Water Resources Research* 26:957-971.

Loi, J., D.G. Fredlund, J.K-M. Gan, and R.A. Widger. 1992. Monitoring soil suction in an indoor test track facility. *Transportation Research Record* 1362:101-110.

Long, I.F. and B.K. French. 1967. Measurements of soil moisture in the field by neutron moderation. *Journal of Soil Science* 18:149-166.

Luebs, R.E., M.J. Brown, and A.E. Laag. 1968. Determining water content of different soils by the neutron method. *Soil Science* 106:207-212.

Lyford, F.P., and H.K. Qashu. 1969. Infiltration rates as affected by desert vegetation. *Water Resources Research* 5:1373-1376.

Mack, M.J. 1995. HER - Hydrologic Evaluation of Runoff: the soil conservation service curve number technique as an interactive computer model. *Computers and Geosciences* 21:929-935.

Mahfouf, J.F., and J. Noilhan. 1991. Comparative study of various formulations of evaporation from bare soil using ain situ data. *Journal of Applied Meteorology* 30:1354-1365.

Maidment, D.R. 1993. Handbook of Hydrology. *McGraw-Hill*, Inc., New York, NY.

Malek, E. 1993. Rapid changes of the surface soil heat flux and its effects on the estimation of evapotranspiration. *Journal of Hydrology* 142:89-97.

Malek, E, and G.E. Bingham. 1993. Comparison of the Bowen ratio-energy balance and the water methods for the measurement of evapotranspiration. *Journal of Hydrology* 146:209-220.

Malek, E. 1994. Calibration of the Penman wind function using the Bowen ratio energy balance method. *Journal of Hydrology* 163:289-298.

Marais, P.G., and W.B. DE V. Smit. 1960. Laboratory calibration of the neutron moisture meter. *South African Journal of Agricultural Science* 3:581-599.

Marais, P.G., and W.B. DE V. Smit. 1962. Effect of bulk density and of hydrogen in forms other than free water on the calibration curve of the neutron moisture meter. *South African Journal of Agricultural Science* 5:225-238.

Martinez-Mena, M., J. Albaladejo, and V.M. Castillo. 1998. Factors influencing runoff generation in a mediterranean semi-arid environment: Chicamo watershed, SE Spain. *Hydrological Processes* 12:741-754.

McCumber, M.C., and R.A. Pielke. 1981. Simulation of the effects of surface fluxes of heat and moisture in a meso-scale numerical model. Part I.: Soil Layer. *Journal of Geophysical Research* 86:9929-9938.

McGuinness, J.L., F.R. Dreibelbis, and L.L. Harrold. 1961. Soil moisture measurement with the neutron method supplement weighing lysimeters. *Soil Science Society of America Proceedings* 25:339-342.

McHenry, F.R. 1963. Theory and application of neutron scattering in the measurement of soil moisture. *Soil Science* 95:294-307.

McHenry, F.R., and C. Gill. 1967. The influence of bulk density, slow neutron absorbers, and time of the calibration of the neutron moisture probes. Isotopes and radiation techniques in soil physics and irrigation studies. *IAEA/FAO Symposium, Istanbul*, pp.83-97. (From Arslan and Razzouk, 1994).

Mein, R.G., and C.L. Larson . 1973. Modeling infiltration during a steady rain. *Water Resources Research* 9:384-394.

Melone, F., C. Corradini, and V.P. Singh. 1998. Simulation of the direct runoff hydrograph at basin outlet. *Hydrological Processes* 12:769-779.

Meneley, W.A., and J.A. Cherry. 1986. Conceptual decommissioning plan: hydrology. Report 0018-070 prepared for Cluff Mining by *W.A. Meneley Consultants Ltd.*, October 1986. (From Ayres 1998).

Milly, P.C.D. 1982. Moisture and heat transport in hysteretic, inhomogeneous porous media: a matric head based formulation and a numerical model. *Water Resources Research* 18:489-498.

Milly, P.C.D. 1984. A simulation analysis of thermal effects on evaporation from soil. *Water Resources Research* 20:1087-1098.

Milly, P.C.D. 1986. An event-based simulation model of moisture and energy fluxes at a bare soil surface. *Water Resources Research* 22:1680-1692.

Mitchell, A.R. and M.T. van Genuchten. 1993. Flood irrigation of a cracked soil. *Soil Science Society of America Journal* 57:490-497.

Mohamed, A-M. O., R.N. Young, F. Caporuscio, E.K. Yanful, and L. Bienvenu. 1993. Chemical interaction and cyclic freeze-thaw effects on the integrity of the soil cover for Waite Amulet tailings. *Joint CSCE-ASCE National Conference on Environmental Engineering*, Montreal, Quebec, pp.259-268.

Monteith, J.L. 1965. Evaporation and Environment. In the State and Movement of Water in Living Organisms, Symposium: *Society of Experimental Biology* 19:205-234. Edited by G.E. Fogg, Academic Press, San Diego, Ca. (From Wilson *et al.*, 1994).

Moore, I.D., and R.B. Grayson. 1991. Terrain based catchment partitioning and runoff prediction using vector elevation data. *Water Resources Research* 27:1177-1191.

Morel-Seytoux, J., and J. Khanji. 1974. Derivation of an equation of infiltration. *Water Resources Research* 10:795-800.

Nagy, A.E. and P. Verites. 1968. Correction for dry bulk density in measurements with neutron moisture gauges. Journal Sci. Instr. 1 E:1097-1100.

Nakayama, F.S. and R.J. Reginato. 1982. Simplifying neutron moisture meter calibration. *Soil Science* 133:48-52.

Nassif, S.H., and E.M. Wilson. 1975. The influence of slope and rain intensity on runoff and infiltration. *Hydrological Sciences Bulletin* 20:539-553. From Dingman.

Newman, G.P., and G.W. Wilson. 1997. Heat and Mass transfer in unsaturated soils during freezing. *Canadian Geotechnical Journal* 34:63-70.

Nicholson, R.V., R.W. Gillham, J.A. Cherry, and E.J. Reardon. 1989. Reduction of acid generation in mine tailings through the use of moisture-retaining cover layers as oxygen barriers. *Canadian Geotechnical Journal* 26:1-8.

Ogden, F.L., and B. Saghaflan. 1997. Green and Ampt infiltration with redistribution. *ASCE Journal of Irrigation and Drainage Engineering* 123:386-393.

Ohmura, A. 1982. Objective criteria for rejecting data for Bowen ratio flux calculations. *Journal of Applied Meteorology* 21:595-598.

O'Kane, M., G.W. Wilson, S.L. Barbour, and D.A. Swanson. 1995. Aspects on the performance of the till cover system at Equity Silver Mines Ltd. *Conference on Mining and the Environment*, Sudbury, Ontario. pp. 565-574.

O'Kane, M. 1996. Instrumentation and monitoring of an engineered soil cover system for acid generating mine waste. M.Sc. Thesis, Department of Civil Engineering, *University of Saskatchewan*, Saskatoon, Saskatchewan.

Oke T.R. 1987. *Boundary Layer Climates, 2nd. Ed.*. Methuen Inc., New York, 1001.

Olgaard, P.L. and V. Haahr. 1968. On the sensitivity of subsurface neutron moisture gauges to variations in bulk density. *Soil Science* 105:62-64.

Passerat de Silans, A., L. Brukler, J.L. Thory, and M. Vauclin. 1989. Numerical modeling of coupled heat and water flows during drying in a stratified bare soil - comparison with filed observations. *Journal of Hydrology* 105:109-138.

Passerat de Silans, A., B.A. Monteny, and J.P. Lhomme. 1997. The correction of soil heat flux measurements to derive an accurate surface energy balance by the Bowen ratio method. *Journal of Hydrology* 188-189:453-465.

Penman, H.L. 1948. Natural evaporation from open water, bare soil, and grass. *Royal Society of London Proceedings*, Series A, 193:120-145 (From Dingman 1994).

Philip, J.R., and D.A. de Vries. 1957. Moisture movement in porous materials under temperature gradients. *Transactions, American Geophysical Union* 38(2):222-232.

Philip, J.R. 1969. Theory of infiltration. *Advances in Hydroscience*, 5:215-296.

Pierpont, G. 1966. Measuring surface soil moisture with the neutron depth probe and a surface shield. *Soil Science* 101:189-192.

Priestley, C.H.B., and R.J. Taylor. 1972. On the assessment of surface heat flux and evaporation using large-scale parameters. *Monthly Weather Review* 100:81-92. (From Dingman 1994).

Rahardjo, H., J. Loi, and D.G. Fredlund. 1989. Typical matric suction measurements in the laboratory and the field using thermal conductivity sensors. *Indian Geotechnical Conference*, pp. 127-133.

Rawls, W.J. and L.E. Asmussen. 1973. Neutron probe field calibration for soils in the Georgia Coastal Plains. *Soil Science* 116:262-265.

Rawls, W.J., and D.L. Brakensiek. 1983. A procedure to predict Green and Ampt infiltration parameters. *In* Advances in infiltration. ASAE Conference, Chicago, IL. pp.102-112.

Rawls, W.J., and D.L. Brakensiek. 1988. Comparison between Green-Ampt and curve number runoff predictions. *Transactions of the ASAE* 26:1597-1599.

Rawls, W.J., D.L. Brakensiek, J.R. Simanton, and K.D. Kohl. 1990. Development of a crust factor for a Green Ampt model. *Transactions of the ASAE* 33:1224-1228.

Reynolds, W.D., D.E. Elrick, and B.E. Clothier. 1985. The constant head well permeameter: the effect of unsaturated flow. *Soil Science* 139:172-180.

Reynolds, W.D., and W.D. Zebchuk. 1996. Hydraulic conductivity in clay soil: Two measurement techniques and spatial characterization. *Soil Science Society of America Journal* 60:1679-1685.

Richards, A.L. 1931. Capillary conduction of liquids through porous media. *Physics* 1:316-333. (From Dingman 1994).

Richardson, M.D., C.A. Meisner, C.S. Hoveland, and K.J. Karnok. 1992. Time domain reflectormety in closed container studies. *Soil Science Society of America Journal* 84:1061-1063.

Risse, L.M., M.A. Nearing, and M.R. Savabi. 1994. Determining the Green-Ampt effective hydraulic conductivity from rainfall-runoff data for the WEPP model. *Transactions of the ASAE* 37:411-418.

Rodda, J.c. 1985. Precipitation research. Transactions of the Geophysical Union 8 Jan 1985:10. (From Dingman 1994)

Ryhiner, A.H. 1969. Soil moisture measurement by the gamma transmission method. *Journal of Hydrology* 9:194-205.

Schieldge, J.P., A.B. Kahle, and R.E. Alley. 1982. A numerical simulation of soil temperature and moisture variations for a bare field. *Soil Science* 133:197-207.

Schroeder, P.R., C.M. Lloyd, P.A. Zappi, N.M. Aziz. 1994. The hydrologic evaluation of landdfill performance (HELP) model: User's guide for Version 3. EPA/600/R-94/168a. *U.S. Environmental Protection Agency*, Cincinnati, Ohio. 93 pp.

Sharma, M.L., and J. Tunny. 1972. Measuring soil moisture near the surface with the neutron sub-surface probe. *Journal of Australian Institute of Agricultural Science* 38:221-223.

Sharma, M.L., G.A. Gander, and G.C. Hunt. 1980. Spatial variability of infiltration in a watershed. *Journal of Hydrology* 45:101-122.

Shuai, F., J. Yazdani, M. Feng, and D.G. Fredlund. 1998. Supplemental report of the thermal conductivity matric suction sensor development (year two). Unsaturated Soils Group, Department of Civil Engineering, *University of Saskatchewan*, Saskatoon, SK. 21 pp.

Silvestri, V., G. Sarkis, N. Bekkouche, M. Soulie, and C. Tabib. 1991. Laboratory and field calibration of a neutron depth moisture gauge for use in high water content soils. *Geotechnical Testing Journal* 14:64-70.

Simanton, J.R., and K.G. Renard. 1982. Seasonal change in infiltration and erosion from USLE plots in southeastern Arizona. *Proceedings of the 1982 Meetings of the Arizona Section, American Water Resources Association and the Hydrology Section*, Arizona Academy of Science, Tempe Arizona.

Sivapalan, M., K. Beven, and E.F. Wood. 1987. On hydrologic similarity 2. A scaled model of storm runoff production. *Water Resources Research* 23:2266-2278.

Smettem, K.R.J., and C. Kirkby. 1990. Measuring the hydraulic properties of a stable aggregated soil. *Journal of Hydrology* 117:1-13.

Smith, R.E., and D.A. Woolhiser. 1971. Overland flow on an infiltrating surface. *Water Resources Research* 7:899-913.

Smith, R.E., and D.L. Cherry, Jr. 1973. Rainfall excess model from soil water flow theory. *Journal of the Hydraulics Division, Proceedings of ASCE* 99:1337-1351.

Smith, R. E. 1976. Approximations for Vertical Infiltration Rate Patterns. *Transactions of the ASAE* 19:505-509.

Smith, C.D. 1962. Brink depth for a circular channel. *Journal of the Hydraulics Division, Proceedings of the ASCE* November p125-134.

SoilCover User's Manual Version 4.01. 1997. Unsaturated Soils Group, *University of Saskatchewan*, Saskatoon, SK.

Soilmoisture Equipment Corp. 1986. Guelph Permeameter 2800KI Operating Instructions. Santa Barbara, California, 28 pp.

Sophocleous, M. 1979. Analysis of water and heat flow in unsaturated-saturated porous media. *Water Resources Research* 15:1195-1206.

Spaans, E.J., and J.M. Baker. 1995. Examining the use of time domain reflectometry for measuring liquid water content in frozen soil. *Water Resources Research* 31:2917-2925.

Springer, E.P., and G.F. Gifford. 1980. Spatial variability of rangeland infiltration rates. *Water Resources Bulletin* 16:550-552.

St-Arnaud, L.C., and M.R. Woyshner. 1992. Hydrological evaluation of the thickened tailings disposal system at Kidd Creek Division, *Falconbridge Ltd. Report V2-1-T01*, Centre de technologie Noranda, Pointe Claire, Quebec (from Ayers 1998).

SRK (Steffen, Robertson and Kirsten) Canada Inc. 1993. Key Lake waste rock characterization. Pepared for Cameco Corporation. Report C101101/2. , Vancouver, B.C.

Stigter, C.J. 1980. Assessment of the quality of generalized wind functions in Penman's equation. *Journal of Hydrology* 45:321-331.

Stolzy, L.H. and G.A. Cahoon. 1957. A field-calibrated portable neutron rate meter for measuring soil moisture in citrus orchards. *Soil Science Society of America Proceedings* 6:571-575.

Stone, J.F., D. Kirkham, and A.A. Read. 1955. Soil moisture meter. *Soil Science Society of America Proceedings* 19:419-423.

Stone, J.F. 1972. Instrumentation effects on errors in nuclear methods for soil water and density determination. *Soil Science Society of America Proceedings* 36:261-264.

Stone, J.J., L.J. Lane, and E.D. Shirley. 1992. Infiltration and runoff simulation on a plane. *Transactions of the ASAE* 35:161-170.

Stone, J.J., E.D. Shirley, and L.J. Lane. 1993. Impact of recession infiltration on runoff volume computed by the kinematic wave model. *Transactions of the ASAE* 36:1353-1361.

Stone, J.J., R.H. Hawkins, and E.D. Shirley. 1994. Approximate form of Green-Ampt infiltration equation. *ASCE Journal of Irrigation and Drainage Engineering* 120:128-137.

Stormant, J.C., and C.E. Morris. 1998. Method to estimate water storage capacity of capillary barriers. *Journal of Geotechnical and Geoenvironmental Engineering* 124(4):297-302.

Swanson, D.A. 1995. Predictive modeling of moisture movement in engineered soil covers for acid generating mine waste. M.Sc. Thesis, Department of Civil Engineering, *University of Saskatchewan*, Saskatoon, Saskatchewan.

Szafron, B.J., and D.G. Fredlund. 1992. Monitoring matric suction in the subgrade of unpaved roads. 45th Canadian Geotechnical Conference, Toronto, Ontario 52:1-10.

Tanner, C.B. 1960. Energy balance approach to evapotranspiration from crops. *Soil Science Society of America Proceedings* 24:1-9.

Thom, A.S. and H.R. Oliver. 1977. On Penman's equation for estimating regional evaporation. *Quarterly Journal of the Royal Meteorological Society* 103:345-357.

Thomas, G.W., and R.E. Phillips. 1979. Consequences of water movement in macropores. *Journal of Environmental Quality* 8:149-152.

Thornthwaite, C.W. 1948. An approach toward a rational classification of climate. *Geographical Review* 38:55-94. (From Dingman 1994).

Topp, G.C., J.L. Davis, and A.P. Annan. Electromagnetic determination of soil water content: measurements in coaxial transmission lines. Water Resources Research 16:574-582.

Tratch, D. 1994. Moisture uptake within the root zone. M.Sc. Thesis, Department of Civil Engineering, *University of Saskatchewan*, Saskatoon, Saskatchewan.

Tricker, A.S. 1978. The infiltration cylinder: some comments on its use. *Journal of Hydrology* 36:383-391.

Tricker, A.S. 1981. Spatial and temporal patterns of infiltration. *Journal of Hydrology* 49:143-147.

Tyler, S.W. 1988. Neutron moisture meter calibration in large diameter boreholes. *Soil Science Society of America Journal* 52:890-893.

University of Saskatchewan. 1993. Laboratory tests to determine the moisture characteristic curves of selected Key Lake soils. Geotechinical Group, *University of Saskatchewan*, Saskatoon, Saskatchewan, pp. 30.

Vanapalli, S., S.L. Barbour, M. O'Kane. 1997. Review of soil cover technologies for acid mine drainage - a peer review of the Waite Amulet and Heath Steele Soil Covers. *MEND Project 2.21.3*

Van Bavel, C.H.M., N. Underwood, and R.W. Swanson. 1956. Soil moisture measurements by neutron moderation. *Soil Science* 82:29-41.

Van Bavel, C.H.M. 1961. Neutron measurement of surface soil moisture. *Journal of Geophysics Research* 66:4193-4198.

van der Raadt, P., D.G. Fredlund, A.W. Clifton, W.E. Jubien. 1987. Soil suction measurements at several sites in western Canada. *Transportation Research Record*, 1137.

Vandervaer, J.P., M. Vauclin, R. Haverkamp, and R.H. Cuenca. 1994a. Error analysis in estimating soil water balance of irrigated fields during the EFEDA experiment. 1: Local standpoint. *Journal of Hydrology* 56:351-370.

Vandervaer, J.P., M. Vauclin, R. Haverkamp, and R.H. Cuenca. 1994b. Error analysis in estimating soil water balance of irrigated fields during the EFEDA experiment. 2: Spatial standpoint. *Journal of Hydrology* 56:371-388.

Van Mullen, J.A. 1991a. Runoff and peak discharge using the Green-Ampt infiltration model. *ASCE Journal of Irrigation and Drainage Engineering* 117:354-370.

Van Mullen, J.A. 1991b. Precipitation distributions and Green-Ampt runoff. *ASCE Journal of Irrigation and Drainage Engineering* 117:944-959.

Vauclin, M., R. Haverkamp, G. Vachaud. 1984. Error analysis in estimating soil water content from neutron probe measurements: 2. Spatial standpoint. *Soil Science* 137:141-148.

Waring, E.A., and J.A.A. Jones. 1980. A snow melt and water equivalent gauges for British conditions. *Hydrological Sciences Bulletin* 25:129-134.

Weeks, O.L., R.S. Mansell, and S.W. McCallister. 1992. Evaluation of soil top-cove systems to minimize infiltration into a sanitary landfill: a case study. *Environmental Geology and Water Sciences* 20(2):139-151.

Whisler, F.C., and H. Bouwer. 1970. Comparison of methods for calculating vertical drainage and infiltration for soils. *Journal of Hydrology* 10:1-19.

Wilcock, D.N., and C.I. Essery. 1984. Infiltration measurements in a small lowland catchment. *Journal of Hydrology* 74:191-204.

Wilson, D.J., A.I.M. Ritchie. 1986. Neutron moisture meters: the dependence of their response on soil parameters. *Australian Journal of Soil Research* 24:11-23.

Wilson, G.W. 1990. Soil evaporative fluxes for geotechnical engineering problems. Ph.D. thesis, University of Saskatchewan, Saskatoon, Saskatchewan, Canada (from Wilson *et al.*, 1994).

Wilson, G.W., R.L. Machibroda, S.L. Barbour, and M.R. Woyshner. 1993. Modeling of soil evaporation from waster disposal sites. Proceedings of the Joint *ASCE-CSCE National Conference on Environmental Engineering*, Montreal, Quebec, pp.281-288.

Wilson, G.W., D.G. Fredlund, and S.L. Barbour. 1994. Coupled soil-atmosphere modeling for soil evaporation. *Canadian Geotechnical Journal* 31:151-161.

Wilson, G.W., D.G. Fredlund, and S.L. Barbour. 1997. The effect of soil suction on evaporative fluxes from soil surfaces. *Canadian Geotechnical Journal* 34:145-155.

Winter, T.C. 1981. Uncertainties in estimating the water balance of lakes. *Water Resources Bulletin* 17:82-115.

Witono, H., and L. Bruckler. 1989. Use of remotely sensed soil moisture content as boundary conditions in soil-atmosphere water transport modeling. 1. Field validation of a water flow model. *Water Resources Research* 25(12): 2423-2435.

Woolhiser, D.A., R.E. Smith, and D.C. Goodrich. 1990. KINEROS, a kinematic runoff and erosion model: documentation and user manual. ARS-77 *US Department of Agriculture*, Agricultural Research Service, Washington, D.C. 130pp.

Wong, D.K.H. 1985. A study of brine flow through saturated-unsaturated potash tailings. M.Sc. Thesis, *University of Saskatchewan*, Saskatoon, Saskatchewan.

Wong, D.K.H., D.G. Fredlund, E. Imre, and G. Putz. 1989. Evaluation of AGWA-II thermal conductivity sensors for soil suction measurement. *Transportation Research Record* 1219:131-143.

Woyshner, M.R., and L.C. St-Arnaud. 1994. Hydrological evaluation and water balance of a thickened tailings deposit near Timmins, Ontario, Canada. In Proceedings, *Third International Conference on the Abatement of Acidic Drainage*, Pittsburgh, PA.

Woyshner, M.R., and E.K. Yanful. 1995. Modeling and field measurements of water perconlation through an experimental soil cover on mine tailings. *Canadian Geotechnical Journal* 32:601-609.

Xu Q., and C. Qiu. 1997. A variation method for computing surface heat fluxes from arm surface energy and radiation balance. *Journal of Applied Meteorology* 36:3-11.

Yanful, E.K. 1991. Engineered soil covers for reactive tailings management: theoretical concept and laboratory development. *Proceedings of the Second International Confenrence on the Abatement of Acidic Drainage*, Montreal, Quebec.

Yazdani, J. 1995 Soil water characteristic curve for mine waste rock containing coarse material. M.Eng Project Report, *University of Saskatchewan*, Saskatoon, Saskatchewan.

Young, M.H., P.J. Wierenga, and C.F. Mancino. 1996. Large weighing lysimeters for water used and deep percolation studies. *Soil Science* 161:491-501.

Young, M.H., P.J. Wierenga, and C.F. Mancino. 1997. Monitoring near surface soil water storage in turfgrass using time domain reflectometry and weighing lysimetry. *Soil Science Society of America Journal* 61:1138-1146.

Youngs, E.G. 1988. Soil Physics and hydrology. Journal of Hydrology 100:411-431.

Zeglin, S.J., I. White, and G.F. Russel. 1992. A critique of the time domain reflectometry technique for determining field soil water content. In *Advances in Measurement of Soil Physical Properties: Bringing Theory into Practice*. Soil Science Society of America Special Publication 30:187-208. (From Ayers, 1998).

Zollweg, J.A., W.J. Gburek, and T.S. Steenhuis. 1996. SmoRMod - a GIS integrated rainfall-runoff model. *Transactions of the ASAE* 39:1299-1307.

Appendix A
POTENTIAL EVAPORATION

A. POTENTIAL EVAPORATION

A direct measurement of evaporation is difficult and expensive, and it is usually impractical. Henceforth, an array of methods have emerged that provide estimates of evaporation based on readily measured climatic parameters. The physics of evaporation involves the energy and water balance at the water-atmosphere interface. There are several methods for estimating the rate of evaporation from free water surface. They are: mass transfer method, energy budget method, empirical method, and direct measurement.

A.1. Mass Transfer Method

Evaporation is a diffusive process that follows Fick's first law. That is, the rate of evaporation is the rate at which water molecules move from the saturated surface layer into the air above. The rate of evaporation is proportional to the difference between the vapour pressure of the surface layer and the vapour pressure of the overlying air. Evaporation can thus be estimated by Dalton's aerodynamic *mass transfer* equation (Dingman 1994):

$$E = f(u)\,(e_s - e_a) \qquad [A.1]$$

where, E = rate of evaporation (mm/day)

$f(u)$ = coefficient that reflects the efficiency of vertical transport of

water vapour by the turbulent eddies

e_s = vapour pressure of an evaporating surface (mm Hg)

e_a = vapour pressure of the overlying air (mm Hg)

Equation *[A.1]* is not easily solved due to the difficulty in estimating *f(u)*. Furthermore, the surface temperature that is needed to estimate e_s is not commonly available. Nonetheless, the mass-transfer approach provides an insight to the physics of the evaporation process, and forms the basis for other methods.

A.2 Energy Balance Method

The *energy balance* approach is based on the theory of *Conservation of Energy*. Evaporation involves some combination of heat inputs from radiation and sensible heat from the atmosphere/ground. Evaporation also involves a loss of heat energy in the evaporating body. Therefore, the rate of evaporation can be calculated from the thermal budget of the evaporating body (Dingman 1994):

$$LE = Q_n - G - H + A_W - \Delta Q/\Delta t \qquad [A.2]$$

where,

LE = latent heat transfer, i.e. energy used for evaporation

Q_n = net radiation

G = net conduction to the ground

H = net sensible heat exchange with the atmosphere

A_W = water advected energy

ΔQ = change in the amount of heat stored in the body per unit area

In natural water bodies, A_W and ΔQ may play a significant role in the energy balance. In estimating free water evaporation, they are insignificant, and equation *[A.2]* simplifies to:

$$LE = Q_n - G - H \qquad [A.3]$$

Evaporation is accompanied by a transfer of latent heat from the evaporating body into the air. This heat loss produces a reduction in surface temperature that is compensated by heat transfer to the surface from within the evaporating body, and/or by radiative or sensible-heat transfer from the overlying air. The rate of latent heat transfer (*LE*) is:

$$LE = \rho_w \lambda_v E \qquad [A.4]$$

where, ρ_w = mass density of water (g/cm^3)

λ_v = latent heat of vaporization

= $597.3 - 0.564\,T$ (cal/g)

The sensible heat exchange, *H,* represents the energy conducted to or from the evaporating body by air. The upward rate of sensible heat exchange by turbulent transfer is dependant on the wind speed (u_a), and the difference between the surface temperature (T_s) and the overlying air temperature (T_a) (Dingman 1994):

$$H = K_H u_a (T_s - T_a) \qquad [A.5]$$

where, K_H = constant reflecting eddy diffusivity of heat.

A direct measurement of *H* is difficult, and therefore it is usually calculated from the *Bowen ratio*. The *Bowen ratio, B,* is the ratio of sensible heat exchange to latent heat exchange. It is expressed as a ratio of surface-air temperature gradient ($T_s - T_a$) to surface-air vapor-pressure gradient ($e_s - e_a$):

$$B = H/LE \qquad [A.6]$$

$$B = \gamma \frac{T_s - T_a}{e_s - e_a} \qquad [A.7]$$

where, γ = psychrometric constant

= $c_a P/0.622\lambda_v$

c_a = heat capacity of air (0.24 cal/g/^{0}C)

P = atmospheric pressure (1013 mb)

The main advantage of using the *Bowen ratio* in an energy balance is that wind data is not required. Using equations *[A.3]*, *[A.4]*, *[A.6]*, and *[A.7]*:

$$E = \frac{Q_n - G}{\rho_w \lambda_v (1 + B)} \qquad [A.8]$$

$$E = \frac{Q_n - G}{\rho_w \lambda_v (1 + \gamma \frac{T_s - T_a}{e_s - e_a})} \qquad [A.9]$$

As with the mass transfer method, the *Bowen ratio* energy balance (BREB) method requires data that are not routinely recorded for most weather monitoring programs. It requires specific instrumentation to acquire the parameters that are needed to estimate evaporation.

A.3 Empirical Method

The energy budget and mass transfer methods require data that are often arduous to obtain and/or are not readily available. An accurate evaluation of the turbulent eddie coefficient, *f(u)*, in the *mass transfer* aerodynamic equation is often rigorous, and the surface temperature and the vapour pressure are difficult to obtain. Henceforth, empirical formulas have been proposed over the years to estimate evaporation using standard meteorological data.

Most empirical equations are based on Dalton's mass transfer aerodynamic equation. Thornthwaite (1948) first developed a complex temperature based empirical formula for calculating potential evaporation using climatic average monthly temperature and day length as input variables. Priestly and Taylor (1972) developed a radiation based equation for

estimating potential evaporation over well watered surfaces using net radiation, air temperature, and pressure as input parameters.

Penman (1948) combined the mass transfer equation with a second simultaneous sensible surface heat flux equation to estimate evaporation using routine climatic parameters such as net radiation, air temperature, relative humidity, and wind speed. Penman also proposed a simplified method of estimating *f(u)* using readily available mean wind speed. The Penman combination approach is most widely applied due to its ease of use, availability of input parameters, and good correlation with measured potential evaporation (Dingman 1994). It has since become the standard hydrologic method for determining free water evaporation. The Penman formulation is given by:

$$E = \frac{\Delta Q_n + \gamma E_a}{\Delta + \gamma} \qquad [A.10]$$

where,

E	=	evaporative flux (mm/day)
Δ	=	slope of the saturation vapour pressure versus temperature curve at the current air temperature T_a (mb/^{0}C)
Q_n	=	net radiation (mm/day of water)
γ	=	psychrometric constant ($\approx$ 0.66 mb/^{0}C)
	=	$c_a P / 0.622\ \lambda_v$
		c_a = heat capacity of air (0.24 cal/g/^{0}C)
		P = atmospheric pressure, function of elevation ($\approx$1013 mb)
		λ_v = latent heat of vaporization = $597.3 - 0.564 T_a$ cal/g
E_a	=	$f(u)\ (e_{sat\ (Ta)} - e_a)$
$f(u)$	=	$0.35\ (1 + 0.146\ u_a)$
u_a	=	wind speed (km/hr)
$e_{sat\ (Ta)}$	=	saturation vapour pressure of air at air temperature T_a (mb)
	=	$6.11\ exp^{[17.3\ Ta\ /\ (Ta\ +\ 237.3)]}$
e_a	=	vapour pressures of the overlying air (mb)
	=	$h_a\ e_{sat\ (Ta)}$

h_a = air relative humidity

A.4 Direct Measurement: Evaporation Pan

A direct measurement of evaporation using evaporation pans has been employed for many years for lakes and reservoirs. Their popularity and widespread use arise from their simplicity and their ease of use. The ratio of evaporation from pans to lake evaporation has been found to remain reasonably constant from year to year thus providing estimates of annual lake evaporation within 10% to 15% of actual lake evaporation amounts (Gray 1973).

The evaporation pan method determines free water evaporation by exposing a cylindrical pan of liquid water to the atmosphere. The water surface is maintained a few centimeters below the pan rim by adding or removing measured amounts of water as needed. Evaporation is estimated by records of water level changes due to precipitation, artificial filling, and evaporation. Intense rainfall often results in errors from water overflow and splash effects.

Class A type pan, used by the U.S. National Weather Service and in Canada, is typically mounted above ground with sides exposed to air and sun. This difference results in an elevated warm season average temperature and vapour pressure of the pan water surface relative to that of a nearby lake. Kohler *et al.* (1955) developed an empirical equation to account for the energy exchange through the sides of a pan:

$$E_{fw} = 0.7\,[\,E_{pan} \pm 0.00064\,P\,\alpha_{pan}\,(0.37 + 0.00255\,v_{pan})]\,[T_{span} - T_a]^{0.88} \qquad [A.11]$$

where,

E_{fw} = daily free water evaporation (mm/day)

E_{pan} = daily pan evaporation (mm/day)

$\pm$ = is + when $T_{span} > T_a$ and - when $T_{span} < T_a$

P = atmospheric pressure (mb)

α_{pan} = proportion of energy exchanged through the sides of the pan

= $0.34 + 0.117\,T_{span} - (3.5 \times 10^{-7})\,(T_{span} + 17.8)^3 + 0.0135\,u_{pan}^{0.36}$

u_{pan} = average wind speed at 15cm height above pan (km/day)

T_{span} = water surface temperature in the pan (^{0}C)

T_a = air temperature (^{0}C)

An evaporation pan also differs from lakes in that it has less heat storage capacity, and it lacks surface or ground water inflows and outflows. Pan evaporation is relatively independent of antecedent weather conditions ,whereas lake evaporation is determined by heat exchange that occurs over a considerable period of time preceding the measurement. Therefore, a large variation may be noted if only short time periods are considered.

The ratio of lake evaporation to pan evaporation is called pan coefficient, and its annual average in the U.S.A. and Canada ranges from 0.6 to 0.8 (Gray 1973; Brutsaert 1982). Heat storage effects cause water temperatures in lakes to be generally lower than those of pans in the spring and higher in the fall, and pan coefficients generally follow the same pattern.

Appendix B

NEUTRON PROBE CALIBRATION CURVE

B. NEUTRON PROBE CALIBRATION CURVE

The shape and the universality of the neutron moisture probe *calibration curve* remains contentious to date. The factors that may affect the shape of this response curve are: the presence of hydrogen in forms other than free water; the presence of absorber elements such as boron, chlorine, iron, potassium; the bulk density and soil texture; the presence of gravel, rock, and air; high clay content; and the type of access hole casing material and its diameter.

B.1 Other Forms of Hydrogen

Hydrogen in forms other than free water, such as mineralogically bound H^- (e.g. gypsum, kaolinite), organic soil compounds (e.g. peat moss), and organic liquids (e.g. petroleum contaminants), could result in high apparent water content. Church and Smith (1955) concluded that count rate was affected by hydrogen in all chemical forms. Van Bavel *et al.* (1956) determined that mineralogically bound hydrogen in clay minerals did not affect count rate in soils of up to 10% clay content.

Marais and Smit (1962) and Holmes (1966) found that for organic soils, or soils rich in clay minerals such as kaolinite, the presence of hydrogen in forms other than free water should be considered. Arslan and Razzouk (1994) found it necessary to correct for the effects of gypsum.

B.2 Strong Absorber Elements

The presence of strong thermal neutron absorber elements, such as boron, chlorine, iron, titanium, and potassium, will also increase the density of thermalized neutrons count rate (Luebs *et al.*, 1968; Greacen and Schrale, 1976; Chanasyk and McKenzie, 1986). In most soils, the proportion of these elements is relatively low.

B.3 Soil Bulk Density and Soil Texture

The effect of soil bulk density and soil texture has been investigated by many researcher with differing results. The mechanism of bulk density effects on the thermal neutron count rate for a given soil moisture content are (Greacen and Schrale, 1976):

- increase in volumetric content of bound hydrogen (i.e. constitutional hydrogen) due to increase in bulk density;
- increase in bulk density which results in increased number of soil atoms per unit volume of soil, consequently restricting the movement of high energy neutrons away from the source; and
- increase in concentration of thermal neutron absorber elements (boron, chlorine, manganese, iron, potassium, titanium) with increase in bulk density.

Some researchers have indicated that sthe oil bulk density did not affect neutron count rate (McHenry and Gill 1967; Hajdukovic *et al.*, 1967; Silvestri, 1991).

Chanasyk and McKenzie (1986), in 29 agricultural study fields near Lethbridge, Alberta (Coaldale clay loam and Lethbridge silt loam), found that in general, as bulk density increased, the intercept of the calibration curve decreased, and the slope of the calibration curve increased. However, there was no apparent trend based on either the soil texture or the bulk density. And although the bulk density did affect calibration, the magnitude of its effect did not warrant calibration based on the bulk density.

Arslan and Razzouk (1994) concluded that the effect of bulk density on the calibration curve was negligible in most cases, but it was significant for organic soils.

Marais and Smit (1962) found that there was no increase in count rate with increase in density other than that due to the change in constitutional hydrogen. While it was possible to obtain a single calibration curve for soils that differ markedly in texture and density, significant differences were noted for a particular soil that was sampled at different layers (i.e. varying densities). The changes in bulk density caused a parallel shift of the calibration curve, however, the slope remained unchanged.

Holmes (1966) attributed the effects of bulk density on the volumetric content of chemically bound hydrogen and the macroscopic absorption cross section. Olgaard and Haahr (1968) attributed it to the impediment of neutron movement (i.e. transport cross section) away from the source with higher soil density, thus resulting in higher count. Luebs *et al.*, (1968) stated that the apparent effect of bulk density is to change the amount of water indicated without markedly changing the slope of the calibration curve (similar to Marais and Smit, 1962) and that soil texture *per se* had no effect. Lal (1974) suggested that for some soils, bulk density had a significant effect, and that this effect was interrelated with the soil texture.

Wilson and Ritchie (1986) concluded that the neutron probe response increases linearly with increase in matrix density over almost the entire range of the soil water mixture, and that the calibration curve was nonlinear. Many other researchers have also concluded that higher neutron count rates were achieved at higher bulk densities for the same volumetric water content (Jensen and Somer, 1967; Damagnez 1967; Greacen and Schrale, 1976).

O'Kane (1996) derived two calibration curves for a till cover material to account for variations in bulk density between the compacted till layer, and the overlying non compacted till layer. However, his data suggested that lower count rates were achieved at higher bulk densities for the same volumetric water content. That is to say, for a given count ratio, the water content in the compacted layer was greater than that of the non compacted layer.

The effects of soil texture on the count rate have also been suggested (McHenry and Gill 1967; De Boodt and Demeester 1968; Gornat and Goldberg 1972). Lal (1974) concluded that the slope of the calibration curve increases for coarse-textured soils as compared to that of fine textured soils, and that the soil texture and density have a significant effect on the neutron probe calibration. He claimed that the usefulness of neutron-scattering technique for inherently heterogeneous tropical soils was very limited.

Greacen and Schrale (1976) proposed a bulk density correction factor to improve the variance of the calibration curve resulting from variations in the soil bulk density:

$$CR_c = CR\ (\rho_s/\rho)^n$$

where, CR_c = corrected count ratio at a chosen standard dry density, ρ_s

CR = observed count rate at dry density ρ

n = some power best represented by 0.5

A count ratio is simply a ratio of observed count rate to the standard count rate. The standard count rate is typically measured in water or within a wax shield encasing the fast neutron source. The count ratio is generally used because it gives an indication of acceptable drift in the electronics, and it is also a means of checking that noise is not affecting the count.

Grismer *et al.* (1995) postulated that if the effects of bulk density are ignored, then the calibration curve would become non-linear. His data suggested that due to field variability of soil textures, correcting the count data and measured moisture contents using the bulk density corrections generally improved the calibration regression slightly. However, it did not improve the standard measurement errors. It was concluded that such correction appeared to be of limited value when using field calibration, and that it may not be worth the effort required to obtain bulk density data.

B.4 Rock and Air Space

McHenry (1963) reported that the presence of rock and air space in the soil decreased the density of thermalized neutron by scattering or reflecting. Lal (1974) also concluded that the concentration of stones decreased the density of thermal neutrons. He stated that the change in the slope of the response curve is due to both the chemical and physical composition of the soil, and that the slope of the calibration curve generally decreased with increase in gravel concentration.

B.5 Clay Content

The application of neutron soil moisture technique in clay soils comprised of over 40% clay fractions remains unresolved (Grismer *et al.*, 1995). In general, it has been found that high clay content will have a positive intercept (Long and French, 1967; Lal 1974). Achieving an accurate calibration curve has proven difficult for soils high in clay content. Best calibrations were achieved as the soil profile dried resulting in a broader range of water contents on which to base the calibration (Grismer *et al.*, 1995). Soil cracking adjacent to the access tube, and clay soil shrinkage and swelling, all contribute to error when performing field calibration (Mitchell and Van Genuchten 1993).

B.6 Access Tube Material and Size

Access tubes enable the neutron probe to be lowered into the soil medium so that soil moisture profile can be estimated. The selection of access tube material, its diameter, and installation technique all have a significant impact on the shape of the calibration curve. The sensitivity of the soil medium response is also affected by the type and the diameter of the tubing material.

Steel, aluminum, and PVC access tubes are commonly used. Aluminum was shown to be transparent to neutrons (Stolzy and Cahoon, 1957; Bell and McCulloch, 1966) and the count

rate was determined to be lower with steel tubes than with aluminum (Stolzy and Cahoon, 1957). However, it was also found that a metal tube tightly fitting into a borehole has the least interference with the neutron measurement (Tyler 1988).

A plastic tubing (PVC) was found to decrease the count rate by at least 15%. Calibration slopes associated with PVC access tubes generally exceed those with steel tubing due to neutron absorption by the PVC (Hanson and Dickey 1993; Dickey *et al.*, 1993). However, Keller *et al.* (1990) also found that the hydrogen in PVC access tubes did not produce a significant measurement by itself, and that the effects of PVC access tubes alone are not distinguishable from the stainless steel tube.

The neutron probes are designed for soil moisture measurements in small diameter, 38 mm (1.5 inches) or 50 mm (2 inch), access tubes. They have been employed in larger diameter access tubes with success (Tyler 1988; Keller *et al.*, 1990; Kramer *et al.*, 1992).

Thermalized neutron count rate and its sensitivity to changes in soil moisture content depend to a large extent on the diameter of the access tube. Neutron reading integrates the moisture of a volume of soil somewhat as a negative exponential function of distance from the neutron source (McGuiness *et al.*, 1961). Consequently, the count rate decreases with increase in access tube diameter (Holmes and Jenkinson 1959). This is reflected by the shape of the calibration curve which becomes more curvilinear with increase in access hole diameter.

Marais and Smit (1960) found calibration curves to be linear using a 5.1 cm access tube. However, with larger 7.6 cm diameter access tube, the calibration curve became nonlinear. Their results indicated that the most important advantage of thinner and smaller diameter access tube was not the increased sensitivity, but the resulting linear calibration curve.

Keller *et al.* (1990) found that an 8 inch (20 cm) diameter PVC tube yielded 62% decrease in neutron density reading. This large decrease is attributed to the back scattering of the PVC itself, air gaps, unexplained deflection effect, or capture of slow neutrons by chloride.

Abeele (1979) found that linear calibration curves could be developed in diameters ranging up to 10.2 cm using aluminum, PVC, and steel casings. Conversely, Tyler (1988) had to resort to a quadratic calibration equation for a 15 cm diameter access tube. The density of thermal neutrons returning to the detector was reduced by approximately 50% over the manufacturer's calibration data. This reduction was attributed to the larger casing cross section available for neutron absorption, and the increased path length associated with the large air gap between the detector and the soil. A decrease in sensitivity at higher water contents was also noted: i.e. the thermal neutron flux rate becomes less dependent upon the soil water content.

Appendix C

DETAILED LABORATORY and FIELD DATA

C.1 DETAILED LABORATORY DATA

C.1.1 Grain Size Distribution

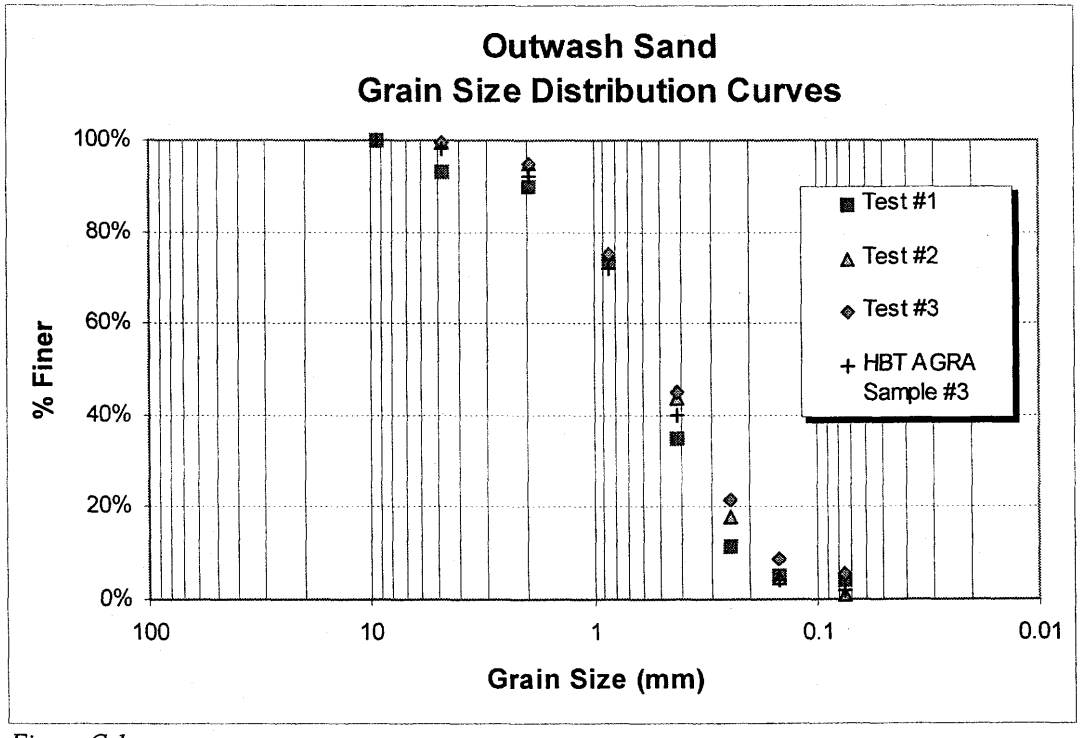

Figure C.1

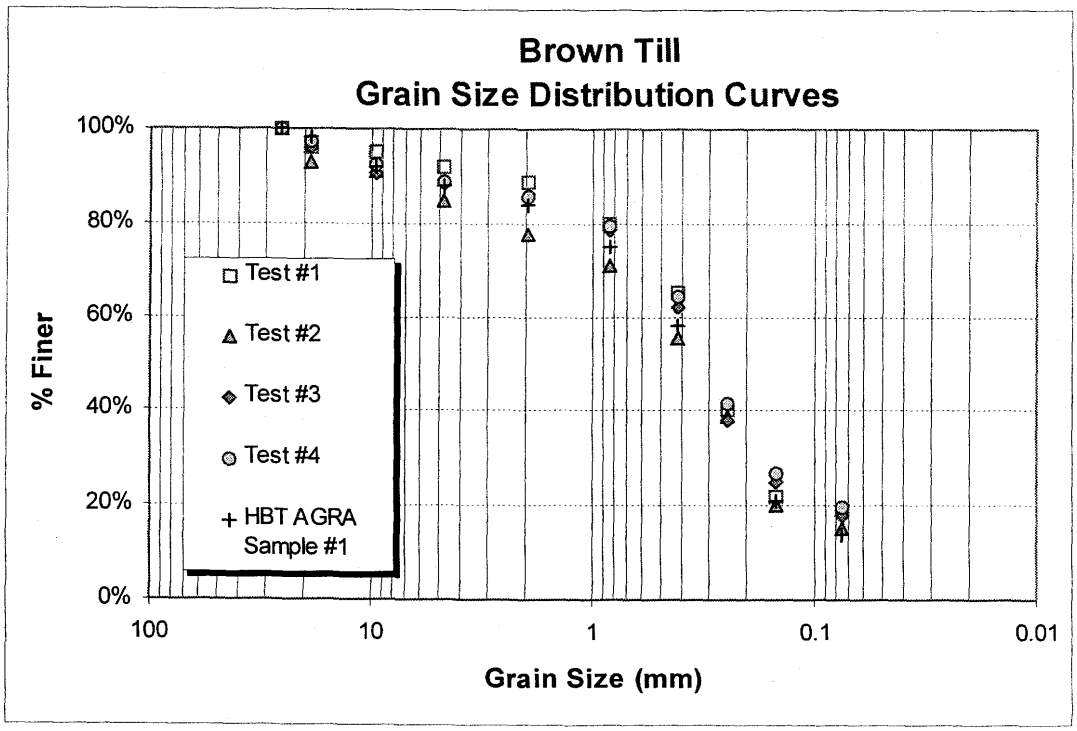

Figure C.2

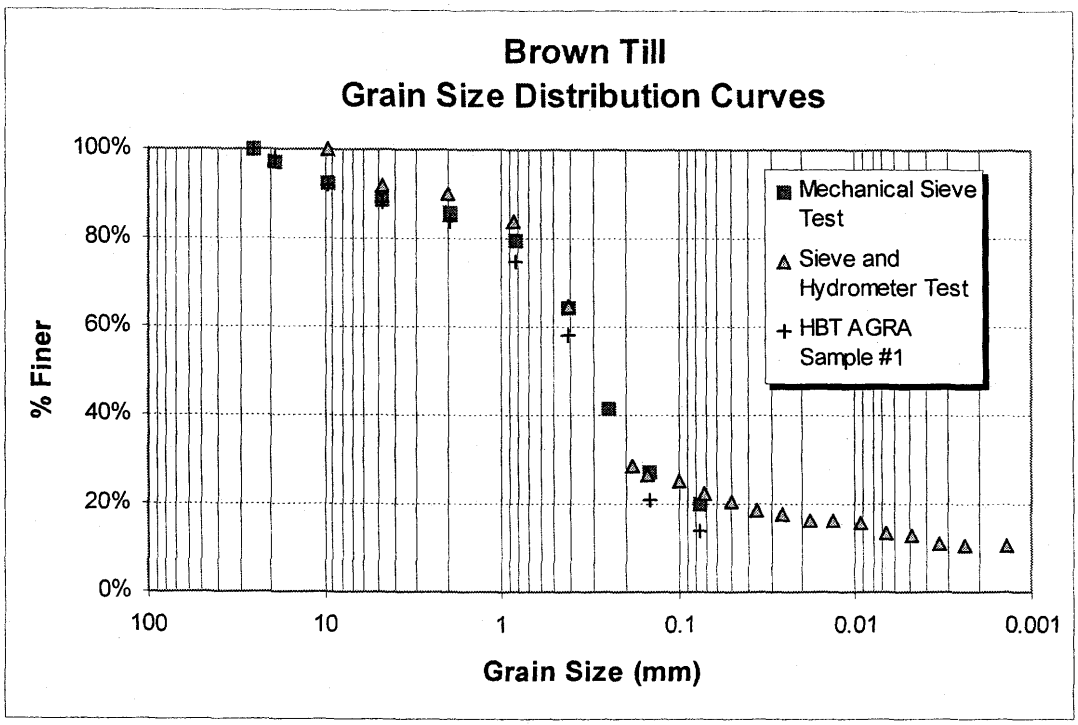

Figure C.3

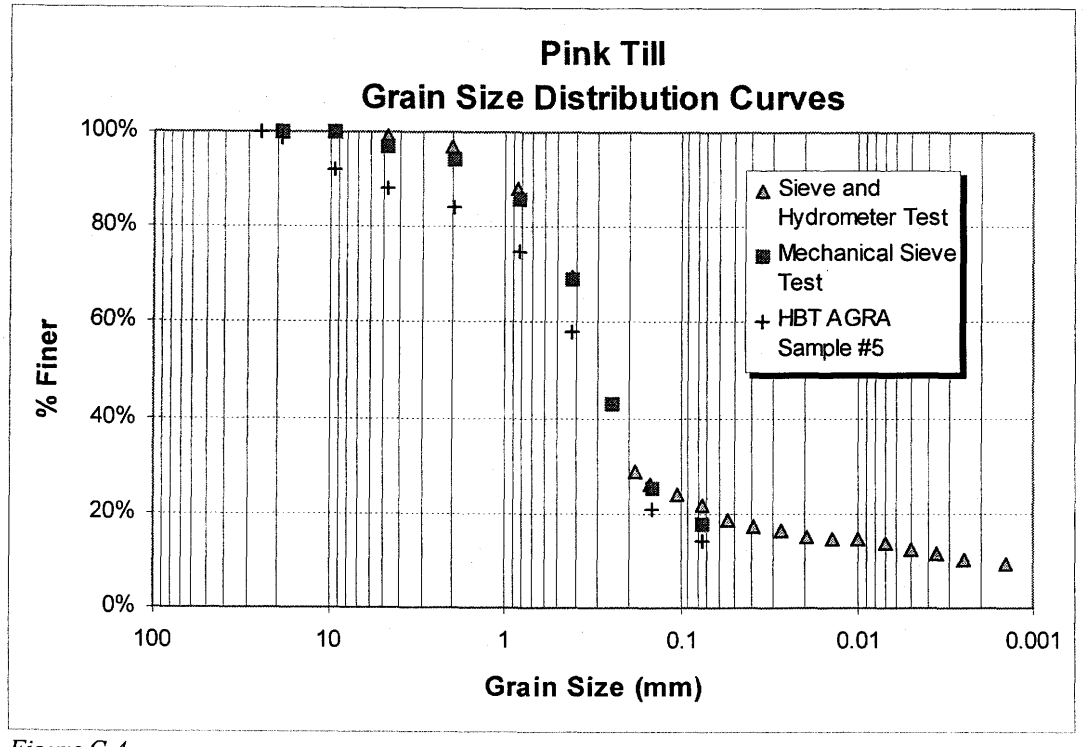

Figure C.4

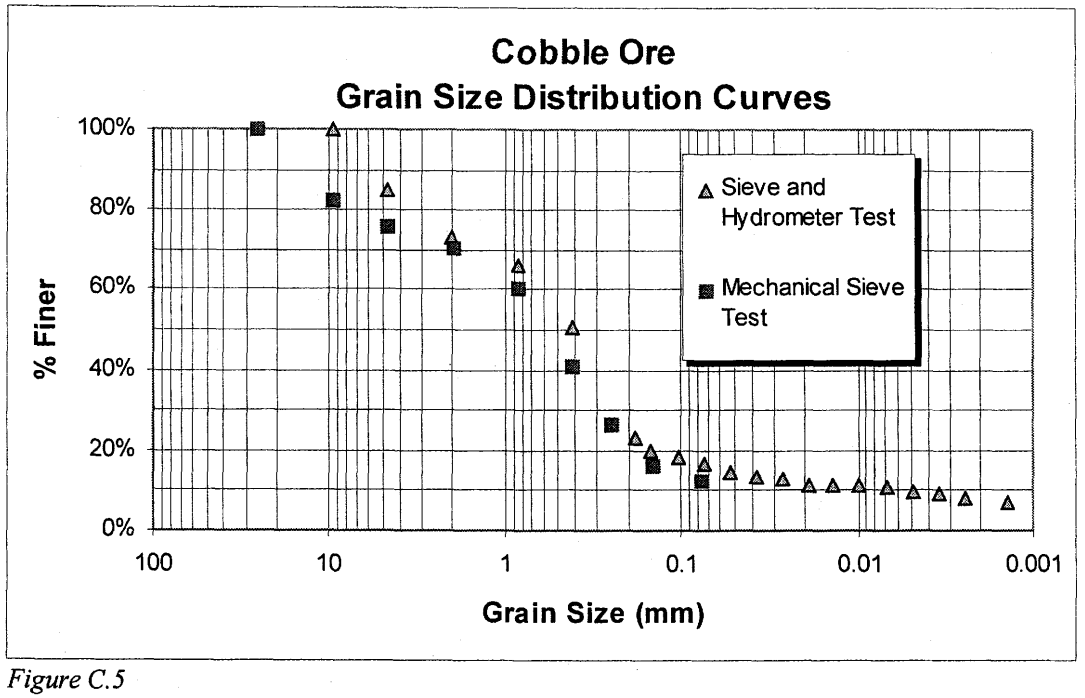

Figure C.5

C.1.2 Hydraulic Conductivity Test Results

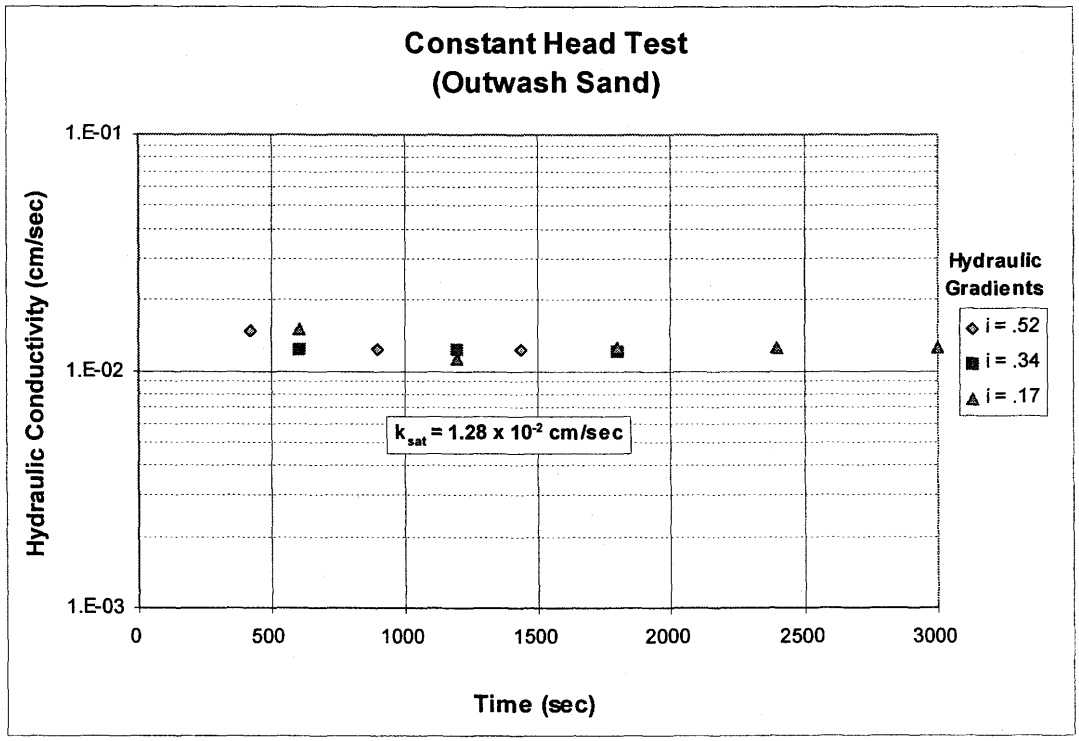

Figure C.6

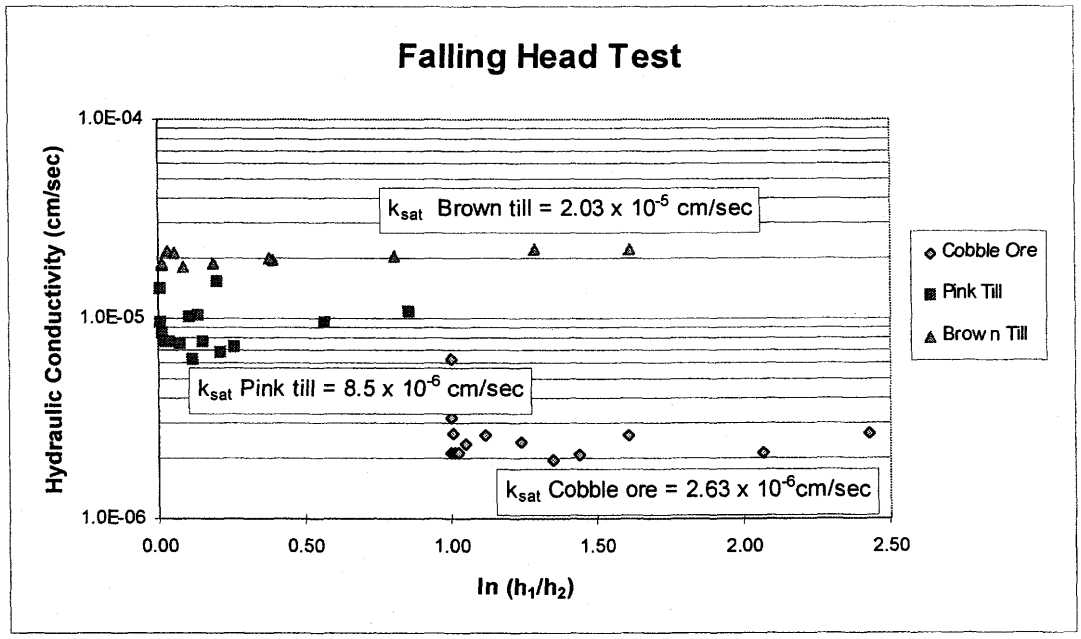

Figure C.7

C.1.3 Soil Water Characteristic Curves

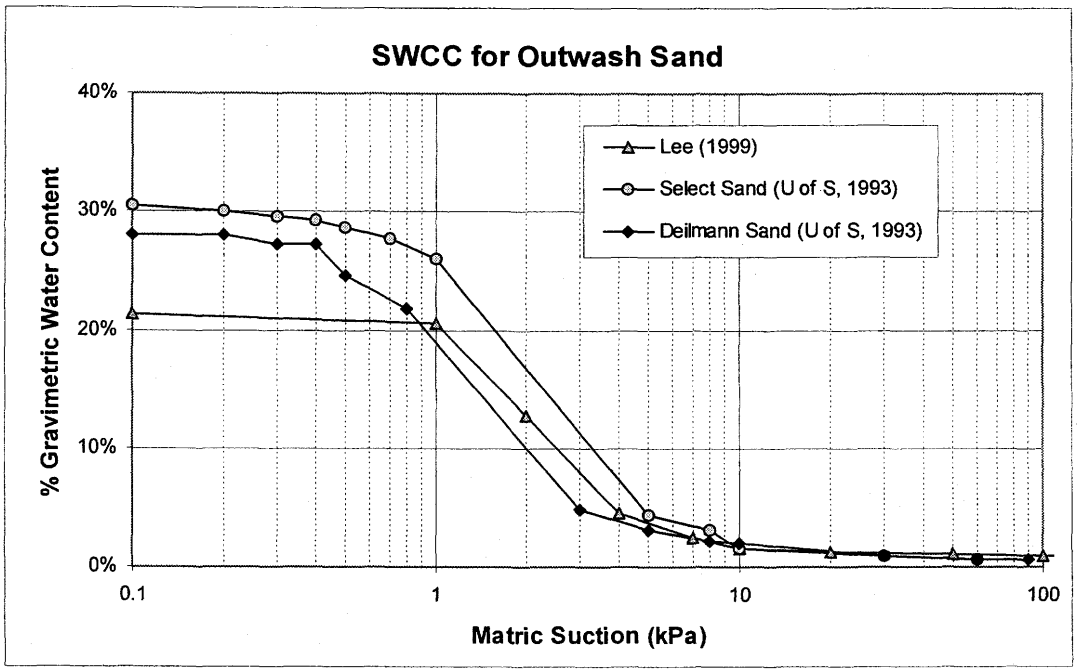

Figure C.8

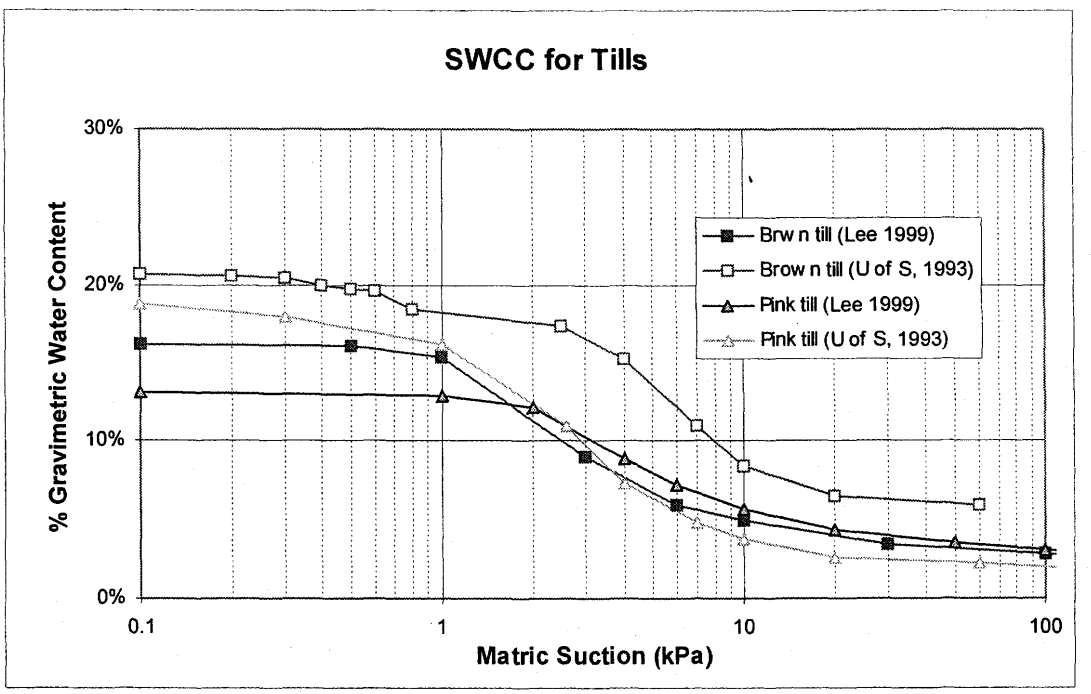

Figure C.9

C.2 DETAILED FIELD DATA

C.2.1 In Situ Density Test

Table C.1 In sity density test results.

Material	*Method*	*Number of samples*	*Dry Density (g/cm^3)*
Brown till	Modified water replacement technique	3	2.12
	Sonic drill sampling	4	1.93
	Maximum dry density (HBT 1992)	2	2.04
Outwash sand	Modified water replacement technique	1	1.79
	Sonic drill sampling	6	1.82
	Maximum dry density (HBT 1992)	2	1.75
Pink till	Modified water replacement technique	1	1.78
	Maximum dry density (HBT 1992)	1	1.90
Cobble Ore	Sonic drill sampling	8	1.90

C.2.2 Sonic Drill Soil Profile Sampling Results

Table C.2 Sonic drill sampling results.

Depth (cm)	*Material*	*Dry Density (g/cm^3)*
0 to 15	Brown till	1.96
15 to 27	Brown till	1.82
27 to 39	Brown till	1.98
39 to 51	Brown till	1.96
51 to 64	Brown till/outwash sand	1.78
64 to 76	Outwash sand	1.67
76 to 88	Outwash sand	1.76
88 to 100	Outwash sand	1.71
100 to 113	Outwash sand	1.78

Depth (cm)	*Material*	*Dry Density (g/cm³)*
113 to 125	Outwash sand	1.85
125 to 137	Outwash sand	2.13
137 to 149	Sand (greenish)	1.61
149 to 161	Sand (greenish)	1.74
161 to 174	Sand (greenish)	1.73
174 to 186	Sand (greenish)	1.69
186 to 198	Till	2.04
198 to 210	Till	1.92
210 to 222	Till	1.75
222 to 235	Till	1.81
235 to 247	Till	1.74
247 to 259	Till	1.83
259 to 269	Cobble ore	1.87
269 to 282	Cobble ore	2.14
282 to 295	Cobble ore	1.70
295 to 308	Cobble ore	2.12
308 to 334	Cobble ore	2.14
334 to 360	Cobble ore	1.88
360 to 386	Cobble ore	1.83
386 to 412	Cobble ore	1.87
412 to 437	Cobble ore	1.66
437 to 457	Cobble ore	1.72

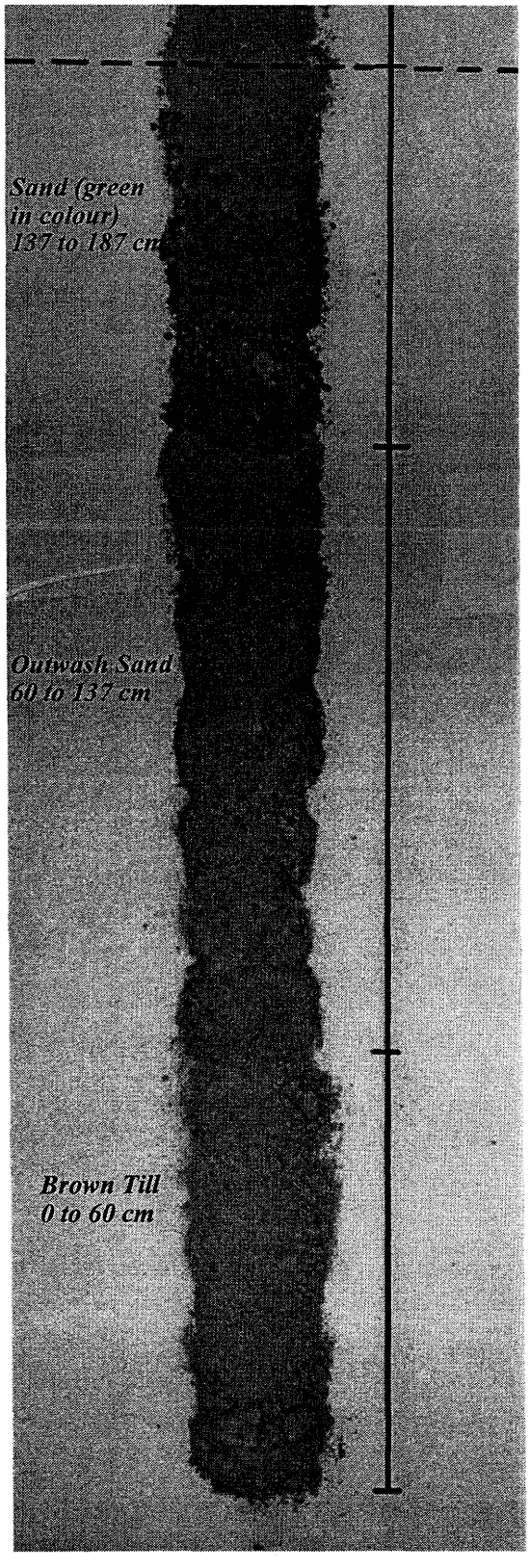

Figure C.10 *Photograph of sonic drill soil profile sampling.*

C.3 THERMISTOR RESULTS

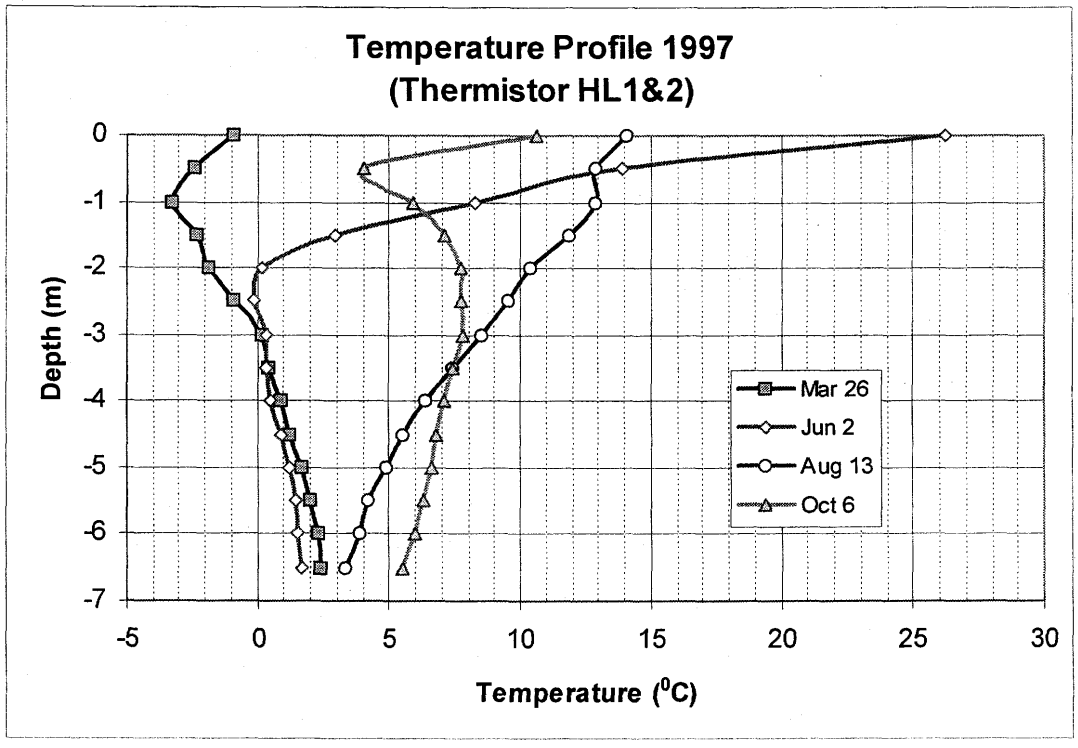

Figure C.11

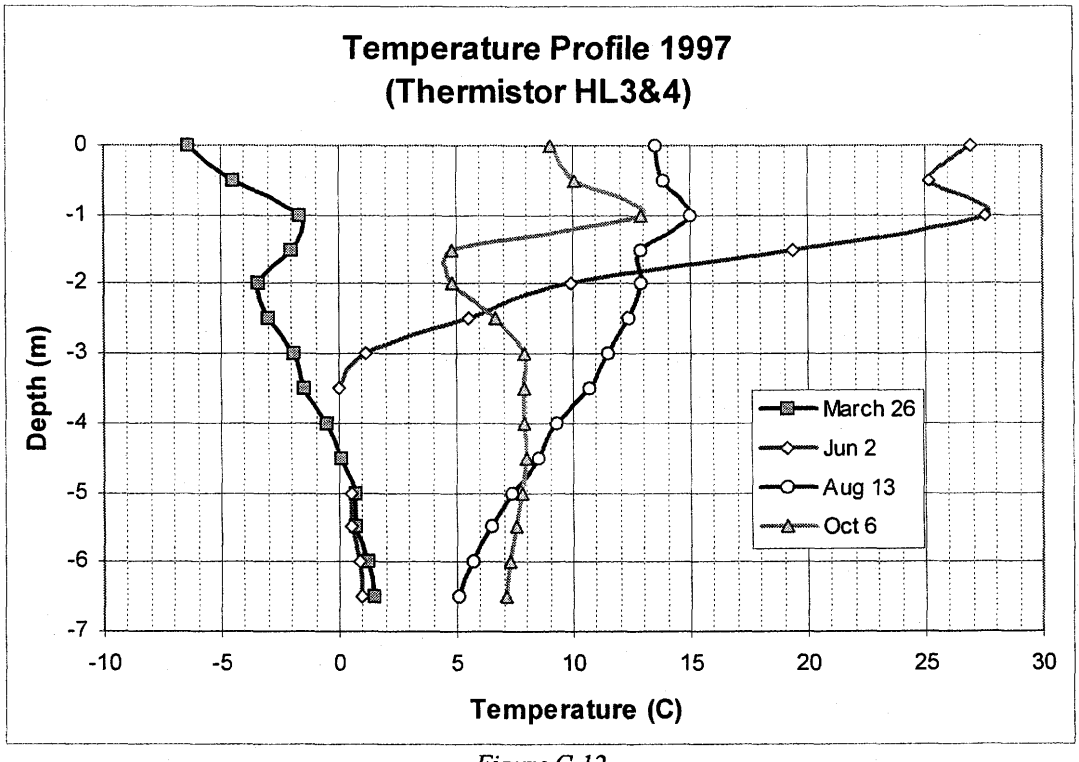

Figure C.12

Appendix D

DETAILED WEATHER DATA

Table D.1 1996 and 1997 monthly weather statistics for Key Lake weather station.

Month	Mean Max Air Temp (^{0}C)	Mean Min Air Temp (^{0}C)	Mean Average Air Temp (^{0}C)	Mean Daily Wind Speed (km/hr)	Monthly Total Rainfall (mm)	Monthly Total Snowfall (mm)
Jan-96	-23.4	-32.6	-28.0	11.1		13.4
Feb-96	-11.7	-22.0	-16.8	10.8		25.1
Mar-96	-9.7	-25.6	-17.8	11.4		41.3
Apr-96	3.0	-13.3	-5.2	11.1	0.4	2.4
May-96	11.6	-2.0	4.6	10.8	8.1	
Jun-96	20.8	7.2	14.0	11.4	72.0	
Jul-96	22.7	10.7	16.7	11.5	88.9	
Aug-96	21.3	10.9	16.1	12.1	41.1	
Sep-96	12.8	3.9	6.4	13.9	59.7	8.0
Oct-96	2.4	-3.5	-0.6	11.8	10.9	15.7
Nov-96	-10.3	-19.9	-15.1	7.7		24.2
Dec-96	-19.0	-28.3	-23.6	8.1		21.0
Jan-97	-18.5	-29.1	-23.8	11.2		32.7
Feb-97	-8.8	-23.2	-16.0	10.1		11.2
Mar-97	-7.2	-22.1	-14.6	9.9		15.2
Apr-97	3.8	-11.5	-3.9	9.2		12.9
May-97	11.1	-1.8	4.6	10.6	27.8	0.1
Jun-97	19.5	7.5	13.5	11.5	70.5	
Jul-97	24.2	11.9	18.1	9.1	154.0	
Aug-97	20.0	10.2	15.1	9.2	101.3	
Sep-97	14.4	4.9	9.6	10.1	142.7	
Oct-97	1.1	-4.0	-1.5	12.1	9.1	21.3
Nov-97	-4.9	-11.4	-8.2	9.4		23.7
Dec-97	-6.3	-18.4	-12.3	8.4		13.7

Table D.2 1996 and 1997 weather statistics for the HLTF.

Month	Mean Max Air Temp (^{0}C)	Mean Min Air Temp (^{0}C)	Mean Average Air Temp (^{0}C)	Mean Net Radiation (MJ/m^2/day)	Mean Max Relative Humidity	Mean Min Relative Humidity	Mean Average Relative Humidity	Mean Daily Wind Speed (km/hr)	Total Rainfall (mm)	Monthly Total Snowfall (mm)
Jan-96	-22.8	-31.4	-27.2	-0.1	78.5%	67.6%	73.2%	8.7		13.4
Feb-96	-11.6	-22.2	-16.5	-0.3	86.3%	55.8%	72.8%	9.0		25.1
Mar-96	-10.5	-22.9	-16.2	-0.6	84.7%	40.3%	64.8%	9.9		41.3
Apr-96	2.7	-8.6	-2.5	3.8	82.1%	33.4%	55.5%	9.4		2.4
May-96	9.0	-0.7	4.4	10.1	82.5%	29.6%	53.7%	8.8		
Jun-96	20.1	9.5	14.5	9.2	88.4%	34.4%	60.7%	10.1	70.0	
Jul-96	21.9	12.0	16.8	9.3	93.1%	35.0%	63.1%	10.1	75.9	
Aug-96	20.1	10.5	15.1	7.6	97.6%	48.5%	76.6%	10.2	86.5	
Sep-96	12.1	4.7	8.3	3.6	91.3%	54.3%	75.1%	12.4	69.1	8.0
Oct-96	2.3	-3.0	-0.5	1.4	96.7%	66.6%	84.8%	10.2	19.3	15.7
Nov-96	-10.4	-17.7	-13.7	-0.5	92.1%	74.9%	85.6%	7.1		24.2
Dec-96	-18.7	-25.5	-21.8	-0.1	86.5%	76.7%	81.8%	8.3		21.0
Jan-97	-19.5	-28.0	-23.7	-0.6	70.1%	59.1%	65.4%	10.6		32.7
Feb-97	-8.7	-19.7	-14.3	-1.4	76.6%	53.9%	67.6%	8.8		11.2
Mar-97	-6.3	-18.1	-12.1	-1.4	75.8%	43.4%	61.1%	8.9		15.2
Apr-97	3.7	-8.5	-2.2	3.3	80.7%	38.4%	83.9%	9.2		12.9
May-97	10.0	-0.3	4.9	9.1	95.8%	36.1%	61.4%	10.6	27.8	0.1
Jun-97	18.7	9.2	14.0	9.1	94.0%	37.8%	64.0%	11.5	64.0	
Jul-97	23.4	12.6	17.9	9.6	94.6%	38.0%	65.5%	9.1	113.9	
Aug-97	19.5	10.9	15.0	7.5	92.9%	49.8%	73.0%	9.2	102.5	
Sep-97	14.0	5.8	9.6	3.5	93.0%	61.6%	80.5%	10.1	112.8	
Oct-97	1.1	-4.1	-1.4	0.2	93.7%	75.8%	86.9%	12.1	14.5	21.3
Nov-97	-5.2	-10.0	-7.6	-0.7	92.2%	78.9%	87.1%	9.4		23.7
Dec-97	-7.1	-15.7	-11.0	-0.6	89.6%	75.8%	83.0%	8.4		13.7

JANUARY 1997 DAILY WEATHER DATA

Date	Julian Day	Max Air Temp (^{0}C)	Min Air Temp (^{0}C)	Mean Air Temp (^{0}C)	Daily Net Radiation MJ/m^2/day	Max RH	Min RH	Mean RH	Mean Wind Speed (km/hr)	Precip (mm)	Runoff (litres)	Water pumped (m^3)
1	1	-22.2	-27.2	-23.8	-0.1	69.9%	65.4%	68.6%	17.9			
2	2	-20.8	-28.5	-23.0	-0.5	71.1%	64.3%	69.3%	10.6			
3	3	-19.8	-28.8	-24.1	0.2	71.1%	64.0%	67.9%	8.9			
4	4	-18.4	-23.2	-20.0	-0.7	73.3%	69.8%	71.9%	5.8			
5	5	-20.4	-30.6	-26.0	-0.4	72.3%	62.4%	66.7%	3.6			
6	6	-16.5	-25.8	-20.5	-0.2	74.8%	67.4%	71.8%	13.3			
7	7	-16.2	-17.4	-17.0	0.3	75.2%	73.7%	74.2%	11.5			
8	8	-16.0	-31.1	-21.8	-0.2	75.2%	62.7%	70.7%	11.5			
9	9	-31.1	-35.3	-33.7	-1.4	62.8%	57.4%	59.3%	13.6			
10	10	-31.3	-37.8	-35.3	-0.5	60.2%	54.7%	57.2%	9.4			
11	11	-24.4	-37.9	-31.5	0.0	67.2%	54.7%	60.7%	5.9			
12	12	-12.3	-27.5	-18.4	-1.1	70.9%	55.4%	65.5%	12.7			
13	13	-10.3	-19.3	-13.9	-0.9	76.5%	54.0%	68.2%	3.2			
14	14	-13.0	-22.0	-17.6	-0.5	75.6%	65.5%	72.0%	8.0			
15	15	-22.0	-30.7	-27.3	-3.4	65.8%	55.3%	60.8%	14.2			
16	16	-23.3	-31.7	-28.3	-3.0	70.7%	46.3%	60.8%	9.2			
17	17	-15.1	-33.2	-23.9	-0.2	71.8%	59.7%	66.4%	7.1			
18	18	-1.4	-15.3	-8.2	-0.8	78.0%	66.1%	73.0%	18.6			
19	19	-4.4	-17.6	-14.5	-1.9	73.7%	63.5%	69.4%	14.6			
20	20	-16.1	-18.4	-17.6	-0.4	72.3%	60.4%	68.8%	5.4			
21	21	-18.3	-27.5	-23.7	-0.4	71.1%	41.1%	57.1%	10.5			
22	22	-22.6	-28.9	-25.3	-0.5	66.8%	52.9%	60.1%	13.4			
23	23	-22.5	-31.2	-26.0	-1.0	69.2%	60.9%	65.3%	9.6			
24	24	-29.3	-36.0	-32.3	0.1	63.5%	56.1%	60.0%	14.4			
25	25	-23.2	-32.7	-28.5	0.4	63.6%	50.8%	59.9%	10.8			
26	26	-23.4	-29.6	-27.0	-0.6	64.7%	45.9%	56.7%	10.5			
27	27	-28.0	-33.6	-30.8	-1.0	65.5%	54.9%	60.6%	12.8			
28	28	-24.3	-37.1	-30.9	0.0	64.4%	51.4%	59.2%	4.8			
29	29	-19.5	-26.2	-21.8	0.3	71.7%	60.3%	67.0%	10.2			
30	30	-21.3	-24.0	-22.5	0.4	71.4%	68.1%	69.8%	16.5			
31	31	-18.0	-21.9	-19.7	0.4	74.0%	66.2%	69.5%	10.0			

FEBRUARY 1997 DAILY WEATHER DATA

Date	Julian Day	Max Air Temp (^{0}C)	Min Air Temp (^{0}C)	Mean Air Temp (^{0}C)	Daily Net Radiation MJ/m^2/day	Max RH	Min RH	Mean RH	Mean Wind Speed (km/hr)	Precip (mm)	Runoff (litres)	Water pumped (m^3)
1	32	-9.7	-18.0	-13.4	0.1	79.5%	73.5%	76.3%	3.8			
2	33	-7.1	-10.1	-8.8	-0.2	81.3%	79.5%	80.3%	6.7			
3	34	-5.7	-11.9	-8.2	-0.8	81.5%	75.7%	80.0%	5.0			
4	35	-0.1	-9.4	-5.9	-1.8	81.9%	48.3%	72.4%	9.4			
5	36	-3.7	-8.6	-5.7	-1.0	81.3%	59.5%	74.0%	11.3			
6	37	-2.4	-8.9	-6.6	-0.7	81.8%	65.0%	78.3%	6.6			
7	38	1.4	-9.8	-5.0	-1.3	81.3%	47.4%	67.8%	10.1			
8	39	0.7	-6.0	-2.5	-3.3	80.9%	53.1%	67.4%	14.5			
9	40	-5.9	-24.7	-18.1	-1.6	77.1%	37.6%	59.2%	8.8			
10	41	-5.8	-24.7	-13.9	-0.7	78.6%	57.3%	71.4%	15.0			
11	42	-17.1	-29.7	-23.2	-2.1	70.0%	43.0%	60.8%	8.2			
12	43	-11.2	-23.5	-18.4	-2.4	75.5%	52.0%	66.5%	9.5			
13	44	-14.0	-23.7	-17.6	-0.9	76.3%	59.4%	70.0%	13.1			
14	45	-17.5	-27.6	-23.0	-0.6	73.0%	53.5%	67.3%	6.7			
15	46	-21.9	-34.6	-27.4	-0.1	68.3%	50.5%	60.4%	3.8			
16	47	-15.9	-23.4	-18.8	0.0	73.4%	59.1%	67.6%	7.5			
17	48	-17.4	-25.5	-20.2	-4.0	73.4%	50.4%	64.2%	9.1			
18	49	-15.3	-25.9	-21.3	-4.5	69.6%	30.1%	54.7%	3.3			
19	50	-10.9	-20.1	-14.5	-0.1	76.5%	69.6%	73.3%	7.1			
20	51	-14.4	-27.3	-20.8	-2.0	73.9%	32.5%	56.1%	7.2			
21	52	-14.0	-25.5	-20.1	-3.3	69.6%	33.0%	54.4%	7.5			
22	53	-15.0	-28.0	-22.1	-1.9	69.0%	48.6%	62.7%	10.6			
23	54	-6.9	-26.7	-16.8	-1.7	73.3%	38.4%	56.5%	8.5			
24	55	4.6	-7.8	-1.4	-0.7	84.4%	59.1%	71.0%	13.5			
25	56	2.5	-19.2	-10.3	-0.7	82.5%	61.0%	72.5%	20.1			
26	57	-9.2	-20.6	-15.0	-0.1	75.1%	57.4%	67.9%	6.6			
27	58	-2.2	-12.3	-8.4	-1.3	77.0%	47.3%	65.4%	3.4			
28	59	-8.3	-19.6	-12.5	-0.3	79.5%	66.6%	73.7%	8.5			

MARCH 1997 DAILY WEATHER DATA

Date	Julian Day	Max Air Temp (^{0}C)	Min Air Temp (^{0}C)	Mean Air Temp (^{0}C)	Daily Net Radiation MJ/m^2/day	Max RH	Min RH	Mean RH	Mean Wind Speed (km/hr)	Precip (mm)	Runoff (litres)	Water pumped (m^3)
1	60	-16.5	-27.3	-22.0	-2.9	71.7%	39.4%	58.9%	7.80			
2	61	-20.7	-30.0	-25.8	-3.4	67.1%	42.3%	57.1%	8.04			
3	62	-19.9	-31.9	-26.0	-3.2	64.1%	46.4%	56.7%	11.06			
4	63	-15.5	-28.6	-22.0	-1.8	68.7%	39.3%	56.1%	9.10			
5	64	-17.2	-25.8	-21.2	-1.9	70.6%	49.2%	61.3%	12.84			
6	65	-11.2	-27.6	-20.0	-1.7	68.9%	31.5%	54.8%	4.29			
7	66	-7.9	-26.7	-15.9	-1.1	70.9%	35.6%	53.3%	10.73			
8	67	-1.2	-10.7	-7.3	0.0	80.3%	40.2%	58.6%	11.29			
9	68	1.1	-11.8	-6.2	-1.0	80.6%	42.7%	69.4%	6.83			
10	69	-7.4	-20.1	-14.2	-1.7	79.1%	40.1%	60.9%	8.80			
11	70	-13.9	-27.4	-20.0	-2.9	68.3%	37.9%	53.7%	7.64			
12	71	-15.5	-26.6	-21.0	-2.5	70.6%	43.9%	59.8%	10.29			
13	72	-17.1	-29.0	-23.2	-1.6	68.6%	46.1%	59.8%	8.86			
14	73	-13.8	-26.6	-20.1	-1.3	70.6%	44.4%	59.9%	6.56			
15	74	-6.9	-25.0	-15.6	-1.8	70.6%	27.9%	51.2%	4.36			
16	75	-5.3	-24.5	-14.7	-1.6	72.9%	26.8%	53.6%	1.94			
17	76	-9.5	-21.9	-15.8	-1.6	74.8%	41.9%	58.5%	9.26			
18	77	-2.5	-19.9	-9.9	-0.1	80.8%	56.1%	67.7%	7.28			
19	78	-1.8	-7.0	-4.5	0.2	82.2%	65.1%	74.6%	11.50			
20	79	-3.6	-6.2	-5.0	-0.1	82.6%	74.5%	79.7%	12.57			
21	80	-0.6	-6.7	-4.4	-0.3	82.8%	55.2%	76.4%	4.15			
22	81	3.7	-6.1	-1.6	-1.8	84.0%	37.7%	65.3%	7.70			
23	82	4.6	-6.7	-0.5	-0.3	83.1%	47.5%	67.4%	6.06			
24	83	3.1	-5.5	-2.4	-1.4	83.2%	33.6%	60.5%	7.00			
25	84	3.0	-3.6	0.0	-0.3	85.1%	55.8%	70.1%	10.61			
26	85	1.7	-11.8	-3.8	-1.0	84.1%	51.4%	69.9%	13.76			
27	86	-8.3	-18.8	-11.8	-1.2	79.6%	48.8%	67.1%	8.54			
28	87	-8.2	-24.1	-14.9	-1.8	73.2%	37.3%	54.1%	9.10			
29	88	0.1	-18.1	-8.8	-1.5	69.1%	40.8%	55.6%	13.53			
30	89	5.2	-5.2	0.1	-1.7	78.5%	31.6%	55.7%	10.39			
31	90	6.2	-0.2	2.7	-0.2	84.2%	35.0%	47.7%	15.13			

APRIL 1997 DAILY WEATHER DATA

Date	Julian Day	Max Air Temp (^{0}C)	Min Air Temp (^{0}C)	Mean Air Temp (^{0}C)	Daily Net Radiation MJ/m^2/day	Max RH	Min RH	Mean RH	Mean Wind Speed (km/hr)	Precip (mm)	Runoff (litres)	Water pumped (m^3)
1	91	-0.1	-7.3	-4.1	-0.2	93.0%	86.7%	90.2%	17.9			
2	92	0.4	-8.2	-3.7	0.0	80.2%	64.1%	89.9%	9.7			
3	93	-0.9	-7.2	-4.0	-0.1	84.5%	71.8%	89.7%	14.9			
4	94	-5.4	-15.3	-10.0	-1.0	79.7%	46.9%	89.4%	7.9			
5	95	-8.1	-18.9	-12.3	-1.7	78.6%	58.1%	89.1%	8.2			
6	96	-13.9	-24.7	-19.0	-1.1	73.8%	51.8%	88.8%	13.3			
7	97	-7.8	-23.3	-16.3	-2.4	70.1%	15.4%	88.5%	5.9			
8	98	-1.5	-21.9	-10.6	-2.8	43.4%	11.7%	88.2%	4.9			
9	99	0.7	-15.6	-6.5	-2.0	50.9%	26.6%	87.9%	9.4			
10	100	3.4	-12.7	-4.0	-2.2	63.5%	26.6%	87.6%	12.1			
11	101	0.4	-8.9	-3.9	-1.1	69.4%	47.9%	87.3%	8.1			
12	102	6.6	-12.4	-1.2	-2.0	81.4%	29.8%	86.9%	5.5			
13	103	7.4	-8.6	-0.2	-0.7	59.1%	21.6%	86.4%	10.1			
14	104	-4.2	-17.6	-10.9	-0.8	70.2%	27.8%	85.7%	6.2			
15	105	7.2	-15.6	-2.4	-1.6	63.6%	30.7%	85.0%	12.7		Snow melt	
16	106	12.3	-1.0	5.4	1.0	64.8%	34.0%	84.3%	11.2		69.0	
17	107	17.5	0.6	7.9	4.5	83.5%	28.9%	83.5%	5.9		2,414.3	
18	108	11.4	2.1	5.1	3.9	86.3%	55.0%	82.8%	6.3		505.0	
19	109	13.4	-1.0	5.6	10.3	83.6%	21.9%	82.0%	5.8		2,773.9	
20	110	6.1	-3.4	2.1	11.4	101.0%	59.2%	81.2%	12.1		431.1	
21	111	7.3	-0.7	2.9	9.9	81.9%	40.4%	80.4%	10.9		Snow melt	
22	112	3.9	-1.9	0.8	4.9	100.8%	57.1%	79.8%	5.3			
23	113	5.9	-1.8	1.6	10.6	100.7%	59.0%	79.2%	10.1			
24	114	4.7	0.1	2.2	7.7	100.8%	53.1%	78.6%	7.2			
25	115	8.1	-1.3	3.1	8.8	98.3%	36.3%	78.1%	5.2			
26	116	11.9	-1.8	5.5	11.7	92.1%	19.4%	77.8%	6.4			
27	117	12.3	-3.5	5.0	6.9	83.1%	28.0%	77.6%	12.6			
28	118	1.0	-7.5	-3.5	10.3	101.0%	26.2%	77.5%	18.7			
29	119	4.3	-9.5	-2.2	7.8	95.6%	17.1%	77.5%	6.4			
30	120	7.9	-7.3	1.3	7.8	86.4%	0.2%	77.6%	5.0			

MAY 1997 DAILY WEATHER DATA

Date	Julian Day	Max Air Temp (^{0}C)	Min Air Temp (^{0}C)	Mean Air Temp (^{0}C)	Daily Net Radiation MJ/m^2/day	Max RH	Min RH	Mean RH	Mean Wind Speed (km/hr)	Key Lake Precip (mm)	Runoff (litres)	Water pumped (m^3)
1	121	8.6	-6.2	2.2	8.6	109.1%	0.2%	38.4%	7.50			
2	122	9.4	-6.3	2.6	8.2	108.3%	0.2%	33.7%	5.39			
3	123	13.0	-2.4	5.7	8.3	50.2%	11.2%	28.3%	5.35			
4	124	9.3	-2.8	3.8	7.7	87.9%	0.2%	38.2%	11.38			
5	125	12.0	-2.4	5.7	10.3	83.8%	22.0%	39.3%	9.52			
6	126	10.2	0.5	5.9	5.3	108.2%	34.3%	59.3%	8.66	2.0		
7	127	7.5	-0.5	3.2	12.6	92.4%	33.8%	61.8%	13.73			
8	128	13.5	-0.9	6.7	8.9	97.1%	13.1%	53.7%	9.35			
9	129	19.0	0.4	9.6	8.6	108.5%	21.6%	58.7%	10.02			
10	130	9.9	0.3	5.2	9.6	108.9%	31.1%	60.8%	12.06			
11	131	8.2	0.5	3.8	8.4	108.8%	29.0%	54.5%	8.33			
12	132	8.0	0.4	3.4	3.6	108.8%	58.5%	79.6%	16.77	9.0		
13	133	1.5	-7.2	-1.1	8.2	108.9%	35.6%	68.5%	17.42			
14	134	4.1	-10.0	-3.1	11.7	98.9%	20.9%	52.1%	9.62			
15	135	13.4	-3.8	2.9	12.5	93.7%	39.4%	65.7%	16.73	4.0		
16	136	2.4	-1.3	0.5	5.4	107.7%	71.8%	83.6%	11.36			
17	137	3.4	-0.8	1.5	4.8	77.7%	50.6%	64.9%	16.83			
18	138	5.3	-0.5	2.1	6.4	79.0%	46.7%	62.5%	8.35			
19	139	6.8	-1.3	2.3	7.5	107.3%	46.7%	68.9%	11.70			
20	140	3.9	-0.7	1.6	6.3	84.4%	52.1%	65.8%	10.28			
21	141	4.0	-0.6	1.3	3.5	93.0%	55.8%	76.7%	10.99			
22	142	4.5	0.4	2.2	6.6	108.7%	80.8%	89.2%	10.92	3.6		
23	143	8.5	1.2	4.0	11.6	92.9%	51.2%	79.4%	7.89			
24	144	11.2	-0.5	5.6	14.3	92.9%	39.3%	71.6%	9.67			
25	145	16.9	5.3	11.2	13.2	85.6%	28.6%	54.8%	6.97	0.6		
26	146	11.6	0.7	5.9	10.9	84.3%	51.6%	67.9%	13.36			
27	147	10.2	1.3	5.5	5.8	105.2%	71.0%	85.9%	11.24	2.6		
28	148	18.2	5.9	11.1	7.8	92.3%	41.2%	70.6%	6.75			
29	149	13.8	7.0	11.2	14.5	86.1%	35.5%	55.8%	9.25			
30	150	19.5	4.7	12.4	13.3	90.7%	20.0%	50.1%	11.11	3.2		
31	151	22.8	10.6	16.3	16.5	107.9%	24.1%	61.6%	9.18	1.0		

JUNE 1997 DAILY WEATHER DATA

Date	Julian Day	Max Air Temp (^{0}C)	Min Air Temp (^{0}C)	Mean Air Temp (^{0}C)	Daily Net Radiation MJ/m^2/day	Max RH	Min RH	Mean RH	Mean Wind Speed (km/hr)	Precip (mm)	Runoff (litres)	Water pumped (m^3)
1	152	25.3	11.9	17.2	8.0	74.6%	29.0%	58.3%	16.1	3.6		
2	153	21.3	11.9	16.3	13.7	91.7%	35.3%	64.0%	13.3			
3	154	23.9	12.4	17.2	8.2	81.8%	26.0%	54.4%	6.4			
4	155	22.5	10.0	16.6	10.4	85.1%	31.8%	54.0%	12.6			
5	156	17.1	8.5	12.6	5.6	74.9%	39.0%	58.7%	16.7			
6	157	24.2	12.3	16.8	8.9	99.4%	34.9%	67.3%	13.9	3.0		
7	158	15.3	9.9	12.9	3.0	93.1%	75.9%	88.3%	11.9	21.5	534.6	
8	159	19.6	7.5	15.0	11.8	92.9%	43.8%	68.5%	9.0			
9	160	21.4	11.1	14.4	9.2	108.0%	22.8%	68.6%	8.5	0.3		
10	161	23.3	9.5	17.2	8.5	89.6%	23.5%	45.9%	9.8			
11	162	20.1	10.3	15.1	11.4	107.7%	34.7%	52.1%	10.8			
12	163	19.9	7.7	14.7	9.6	108.1%	35.3%	57.4%	6.5			
13	164	22.7	9.8	17.4	9.9	83.9%	25.3%	43.1%	7.8			
14	165	15.9	10.7	12.1	1.9	107.9%	47.5%	91.0%	11.9	12.3	481.9	
15	166	18.0	10.3	13.2	11.6	93.7%	41.0%	74.2%	9.5	3.4	224.1	
16	167	19.8	9.0	13.9	11.0	98.6%	36.0%	68.9%	10.5	5.2	77.5	
17	168	14.2	9.0	11.5	7.4	108.1%	70.6%	80.2%	18.6	1.4		6.8
18	169	18.5	11.6	14.5	9.9	84.9%	56.6%	71.4%	19.0	0.7		6.7
19	170	12.6	10.0	11.0	4.2	93.3%	73.7%	91.0%	20.5	5.5	72.4	
20	171	14.3	9.4	11.3	5.8	93.5%	65.0%	85.0%	16.0	0.1		30.4
21	172	19.1	9.0	14.3	13.9	89.9%	24.5%	50.0%	9.7			
22	173	22.0	6.9	15.8	11.7	83.2%	24.0%	49.8%	4.7			
23	174	19.6	9.0	14.7	6.2	90.2%	38.0%	64.9%	8.3			
24	175	17.3	10.2	13.8	11.4	91.5%	29.1%	60.4%	10.4			13.6
25	176	18.8	6.8	13.9	10.1	100.5%	20.7%	47.9%	13.5			19.8
26	177	18.8	9.4	14.1	9.9	107.9%	0.2%	58.3%	12.1	0.6		
27	178	13.0	8.6	10.4	10.3	108.0%	46.3%	71.3%	8.7	5.1	190.3	
28	179	13.1	5.8	9.4	11.6	87.1%	38.0%	63.2%	10.3	1.3	9.0	
29	180	14.2	4.4	9.8	8.4	101.1%	36.6%	59.7%	11.4			
30	181	16.2	4.6	11.9	9.3	89.7%	29.7%	51.7%	5.0			

JULY 1997 DAILY WEATHER DATA

Date	Julian Day	Max Air Temp (^{0}C)	Min Air Temp (^{0}C)	Mean Air Temp (^{0}C)	Daily Net Radiation MJ/m^2/day	Max RH	Min RH	Mean RH	Mean Wind Speed (km/hr)	Precip (mm)	Runoff (litres)	Water pumped (m^3)
1	182	19.0	7.9	13.5	9.2	107.6%	32.2%	55.5%	6.0	1.6		19.0
2	183	22.1	9.3	15.0	6.4	107.8%	35.6%	61.3%	6.9	0.2		
3	184	21.8	10.5	16.5	7.6	107.3%	0.2%	61.0%	10.5			
4	185	16.1	8.7	12.8	9.2	100.7%	35.4%	63.5%	12.4	0.3		
5	186	20.4	4.2	12.9	10.5	108.3%	21.7%	47.2%	5.8			
6	187	25.0	9.6	16.1	5.9	85.9%	36.9%	62.4%	7.0	4.1	280	
7	188	26.3	14.3	18.8	9.8	93.1%	39.6%	69.1%	10.0	4.2	411	
8	189	23.4	10.9	18.3	10.9	96.4%	31.3%	57.1%	6.6	0.1		
9	190	26.7	14.7	20.3	12.3	91.2%	39.3%	63.3%	9.8	6.5	813	
10	191	28.0	14.8	21.1	17.3	93.7%	39.8%	69.0%	4.7	12.6	5962	
11	192	24.5	16.1	20.3	5.6	90.8%	53.6%	76.6%	8.9	0.8		
12	193	27.0	15.4	21.1	14.9	94.0%	19.2%	56.3%	9.2			
13	194	22.1	13.2	16.7	9.5	107.6%	40.8%	69.7%	8.3	8.3	1492	
14	195	22.9	12.6	17.3	11.1	103.9%	50.0%	76.5%	10.6	0.6		6.8
15	196	23.4	14.1	18.1	9.4	85.7%	46.1%	71.1%	16.2	0.1		14.1
16	197	21.5	12.7	17.0	8.0	90.9%	48.1%	73.3%	9.7	0.1		
17	198	24.8	13.1	18.5	10.0	86.7%	38.8%	65.2%	7.9			
18	199	21.2	14.4	17.2	5.9	92.3%	60.2%	81.3%	16.2	20.0	7209	19.5
19	200	18.2	13.7	15.7	9.5	92.3%	66.9%	84.8%	10.1	2.3	15	
20	201	26.0	12.7	20.2	13.9	91.8%	35.4%	62.2%	5.4			
21	202	28.5	15.9	22.5	8.8	87.1%	33.2%	59.0%	9.5			
22	203	27.5	16.9	22.6	12.0	77.8%	35.8%	57.4%	12.7	1.5		
23	204	22.5	14.5	18.9	12.2	91.4%	43.8%	72.0%	11.9	4.0	77	
24	205	21.4	11.7	16.4	8.9	90.4%	35.1%	67.2%	10.9	0.1		
25	206	22.5	11.6	16.0	8.2	92.1%	35.3%	68.9%	5.6	0.4		11.7
26	207	18.5	11.2	14.6	8.1	107.9%	49.2%	76.5%	8.2			17.1
27	208	20.1	12.3	15.9	10.2	107.8%	35.7%	64.3%	9.7	0.5		
28	209	24.5	10.8	18.1	7.4	85.4%	28.2%	50.2%	5.8			
29	210	28.0	12.7	21.3	9.9	83.0%	31.9%	51.5%	10.0			
30	211	30.5	16.1	22.5	11.6	89.9%	25.2%	59.5%	7.9	10.9	4851	
31	212	22.4	15.6	19.1	3.8	93.1%	53.8%	76.5%	6.8	34.7	23489	

AUGUST 1997 DAILY WEATHER DATA

Date	Julian Day	Max Air Temp (^{0}C)	Min Air Temp (^{0}C)	Mean Air Temp (^{0}C)	Daily Net Radiation MJ/m^2/day	Max RH	Min RH	Mean RH	Mean Wind Speed (km/hr)	Precip (mm)	Runoff (litres)	Water pumped (m^3)
1	213	15.7	10.1	13.3	5.1	93.4%	72.8%	86.2%	10.2	16.0	4,826	
2	214	21.2	11.3	16.4	14.6	93.4%	38.5%	69.1%	10.9			
3	215	21.9	9.7	16.9	10.7	93.0%	39.4%	63.7%	5.6			
4	216	25.8	11.4	19.4	9.7	89.4%	27.8%	55.5%	6.7			
5	217	27.7	13.0	21.3	11.5	87.9%	26.8%	51.4%	6.6			
6	218	30.1	15.9	23.3	10.7	76.2%	28.0%	52.2%	10.0			
7	219	33.8	17.5	24.9	7.9	83.1%	21.2%	54.4%	9.5	0.1		
8	220	18.9	7.9	11.8	2.1	106.8%	62.8%	82.8%	16.3	1.2		
9	221	16.2	6.9	11.2	8.9	85.2%	41.2%	64.7%	10.3	0.8		
10	222	16.1	8.3	12.0	12.1	95.8%	43.9%	73.2%	10.4	32.9	10,314	6.1
11	223	14.4	6.3	10.4	10.9	108.3%	41.6%	69.5%	14.9	6.0	1,915	
12	224	18.7	6.2	13.0	8.9	89.3%	26.5%	58.5%	5.7			
13	225	14.7	10.4	12.1	2.4	89.7%	60.5%	76.6%	13.6	4.2	156	
14	226	15.1	10.4	12.6	1.8	92.6%	76.3%	86.1%	13.9	2.3	17	
15	227	18.9	10.7	14.7	10.3	85.0%	41.5%	64.4%	10.1			
16	228	17.1	8.8	12.9	5.6	91.6%	52.3%	76.0%	6.0			
17	229	17.7	10.5	13.4	8.0	95.2%	58.2%	83.1%	6.3	2.6		
18	230	19.0	10.5	13.8	7.8	92.5%	46.6%	78.5%	6.7	0.8		
19	231	19.6	10.1	14.7	9.0	92.8%	51.7%	76.8%	3.5	2.7	186	
20	232	21.9	12.0	15.9	10.7	101.8%	44.2%	72.3%	5.1	2.2	73	
21	233	23.0	10.5	16.6	8.2	107.3%	39.9%	63.6%	5.5			
22	234	16.1	14.1	15.0	2.2	94.0%	72.1%	83.2%	8.0	3.7	7	
23	235	23.5	14.7	18.3	11.6	94.0%	39.8%	69.7%	8.7			
24	236	16.9	14.1	15.1	2.5	95.0%	71.6%	87.9%	11.2	13.1	364	
25	237	15.6	13.2	14.1	3.6	93.5%	80.2%	89.5%	9.5	3.9	60	
26	238	19.8	11.8	15.0	8.4	93.6%	52.3%	76.8%	5.3			
27	239	20.8	11.8	16.0	6.6	89.9%	54.3%	73.6%	13.9			
28	240	20.4	14.0	16.4	3.7	92.6%	69.9%	85.1%	6.8	0.2		
29	241	21.5	12.3	16.2	5.5	94.4%	37.8%	76.4%	7.1	1.4		
30	242	14.5	7.8	11.8	5.5	91.4%	61.9%	81.7%	13.9	6.5	365	
31	243	9.3	5.2	7.0	6.0	91.1%	63.1%	79.9%	14.0	1.9	30	

SEPTEMBER 1997 DAILY WEATHER DATA

Date	Julian Day	Max Air Temp (^{0}C)	Min Air Temp (^{0}C)	Mean Air Temp (^{0}C)	Daily Net Radiation MJ/m^2/day	Max RH	Min RH	Mean RH	Mean Wind Speed (km/hr)	Precip (mm)	Runoff (litres)	Water pumped (m^3)
1	244	16.7	3.3	9.9	7.5	94.4%	39.5%	67.7%	5.3			
2	245	19.5	8.0	14.1	5.4	87.9%	37.6%	60.5%	13.4			
3	246	22.7	12.0	15.9	3.6	94.3%	60.2%	79.1%	6.8	3.9	175	
4	247	19.9	11.0	15.6	3.3	95.3%	55.2%	79.9%	6.3	0.2		12.9
5	248	13.8	9.9	11.1	1.2	95.9%	83.4%	87.3%	11.0	0.2		
6	249	12.3	10.0	11.2	2.0	96.6%	88.8%	94.9%	14.1	14.0	1372	
7	250	14.1	7.4	10.3	6.6	96.5%	65.9%	89.2%	6.8	4.0	234	
8	251	14.5	8.2	10.2	5.1	95.6%	55.8%	81.6%	8.2	0.3		
9	252	20.6	8.5	13.6	7.8	93.6%	41.5%	75.5%	6.9	0.8		
10	253	18.6	10.0	13.9	7.3	95.9%	48.8%	79.9%	6.8	2.0	86	
11	254	13.5	8.3	11.1	2.7	94.5%	65.7%	84.4%	9.1	0.2		
12	255	12.3	10.0	11.0	1.6	96.8%	89.7%	94.1%	19.0	1.1		
13	256	12.2	1.0	6.8	1.7	96.8%	90.5%	94.9%	14.4	20.3	1111	
14	257	5.6	0.6	2.6	5.4	94.1%	67.4%	84.6%	11.3	0.6		
15	258	5.1	2.9	3.8	1.1	95.0%	82.8%	89.6%	21.0	5.1	79	
16	259	3.8	0.0	1.8	0.1	97.1%	92.2%	95.6%	12.3	24.3	17422	
17	260	4.2	0.0	1.5	3.5	97.2%	78.7%	91.3%	12.7	11.1	2170	
18	261	5.2	-0.1	2.1	6.4	96.9%	66.2%	88.0%	7.3	0.5		
19	262	8.9	-1.0	3.6	5.8	97.0%	48.8%	79.5%	5.0	0.1		
20	263	18.0	3.4	10.7	5.9	91.3%	44.4%	69.7%	8.8			
21	264	12.1	5.2	9.3	1.5	90.8%	55.5%	76.2%	12.1			
22	265	12.5	3.1	8.3	4.5	96.0%	46.1%	72.2%	7.4			26.3
23	266	21.9	7.4	13.5	3.0	80.0%	36.5%	62.9%	11.5			151.3
24	267	20.3	10.0	14.9	1.9	75.1%	35.4%	57.3%	13.5			
25	268	22.3	7.2	14.4	1.2	78.9%	35.4%	60.7%	6.8			
26	269	24.0	9.1	15.4	1.6	83.6%	39.6%	65.9%	5.3			
27	270	14.8	7.9	12.0	-0.1	91.9%	57.1%	77.0%	7.3		332	
28	271	10.6	5.0	7.2	0.2	96.3%	80.8%	94.2%	8.8	9.0		
29	272	6.5	3.6	4.8	2.0	97.0%	93.8%	95.7%	13.9	14.7	600	
30	273	12.5	3.6	7.9	4.3	96.6%	65.5%	85.7%	9.2	0.4		

OCTOBER 1997 DAILY WEATHER DATA

Date	Julian Day	Max Air Temp (^{0}C)	Min Air Temp (^{0}C)	Mean Air Temp (^{0}C)	Daily Net Radiation MJ/m^2/day	Max RH	Min RH	Mean RH	Mean Wind Speed (km/hr)	Precip (mm)	Runoff (litres)	Water pumped (m^3)
1	274	9.5	7.0	8.2	1.5	96.4%	88.8%	94.1%	10.1	4.4	6.4	
2	275	9.5	6.0	7.7	1.6	96.0%	82.0%	89.8%	21.3	1.8	5.2	
3	276	11.4	1.2	7.1	2.6	94.1%	50.5%	83.5%	16.1	0.3		
4	277	4.9	-1.2	1.9	0.3	95.3%	52.1%	74.3%	15.3	0.1		97.5
5	278	4.4	-2.1	1.1	0.0	85.2%	42.9%	69.3%	16.3			80.8
6	279	8.7	-0.2	3.6	-0.3	90.9%	47.4%	75.1%	7.3			55.5
7	280	2.1	-2.0	0.0	0.5	96.5%	71.8%	86.7%	13.3			44.3
8	281	-0.9	-3.8	-2.4	-0.3	96.8%	82.7%	92.3%	17.6			18.5
9	282	-3.3	-5.7	-4.6	-0.3	89.5%	75.3%	84.0%	9.8	0.4		27.6
10	283	-0.7	-5.1	-2.7	-0.1	94.5%	88.6%	91.6%	17.2			94.1
11	284	1.3	-0.9	0.3	0.4	97.4%	94.0%	96.6%	9.9	1.6		
12	285	0.7	-1.8	-0.5	0.0	97.5%	95.8%	97.0%	11.8	0.2		
13	286	-1.5	-4.4	-2.8	0.7	96.9%	79.1%	90.9%	21.0	0.1	turned off	
14	287	-1.6	-5.8	-4.3	0.3	86.5%	67.9%	78.4%	21.3			9.1
15	288	3.1	-9.4	-2.6	-0.1	92.0%	54.6%	81.3%	9.4	2.2		
16	289	7.9	2.5	4.5	1.8	97.4%	86.5%	92.9%	7.1	3.4		
17	290	4.4	-1.8	0.9	2.1	97.6%	84.1%	93.0%	8.1	tuned off		
18	291	0.1	-2.1	-1.1	1.4	94.8%	84.6%	90.0%	7.8			
19	292	0.4	-5.0	-1.6	-0.5	96.3%	79.6%	91.3%	12.4			
20	293	-5.0	-8.9	-7.8	-0.7	88.4%	78.2%	85.7%	9.5			20.2
21	294	-1.9	-6.7	-3.6	0.3	94.1%	81.9%	88.0%	12.6			
22	295	-1.5	-3.3	-2.2	-0.2	95.4%	87.8%	92.2%	11.4			
23	296	-3.2	-6.7	-4.2	-0.3	94.1%	81.9%	88.7%	11.9			
24	297	-1.4	-7.7	-4.9	-1.0	92.2%	61.6%	81.2%	4.8			
25	298	-0.3	-9.2	-3.6	-0.7	91.0%	73.0%	81.4%	12.4			
26	299	4.1	-2.6	0.7	0.3	91.5%	72.9%	82.7%	13.1			
27	300	3.1	-4.4	0.8	0.4	96.3%	84.4%	93.1%	7.5			
28	301	-4.2	-11.5	-6.9	-1.0	92.5%	75.5%	84.6%	9.7			
29	302	-8.4	-15.8	-11.9	-1.3	90.9%	70.2%	83.8%	7.5			
30	303	-5.9	-9.9	-7.8	-0.2	93.2%	86.9%	90.4%	14.2			
31	304	-2.0	-5.9	-3.9	0.0	93.9%	86.3%	91.3%	7.4			

NOVEMBER 1997 DAILY WEATHER DATA

Date	Julian Day	Max Air Temp (^{0}C)	Min Air Temp (^{0}C)	Mean Air Temp (^{0}C)	Daily Net Radiation MJ/m^2/day	Max RH	Min RH	Mean RH	Mean Wind Speed (km/hr)	Precip (mm)	Runoff (litres)	Water pumped (m^3)
1	305	0.3	-2.8	-1.2	0.0	95.8%	87.2%	93.3%	3.5			
2	306	-0.2	-3.6	-1.8	-0.1	97.1%	93.6%	95.7%	8.9			
3	307	-1.9	-6.8	-4.3	-0.5	96.3%	81.8%	89.9%	14.7			
4	308	-2.8	-6.8	-4.6	-0.2	95.3%	84.0%	89.4%	8.9			
5	309	3.1	-2.8	0.8	-0.4	96.6%	84.6%	90.6%	14.6			
6	310	5.0	-2.4	1.5	-2.3	94.0%	60.6%	81.3%	9.3			
7	311	0.2	-5.6	-2.7	-0.9	93.7%	72.9%	86.0%	7.7			
8	312	-2.3	-6.3	-3.8	-0.5	90.7%	68.5%	79.9%	13.4			
9	313	-6.2	-10.4	-8.0	-0.8	91.6%	81.7%	86.9%	6.1			
10	314	-8.5	-12.1	-10.0	-1.1	90.6%	75.8%	86.1%	9.2			
11	315	-0.2	-8.7	-4.7	-2.4	90.6%	60.8%	80.4%	12.2			
12	316	-4.9	-7.8	-6.7	-0.8	93.1%	83.3%	91.1%	10.2			
13	317	-5.4	-11.1	-8.2	-1.8	89.8%	62.8%	82.1%	7.1			
14	318	-7.3	-9.4	-8.3	-0.3	92.5%	83.4%	88.8%	4.1			
15	319	-4.1	-11.9	-7.9	-0.3	92.9%	75.8%	87.6%	9.7			
16	320	-5.4	-9.5	-7.0	-0.5	93.0%	72.5%	82.2%	12.0			
17	321	-8.9	-11.3	-10.0	-0.5	88.6%	73.0%	81.4%	5.1			
18	322	-9.6	-14.3	-11.1	-1.0	89.3%	78.6%	85.9%	6.6			
19	323	-12.3	-16.4	-13.6	-2.1	85.3%	75.2%	81.4%	12.5			
20	324	-13.2	-15.8	-14.8	-1.1	87.4%	77.0%	82.4%	9.5			
21	325	-15.1	-18.5	-17.2	-1.5	86.0%	66.3%	81.7%	5.6			
22	326	-13.2	-16.8	-15.1	-0.9	87.8%	78.9%	85.6%	4.5			
23	327	-7.2	-14.1	-10.2	0.1	92.1%	87.5%	90.1%	13.2			
24	328	-5.9	-7.2	-6.5	0.2	93.6%	88.4%	90.9%	12.2			
25	329	-2.0	-7.0	-5.2	0.1	96.0%	84.8%	92.6%	11.7			
26	330	-4.6	-13.4	-9.1	0.1	94.7%	79.9%	89.0%	7.9			
27	331	-5.2	-9.6	-7.6	-0.2	93.9%	89.4%	91.9%	5.2			
28	332	-1.5	-10.0	-6.9	-0.1	93.2%	84.8%	90.2%	12.4			
29	333	-9.9	-15.8	-13.3	-0.1	90.8%	84.8%	88.0%	9.2			
30	334	-6.4	-13.5	-9.7	-0.3	93.0%	88.1%	90.7%	14.8			

DECEMBER 1997 DAILY WEATHER DATA

Date	Julian Day	Max Air Temp (^{0}C)	Min Air Temp (^{0}C)	Mean Air Temp (^{0}C)	Daily Net Radiation MJ/m^2/day	Max RH	Min RH	Mean RH	Mean Wind Speed (km/hr)	Precip (mm)	Runoff (litres)	Water pumped (m^3)
1	335	-3.3	-9.3	-5.7	-0.1	92.3%	80.7%	89.7%	12.5			
2	336	-6.7	-13.3	-9.8	-0.1	91.0%	85.8%	88.5%	4.7			
3	337	-11.1	-17.4	-12.9	-0.2	87.1%	82.8%	85.8%	3.1			
4	338	-10.2	-20.7	-16.0	-0.2	86.4%	79.6%	83.5%	0.4			
5	339	-6.3	-17.1	-10.1	0.0	90.9%	82.9%	88.0%	0.0			
6	340	-6.0	-9.5	-6.7	0.0	91.1%	88.7%	90.6%	3.0			
7	341	-7.9	-15.4	-11.4	-0.1	89.9%	84.4%	87.1%	3.1			
8	342	-8.3	-10.6	-9.0	-0.1	89.4%	87.7%	88.9%	6.2			
9	343	-8.7	-13.5	-10.4	-0.2	89.3%	85.9%	87.9%	6.5			
10	344	-6.5	-13.6	-9.1	0.0	90.7%	80.3%	87.1%	12.2			
11	345	0.9	-12.5	-4.5	-1.3	108.1%	73.3%	83.8%	13.5			
12	346	1.0	-5.8	-1.6	-5.0	80.7%	60.2%	72.6%	19.9			
13	347	-2.0	-8.1	-5.0	-1.3	109.6%	76.8%	87.2%	7.8			
14	348	3.4	-3.0	-0.3	-1.7	77.2%	45.9%	61.6%	6.6			
15	349	1.6	-17.6	-6.5	-2.1	106.7%	49.2%	76.5%	15.1			
16	350	-9.1	-23.4	-16.1	-0.4	83.3%	52.4%	73.1%	8.0			
17	351	-8.7	-11.3	-9.7	-0.1	85.5%	58.8%	76.4%	9.3			
18	352	-8.0	-15.6	-11.5	-0.6	87.9%	80.1%	83.6%	10.3			
19	353	-12.7	-22.6	-17.6	-0.9	83.7%	77.5%	80.6%	8.5			
20	354	-9.8	-14.1	-12.0	0.3	88.0%	77.2%	84.1%	4.5			
21	355	-6.6	-14.3	-10.1	-0.1	88.2%	82.0%	85.4%	12.1			
22	356	-10.5	-16.4	-12.6	-0.7	87.7%	82.9%	85.3%	12.9			
23	357	-1.1	-12.3	-6.0	-0.4	91.2%	79.2%	87.7%	13.2			
24	358	-5.0	-18.4	-13.7	-1.3	88.3%	64.8%	79.9%	13.3			
25	359	-1.6	-17.6	-8.4	-1.0	88.1%	80.2%	84.2%	18.1			
26	360	-5.7	-19.9	-14.0	-0.2	90.9%	80.5%	85.0%	6.0			
27	361	-6.1	-15.2	-9.6	-0.1	90.8%	84.4%	88.4%	6.7			
28	362	-13.6	-16.9	-15.4	-0.2	85.5%	82.9%	84.1%	3.4			
29	363	-14.6	-28.3	-19.6	-0.2	84.7%	73.4%	80.7%	5.0			
30	364	-18.8	-28.9	-23.8	-0.2	82.3%	72.8%	77.4%	7.0			
31	365	-17.6	-23.9	-20.8	-0.3	90.1%	76.1%	79.9%	8.5			

Appendix E

SURFACE RUNOFF DATA

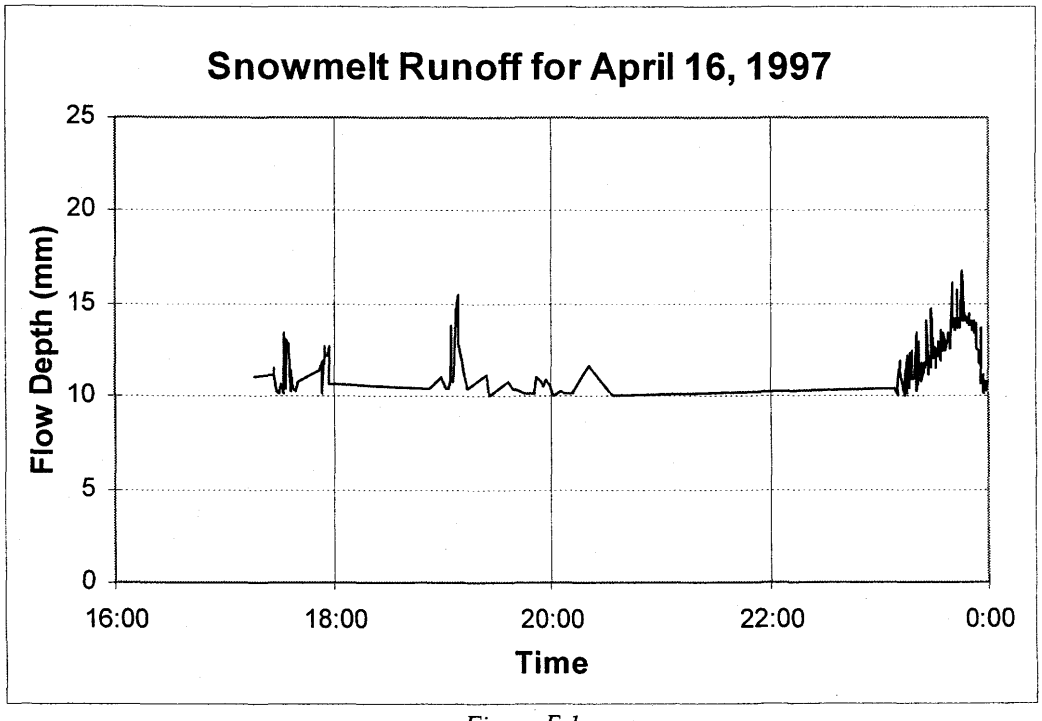

Figure E.1

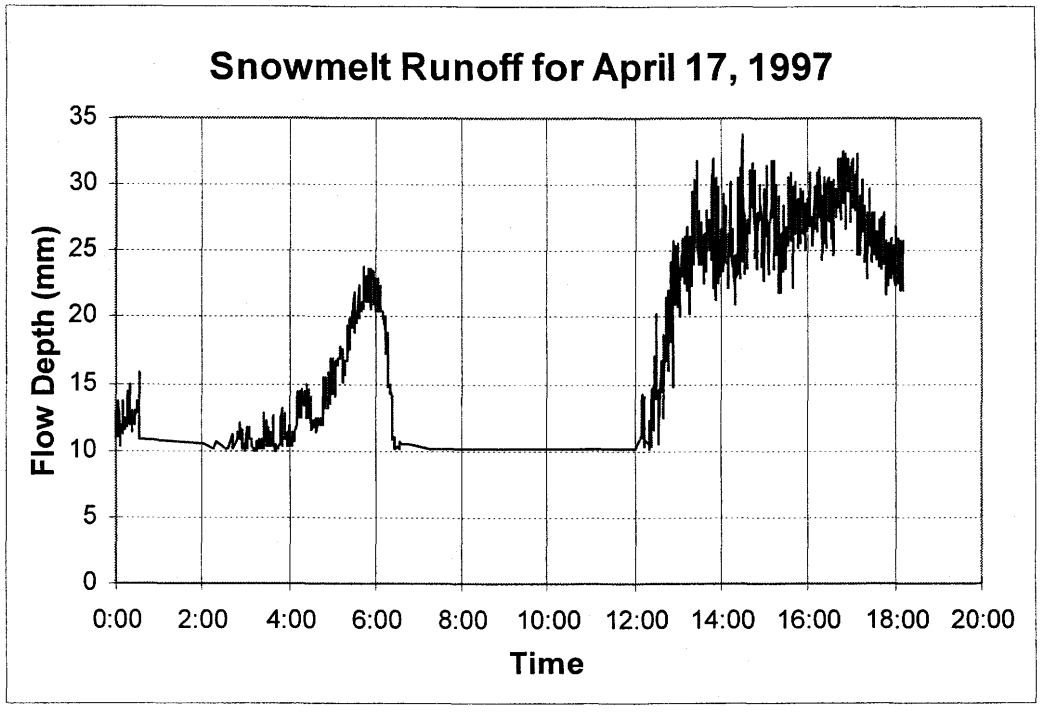

Figure E.2

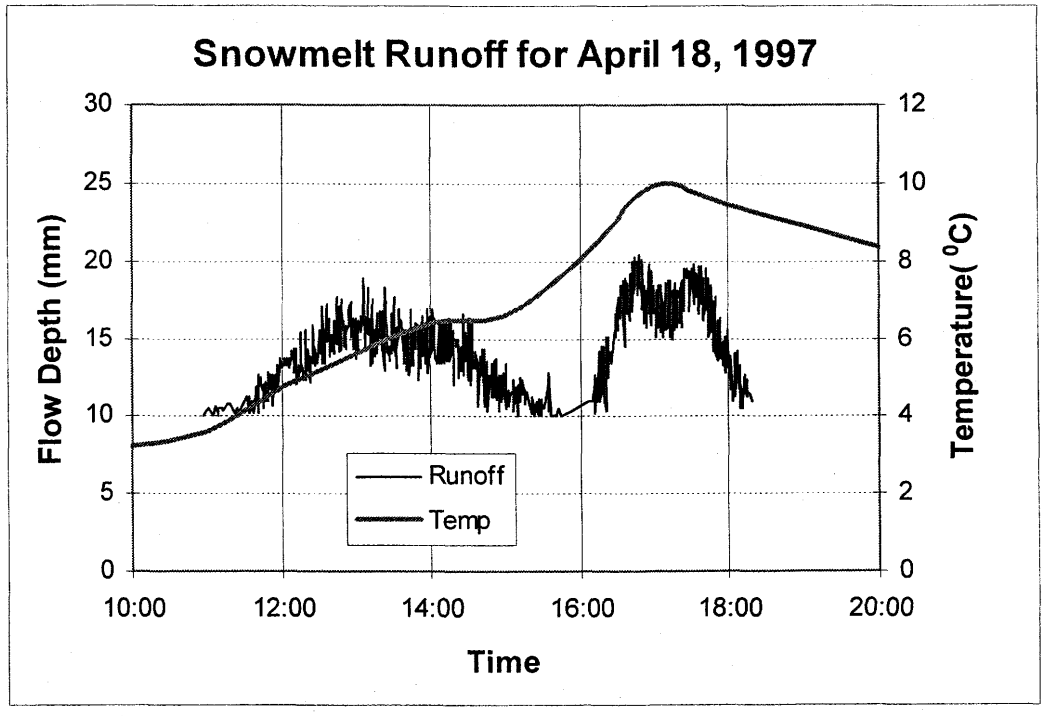

Figure E.3

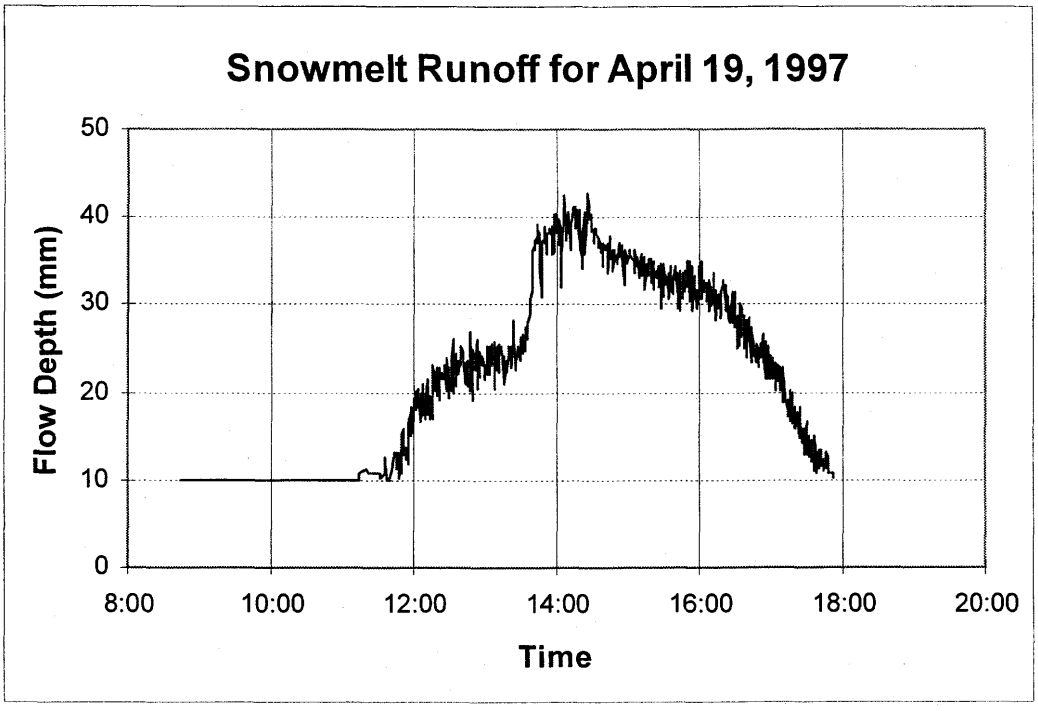

Figure E.4

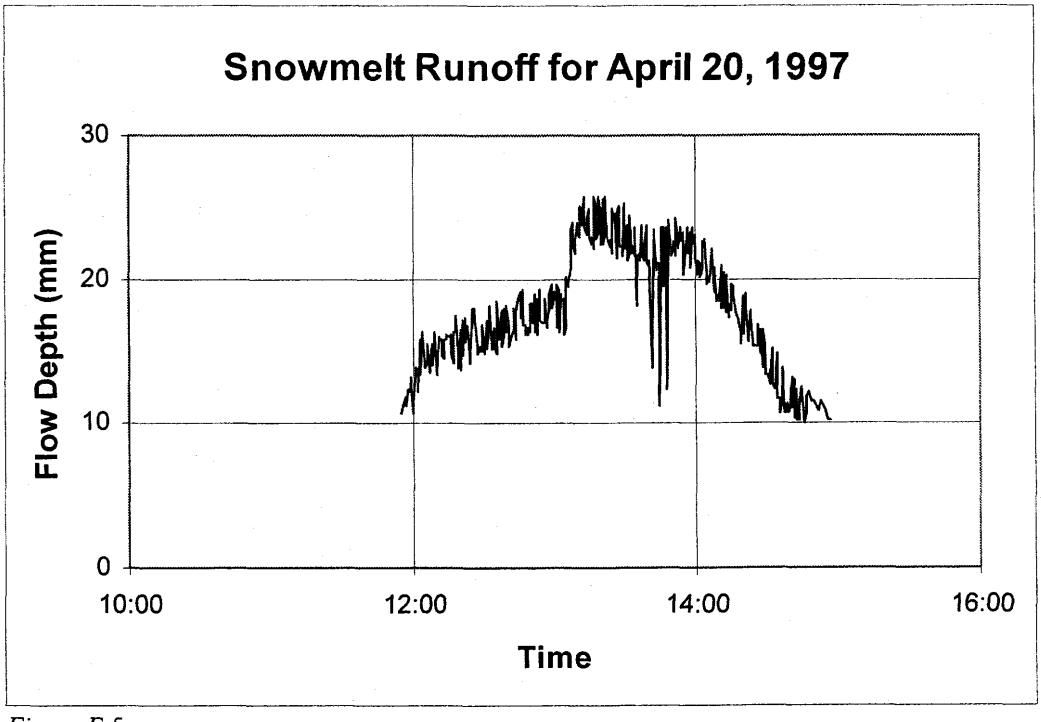

Figure E.5

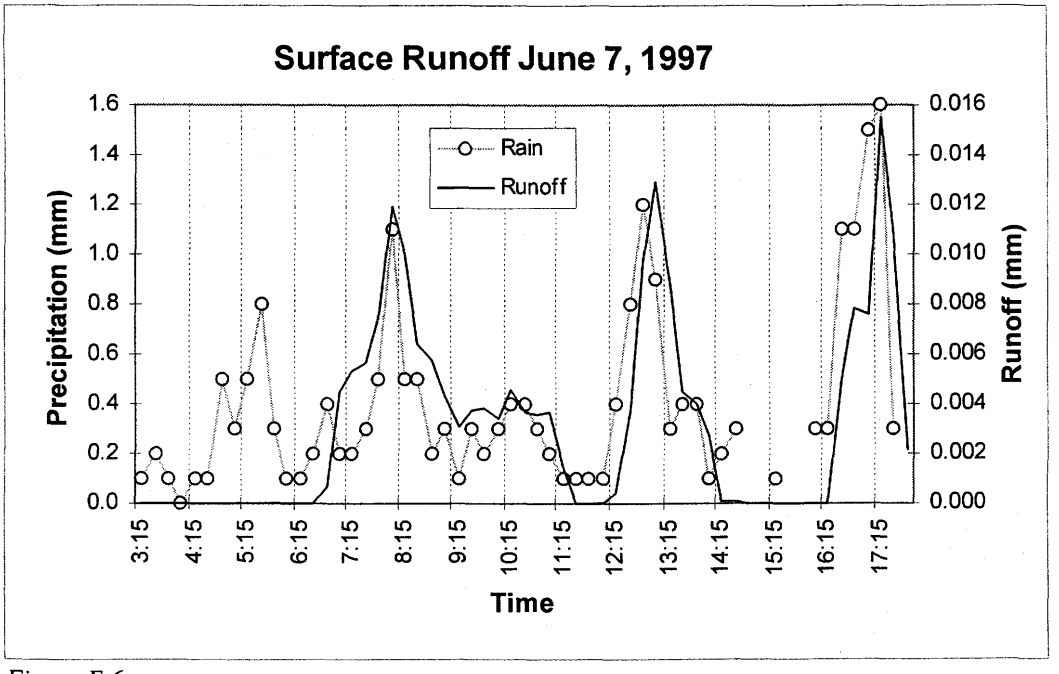

Figure E.6

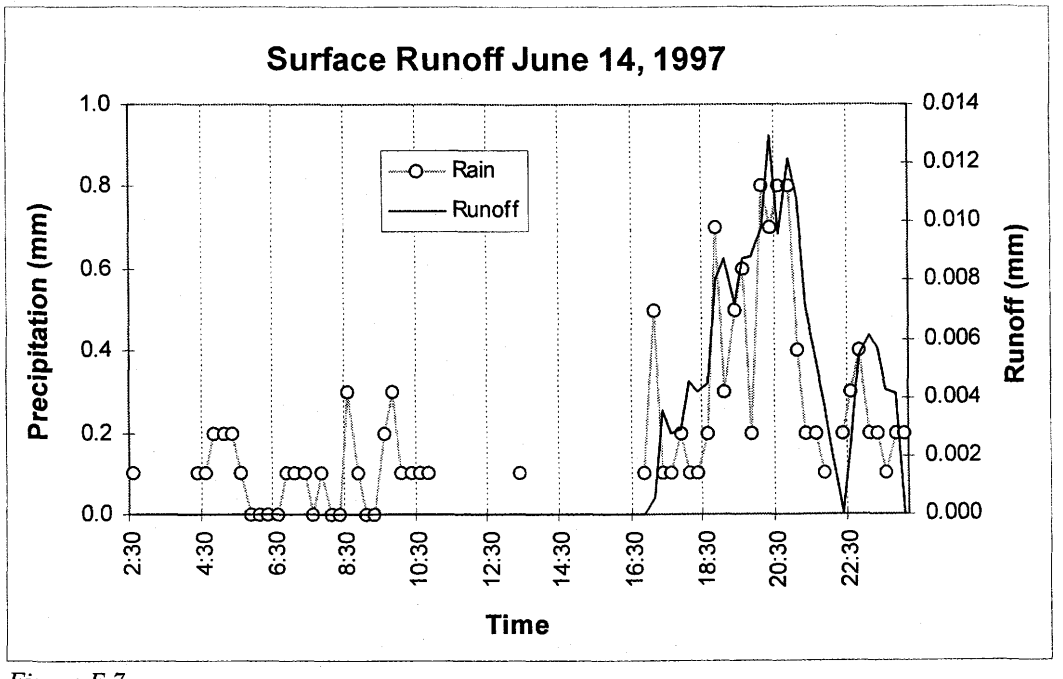

Figure E.7

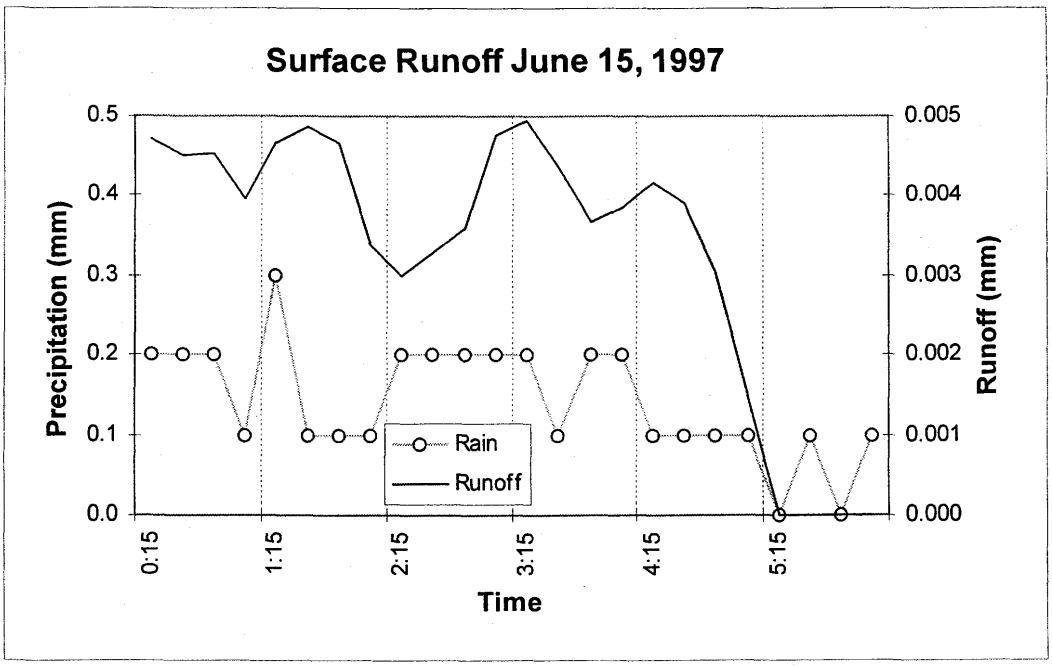

Figure E.8

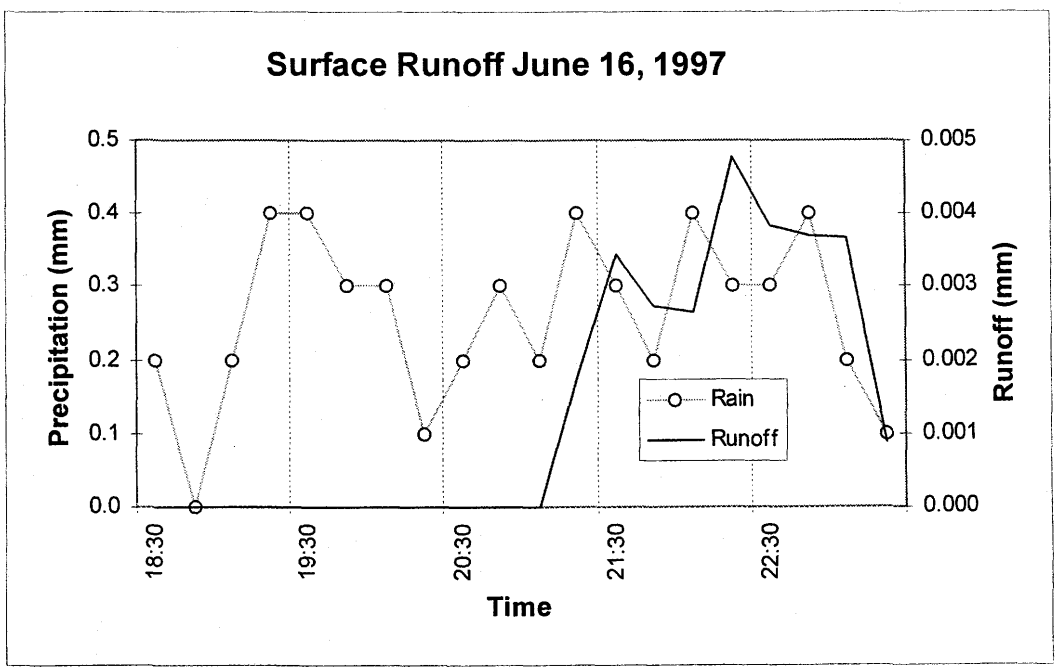

Figure E.9

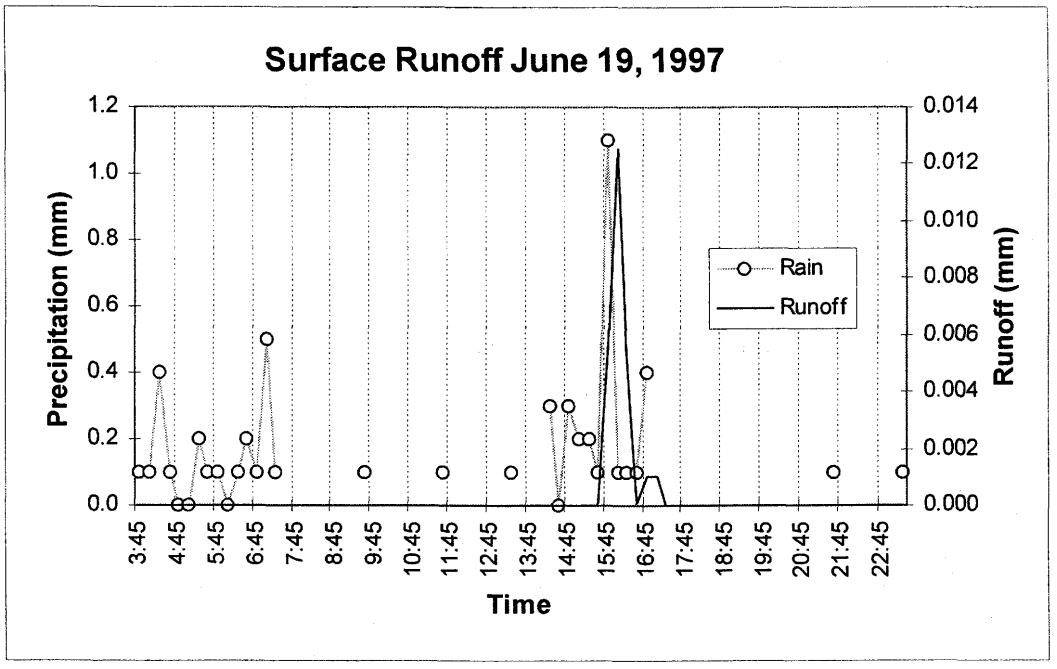

Figure E.10

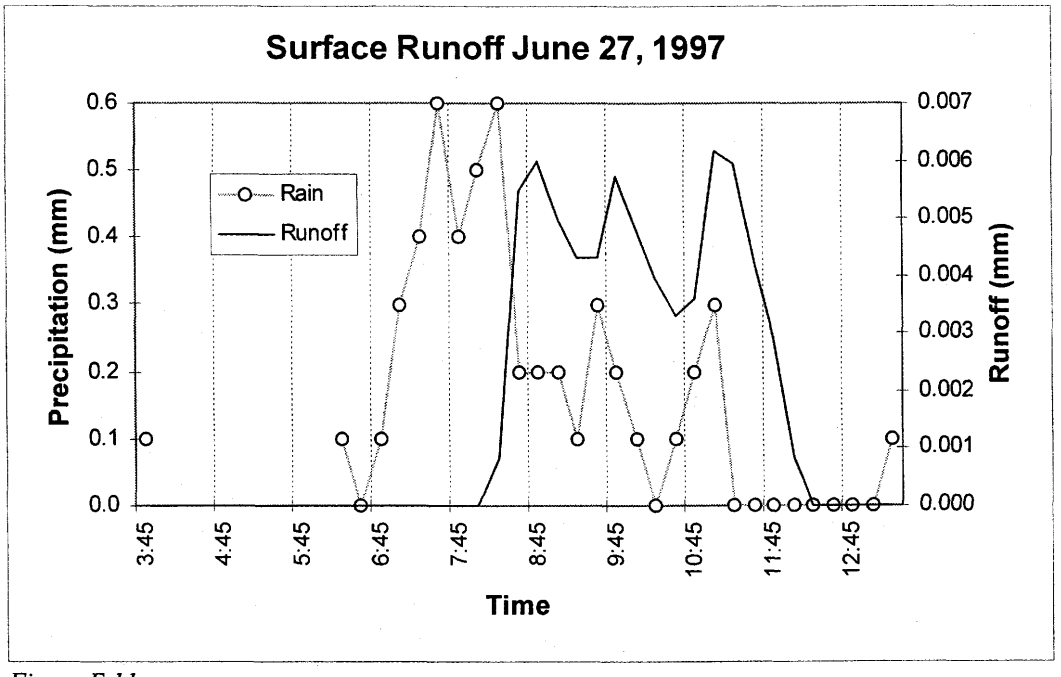

Figure E.11

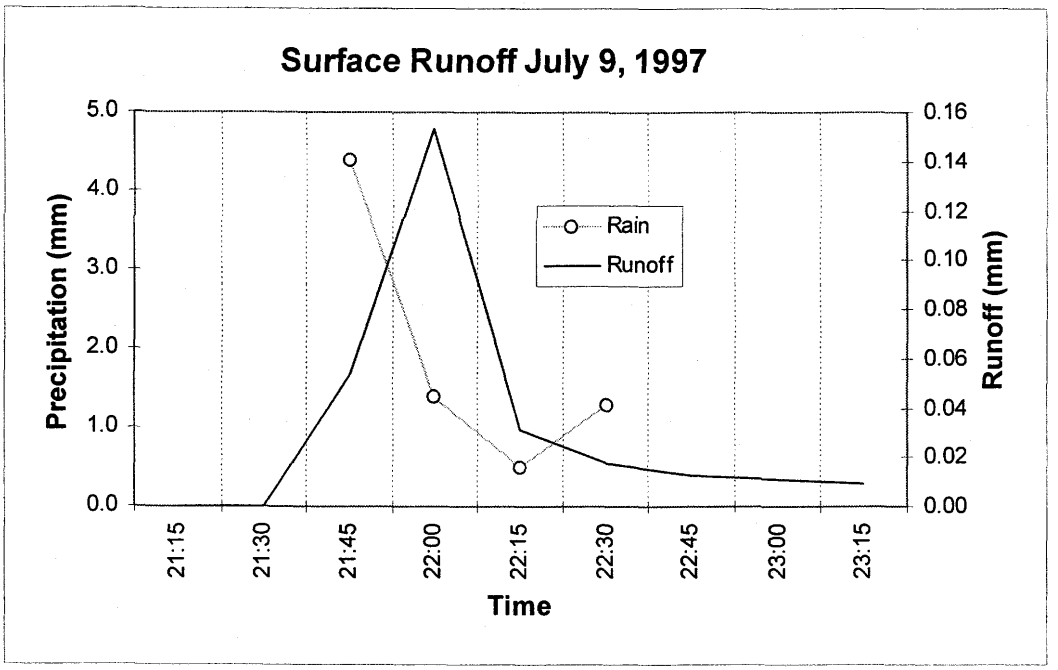

Figure E.12

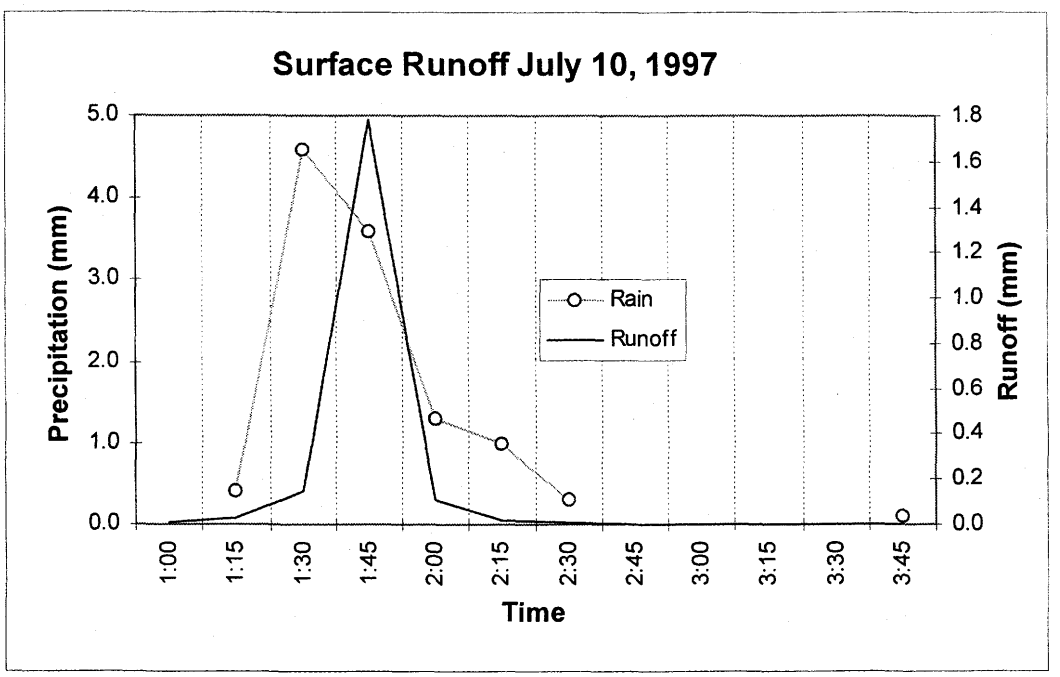

Figure E.13

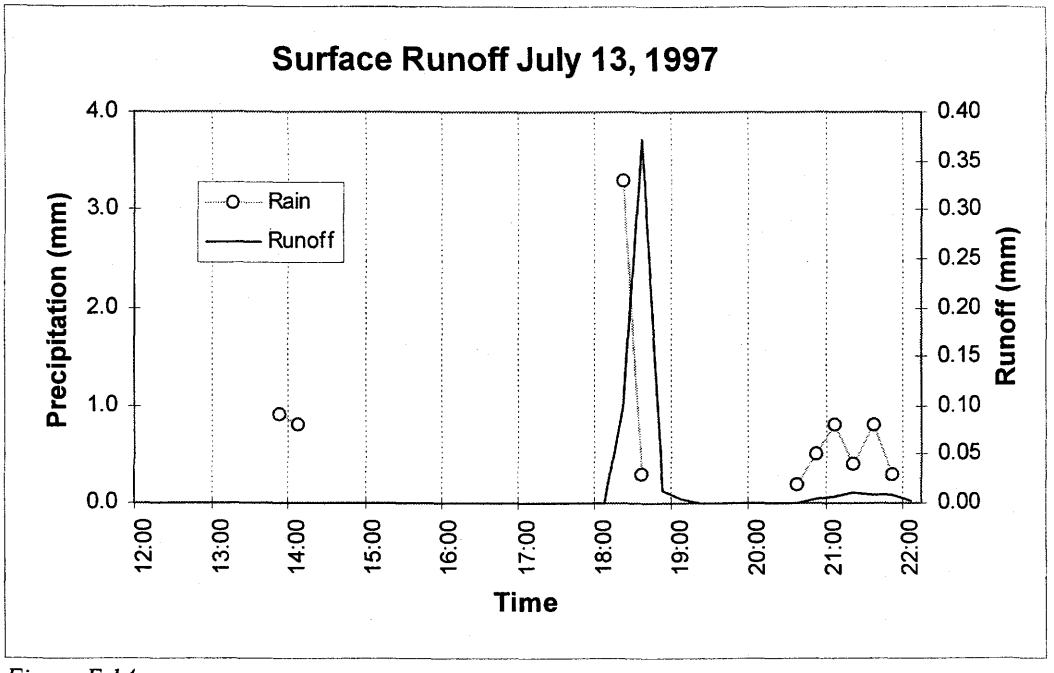

Figure E.14

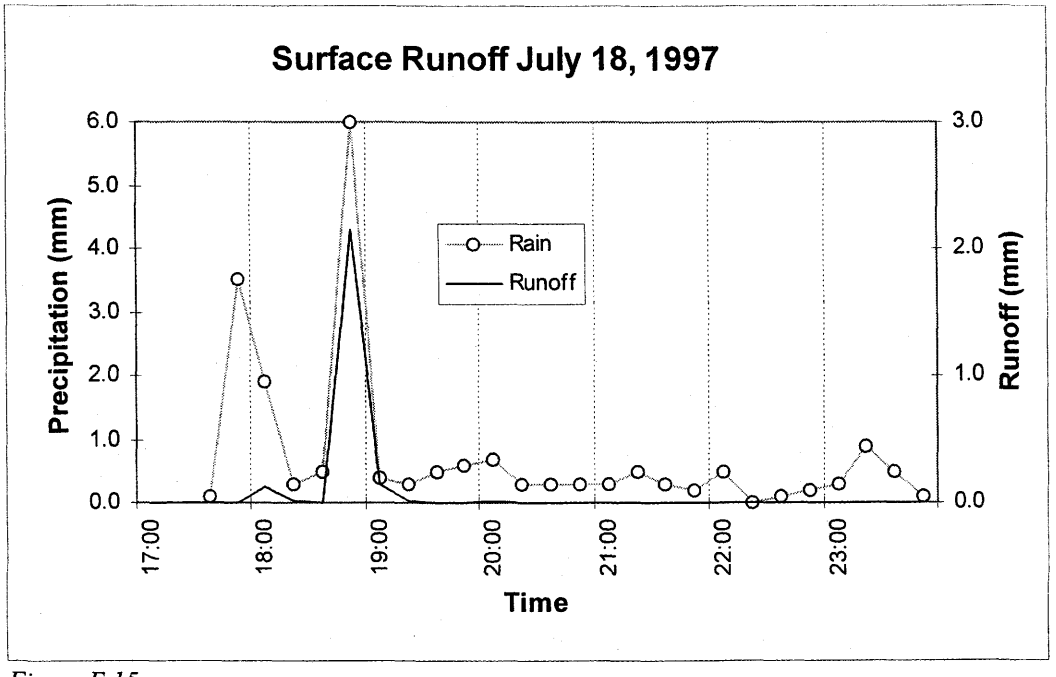

Figure E.15

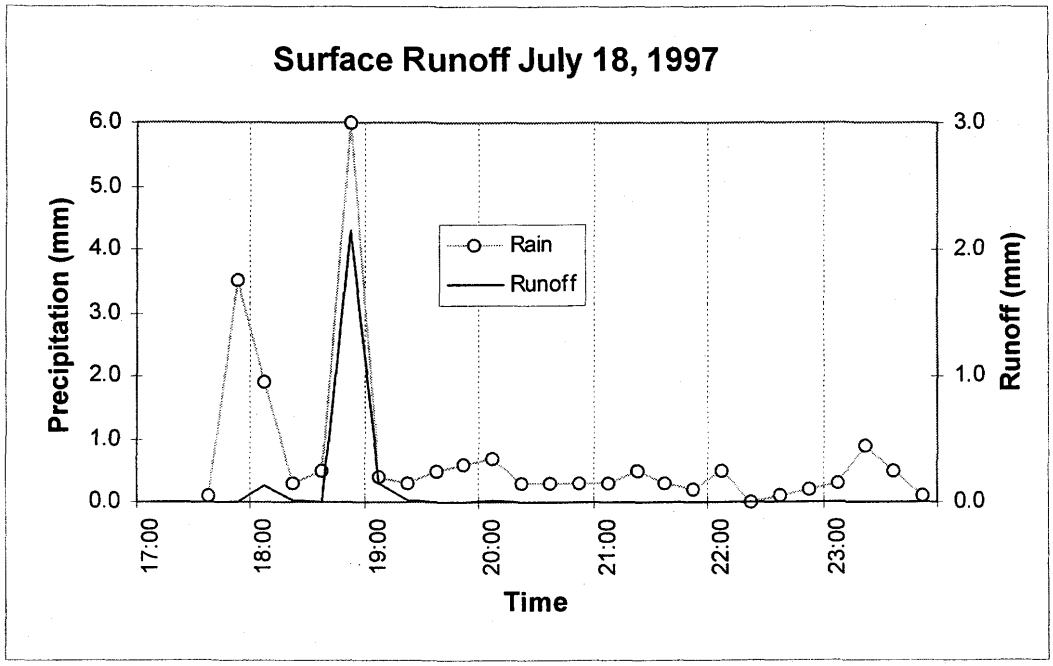

Figure E.16

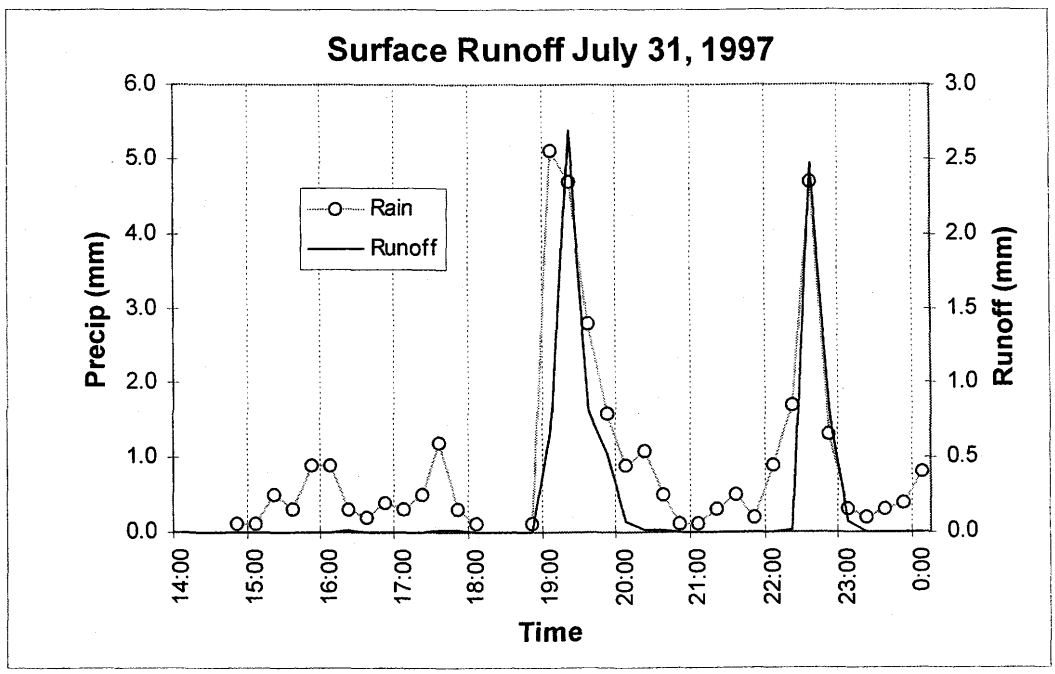

Figure E.17

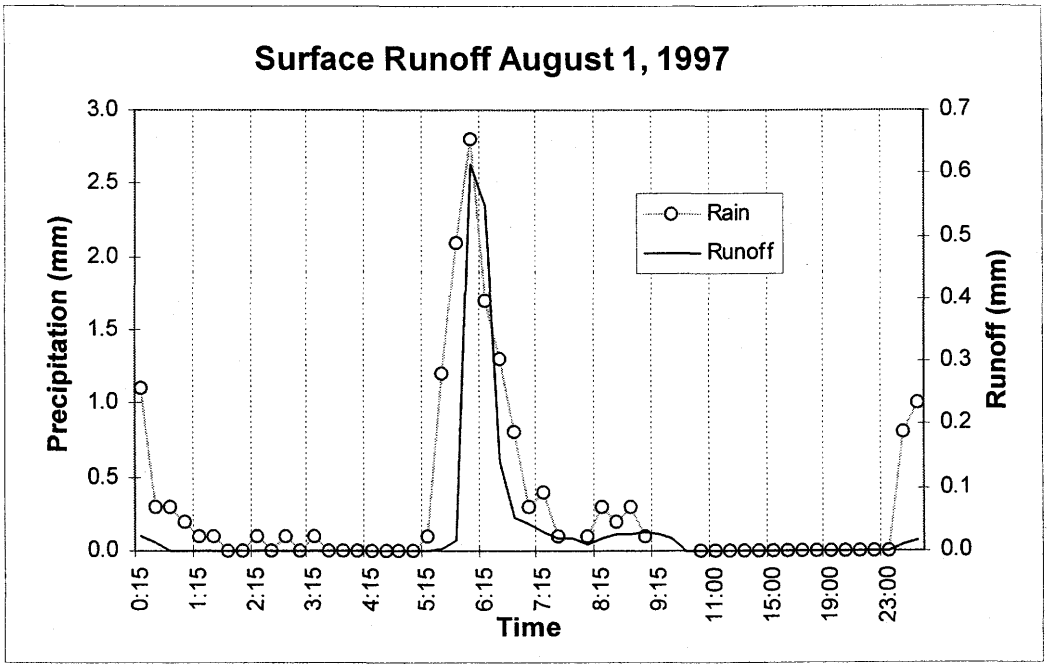

Figure E.18

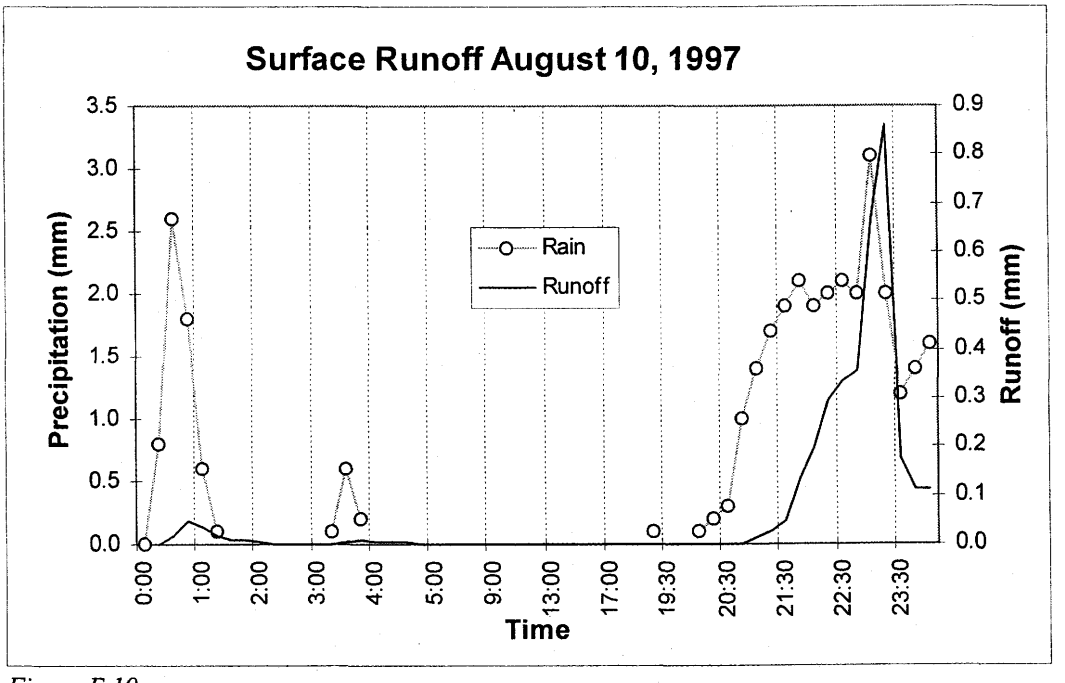

Figure E.19

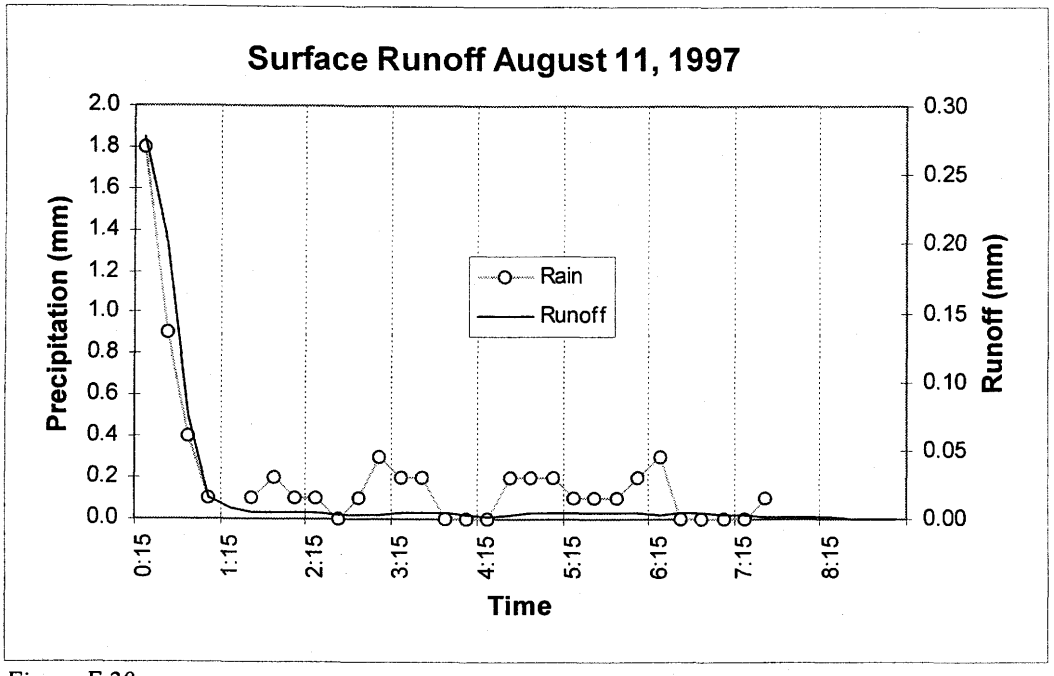

Figure E.20

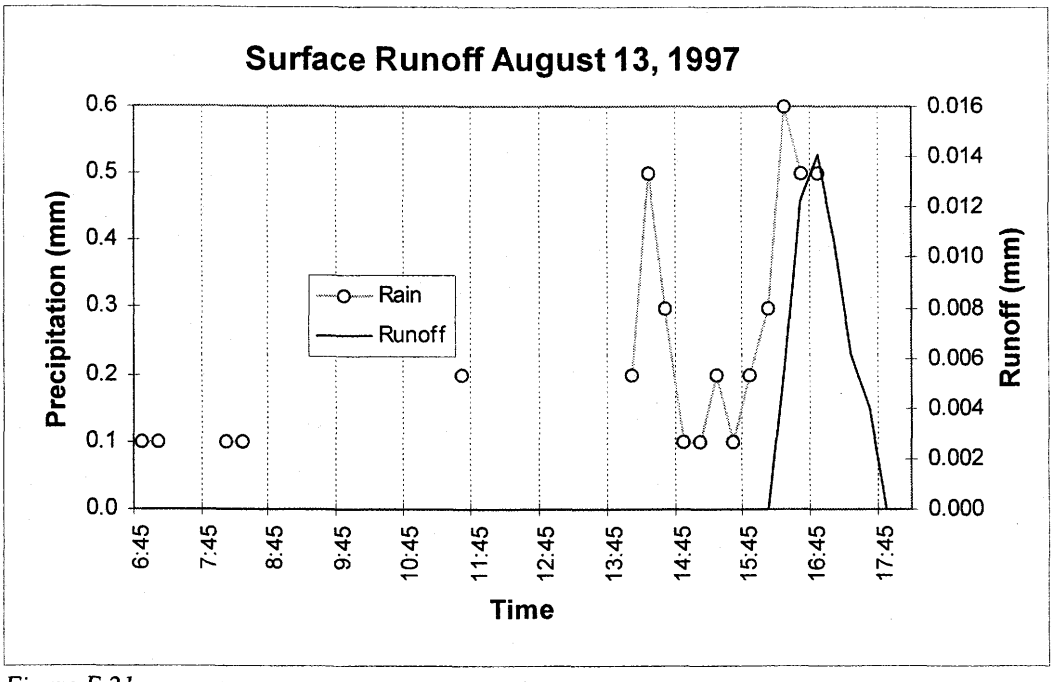

Figure E.21

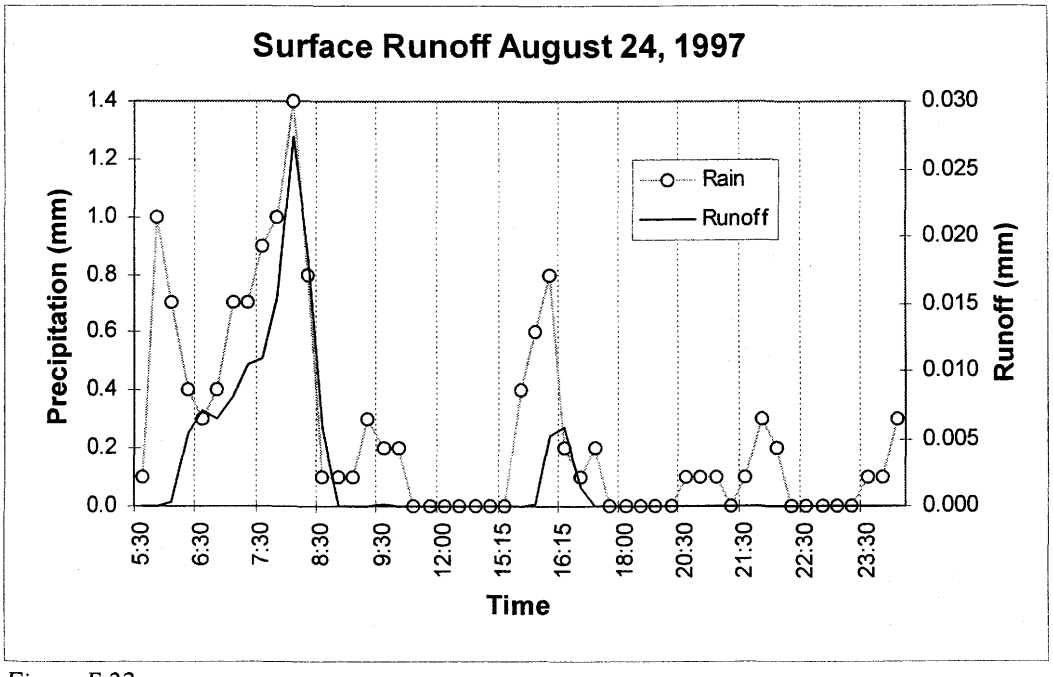

Figure E.22

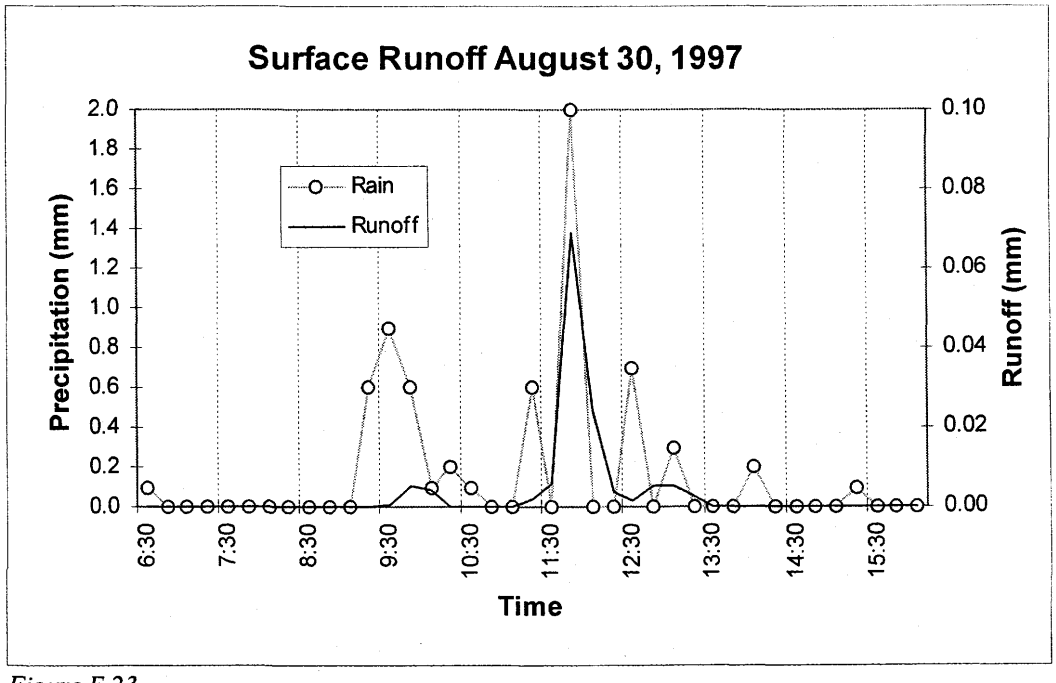

Figure E.23

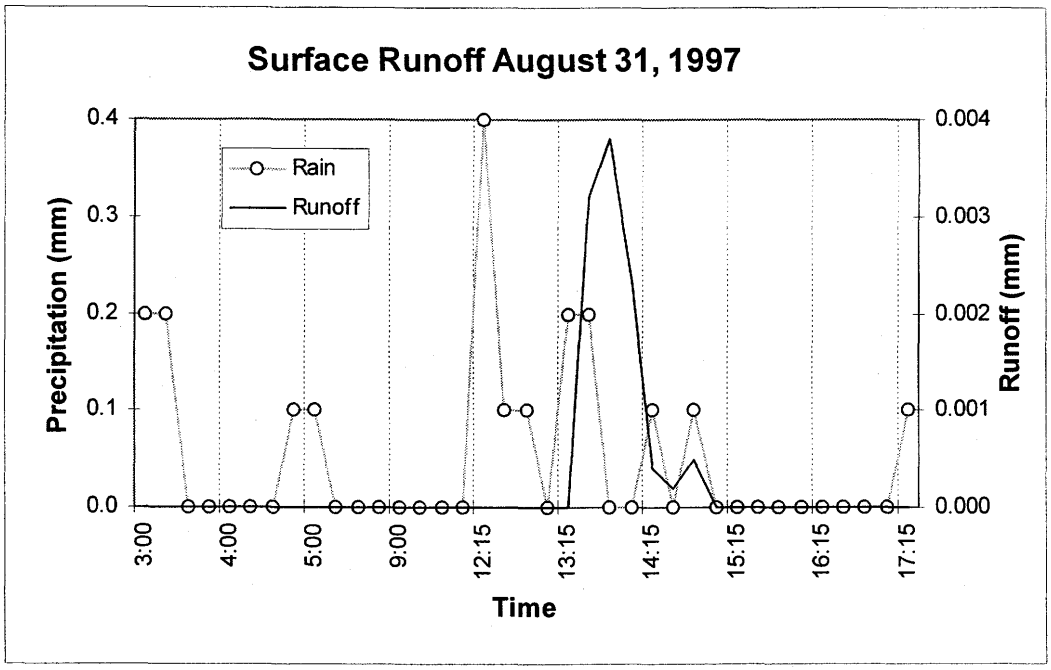

Figure E.24

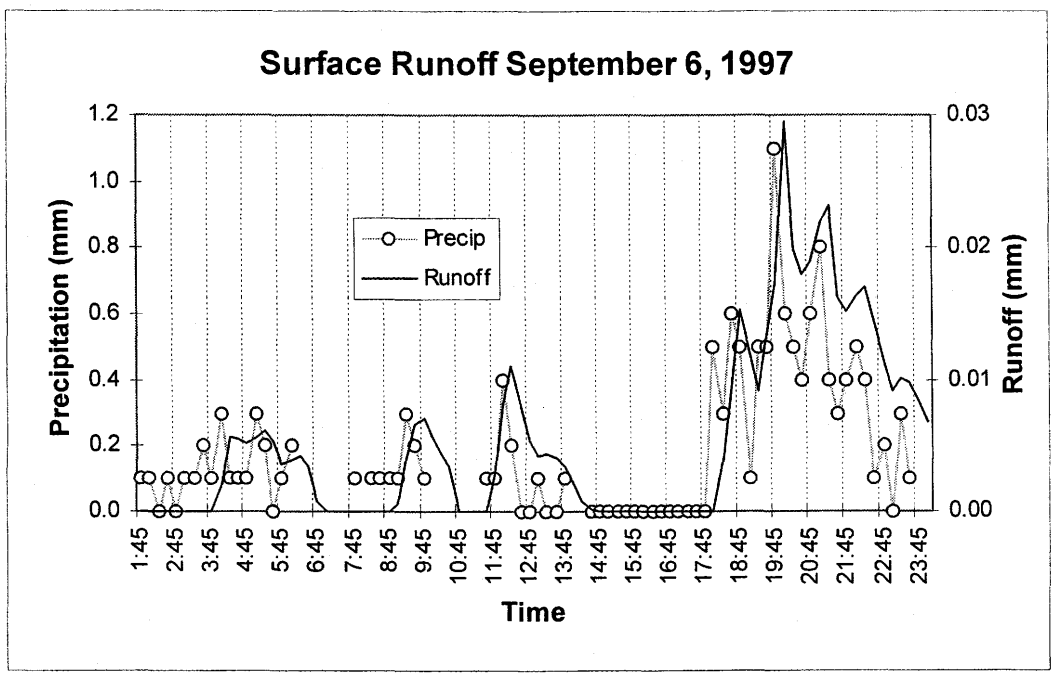

Figure E.25

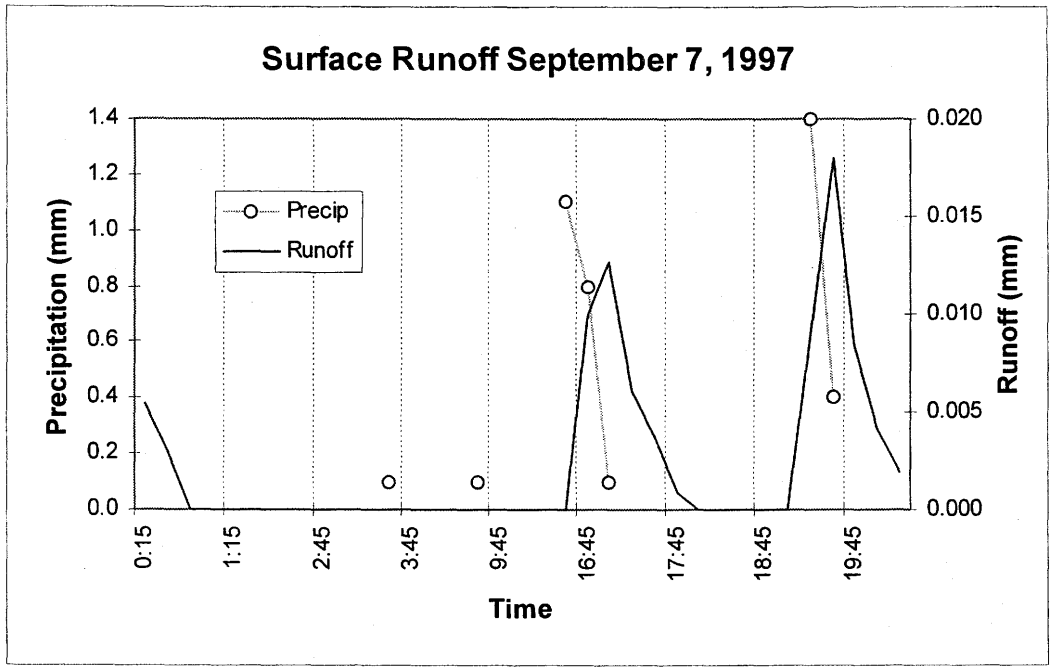

Figure E.26

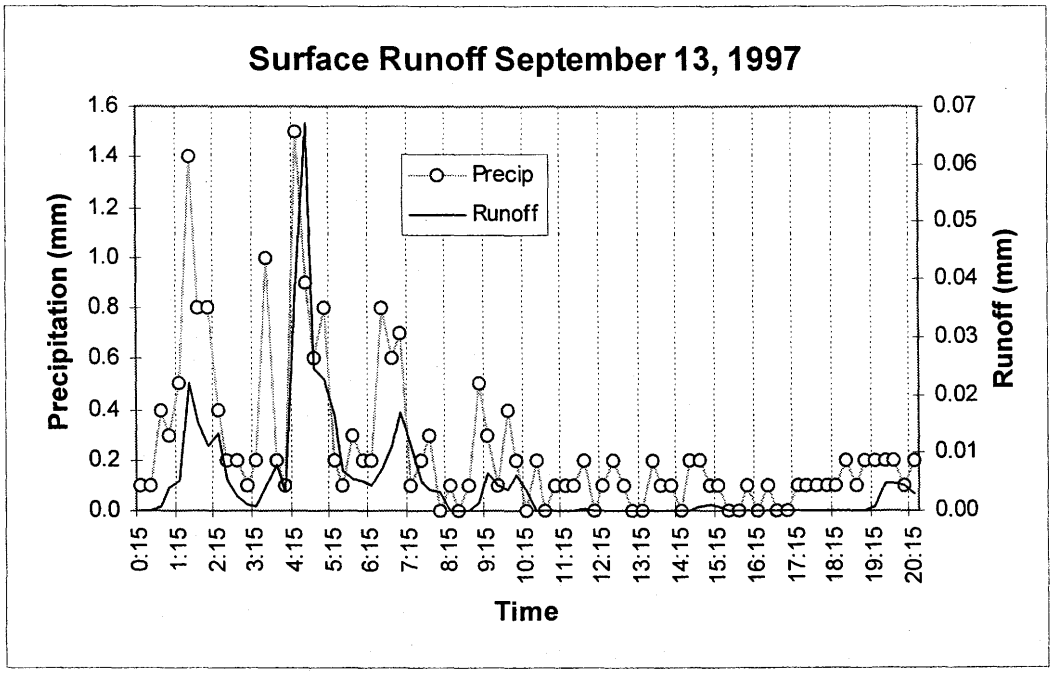

Figure E.27

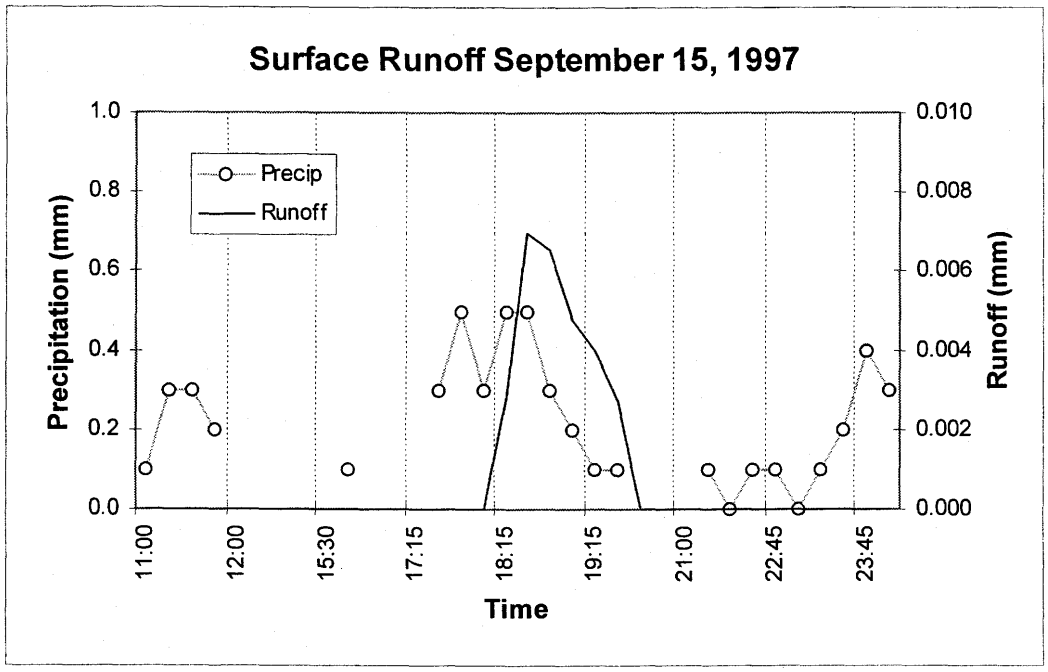

Figure E.28

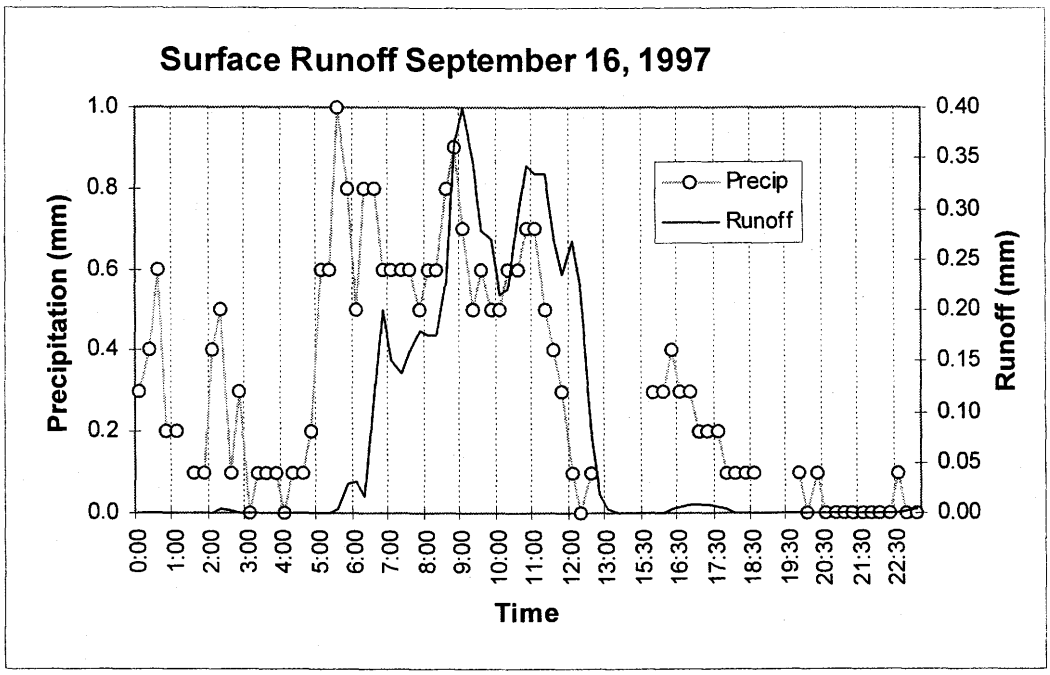

Figure E.29

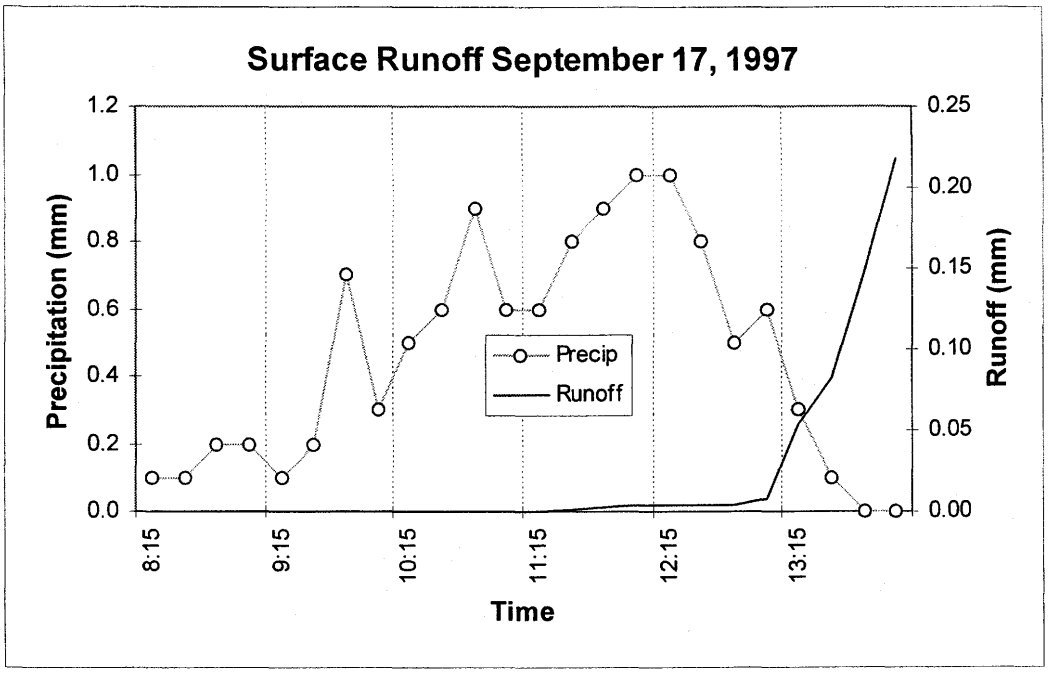

Figure E.30

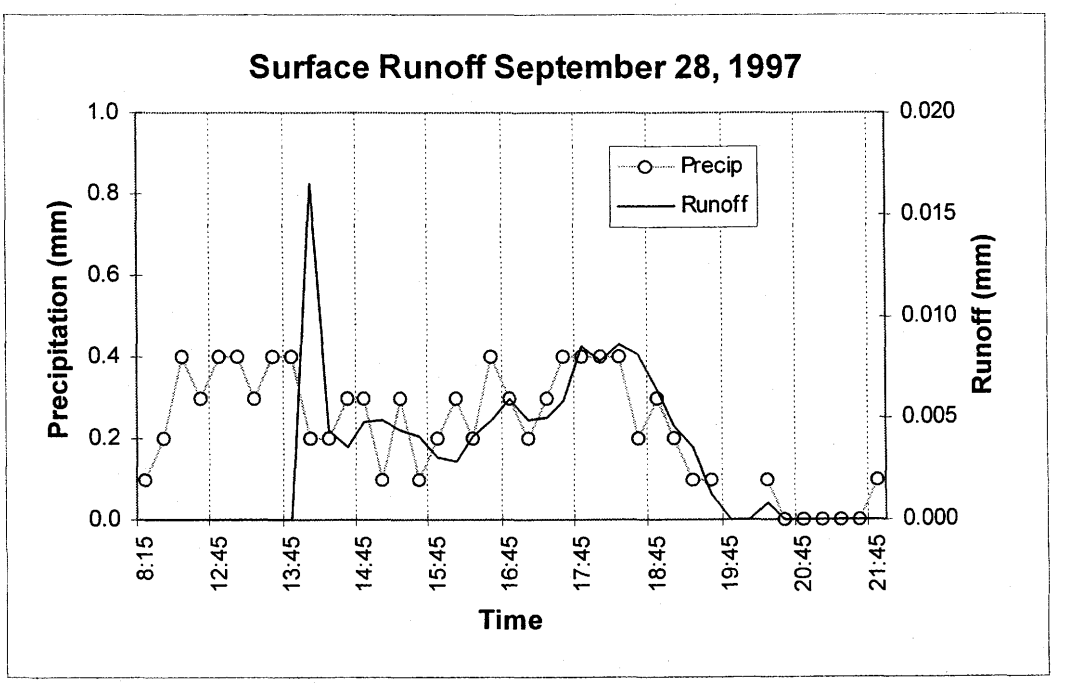

Figure E.31

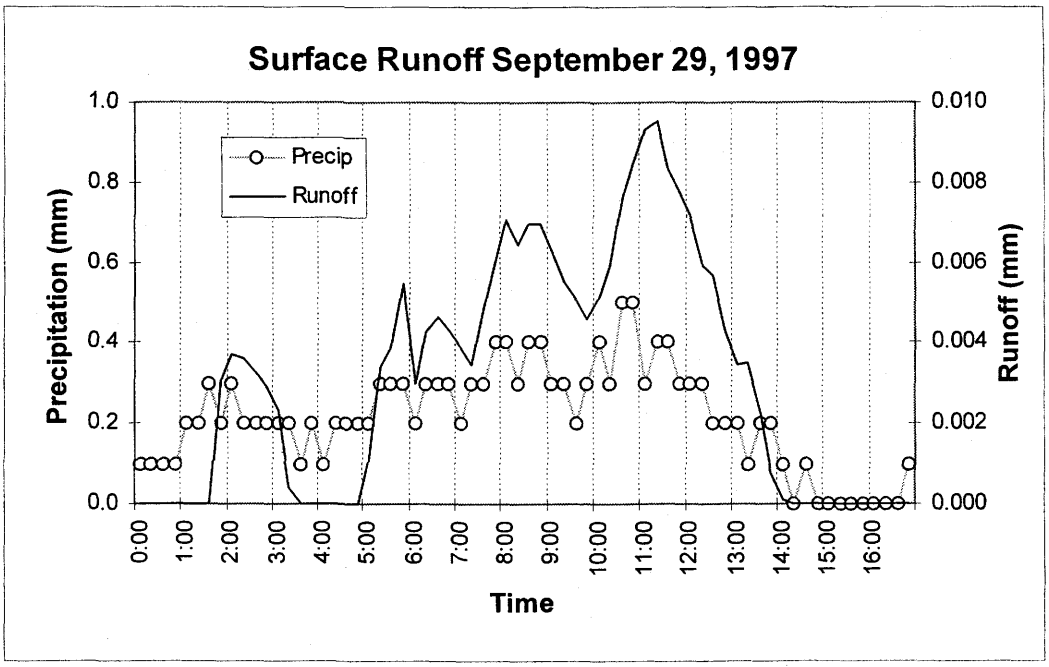
Surface Runoff September 29, 1997
Precip
Runoff
Precipitation (mm)
Runoff (mm)
Time
1.0
0.8
0.6
0.4
0.2
0.0
0.010
0.008
0.006
0.004
0.002
0.000
0:00
1:00
2:00
3:00
4:00
5:00
6:00
7:00
8:00
9:00
10:00
11:00
12:00
13:00
14:00
15:00
16:00

Figure E.32

Appendix F

SOIL SUCTION AND SOIL MOISTURE

F.1 SOIL SUCTION DATA

F.1.1 Beta-97 Sensor Calibration Data

Figure F.1

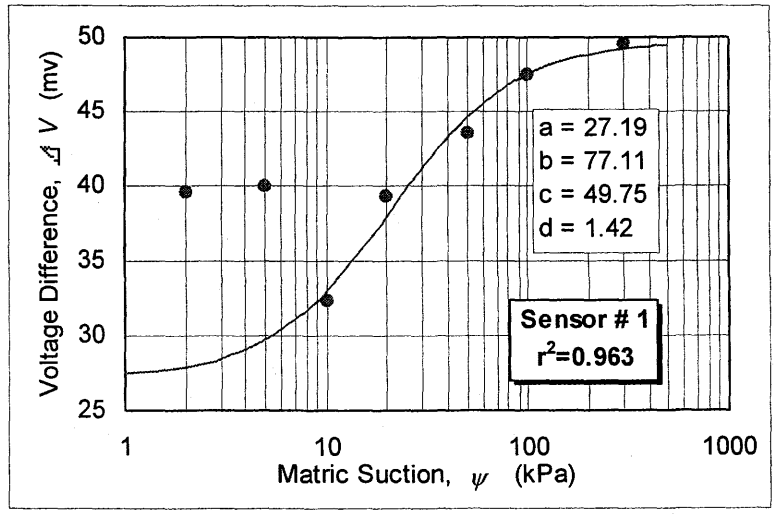

Figure F.2

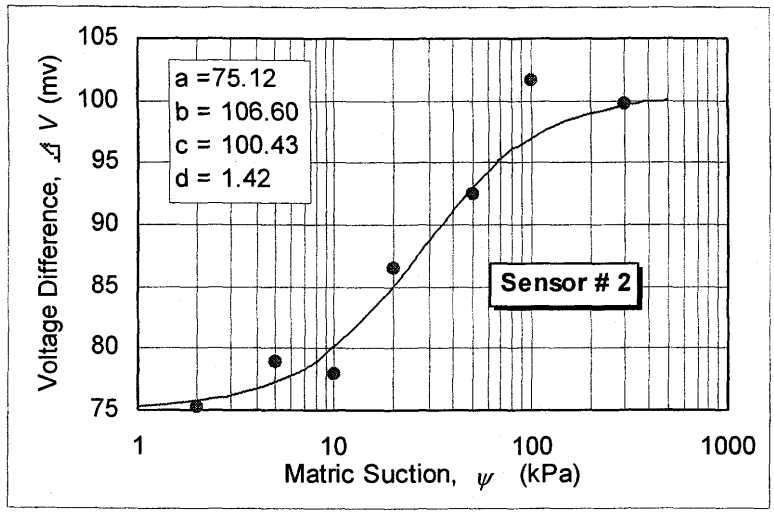

Figure F.3

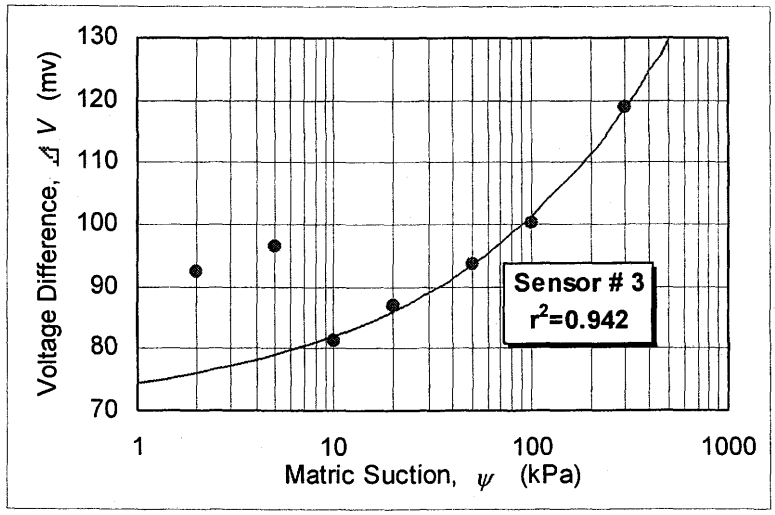

Figure F.4

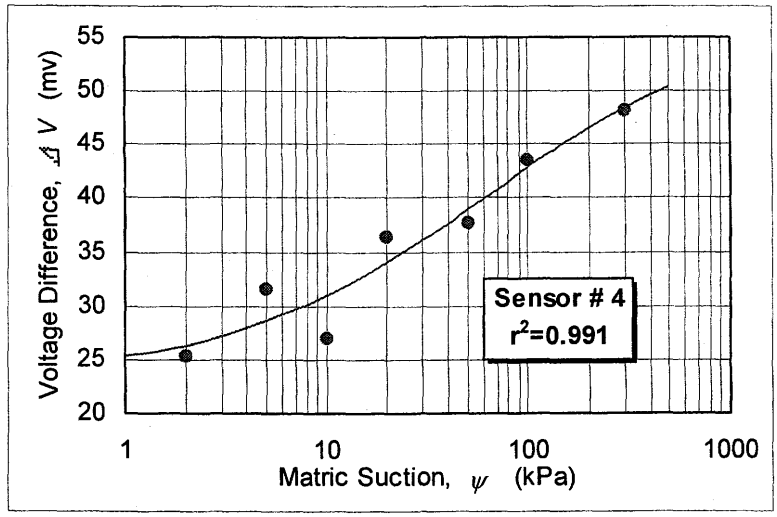

Figure F.5

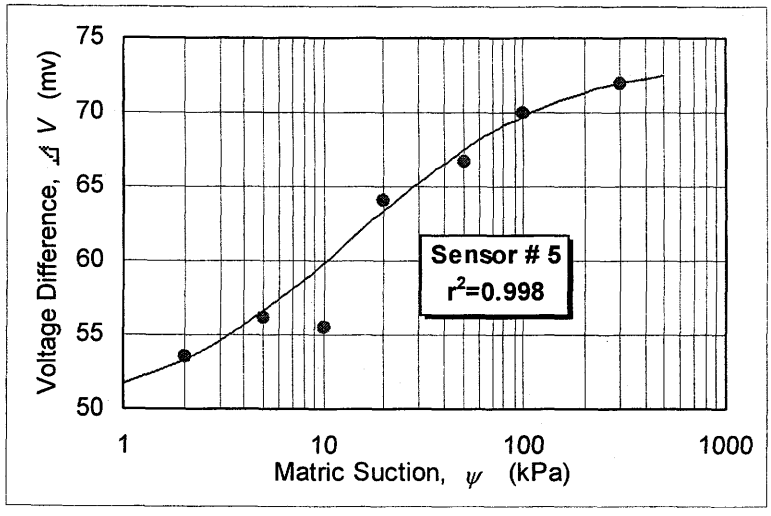

Figure F.6

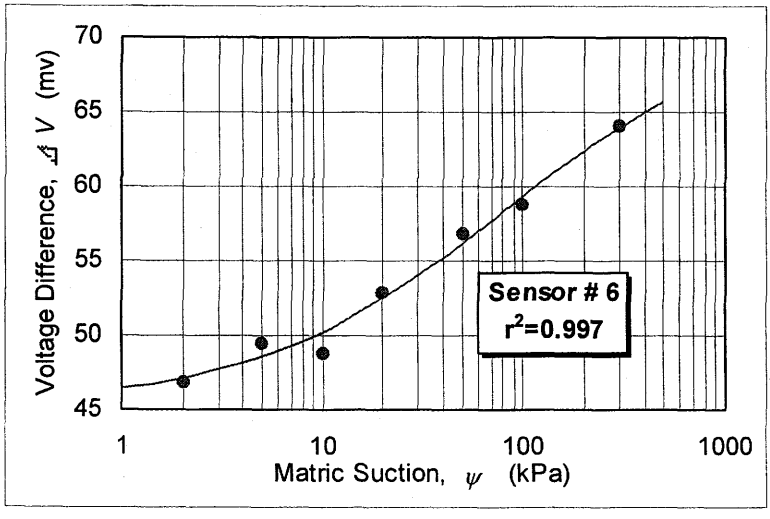

Figure F.7

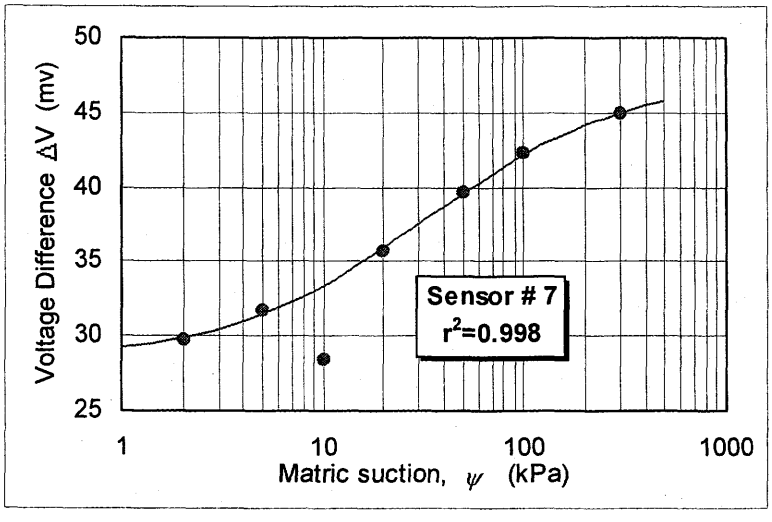

Figure F.8

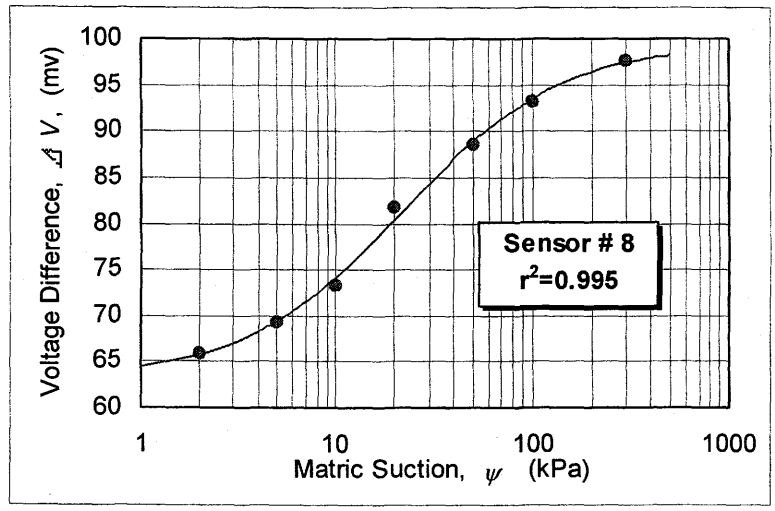

Figure F.9

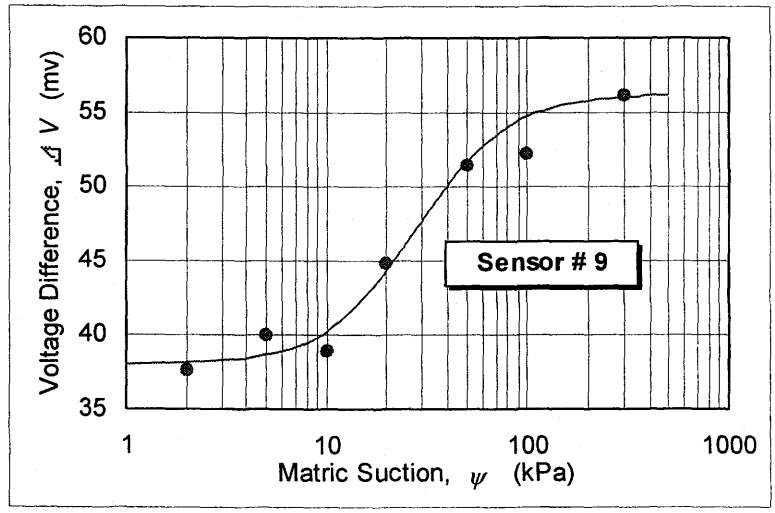

Figure F.10

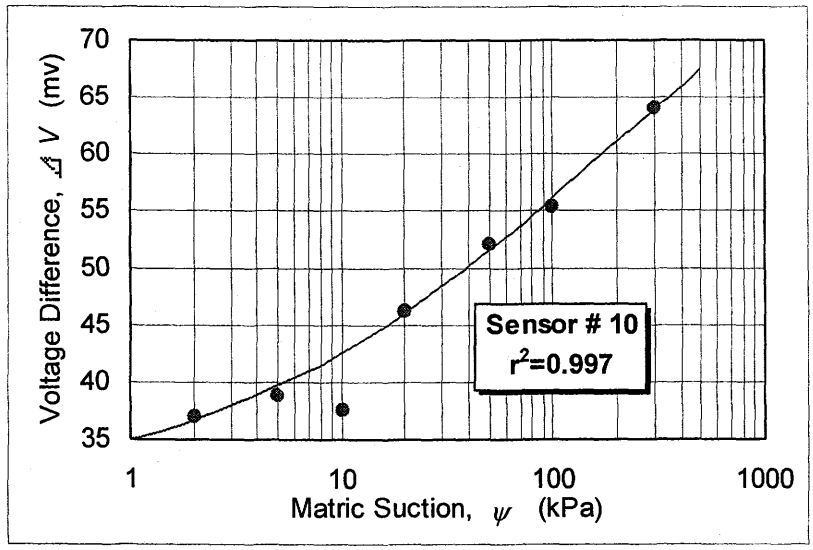

Figure F.11

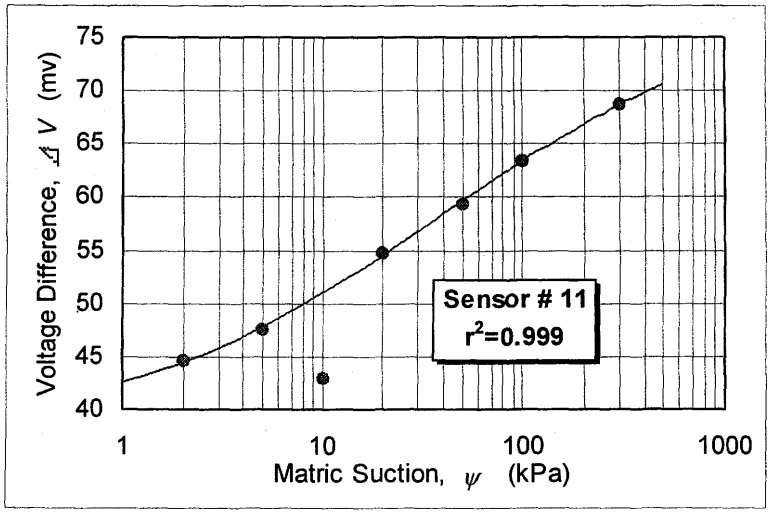

Figure F.12

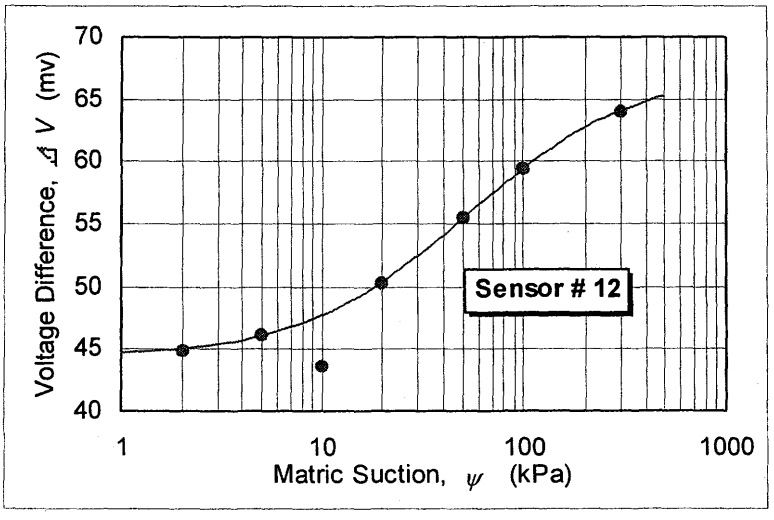

Figure F.13

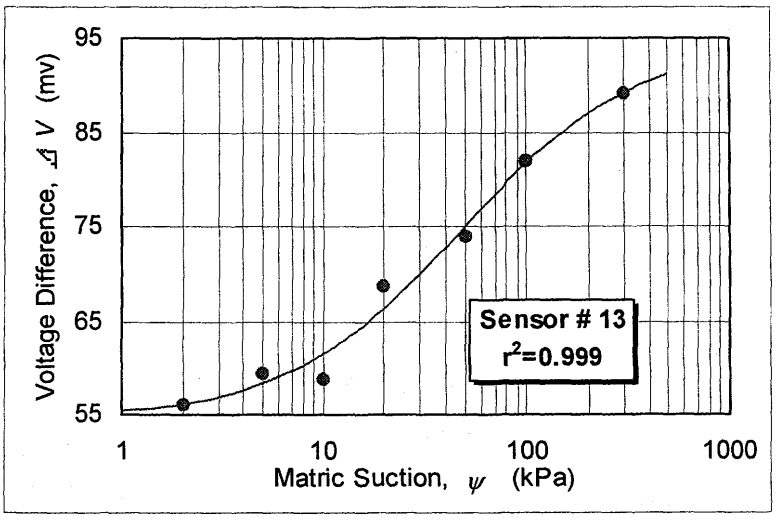

Figure F.14

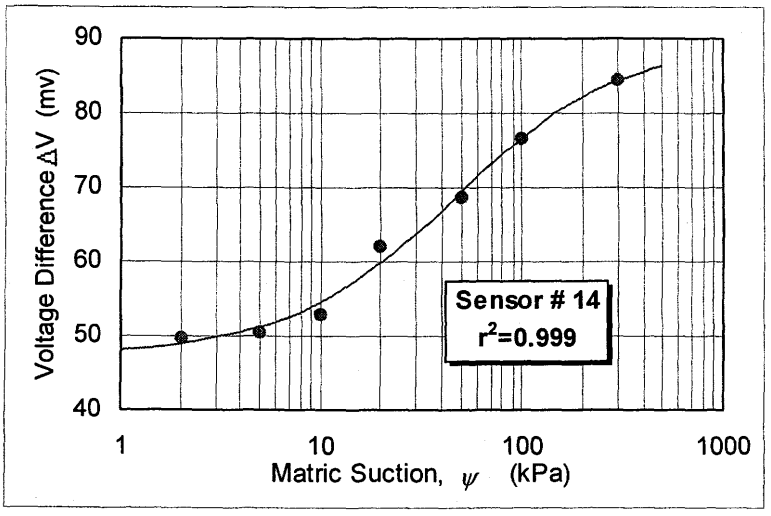

Figure F.15

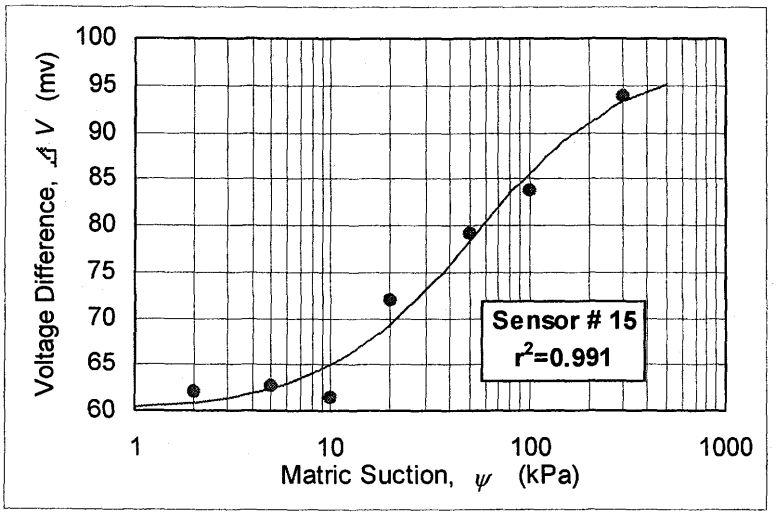

Figure F.16

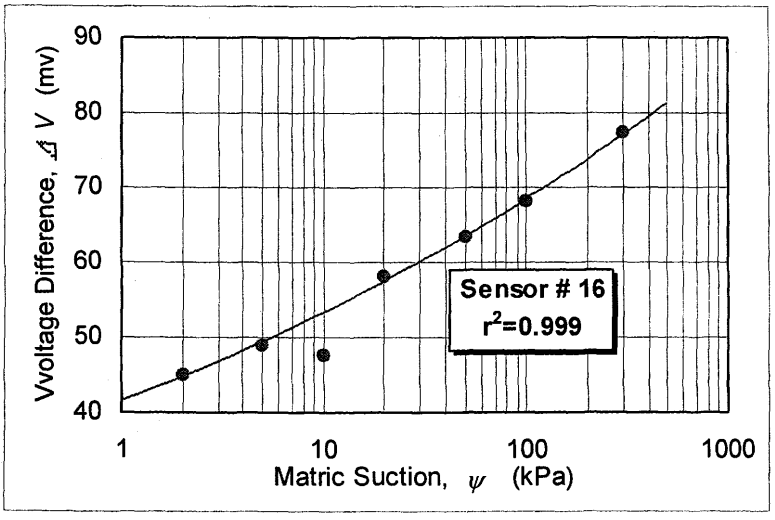

Figure F.17

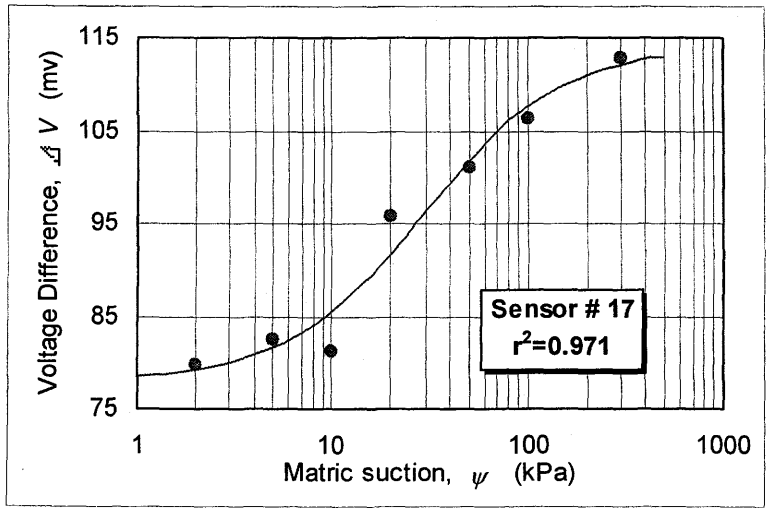

Figure F.18

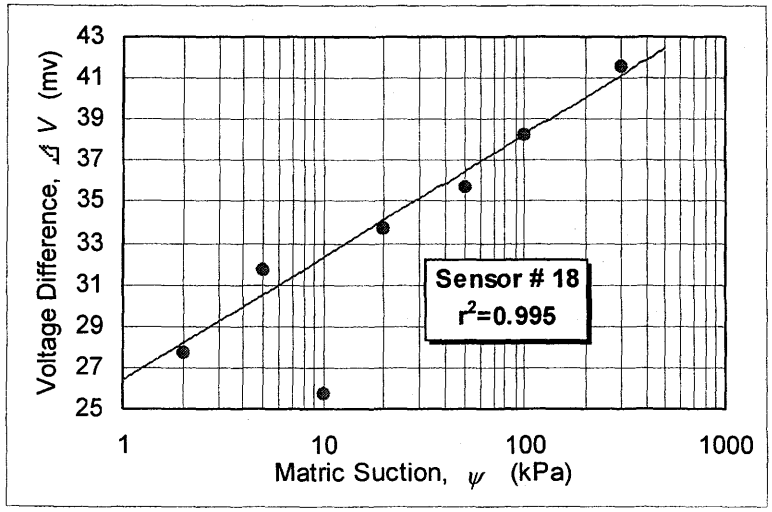

Figure F.19

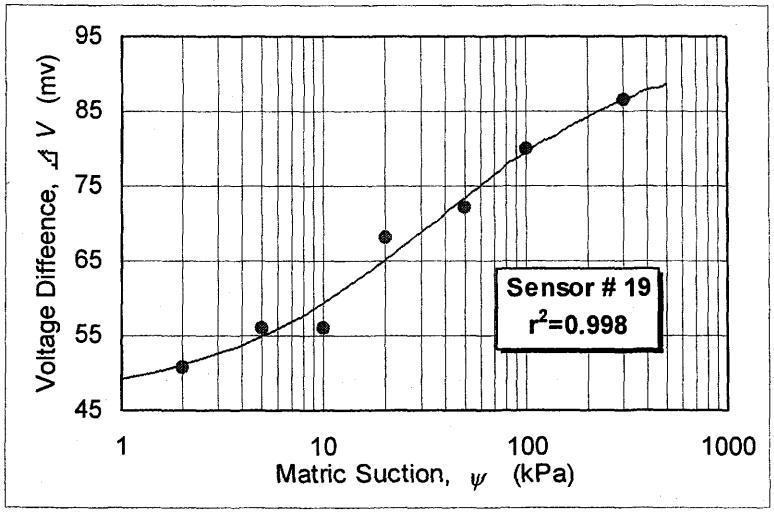

Figure F.20

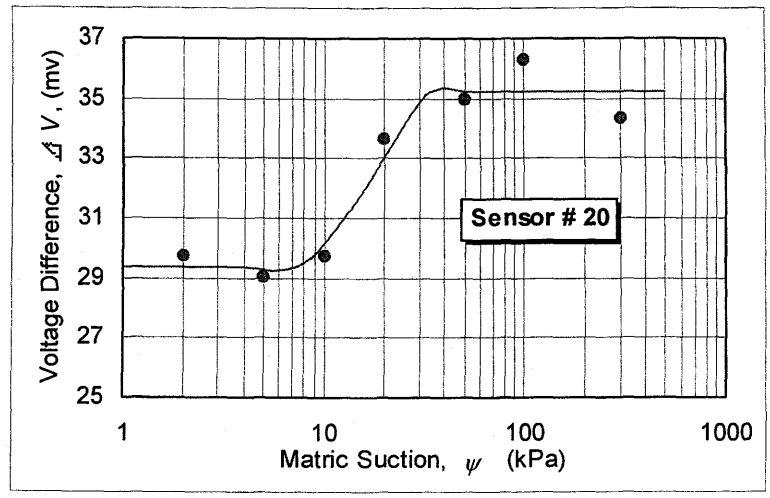

Figure F.21

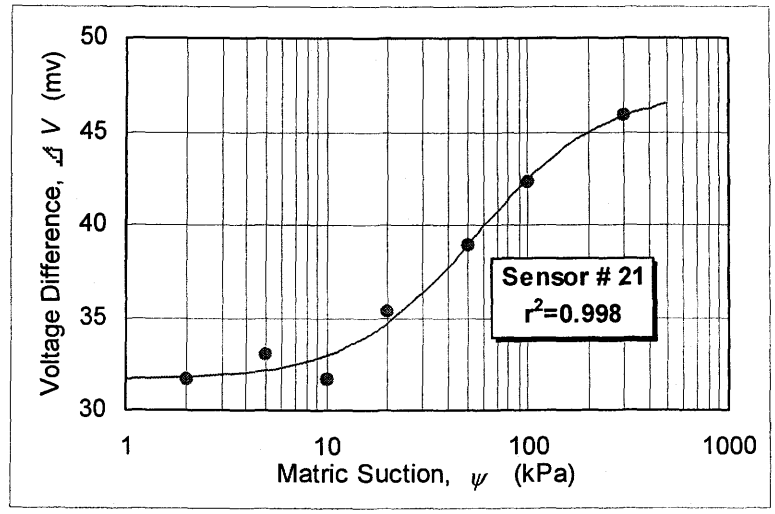

Figure F.22

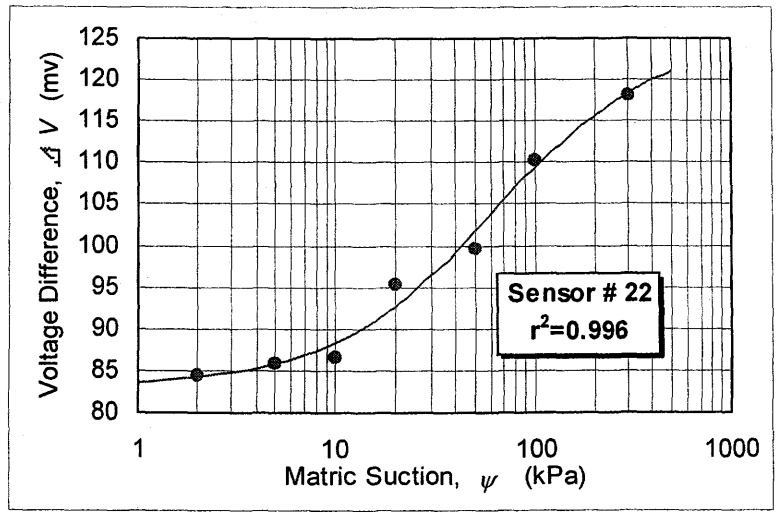

Table F.1 Beta-97 sensor calibration equations.

Sensor Number	a	b	c	d
# 1	27.19	77.11	49.75	0.70
# 2	75.12	106.60	100.43	0.71
# 3	69.24	1006.88	5201.79	2.50
# 4	23.27	15.99	57.26	1.50
# 5	49.22	8.92	73.68	1.20
# 6	45.19	20.89	71.45	1.44
# 7	28.30	20.45	47.41	1.15
# 8	63.01	25.57	99.55	0.95
# 9	38.01	605.99	56.23	0.52
# 10	30.10	11.33	90.08	2.13
# 11	37.59	7.32	79.06	1.85
# 12	44.33	67.88	67.20	0.94
# 13	54.52	47.54	94.74	1.00
# 14	47.52	57.15	89.38	0.94
# 15	59.97	85.54	97.95	0.89
# 16	9.21	10.34	375.76	6.68
# 17	77.98	64.99	113.97	0.81
# 18	-21.05	1.55	100.20	11.62
# 19	46.61	17.11	93.61	1.25
# 20	29.38	#######	35.23	0.18
# 21	31.61	242.28	47.22	0.73
# 22	83.09	79.11	125.01	0.94

F.2 Beta-97 Sensor Field Data

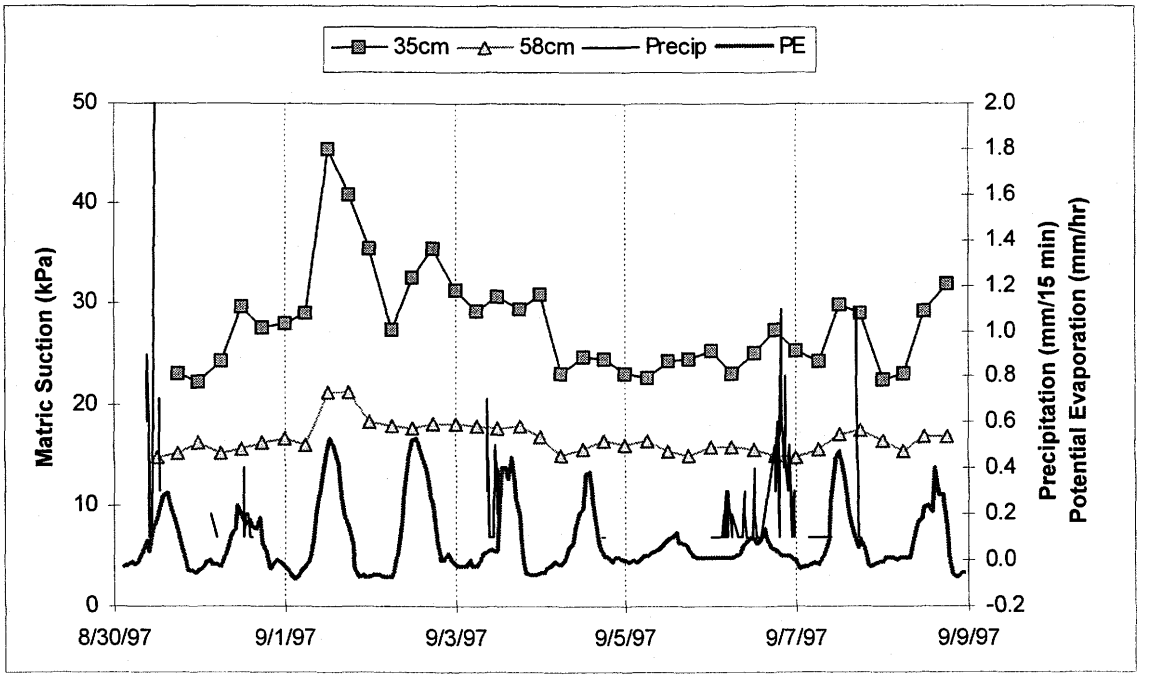

Figure F.23

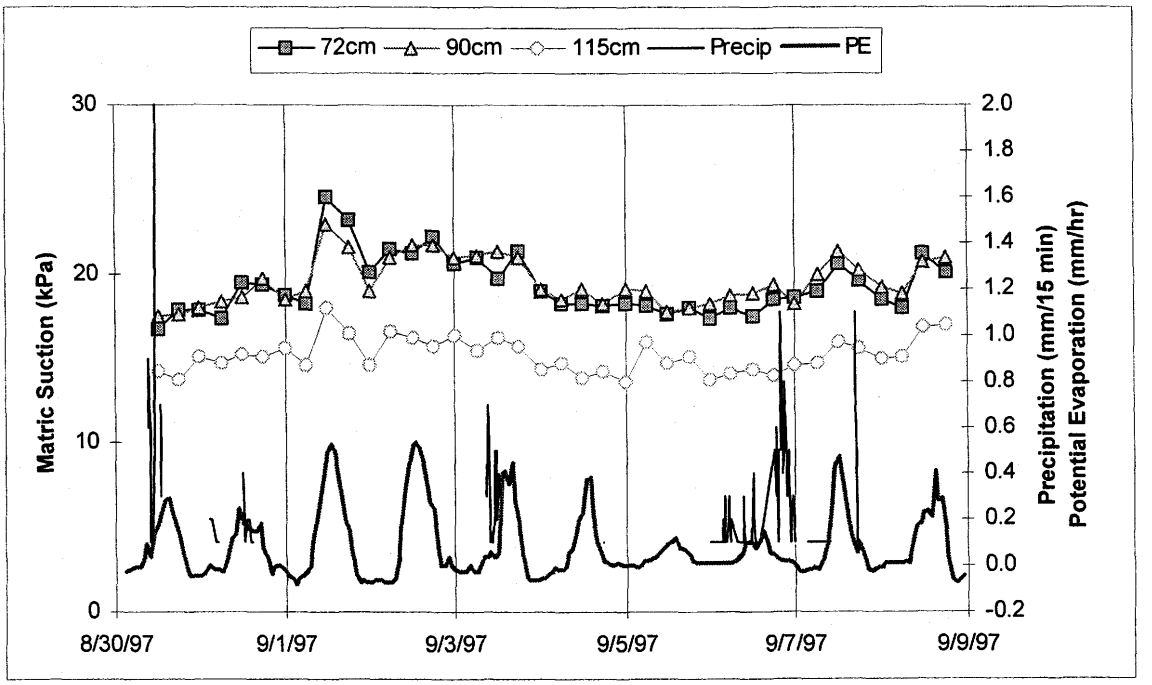

Figure F.24

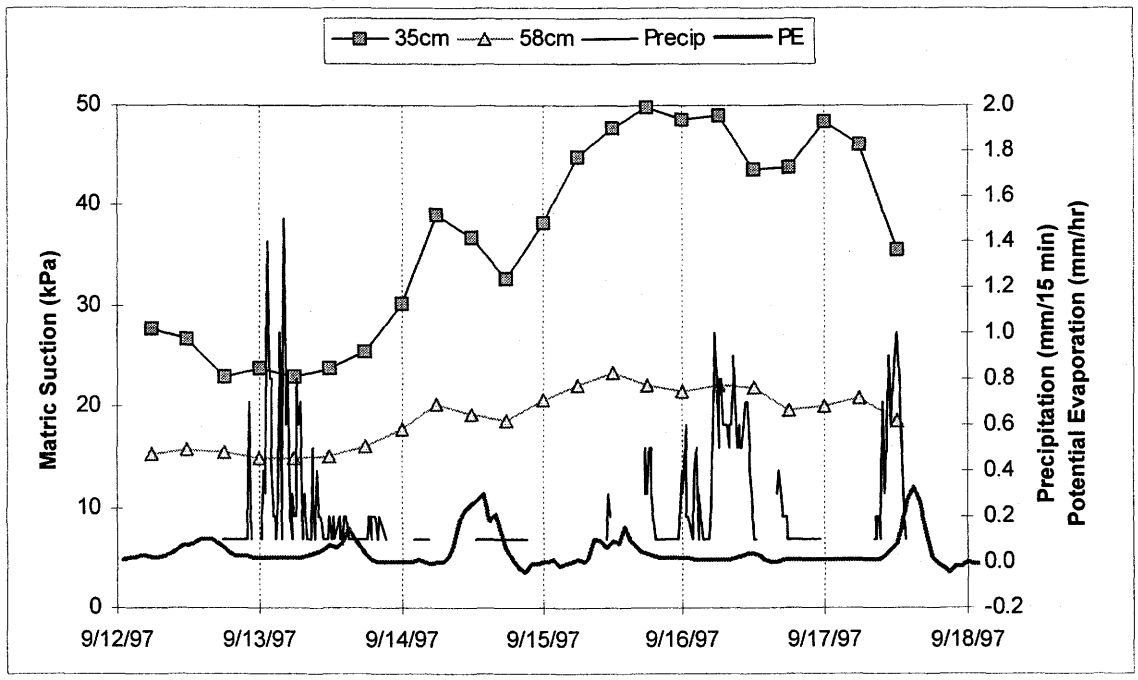

Figure F.25

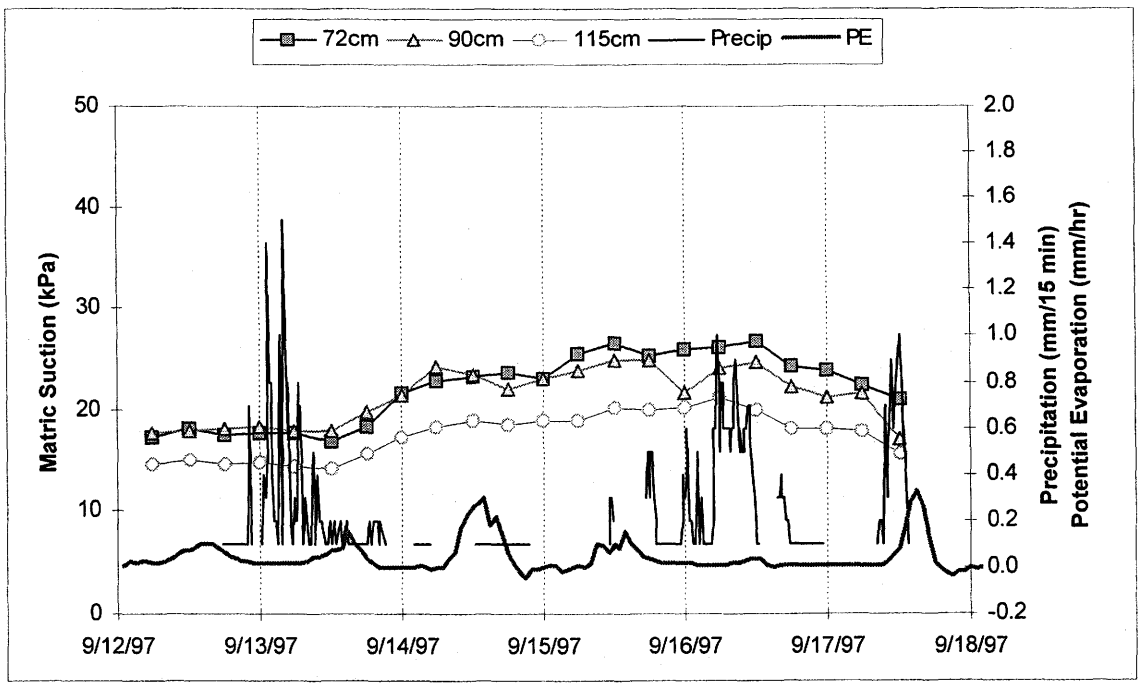

Figure F.26

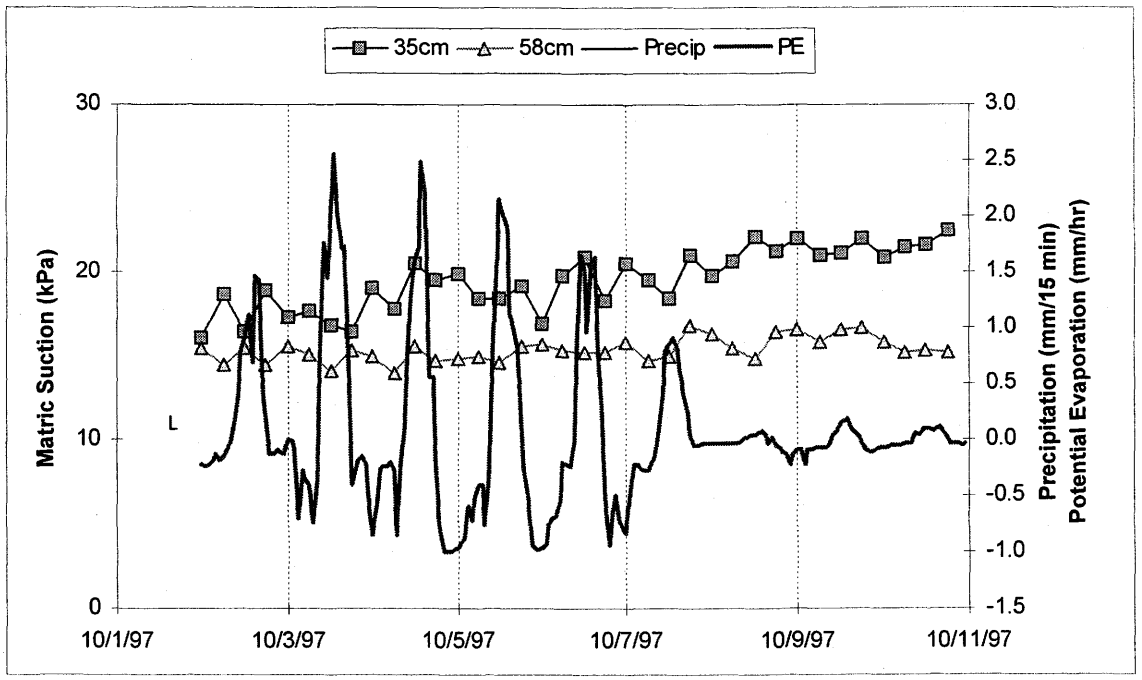

Figure F.27

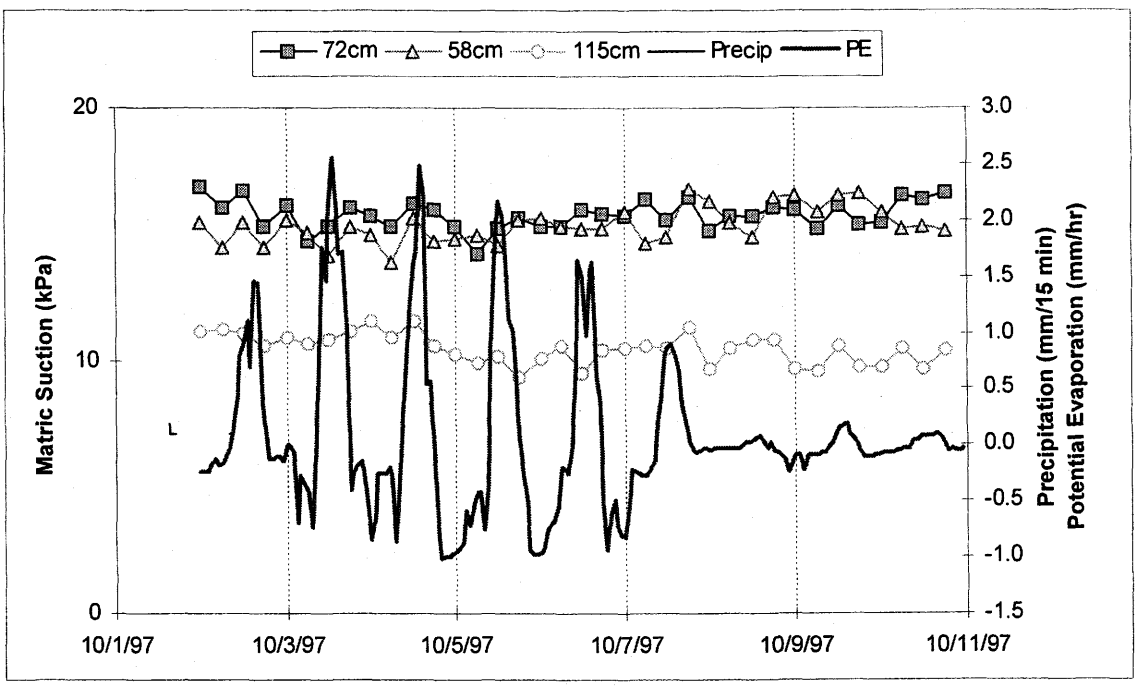

Figure F.28

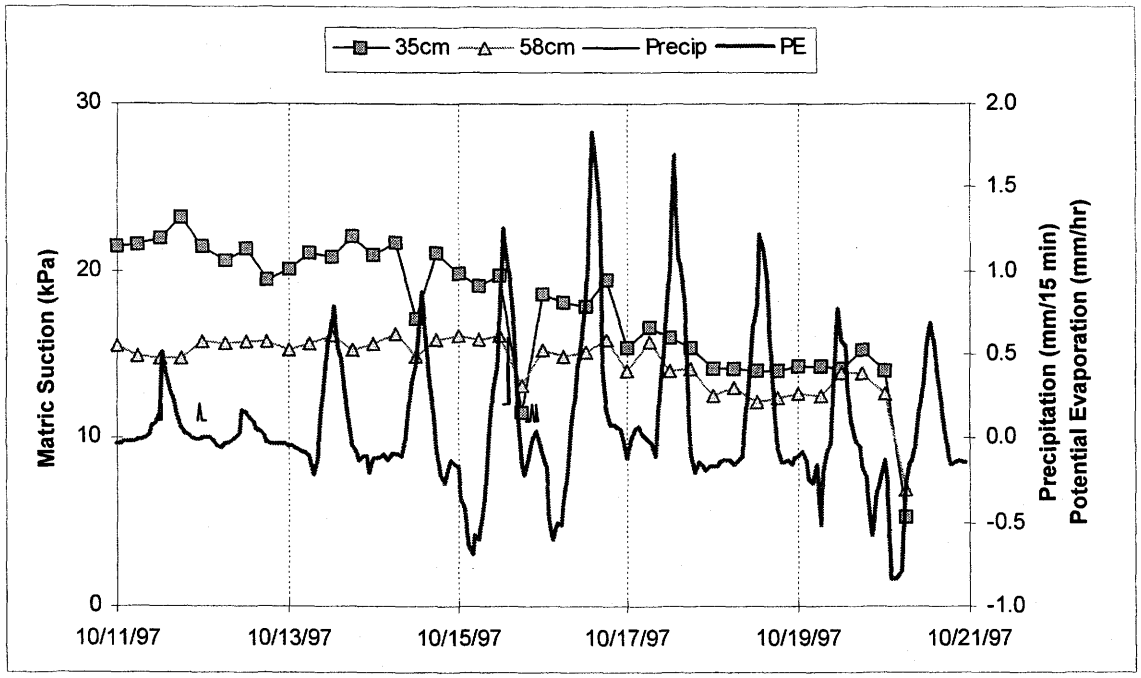

Figure F.29

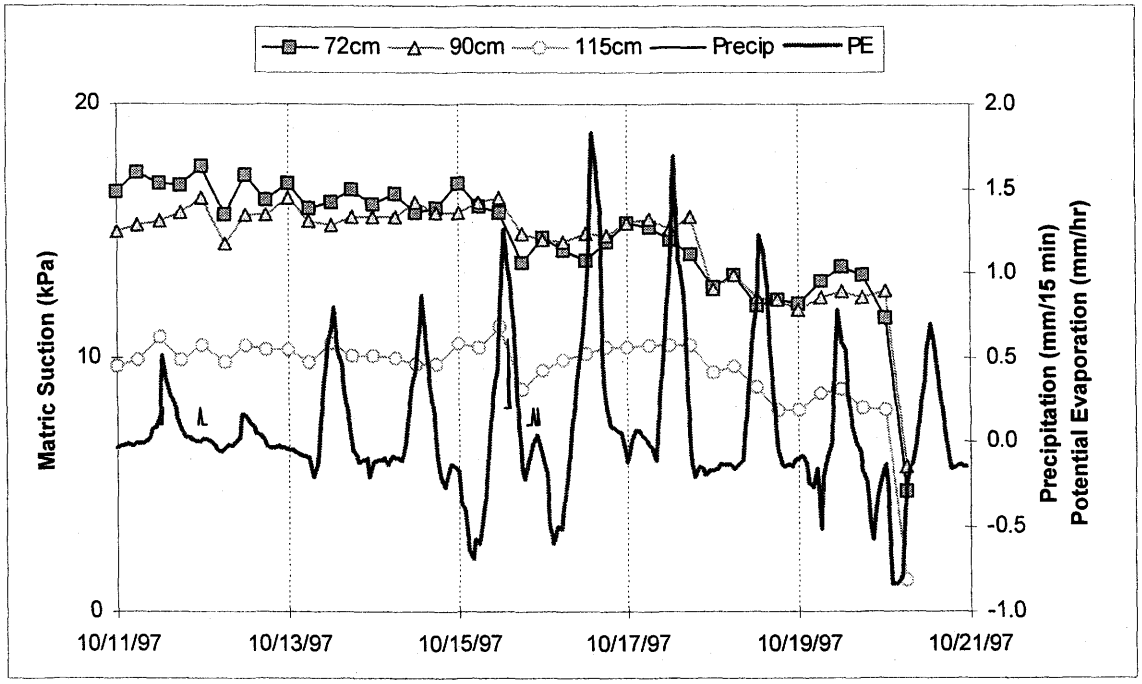

Figure F.30

F.3 NEUTRON PROBE DATA

F.3.1 Neutron Probe Calibration Equations and Regressions

Table F.2 Neutron Probe Laboratory calibration equations

Data Type	Bulk	Regression	Regression Equation	r^2
Sand	various	linear	$\theta = 0.616\ (CR) - 0.061$	0.972
Till combined	various	linear	$\theta = 0.503\ (CR) - 0.054$	0.898
All soil types	various	linear	$\theta = 0.573\ (CR) - 0.064$	0.922
Sand	1.76	linear	$\theta = 0.637\ (CR) - 0.061$	0.964
Till combined	2.02	linear	$\theta = 0.508\ (CR) - 0.050$	0.864
All soil types	1.80	linear	$\theta = 0.566\ (CR) - 0.059$	0.874
Sand	various	power	$\theta = 0.942\ (CR)^{2.29}$	0.994
Till combined	various	power	$\theta = 0.886\ (CR)^{2.43}$	0.998
All soil types	various	power	$\theta = 0.890\ (CR)^{2.33}$	0.993
All soil types	various	polynomial	$\theta = 0.867\ (CR)^2 - 0.0763$	0.978
Sand	1.76	power	$\theta = 1.01\ (CR)^{2.28}$	0.995
Till combined	2.02	power	$\theta = 0.916\ (CR)^{2.39}$	0.995
All soil types	1.80	power	$\theta = 0.874\ (CR)^{2.20}$	0.987
All soil types	1.80	polynomial	$\theta = 0.946\ (CR)^2 - 0.115\ (CR)$	0.978

F.3.2 Neutron Probe Field Data

Table F.3 Neutron Probe HL101-N Results.

Date	*27/11/96*		*8/4/97*		*26/5/97*		*22/8/97*		*7-Oct-97*	
χ^2	1.15		1.09		0.98		0.92		0.94	
Depth (m)	**Count**	θ	**Count**	θ	**Count**	θ	**Count**	θ	**Count**	θ
0.51	0.45	12.6%	0.41	10.4%	0.42	10.9%	0.43	11.3%	0.43	11.6%
0.82	0.50	15.9%	0.39	9.1%	0.40	9.4%	0.41	10.2%	0.44	11.7%
1.12	0.51	16.6%	0.32	5.6%	0.34	6.6%	0.37	8.1%	0.38	8.7%
1.43	0.37	8.2%	0.27	4.0%	0.32	5.7%	0.30	4.9%	0.29	4.6%
1.73	0.33	6.1%	0.34	6.7%	0.44	12.2%	0.39	9.1%	0.37	8.2%
2.04	0.41	10.2%	0.36	7.6%	0.45	12.9%	0.65	29.2%	0.45	12.3%

Table F.4 Neutron Probe HL102-N Results.

Date	*27/11/96*		*8/4/97*		*26/5/97*		*22/8/97*		*7-Oct-97*	
χ^2	1.15		1.09		0.98		0.98		0.92	
Depth (m)	**Count**	θ	**Count**	θ	**Count**	θ	**Count**	θ	**Count**	θ
0.41	0.24	2.9%	0.46	13.3%	0.41	10.1%	0.42	11.1%	0.44	11.8%
0.72	0.48	14.8%	0.35	7.2%	0.44	11.8%	0.42	11.0%	0.47	13.8%
1.02	0.41	10.5%	0.32	5.9%	0.38	8.5%	0.40	9.4%	0.43	11.2%
1.33	0.44	12.1%	0.36	7.5%	0.45	12.4%	0.47	14.0%	0.46	13.5%
1.63	0.52	17.6%	0.51	16.8%	0.61	25.4%	0.52	17.9%	0.52	17.7%
1.94	0.56	20.8%	0.43	11.4%	0.46	13.1%	0.63	27.3%	0.54	19.3%
2.24			0.45	12.7%	0.47	13.6%	0.68	32.0%	0.59	23.5%

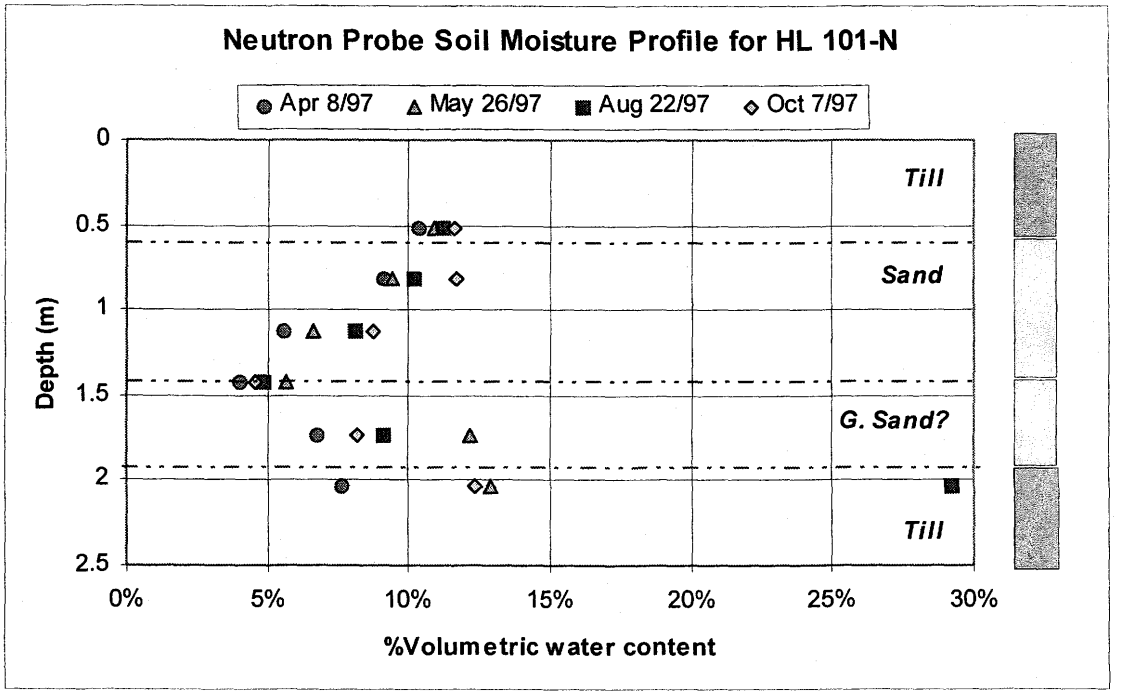

Figure F.31

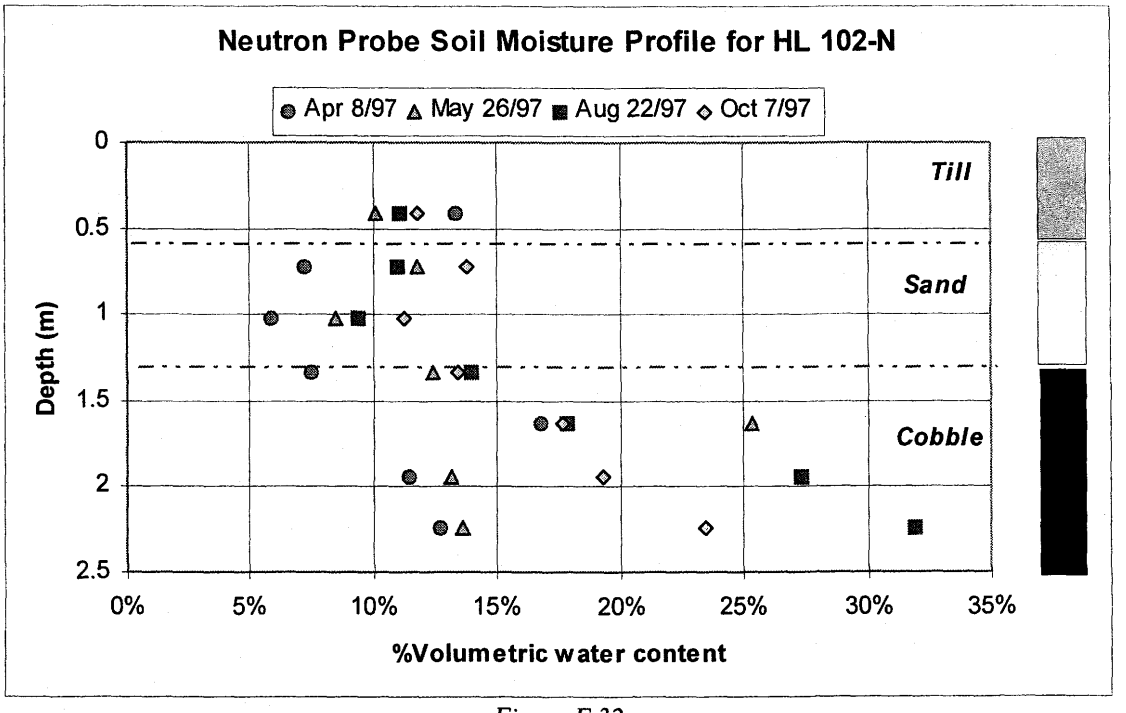

Figure F.32